

10-45

NASA/TP-2000-210016

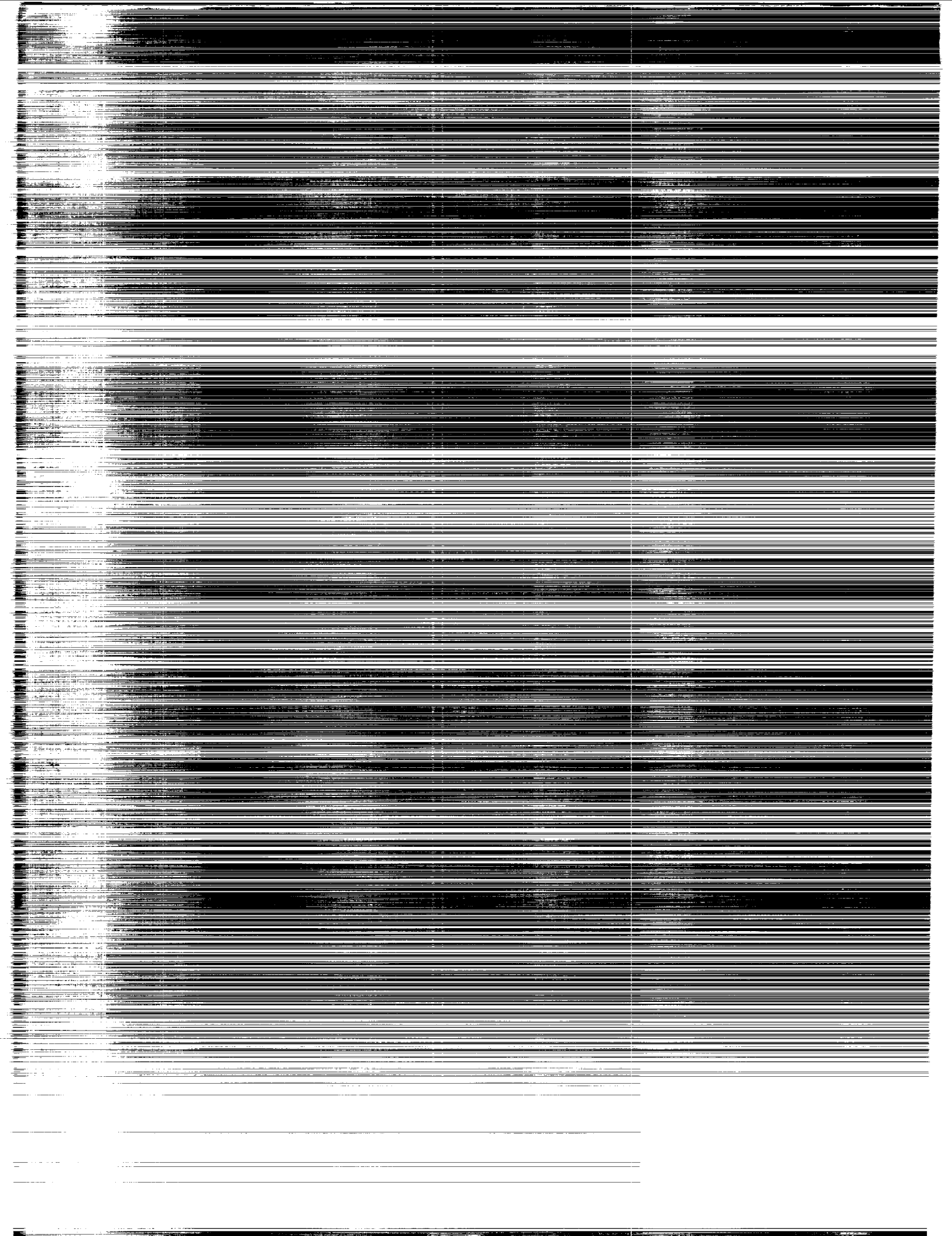
March 2000

Present State of Knowledge of the Upper Atmosphere 1999: An Assessment Report

*Report to Congress
and the Environmental
Protection Agency*

M. J. Kurylo
P. L. DeCola
J. A. Kaye





NASA/TP-2000-210016

March 2000

Present State of Knowledge
of the Upper Atmosphere 1999:
An Assessment Report

*Report to Congress
and the Environmental
Protection Agency*

M. J. Kurylo
P. L. DeCola
J. A. Kaye

*NASA Office of Earth Science Research Division
Washington, DC*



1. The first part of the document discusses the importance of maintaining accurate records of all transactions.

2. It is essential to ensure that all data is entered correctly and consistently across all systems.

3. Regular audits should be conducted to verify the integrity and accuracy of the information.

4. The second section outlines the various methods used to collect and analyze data.

5. These methods include surveys, interviews, and focus groups, each with its own strengths and limitations.

6. The choice of method depends on the specific research objectives and the nature of the data being collected.

7. It is important to select the most appropriate method to ensure the reliability and validity of the results.

8. The third section describes the process of data analysis and interpretation.

9. This involves identifying patterns, trends, and relationships within the data set.

10. Statistical techniques are often used to quantify these findings and test hypotheses.

11. The final part of the document provides a summary of the key findings and conclusions.

12. It emphasizes the need for ongoing monitoring and evaluation to ensure the continued relevance and accuracy of the data.

13. The document concludes by highlighting the importance of transparency and accountability in the data management process.

14. Finally, it offers recommendations for best practices to improve data management and reporting.

Page 1 of 1

TABLE OF CONTENTS

A	INTRODUCTION.....	1
B	SCIENTIFIC ASSESSMENT OF OZONE DEPLETION: 1998.....	5
	EXECUTIVE SUMMARY	5
	Recent Major Scientific Findings and Observations.....	5
	Supporting Scientific Evidence and Related Issues	8
	Recent Halogen and Methane Changes.....	8
	Stratospheric Particles	10
	Ozone in the Midlatitudes and Tropics	10
	Ozone in High-Latitude Polar Regions.....	12
	Stratospheric Temperatures.....	13
	Tropospheric Ozone	14
	Changes in UV Radiation.....	14
	Changes in Climate Parameters	15
	Future Halogen Changes.....	16
	Recovery of the Ozone Layer.....	16
	Implications for Policy Formulation	17
	CHAPTER SUMMARIES.....	21
	1 Long-Lived Ozone-Related Compounds	21
	2 Short-Lived Ozone-Related Compounds.....	25
	3 Global Distributions and Changes in Stratospheric Particles	30
	4 Ozone Variability and Trends.....	31
	5 Trends in Stratospheric Temperatures	34
	6 Upper Stratospheric Processes	38
	7 Lower Stratospheric Processes.....	39
	8 Tropospheric Ozone and Related Processes	42
	9 Ultraviolet Radiation at the Earth's Surface.....	44
	10 Climate Effects of Ozone and Halocarbon Changes	46
	11 Halocarbon Scenarios for the Future Ozone Layer and Related Consequences.....	48
	12 Predicting Future Ozone Changes and Detection of Recovery.....	51

C	SUMMARY OF THE STRATOSPHERIC PROCESSES AND THEIR ROLE IN CLIMATE/INTERNATIONAL OZONE COMMISSION/GLOBAL ATMOSPHERIC WATCH (SPARC/IOC/GAW) ASSESSMENT OF TRENDS IN THE VERTICAL DISTRIBUTION OF OZONE.....	55
	INTRODUCTION.....	55
	FINDINGS.....	56
	Validity of the Data Sets.....	56
	Trend Analyses.....	60
D	POLICYMAKERS SUMMARY OF THE INTERGOVERNMENTAL PANEL ON CLIMATE CHANGE (IPCC) SPECIAL REPORT ON AVIATION AND THE GLOBAL ATMOSPHERE.....	63
	INTRODUCTION.....	63
	HOW DO AIRCRAFT AFFECT CLIMATE AND OZONE?.....	64
	HOW ARE AVIATION EMISSIONS PROJECTED TO GROW IN THE FUTURE?.....	66
	WHAT ARE THE CURRENT AND FUTURE IMPACTS OF SUBSONIC AVIATION ON RADIATIVE FORCING AND UV RADIATION?.....	68
	Carbon Dioxide.....	68
	Ozone.....	68
	Methane.....	69
	Water Vapor.....	69
	Contrails.....	69
	Cirrus Clouds.....	69
	Sulfate and Soot Aerosols.....	70
	What are the Overall Climate Effects of Subsonic Aircraft?.....	70
	What are the Overall Climate Effects of Subsonic Aircraft on UV-B?.....	72
	WHAT ARE THE CURRENT AND FUTURE IMPACTS OF SUPERSONIC AVIATION ON RADIATIVE FORCING AND UV RADIATION?.....	73
	WHAT ARE THE OPTIONS TO REDUCE EMISSIONS AND IMPACTS?.....	74
	Aircraft and Engine Technology Options.....	75
	Fuel Options.....	75
	Operational Options.....	76
	Regulatory, Economic and Other Options.....	76
	ISSUES FOR THE FUTURE.....	78

E	ASSESSMENT OF THE EFFECTS OF HIGH-SPEED AIRCRAFT IN THE STRATOSPHERE: 1998	79
	INTRODUCTION	79
	EXECUTIVE SUMMARY	79
F	MODELS AND MEASUREMENTS INTERCOMPARISON II	89
	EXECUTIVE SUMMARY	89
	New Data Used for M&M II.....	89
	Strategy for Model Testing.....	90
	Focus on Transport.....	91
	Focus on Chemistry	92
	Results of M&M II.....	93
	Transport Exercises.....	93
	Chemistry Partitioning	95
	Chemical Tracers.....	95
	Ozone Comparison	96
G	PHOTOCHEMISTRY OF OZONE LOSS IN THE ARCTIC REGION IN SUMMER (POLARIS) END OF MISSION STATEMENT.....	101
	INTRODUCTION	101
	DEPLOYMENT DESCRIPTIONS	102
	Phase I.....	102
	Phase II.....	102
	Phase III.....	102
	POLARIS SCIENCE SUMMARY	103
H	CHEMICAL KINETICS AND PHOTOCHEMICAL DATA FOR USE IN STRATOSPHERIC MODELING: SUPPLEMENT TO EVALUATION NUMBER 12 OF THE NASA PANEL FOR DATA EVALUATION	123
	SCOPE OF THE EVALUATION.....	123

I	AUTHORS, CONTRIBUTORS, AND REVIEWERS.....	131
	A.....	131
	B.....	131
	C.....	148
	D.....	151
	E.....	166
	F.....	167
	G.....	169
	H.....	170

PREFACE

NASA has relied heavily on the entire scientific community, national and international, in its effort to provide a better understanding of the upper atmosphere and its perturbation in response to natural phenomena and human activities. The lists of contributors to the individual sections in this report are given in Section I. We are indebted to those who gave their time and knowledge. We also thank Rose Kendall and Kathy Wolfe for compiling the report and providing editorial support.

Michael J. Kurylo

Philip L. DeCola

Jack A. Kaye

1. The first part of the document is a list of names and addresses of the members of the committee.

MEMBERS OF THE COMMITTEE

1. Mr. J. H. Smith

2. Mr. W. B. Jones



SECTION A

INTRODUCTION

In compliance with the Clean Air Act Amendments of 1990, Public Law 101-549, the National Aeronautics and Space Administration (NASA) has prepared this report on the state of our knowledge of the Earth's upper atmosphere, and particularly, of the stratospheric ozone layer. The present report presents new findings since the last report in 1996 and is printed in two parts. Part I (Research Summaries) summarizes the objectives, status, and accomplishments of the research tasks supported under NASA's Upper Atmosphere Research Program (UARP) and Atmospheric Chemistry Modeling and Analysis Program (ACMAP) for the period of 1997-1999. Part II (this document) is a compilation of several scientific assessments, reviews, and summaries. Section B (*Scientific Assessment of Ozone Depletion: 1998*), Section C (a summary of the 1998 Stratospheric Processes and Their Role in Climate/Intergovernmental Ozone Commission/Global Atmospheric Watch (SPARC/IOC/GAW) Assessment of Trends in the Vertical Distribution of Ozone *SPARC Report No. 1, WMO Ozone Research and Monitoring Project Report No. 43*), Section D (the Policymakers Summary of the Intergovernmental Panel on Climate Change, IPCC, special report on *Aviation and the Global Atmosphere*), and Section E (the executive summary of the *NASA Assessment of the Effects of High-Speed Aircraft in the Stratosphere: 1998*) are summaries of the most recent assessments of our current understanding of the chemical composition and the physical structure of the stratosphere, with particular emphasis on how the abundance and distribution of ozone is predicted to change in the future. Section F (the executive summary of NASA's Second Workshop on Stratospheric Models and Measurements, M&M II) and Section G (the end-of-mission statement for the Photochemistry of Ozone Loss in the Arctic Region in Summer, POLARIS, campaign) describe the scientific results for a comprehensive modeling intercomparison exercise and an aircraft and balloon measurement campaign, respectively. Section H (*Chemical Kinetics and Photochemical Data for Use in Stratospheric Modeling: Supplement to Evaluation Number 12 of the NASA Panel for Data Evaluation*) highlights the latest of NASA's reviews of this important aspect of the atmospheric sciences.

For over two decades, scientists have postulated that certain pollutants directly associated with human activity could cause harmful effects by reducing the amount of stratospheric ozone. Initial concerns focused on supersonic aircraft emissions of NO and NO₂, and then shifted to the issue of chlorine and bromine loading of the stratosphere from chlorofluorocarbons (CFCs) and halons. Now there is compelling evidence that human activity has, in fact, changed the atmospheric environment on a global scale. In recognition of the importance of understanding such perturbations, Congress directed NASA in June 1975 to "develop and carry out a comprehensive program of research, technology, and monitoring of the phenomena of the upper atmosphere so as to provide for an understanding of and to maintain the chemical and physical integrity of Earth's upper atmosphere." Responding to this Congressional mandate, NASA implemented a long-range scientific research program, conducted through UARP and ACPMAP, aimed at developing a comprehensive understanding of processes in the upper atmosphere. Additional activities are carried out through the NASA space flight programs. In the near-term, NASA has the

responsibility of providing triennial reports to Congress and concerned regulatory agencies on the status of upper atmospheric research, including scientific assessments of potential effects of human activities on the atmosphere, and particularly, on stratospheric ozone.

Many governments around the world, including the United States, have recognized that the ozone layer must be protected in order to preserve human health and aquatic and terrestrial ecosystems from damage due to enhanced levels of ultraviolet radiation. In particular, it was recognized that the use of chemicals containing chlorine (in the form of CFCs, hydrochlorofluorocarbons (HCFCs), and other chlorinated hydrocarbons such as methyl chloroform and carbon tetrachloride) and bromine (mainly in the form of halons and methyl bromide) constitute a potential threat to the ozone layer. More than twenty nations, including the United States, signed the Vienna Convention for the Protection of the Ozone Layer in Vienna, Austria, in 1985, and the Montreal Protocol on Substances That Deplete the Ozone Layer, in Montreal, Canada, in 1987. Subsequent Amendments and Adjustments (London, UK, 1990; Copenhagen, Denmark, 1992; Vienna, Austria, 1995; and Montreal, Canada, 1997) strengthened the Montreal Protocol by calling for an accelerated CFC phase-out schedule and adding to the list of regulated compounds.

The Vienna Convention and the Montreal Protocol both call for all regulatory decisions to be based on a scientific understanding of the issues, and the Montreal Protocol specifically called for international scientific assessments at least every four years. The 1998 scientific assessment was coordinated by NASA, the National Oceanic and Atmospheric Administration (NOAA), the United Nations Environment Program (UNEP), the World Meteorological Organization (WMO), and the European Commission (EC). The executive summary of the overall assessment and scientific summaries of the assessment chapters are reproduced in Section B.

One of the largest uncertainties in determining the effect of CFCs on stratospheric ozone has been the magnitude of the trends in the altitude region between 15 and 20 km. In 1996 the SPARC panel on Understanding Ozone Trends and the International Ozone Commission decided to collaborate, under the auspices of the World Climate Research Programme and the World Meteorological Organisation, on a study to carefully re-evaluate the ground-based and satellite data to resolve differences in the interpretation of the various ozone profile data records. The philosophy of the study was similar to that of the International Ozone Trends Panel of 1988 which addressed the total ozone measurements. The summary of this report is presented in Section C.

Aviation has experienced rapid expansion as the world economy has grown. This expansion has led to an increase in aviation emissions. In light of the concern about the possible effects of aircraft emissions on global climate and atmospheric ozone, the Intergovernmental Panel on Climate Change has prepared an assessment report addressing these issues. Section D consists of the policymakers summary from this special report.

The environmental impact of a proposed fleet of high-speed (i. e., supersonic) civil transport (HSCT) aircraft on the ozone layer has also been assessed. The interim assessment report from NASA's High-Speed Research Program, issued in January 1995, has been superceded by a more recent 1998 assessment on the effects of high-speed aircraft in the stratosphere. The executive summary from this assessment report is included as Section E of this document.

NASA's Second Workshop on Stratospheric Models and Measurements (M&M II) is a continuation of the effort previously started in M&M I held in 1992. As originally stated, the aim of M&M was to provide a foundation for establishing the credibility of stratospheric models used in environmental assessments of the ozone response to chlorofluorocarbons, aircraft emissions, and other climate-chemistry interactions. To accomplish this, a set of measurements of the present day atmosphere was selected. The intent was that successful simulations of the set of measurements should become the prerequisite for the acceptance of these models as having a reliable prediction for future ozone behavior. The executive summary of the M&M II report comprises Section F of this document.

Process studies conducted via field campaigns, involving focused measurements within a particular atmospheric region so that specific chemical and physical processes can be understood and theories can be quantitatively tested, are fundamental to the assessment process. Such campaigns rely extensively on *in situ* and remote-sensing aircraft measurements as well as those from ground-, balloon-, and space-based instruments. Section G describes the results of the Photochemistry of Ozone Loss in the Arctic Region in Summer (POLARIS) field campaign that was designed to understand the seasonal behavior of polar stratospheric ozone as it changes from very high concentrations in spring down to very low concentrations in autumn. This behavior has been attributed to an increased role of NO_x catalytic cycles for ozone destruction during periods of prolonged solar illumination such as occur at high latitudes during summer. The detail with which current photochemical models can describe this large natural change in ozone serves as an indication of how well the role of increased stratospheric NO_x from anthropogenic sources can be quantified. Additional information on the POLARIS measurement campaign, including an unabridged version of the end-of-mission statement, is available at the following website: <http://cloud1.arc.nasa.gov/polaris/index.html>.

Also fundamental to the assessment process is a solid quantitative foundation of laboratory-derived photochemical reaction rates for use in predictive models. The periodic review and evaluation of kinetic and photochemical data by the NASA Panel for Data Evaluation is an important unifying document for the atmospheric sciences community. It offers a standard reference database for atmospheric modeling (for both assessment and research) thereby providing a common focus for laboratory measurements and theoretical studies. The most recent recommendations of this panel are being published as an update to Evaluation Number 12 of the NASA Panel for Data Evaluation, and details on the scope of the re-evaluation as well as pertinent sections are included as Section H of this document.

The contributors to all of the sections mentioned above are listed in Section I.

1. The first part of the document discusses the importance of maintaining accurate records of all transactions and activities. It emphasizes that this is crucial for ensuring transparency and accountability in the organization's operations.

2. The second part of the document outlines the various methods and tools used to collect and analyze data. It highlights the need for consistent data collection practices and the use of advanced analytical techniques to derive meaningful insights from the data.

3. The third part of the document focuses on the implementation of data-driven decision-making processes. It provides a detailed overview of the steps involved in identifying key performance indicators (KPIs) and using data to inform strategic decisions.

4. The fourth part of the document discusses the challenges and risks associated with data management and analysis. It offers practical advice on how to mitigate these risks and ensure the integrity and security of the data.

5. The fifth part of the document concludes by summarizing the key findings and recommendations. It stresses the importance of ongoing monitoring and evaluation to ensure that the data-driven approach remains effective and relevant over time.

6. The final part of the document provides a list of references and resources for further reading. It includes links to relevant articles, books, and online resources that can provide additional information on the topics discussed in the document.

SECTION B

SCIENTIFIC ASSESSMENT OF OZONE DEPLETION: 1998 EXECUTIVE SUMMARY

The 1987 Montreal Protocol on Substances that Deplete the Ozone Layer commemorated its 10th anniversary in September 1997. Among the provisions of the Protocol was the requirement that the Parties to the Protocol base their future decisions on the available scientific, environmental, technical, and economic information as assessed by the worldwide expert communities. The advances of the understanding in ozone science over this decade were assessed in 1988, 1989, 1991, and 1994. This information was input to the subsequent Amendments and Adjustments of the 1987 Protocol. The Assessment summarized here is the fifth in that series.

RECENT MAJOR SCIENTIFIC FINDINGS AND OBSERVATIONS

Since the *Scientific Assessment of Ozone Depletion: 1994*, significant advances have continued to be made in the understanding of the impact of human activities on the ozone layer, the influence of changes in chemical composition on the radiative balance of the Earth's climate, and, indeed, the coupling of the ozone layer and the climate system. Numerous laboratory investigations, atmospheric observations, and theoretical and modeling studies have produced several key ozone- and climate-related findings:

- **The total combined abundance of ozone-depleting compounds in the lower atmosphere peaked in about 1994 and is now slowly declining. Total chlorine is declining, but total bromine is still increasing.** As forecast in the 1994 Assessment, the long period of increasing total chlorine abundances – primarily from the chlorofluorocarbons (CFCs), carbon tetrachloride (CCl₄), and methyl chloroform (CH₃CCl₃) – has ended. The peak total tropospheric chlorine abundance was 3.7 ± 0.1 parts per billion (ppb) between mid-1992 and mid-1994. The declining abundance of total chlorine is due principally to reduced emissions of methyl chloroform. Chlorine from the major CFCs is still increasing slightly. The abundances of most of the halons continue to increase (for example, Halon-1211, almost 6% per year in 1996), but the rate has slowed in recent years. These halon increases are likely to be due to emissions in the 1990s from the halon “bank,” largely in developed countries, and new production of halons in developing countries. The observed abundances of CFCs and chlorocarbons in the lower atmosphere are consistent with reported emissions.
- **The observed abundances of the substitutes for the CFCs are increasing.** The abundances of the hydrochlorofluorocarbons (HCFCs) and hydrofluorocarbons (HFCs) are increasing as a result of a continuation of earlier uses and of their use as substitutes for the CFCs. In 1996, the HCFCs contributed about 5% to the tropospheric chlorine from the long-lived gases. This addition from the substitutes offsets some of the decline in tropospheric chlorine associated with methyl chloroform, but is nevertheless about 10 times less than that from the total tropospheric chlorine growth rate throughout the 1980s. The

atmospheric abundances of HCFC-141b and HCFC-142b calculated from reported emissions data are factors of 1.3 and 2, respectively, smaller than observations. Observed and calculated abundances agree for HCFC-22 and HFC-134a.

- **The combined abundance of stratospheric chlorine and bromine is expected to peak before the year 2000.** The delay in this peak in the stratosphere compared with the lower atmosphere reflects the average time required for surface emissions to reach the lower stratosphere. The observations of key chlorine compounds in the stratosphere up through the present show the expected slower rate of increase and show that the peak had not occurred at the time of the most recent observations that were analyzed for this Assessment.
- **The role of methyl bromide as an ozone-depleting compound is now considered to be less than was estimated in the 1994 Assessment, although significant uncertainties remain.** The current best estimate of the Ozone Depletion Potential (ODP) for methyl bromide (CH_3Br) is 0.4, compared with an ODP of 0.6 estimated in the previous Assessment. The change is due primarily to both an increase in the estimate of ocean removal processes and the identification of an uptake by soils, with a smaller contribution from the change in our estimate of the atmospheric removal rate. Recent research has shown that the science of atmospheric methyl bromide is complex and still not well understood. The current understanding of the sources and sinks of atmospheric methyl bromide is incomplete.
- **The rate of decline in stratospheric ozone at midlatitudes has slowed; hence, the projections of ozone loss made in the 1994 Assessment are larger than what has actually occurred.** Total column ozone decreased significantly at midlatitudes (25-60°) between 1979 and 1991, with estimated linear downward trends of 4.0, 1.8, and 3.8% per decade, respectively, for northern midlatitudes in winter/spring, northern midlatitudes in summer/fall, and southern midlatitudes year round. However, since 1991 the linear trend observed during the 1980s has not continued, but rather total column ozone has been almost constant at midlatitudes in both hemispheres since the recovery from the 1991 Mt. Pinatubo eruption. The observed total column ozone losses from 1979 to the period 1994-1997 are about 5.4, 2.8, and 5.0%, respectively, for northern midlatitudes in winter/spring, northern midlatitudes in summer/fall, and southern midlatitudes year round, rather than the values projected in the 1994 Assessment assuming a linear trend: 7.6, 3.4, and 7.2%, respectively. The understanding of how changes in stratospheric chlorine/bromine and aerosol loading affect ozone suggests some of the reasons for the unsuitability of using a linear extrapolation of the pre-1991 ozone trend to the present.
- **The link between the long-term build-up of chlorine and the decline of ozone in the upper stratosphere has been firmly established.** Model predictions based on the observed build-up of stratospheric chlorine in the upper stratosphere indicate a depletion of ozone that is in good quantitative agreement with the altitude and latitude dependence of the measured ozone decline during the past several decades, which peaks at about 7% per decade near 40 km at midlatitudes in both hemispheres.
- **The springtime Antarctic ozone hole continues unabated.** The extent of ozone depletion has remained essentially unchanged since the early 1990s. This behavior is expected given

the near-complete destruction of ozone within the Antarctic lower stratosphere during springtime. The factors contributing to the continuing depletion are well understood.

- **The late-winter/spring ozone values in the Arctic were unusually low in 6 out of the last 9 years, the 6 being years that are characterized by unusually cold and protracted stratospheric winters.** The possibility of such depletions was predicted in the 1989 Assessment. Minimum Arctic vortex temperatures are near the threshold for large chlorine activation. Therefore, the year-to-year variability in temperature, which is driven by meteorology, leads to particularly large variability in ozone for current chlorine loading. As a result, it is not possible to forecast the behavior of Arctic ozone for a particular year. Elevated stratospheric halogen abundances over the next decade or so imply that the Arctic will continue to be vulnerable to large ozone losses.
- **The understanding of the relation between increasing surface UV-B radiation and decreasing column ozone has been further strengthened by ground-based observations, and newly developed satellite methods show promise for establishing global trends in UV radiation.** The inverse dependence of surface UV radiation and the overhead amount of ozone, which was demonstrated in earlier Assessments, has been further demonstrated and quantified by ground-based measurements under a wide range of atmospheric conditions. In addition, the influences of other variables, such as clouds, particles, and surface reflectivity, are better understood. These data have assisted the development of a satellite-based method to estimate global UV changes, taking into account the role of cloud cover. The satellite estimates for 1979-1992 indicate that the largest UV increases occur during spring at high latitudes in both hemispheres.
- **Stratospheric ozone losses have caused a cooling of the global lower stratosphere and global-average negative radiative forcing of the climate system.** The decadal temperature trends in the stratosphere have now been better quantified. Model simulations indicate that much of the observed downward trend in lower stratospheric temperatures (about 0.6°C per decade over 1979-1994) is attributed to the ozone loss in the lower stratosphere. A lower stratosphere that is cooler results in less infrared radiation reaching the surface/troposphere system. Radiative calculations, using extrapolations based on the ozone trends reported in the 1994 Assessment for reference, indicate that stratospheric ozone losses since 1980 may have offset about 30% of the positive forcing due to increases in the well-mixed greenhouse gases (i.e., carbon dioxide, methane, nitrous oxide, and the halocarbons) over the same time period. The climatic impact of the slowing of midlatitude ozone trends and the enhanced ozone loss in the Arctic has not yet been assessed.
- **Based on past emissions of ozone-depleting substances and a projection of the maximum allowances under the Montreal Protocol into the future, the maximum ozone depletion is estimated to lie within the current decade or the next two decades, but its identification and the evidence for the recovery of the ozone layer lie still further ahead.** The falloff of total chlorine and bromine abundances in the stratosphere in the next century will be much slower than the rate of increase observed in past decades, because of the slow rate at which natural processes remove these compounds from the stratosphere. The most vulnerable period for ozone depletion will be extended into the

coming decades. However, extreme perturbations, such as natural events like volcanic eruptions, could enhance the loss from ozone-depleting chemicals. Detection of the beginning of the recovery of the ozone layer could be achievable early in the next century if decreasing chlorine and bromine abundances were the only factor. However, potential future increases or decreases in other gases important in ozone chemistry (such as nitrous oxide, methane, and water vapor) and climate change will influence the recovery of the ozone layer. When combined with the natural variability of the ozone layer, these factors imply that unambiguous detection of the beginning of the recovery of the ozone layer is expected to be well after the maximum stratospheric loading of ozone-depleting gases.

SUPPORTING SCIENTIFIC EVIDENCE AND RELATED ISSUES

Recent Halogen and Methane Changes

- Tropospheric abundances of total organic chlorine (Cl) contained in long- and short-lived halocarbons reached maximum values of 3.7 ± 0.1 parts per billion (ppb) between mid-1992 and mid-1994 and are beginning to decrease slowly in the global troposphere. The decline in the tropospheric abundance of methyl chloroform (CH_3CCl_3) (at a rate of about 40 to 42 parts per trillion (ppt) Cl yr^{-1} in 1996) is the principal cause of the decrease and reversal in the Cl growth rate. At the same time, chlorine from the sum of the major CFCs grew at 7 ppt Cl yr^{-1} (CFC-12, 9 ppt Cl yr^{-1} ; CFC-11, -2 ppt Cl yr^{-1} ; CFC-113, 0 ppt Cl yr^{-1}) and by 10 ppt Cl yr^{-1} from the three major hydrochlorofluorocarbons (HCFCs) (HCFC-22, 5 ppt Cl yr^{-1} ; HCFC-141b, 4 ppt Cl yr^{-1} ; HCFC-142b, 1 ppt Cl yr^{-1}). The rate of decay of CH_3CCl_3 is expected to slow down to less than 10 ppt Cl yr^{-1} by 2005. By that point its concentration should be so small that it will no longer be an important contributor to atmospheric organic chlorine.
- Space-based remote measurements of hydrogen chloride (HCl), hydrogen fluoride (HF), and total chlorine in the stratosphere, as well as column abundances of HCl, chlorine nitrate (ClONO_2), HF, and carbonyl difluoride (COF_2) from the ground, are consistent with the content and rate of change of the total organic chlorine and fluorine abundance of the troposphere. These observations provide evidence that the rate of increase of stratospheric chlorine loading has slowed in recent years.
- Growth in the tropospheric concentrations of HCFCs and hydrofluorocarbons (HFCs) has been observed as expected from continuation of previous uses and from their use as replacements for chlorofluorocarbons (CFCs). Emissions calculated by industry from sales and use data are in accordance with the current global abundances of HCFC-22 and HFC-134a. For HCFC-141b and -142b, the industry data underestimate the current global abundances by factors of approximately 1.3 and 2 respectively. No production and sales data are currently available for other HCFCs and HFCs being used as CFC alternatives.
- New studies suggest a major reduction in the magnitude of the estimated oceanic source of methyl chloride (CH_3Cl). As a result, the sum of known sources is inadequate to explain the observed atmospheric burden of CH_3Cl , thus requiring a larger contribution from other sources, either natural or anthropogenic.

- Tropospheric bromine loading continues to rise largely because of the ongoing growth of Halon-1211 (almost 6% yr⁻¹), Halon-2402 (2% yr⁻¹), and Halon-1301 (1% yr⁻¹). Possible causes are the large “banking” in developed countries of that compound during the 1980s and its subsequent use and release during the 1990s, and new production in developing countries. Continued increases of halons over the next few years could cause the abundance of equivalent chlorine to decline more slowly than predicted in the 1994 Assessment.
- Recent measurements and intercomparisons of calibration standards have confirmed that the average global mixing ratio of methyl bromide (CH₃Br) is between 9 and 10 ppt and that the interhemispheric ratio is 1.3 ± 0.1 (north/south). New estimates of methyl bromide losses yield magnitudes of 77 Gg yr⁻¹ (ranging from 37 to 133 Gg yr⁻¹) for ocean uptake; 42 Gg yr⁻¹ (ranging from 10 to 214 Gg yr⁻¹) for soil uptake; and 86 Gg yr⁻¹ (ranging from 65 to 107 Gg yr⁻¹) for removal by hydroxyl radical (OH), for a total removal rate of 205 Gg yr⁻¹ with a range of about 110 to 450 Gg yr⁻¹. The current best estimate of the lifetime of atmospheric CH₃Br, as calculated from losses within the atmosphere, to the ocean, and to soils, is 0.7 years, with a range of 0.4 to 0.9 years. The Ozone Depletion Potential (ODP) of methyl bromide is 0.4, with a range of 0.2 to 0.5.
- No new important sources of methyl bromide have been identified. The ocean now appears to be a net sink, with an estimated net flux from the atmosphere of -21 Gg yr⁻¹ (ranging from -3 to -32 Gg yr⁻¹). Estimates of ocean emissions of order 60 Gg yr⁻¹ can be directly deduced from the above estimates for uptake and net ocean flux. The total emission of CH₃Br from identified sources is 122 Gg yr⁻¹, with a range of 43 to 244 Gg yr⁻¹. The best-quantified source is fumigation, with a magnitude of 41 Gg yr⁻¹ and a range of 28 to 64 Gg yr⁻¹. Other anthropogenic sources include biomass burning (20 Gg yr⁻¹, ranging from 10 to 40 Gg yr⁻¹) and leaded gasoline use (5 Gg yr⁻¹, ranging from negligible to 10 Gg yr⁻¹). Identified sources of CH₃Br thus constitute only about 60% of identified sinks on a globally averaged basis. This disagreement is difficult to reconcile with estimated uncertainties in the source and sink terms. The short lifetime of methyl bromide, coupled with the inhomogeneity of its sources and sinks, complicates the interpretation of its global budget.
- Based on the most recent analysis of the methyl chloroform (CH₃CCl₃) observational record (including a refinement in calibration), the estimated atmospheric lifetimes (with respect to reactive removal by OH) of CH₃CCl₃, HCFCs, HFCs, and CH₄ have been reduced by about 15% since the 1994 Assessment. The 1995 assessment of the Intergovernmental Panel on Climate Change (IPCC) mostly reflected these revisions, with a slightly smaller correction factor of about 10%. For species whose chemical lifetime is shorter than 1 to 2 years, the use of a global-mean lifetime may not be appropriate.
- The atmospheric abundance of CH₄ continues to increase, but with a declining growth rate. The average growth rate between 1980 and 1992 of about 10 ppb yr⁻¹ can be compared with the 1996-1997 rate of approximately 3 to 4 ppb yr⁻¹. The current best estimate for the total atmospheric lifetime of methane has been lowered to 8.9 ± 0.6 years.

Stratospheric Particles

- Observations and models have further confirmed that stratospheric sulfate aerosol (SSA) and polar stratospheric clouds (PSCs) play a key role in ozone loss chemistry through heterogeneous reactions that activate halogen species and deactivate nitrogen species.
- Observations have increased our knowledge of particle formation processes, the dispersal and decay of volcanic SSA, and particle climatology. They show that supercooled ternary solution (STS) droplets that form from SSA without a nucleation barrier are an important class of PSC particles. The formation processes of solid PSC particles that play a significant role in denitrification of the polar vortices remain uncertain. Recent studies suggest that mesoscale temperature fluctuations, especially over mountain ranges, may be important in PSC formation processes, particularly in the Arctic.
- The two most recent major volcanic eruptions, El Chichón (1982) and Mt. Pinatubo (1991), both temporarily increased SSA amounts by more than an order of magnitude.
- There is no clear trend in SSA abundances from 1979 to 1997, demonstrating that any anthropogenic contribution must be smaller than thought in the 1994 Assessment. SSA models including known tropospheric sulfur sources underpredict 1979 values, which were thought to represent the non-volcanic background, but it is not clear that this period was truly free of volcanic influence.

Ozone in the Midlatitudes and Tropics

- As noted in the 1994 Assessment, Northern Hemisphere midlatitude column ozone decreased markedly in 1992-1993, following the large enhancement of stratospheric aerosol caused by the eruption of Mt. Pinatubo in 1991. Column ozone has now reached amounts higher than a linear extrapolation of the pre-Pinatubo trend would predict. Between 25 and 60°N, ozone abundances for 1994-1997 averaged about 4% below 1979 values, although with large variability, while extrapolation of the pre-1991 trend would predict current (1997) abundances about 5.5% below 1979 values. The corresponding winter/spring and summer/fall losses average about 5.4 and 2.8%, respectively, while a linear extrapolation would predict 7.6 and 3.4%, respectively. The average ozone abundances between 25 and 60°S are currently about 4% (satellite) or 5% (ground) below 1979 values, while the linear extrapolation would predict 7.2% (both satellite and ground).
- Our understanding of how changes in halogen and aerosol loading affect ozone suggests some of the reasons for the unsuitability of using a linear extrapolation of the pre-1991 ozone trend to the present. For example, observations of stratospheric HCl and ClONO₂ show a build-up of stratospheric chlorine in recent years consistent with halocarbon emissions, but slower than would have been predicted by the chlorine trends observed before 1992. In addition, enhanced stratospheric aerosol was also present throughout much of the decade of the 1980s due to earlier volcanic eruptions (e.g., El Chichón and Ruiz), likely enhancing the downward trend of ozone observed even before Pinatubo.

- There are no statistically significant trends in total ozone in the equatorial regions (20°S to 20°N).
- The amplitude of the annual cycle of ozone at middle to high latitudes has decreased by approximately 15% in the last decades because larger declines have occurred during the season of maximum ozone values.
- For northern midlatitudes, combined vertical profile ozone trends through 1996 are negative at all altitudes between 12 and 45 km and are statistically significant at the 2σ level. The downward trend is largest near 40 and 15 km (approximately 7% per decade) and is smallest at 30 km (2% per decade). The bulk of column ozone decline is between the tropopause and 25 km.
- The re-evaluation of the Stratospheric Aerosol and Gas Experiment (SAGE) III satellite data indicates that there are no significant interhemispheric differences in upper stratospheric trends through 1996. Agreement is good, within estimated uncertainties, between SAGE III and ozonesonde trends in the lower to middle stratosphere in northern midlatitudes.
- The total ozone and the vertical profile trends derived for the northern midlatitudes are consistent with each other over the periods studied.
- Most of the midlatitude column ozone decline during the last two decades arose because of depletion in the lower stratosphere. That region is influenced by local chemical ozone loss that is enhanced by volcanic aerosol, and by transport from other regions. The vertical, latitudinal, and seasonal characteristics of the depletion of midlatitude ozone are broadly consistent with the understanding that halogens are the primary cause. The expected low ozone amounts in the midlatitude lower stratosphere following the Mt. Pinatubo eruption further strengthened the connection between ozone destruction and anthropogenic chlorine.
- Models that represent processes affecting ozone are able to calculate variations in ozone abundances that are broadly consistent with the observed midlatitude column ozone trend as well as the response to volcanic enhancement of stratospheric sulfate aerosol. In particular, models reproduce the lower ozone abundances observed immediately following Mt. Pinatubo and the subsequent increases as the aerosol disappeared.
- Current two-dimensional (2-D) assessment models that allow for the observed build-up of stratospheric chlorine calculate reductions in ozone that are in good quantitative agreement with the altitude and latitude dependence of the measured decline in upper stratospheric ozone during the past several decades. This clearly confirms the hypothesis put forth in 1974 that release of CFCs to the atmosphere would lead to a significant reduction of upper stratospheric ozone, with the peak percentage decline occurring around 40 km.
- Comparison of recent observations and model results shows that the overall partitioning of reactive nitrogen and chlorine species is well understood for the upper stratosphere. The previously noted discrepancy for the chlorine monoxide/hydrogen chloride (ClO/HCl) ratio has been resolved based on new kinetic information. Balloonborne observations of OH and

hydroperoxyl radicals (HO_2) agree well with theory, but satellite and ground-based observations of these species exhibit systematic differences compared with model calculations.

- An improved understanding of the relevant kinetic processes has resulted in a close balance between the calculated production and loss of ozone at 40 km (i.e., the long-standing difference between calculated and observed ozone abundance has been mostly resolved).
- Constituent measurements show that the tropics are relatively isolated from midlatitudes in the lower stratosphere. The extent of isolation affects the budgets (and lifetimes) of chemical species that affect ozone abundance.

Ozone in High-Latitude Polar Regions

- The large ozone losses in the Southern Hemisphere polar region during spring continued unabated with approximately the same magnitude and areal extent as in the early 1990s. In Antarctica, the monthly total ozone in September and October has continued to be 40 to 55% below the pre-ozone-hole values of approximately 320 m-atm cm ("Dobson units"), with up to a 70% decrease for periods of a week or so. This depletion occurs primarily over the 12- to 20-km altitude range, with most of the ozone in this layer disappearing during early October. These ozone changes are consistent overall with our understanding of chemistry and dynamics.
- In the Arctic vortex, low column ozone values were observed in the late-winter/spring for 6 out of the last 9 years. Monthly mean values were about 100 m-atm cm below 1960-1970 averages, with shorter-period differences exceeding 200 m-atm cm (equivalent to about 20 to 45% of values found in the 1960s and early 1970s). Within the column, the largest ozone differences were observed in the lower stratosphere.
- Years with large seasonal ozone depletion in the late-winter/spring Arctic are characterized by specific meteorological conditions. These conditions are lower-than-normal late-winter Arctic temperatures, which lead to enhanced activated chlorine, and a more isolated vortex and weaker planetary-wave driving, which lead to less transport of ozone-rich air into the Arctic. Low temperatures, an isolated vortex, and reduced wave driving are coupled processes that occur in concert in the stratosphere. Chemical ozone losses have been identified within the Arctic vortex and are associated with activated chlorine augmented by bromine. The total seasonal chemical ozone losses within the vortex have been estimated to be approximately 100 m-atm cm.
- With the present high abundances of chlorine loading, late-winter/spring Arctic chemical ozone loss is particularly sensitive to meteorological conditions (temperature and vortex isolation) because minimum vortex temperatures are at a critical value in terms of activating chlorine. Winter vortex temperatures in the 1990s have been particularly low. In the absence of low temperatures and an isolated vortex, reduced chemical ozone loss would be expected. However, such a reduced ozone loss would not indicate chemical recovery. The Arctic will remain vulnerable to extreme seasonal loss as long as chlorine loading remains high.

- Chlorine activation in liquid particles in the lower stratosphere (both SSA and liquid PSCs) increases strongly with decreases in temperature and is at least as effective as that on solid particles. Thus, chlorine activation is to a first approximation controlled by temperature and water vapor pressure and only secondarily by particle composition.
- Rapid polar ozone loss requires enhanced chlorine monoxide in the presence of sunlight. Maintenance of elevated ClO in late-winter/spring is dependent upon temperature and requires either repeated heterogeneous processing or denitrification. Since the 1994 Assessment, new understanding has shown that cold liquid aerosol can maintain elevated ClO in non-denitrified air.

Stratospheric Temperatures

- Radiosonde and satellite observations indicate a decadal cooling trend of the global, annual-mean lower stratosphere (approximately 16 to 21 km) since about 1980. Over the period 1979 to 1994, its amplitude is approximately 0.6°C per decade. At midlatitudes the trend is larger (approximately 0.75°C per decade) and broadly coherent among the various datasets with regard to the magnitude and statistical significance.
- Substantial cooling (approximately 3°C per decade) is observed in the polar lower stratosphere during late-winter/spring in both hemispheres. A decadal-scale cooling is evident in the Antarctic since the early 1980s and in the Arctic since the early 1990s. However, the dynamical variability is large in these regions, particularly in the Arctic, and this introduces difficulties in establishing the statistical significance of trends.
- The vertical profile of the annual-mean stratospheric temperature change observed in the Northern Hemisphere midlatitudes is robust for the 1979-1994 period within the different datasets. The trend consists of an approximately 0.75°C per decade cooling of the 15- to 35-km region, a slight reduction in the cooling at about 35 km, and increased cooling with height above 35 km (approximately 2°C per decade at 50 km).
- Model simulations based on known changes in the stratospheric concentrations of various radiatively active species indicate that the depletion of lower stratospheric ozone is the dominant radiative factor in the explanation of the observed global-mean lower stratospheric cooling trends for the period 1979-1990 (approximately 0.5°C per decade). The contribution to these trends from increases in well-mixed greenhouse gases is estimated to be less than one-fourth that due to ozone loss.
- Model simulations indicate that ozone depletion is an important causal factor in the latitude-month pattern of the decadal (1979-1990) lower stratospheric cooling. The simulated lower stratosphere in Northern and Southern Hemisphere midlatitudes and in the Antarctic springtime generally exhibit a statistically significant cooling trend over this period consistent with observations.
- In the middle and upper stratosphere, both the well-mixed greenhouse gases and ozone change contribute in an important manner to the cooling. However, the computed cooling due to these gases underestimates the observed decadal trend.

Tropospheric Ozone

- Trends in tropospheric ozone since 1970 in the Northern Hemisphere show large regional differences, with increases in Europe and Japan, decreases in Canada, and only small changes in the United States. The trend in Europe since the mid-1980s has reduced to virtually zero (at two recording stations). In the Southern Hemisphere, small increases have now been observed in surface ozone.
- Recent field studies have shown that anthropogenic emissions of ozone precursors (nitrogen oxides, carbon monoxide, and hydrocarbons) lead to large-scale production of ozone, which, through long-range transport, influences the ozone concentration in large regions of the troposphere in both hemispheres. However, significant uncertainties remain in the budget of tropospheric ozone, its precursors, and the chemical and physical processes involved. Large spatial and temporal variability is observed in tropospheric ozone, resulting from important regional differences in the factors controlling its concentration.
- Important improvements in global chemical transport models (CTMs) have allowed better simulations of tropospheric ozone distributions and of ozone perturbations resulting from anthropogenic emissions.
- Considerable progress has been made in testing tropospheric photochemistry through field measurements. Our theoretical understanding of tropospheric OH is nevertheless incomplete, specifically in regard to sources of upper tropospheric OH and polluted conditions.
- Increases in air traffic and the resulting emissions could have impacts on atmospheric chemistry and cloud formation, with implications for the ozone layer and the climate system. The understanding of the effects of aircraft emissions are currently being assessed as part of the Intergovernmental Panel on Climate Change (IPCC) special report *Aviation and the Global Atmosphere: 1999*. Consequently, this topic is not included in the scope of the present Assessment.

Changes in UV Radiation

- The inverse correlation between ozone column amounts and ultraviolet-B (UV-B) irradiance has been reconfirmed and firmly established by numerous ground-based measurements. The ground-based measurements have increased our understanding of additional effects such as albedo, altitude, clouds and aerosols, and geographic differences on UV irradiance at the Earth's surface.
- A controversy concerning anomalous UV-trend estimates from the Robertson-Berger (RB) meter network located in the continental United States (1974-1985) has been explained in terms of poor calibration stability. The reanalysis of this U.S. RB-meter dataset shows that the errors are too large for determining UV-irradiance trends over that period.
- Increases in UV-B irradiance (e.g., 1989-1997; 1.5% yr⁻¹ at 300 nm, 0.8% yr⁻¹ at 305 nm) have been detected with a few ground-based spectroradiometers at midlatitudes (near 40°) and are consistent with expected changes from the decreasing amounts of ozone. Although

these UV changes are consistent with those estimated from satellite data, the ground-based data records from suitably stable and calibrated instruments are not yet long enough to determine decadal trends. Local irradiance changes, not seen in the coarse-spatial-resolution satellite data, caused by pollution and aerosols have been detected in both UV-B (280 to 315 nm) and UV-A (315 to 400 nm).

- New satellite estimates of global ($\pm 65^\circ$) UV irradiance that now include cloud, surface reflectivity, and aerosol effects have been estimated from measured backscattered radiances from the Total Ozone Mapping Spectrometer (TOMS) using radiative transfer models. Climatological maps of UV irradiance can be produced from the daily data. In addition, the satellite data have been used to estimate zonally averaged global and seasonal trends in UV irradiance from 1979 to 1992. For this period, annual erythemal UV-irradiance decadal increases were estimated to be $3.7 \pm 3\%$ at 60°N and $3 \pm 2.8\%$ at 40°N . Larger decadal increases were observed in the Southern Hemisphere: $3.6 \pm 2\%$ at 40°S and $9 \pm 6\%$ at 60°S . No statistically significant trends were observed between $\pm 30^\circ$ latitude. Zonally averaged UV-A irradiances have not changed.
- Current zonal-average UV-irradiance trend estimations from satellite data that include cloud effects are nearly identical to clear-sky estimates. The currently estimated trends are slightly lower than the clear-sky trend estimates in the 1994 Assessment because of the new TOMS retrieval algorithm.
- Instrument intercomparison and newly developed calibration and database centers have improved the quality and availability of ground-based data.

Changes in Climate Parameters

- Increased penetration of UV radiation to the troposphere as a result of stratospheric ozone depletion influences key photochemical processes in the troposphere. Model results suggest that a 1% decrease in global total ozone leads to a global increase of 0.7 to 1% in globally averaged tropospheric OH, which would affect the lifetimes of several climate-related gases.
- The global average radiative forcing due to changes in stratospheric ozone since the late 1970s, using extrapolations based on the ozone trends reported in the 1994 Assessment for reference, is estimated to be $-0.2 \pm 0.15 \text{ Wm}^{-2}$, which offsets about 30% of the forcing due to increases in other greenhouse gases over the same period. The climatic impact of the slowing of midlatitude trends and the enhanced ozone loss in the Arctic has not yet been assessed. Recovery of stratospheric ozone would reduce the offset to the radiative forcing of the other greenhouse gases. The ozone recovery will therefore lead to a more rapid increase in radiative forcing than would have occurred due to increases in other greenhouse gases alone.
- The global average radiative forcing due to increases in tropospheric ozone since preindustrial times is estimated to be $+0.35 \pm 0.15 \text{ Wm}^{-2}$, which is about 10 to 20% of the forcing due to long-lived greenhouse gases over the same period.

- Coupled ocean-atmosphere general circulation models (GCMs) have been used to calculate the impact of stratospheric ozone loss on the thermal structure of the atmosphere. The calculated altitude of the transition from tropospheric warming to stratospheric cooling due to increases in well-mixed greenhouse gases is in better agreement with observations when ozone depletion is taken into account.
- Radiative forcings and Global Warming Potentials (GWPs) are now available for an expanded set of gases. New categories include fluorinated organic molecules. The CFC-11 radiative forcing has been revised by +12% from the value used since IPCC (1990), primarily because of the use of an improved vertical profile of CFC-11 mixing ratio. This and other updates lead to GWPs relative to CO₂ that are typically 20% higher than those in IPCC (1995).

Future Halogen Changes

- Large reductions in the production and atmospheric release of ozone-depleting substances (ODSs) have been achieved by international regulations (Montreal Protocol and its Amendments and Adjustments). Without such controls, and assuming a (conservative) 3% annual growth rate in production, ODSs would have led to an equivalent effective chlorine loading of around 17 ppb in 2050. The control measures of the original Montreal Protocol (1987) reduce this to approximately 9 ppb; the Amendments of London (1990) to about 4.6 ppb; and the Amendments of Copenhagen (1992) to approximately 2.2 ppb (but with stratospheric halogen loading increasing again in the second half of the 21st century). The Adjustments of Vienna (1995) and the Amendments of Montreal (1997) further reduce this to about 2.0 ppb (approximately the 1980 abundance) around the year 2050.
- Stratospheric halogen loading lags tropospheric loading by up to 6 years. Given that tropospheric halogen loading peaked around 1994 and assuming a scenario with a 3-yr lag time, the equivalent effective stratospheric chlorine loading is estimated to have peaked in 1997, at an abundance 1.7 times higher than in 1980. If annual ozone trends observed in the 1980s are attributed solely to these halogen increases, the peak ozone reductions in 1997, relative to 1980, are estimated to be about 5% at 45°N and 6% at 45°S. The corresponding increases in erythemally weighted UV radiation in 1997 are estimated to be 5% at 45°N and 8% at 45°S relative to the 1980 values.

Recovery of the Ozone Layer

- In the absence of other changes, stratospheric ozone abundances should rise in the future as the halogen loading falls in response to regulation. However, the future behavior of ozone will also be affected by the changing atmospheric abundances of methane (CH₄), nitrous oxide (N₂O), water vapor (H₂O), sulfate aerosol, and changing climate. Thus, for a given halogen loading in the future, the atmospheric ozone abundance may not be the same as found in the past for that same halogen loading.
- Several two-dimensional models were used to look at the response of ozone to past and future changes in atmospheric composition. Future global ozone abundances are predicted to recover only slowly toward their 1980 values. The return toward 1980 ozone values in

the models depends sensitively on the emission scenarios used. The CH₄ scenario used here has a lower growth rate than in previous assessments, which slows the modeled ozone recovery significantly. Understanding the methane trend is an important priority for understanding the future ozone recovery.

- Temperatures in the Arctic winter lower stratosphere are generally close to the threshold for substantial chlorine activation, making Arctic ozone particularly sensitive to small changes in temperature (e.g., cooling of the lower stratosphere by changes in greenhouse gases). Preliminary calculations with coupled chemistry/climate models suggest that recovery in the Arctic could be delayed by this cooling and, because of the large natural variability, recovery will be difficult to detect unambiguously until well into the next century.
- The detection of the onset of ozone recovery from halogen-induced depletion should be possible earlier in the Antarctic than in the Arctic or globally because there is less variability in the ozone loss in the Antarctic. Estimates of the timing of the detection of the onset of ozone recovery are uncertain. However, it is clear that unambiguous detection of the beginning of recovery will be delayed beyond the maximum loading of stratospheric halogens.

IMPLICATIONS FOR POLICY FORMULATION

The results from more than two decades of research have provided a progressively better understanding of the interaction of human activities and the chemistry and physics of the global atmosphere. New policy-relevant insights to the roles of trace atmospheric constituents have been conveyed to decision-makers through the international state-of-the-understanding assessment process. This information has served as a key input to policy decisions by governments, industry, and other organizations worldwide to limit the anthropogenic emissions of gases that cause environmental degradation: (1) the 1987 Montreal Protocol on ozone-depleting substances, and its subsequent Amendments and Adjustments, and (2) the 1997 Kyoto Protocol on substances that alter the radiative forcing of the climate system.

The research findings that are summarized above are of direct interest and significance as scientific input to governmental, industrial, and other policy decisions associated with the Montreal Protocol (ozone layer) and the Kyoto Protocol (climate change):

- **The Montreal Protocol is working.** Global observations have shown that the combined abundance of anthropogenic chlorine-containing and bromine-containing ozone-depleting substances in the lower atmosphere peaked in 1994 and has now started to decline. One measure of success of the Montreal Protocol and its subsequent Amendments and Adjustments is the forecast of “the world that was avoided” by the Protocol:
 - The abundance of ozone-depleting gases in 2050, the approximate time at which the ozone layer is now projected to recover to pre-1980 levels, would be at least 17 ppb of equivalent effective chlorine (this is based on the conservative assumption of a 3% per annum growth in ozone-depleting gases), which is about 5 times larger than today’s value.

- Ozone depletion would be at least 50% at midlatitudes in the Northern Hemisphere and 70% at midlatitudes in the Southern Hemisphere, about 10 times larger than today.
- Surface UV-B radiation would at least double at midlatitudes in the Northern Hemisphere and quadruple at midlatitudes in the Southern Hemisphere compared with an unperturbed atmosphere. This compares to the current increases of 5% and 8% in the Northern and Southern Hemispheres, respectively, since 1980.

Furthermore, all of the above impacts would have continued to grow in the years beyond 2050. It is important to note that, while the provisions of the original Montreal Protocol in 1987 would have lowered the above growth rates, recovery (i.e., an improving situation) would have been impossible without the Amendments and Adjustments (London, 1990; Copenhagen, 1992; and Vienna, 1995).

- **The ozone layer is currently in its most vulnerable state.** Total stratospheric loading of ozone-depleting substances is expected to maximize before the year 2000. All other things being equal, the current ozone losses (relative to the values observed in the 1970s) would be close to the maximum. These are:
 - about 6% at Northern Hemisphere midlatitudes in winter/spring;
 - about 3% at Northern Hemisphere midlatitudes in summer/fall;
 - about 5% at Southern Hemisphere midlatitudes on a year-round basis;
 - about 50% in the Antarctic spring; and
 - about 15% in the Arctic spring.

Such changes in ozone are predicted to be accompanied by increases in surface erythemal radiation of 7, 4, 6, 130, and 22%, respectively, if other influences such as clouds remain constant. It should be noted that these values for ozone depletion at midlatitudes are nearly a factor of 2 lower than projected in 1994, primarily because the linear trend in ozone observed in the 1980s did not continue in the 1990s. However, springtime depletion of ozone in Antarctica continues unabated at the same levels as observed in the early 1990s, and large depletions of ozone have been observed in the Arctic in most years since 1990, which are characterized by unusually cold and protracted winters.

Some natural and anthropogenic processes that do not in themselves cause ozone depletion can modulate the ozone loss from chlorine and bromine compounds, in some cases very strongly. For example, in coming decades midlatitude ozone depletion could be enhanced by major volcanic eruptions, and Arctic ozone depletion could be increased by cold polar temperatures, which in turn could be linked to greenhouse gases or to natural temperature fluctuations. On the other hand, increases in methane would tend to decrease chlorine-catalyzed ozone loss.

The current vulnerability to ozone depletion over the next few decades is primarily due to past use and emissions of the long-lived ozone-depleting substances. The options to reduce this vulnerability over the next two decades are thus rather limited. The main drivers of

ozone change could be natural and anthropogenic processes not related to chlorine and bromine compounds, but to which the ozone layer is sensitive because of the elevated abundances of ozone-depleting substances.

- **The ozone layer will slowly recover over the next 50 years.** The stratospheric abundance of halogenated ozone-depleting substances is expected to return to its pre-1980 (i.e., “unperturbed”) level of 2 ppb chlorine equivalent by about 2050, assuming full compliance with the Montreal Protocol and its Amendments and Adjustments. The atmospheric abundances of global and Antarctic ozone will start to slowly recover within coming decades toward their pre-1980 levels once the stratospheric abundances of ozone-depleting (halogen) gases start to decrease. However, the future abundance of ozone will be controlled not only by the abundance of halogens, but also by the atmospheric abundances of methane, nitrous oxide, water vapor, and sulfate aerosols and by the Earth’s climate. Therefore, for a given halogen loading in the future, atmospheric ozone abundance is unlikely to be the same as found in the past for the same halogen loading.
- **Few policy options are available to enhance the recovery of the ozone layer.** Relative to the current, but not yet ratified, control measures (Montreal, 1997), the equivalent effective chlorine loading above the 1980 level, integrated from now until the 1980 level is re-attained, could be decreased by:
 - 9% by eliminating global Halon-1211 emissions in the year 2000, thus requiring the complete elimination of all new production and destruction of all Halon-1211 in existing equipment;
 - 7% by eliminating global Halon-1301 emissions in the year 2000, thus requiring the complete elimination of all new production and destruction of all Halon-1301 in existing equipment;
 - 5% by eliminating the global production of all HCFCs in the year 2004;
 - 2.5% by eliminating the global production of all CFCs and carbon tetrachloride in the year 2004;
 - 1.6% by reducing the cap on HCFC production in developed countries from 2.8% to 2.0% in the year 2000, by advancing the phase-out from the year 2030 to 2015, and by instituting more rapid intermediate reductions; and
 - about 1% by eliminating the global production of methyl bromide beginning in 2004.

These policy actions would advance the date at which the abundance of effective chlorine returns to the 1980 value by 1-3 years. A complete and immediate global elimination of all emissions of ozone-depleting substances would result in the stratospheric halogen loading returning to the pre-1980 values by the year 2033. It should also be noted that if the currently allowed essential uses for metered dose inhalers are extended from the year 2000 to 2004, then the equivalent effective chlorine loading above the 1980 level would increase by 0.3%.

- **Failure to comply with the international agreements of the Montreal Protocol will affect the recovery of the ozone layer.** For example, illegal production of 20-40 ktonnes per year of CFC-12 and CFC-113 for the next 10-20 years would increase the equivalent effective chlorine loading above the 1980 abundance, integrated from now until the 1980 abundance is re-attained, by about 1-4% and delay the return to pre-1980 abundances by about a year.
- **The issues of ozone depletion and climate change are interconnected; hence, so are the Montreal and Kyoto Protocols.** Changes in ozone affect the Earth's climate, and changes in climate and meteorological conditions affect the ozone layer, because the ozone depletion and climate change phenomena share a number of common physical and chemical processes. Hence, decisions taken (or not taken) under one Protocol have an impact on the aims of the other Protocol. For example, decisions made under the Kyoto Protocol with respect to methane, nitrous oxide, and carbon dioxide will affect the rate of recovery of ozone, while decisions regarding controlling HFCs may affect decisions regarding the ability to phase out ozone-depleting substances.

SCIENTIFIC ASSESSMENT OF OZONE DEPLETION: 1998

CHAPTER SUMMARIES

CHAPTER 1: LONG-LIVED OZONE-RELATED COMPOUNDS

Since the previous Assessment (WMO, 1995), significant progress has been achieved in determining and understanding the distributions of long-lived ozone-related gases in both the troposphere and stratosphere. In this chapter, we deal primarily with long-lived halocarbons (chlorofluorocarbons (CFCs), halons, perfluorinated and perchlorinated compounds) and other significant long-lived non-halocarbon species.

- Tropospheric measurements show that:
 - (a) International “compliance” with the Montreal Protocol and its Amendments has resulted in the amounts of most CFC’s and chlorocarbons in the atmosphere being equal to or lower than amounts that are consistent with the Protocol’s provisions regarding production and emission.
 - (b) The total amount of organic chlorine (CCl_y) contained in long- and short-lived chlorocarbons reached maximum values of 3.7 ± 0.1 parts per billion (ppb) between mid-1992 and mid-1994 and is beginning to decrease slowly in the global troposphere. This slowing down and reversal in the growth rate resulted primarily from reduced emissions of methyl chloroform (CH_3CCl_3).
 - (c) Despite significant reduction in the emission of halons, the total amount of organic bromine in the troposphere continues to rise, largely because of the ongoing growth of Halon-1211 (CBrClF_2). Possible causes are releases during the 1990s from the large halon “bank” that accumulated in developed countries during the 1980s and from increased production of Halon-1211 in developing countries. The recent observations of Halon-1211 concentrations are higher and growing faster than concentrations calculated from emissions derived from industry and United Nations Environment Programme (UNEP) data. Halon increases over the next few years could delay the time of the currently expected total organic bromine maximum in the troposphere.
 - (d) The amount of nitrous oxide (N_2O) in the troposphere continues to increase at 0.2 to 0.3% per year. As concluded in previous assessments, this trend indicates that the global sources exceed the sinks by approximately 30%. The imbalance appears to be caused by anthropogenic sources whose relative strengths remain uncertain.
- Stratospheric measurements reflect the tropospheric chlorocarbon changes with a time delay ranging from 3 to 6 years, depending on latitude and altitude. Assuming the maximum delay, the peak in chlorine loading in the middle stratosphere (and consequently chlorine-catalyzed ozone loss) is expected to be reached around the year 2000. The impact of organic bromine is not going to significantly alter the time of maximum ozone depletion.

Specifically:

- (a) Space-based measurements of hydrogen chloride (HCl) near the stratopause and of total chlorine throughout the stratosphere are consistent with the amount and rate of change of total CCl_y in the troposphere. The rate of increase of stratospheric chlorine has slowed in recent years.
 - (b) The rate of increase of the total amount of inorganic chlorine (Cl_y) in the atmosphere obtained by combining HCl and chlorine nitrate (ClONO_2) ground-based measurements and a model-computed chlorine monoxide (ClO) background has slowed significantly, from about 3.7% per year in 1991 to 1992 to about 1.8% per year in 1995 to 1996.
 - (c) The long-term remote monitoring of hydrogen fluoride (HF) near 55 km altitude from space and of total column amounts of HF and carbonyl fluoride (COF_2) from the ground, along with the HCl trends, have confirmed that CFC and chlorocarbon compounds included in the Montreal Protocol have been the principal sources of both inorganic fluorine and Cl_y in the stratosphere.
 - (d) Volcanoes have not contributed significantly in recent decades to the total amount of chlorine in the stratosphere.
- Industrial production, sales data, and end-use modeling indicate that global emissions of the long-lived CFCs (-11, -12, -113, -114, and -115), carbon tetrachloride (CCl_4), and Halon-1211 and -1301 (CBrF_3) are all in decline. For CFC-12 (CCl_2F_2) and Halon-1211, the emissions still exceed their atmospheric removal rates; hence, their concentrations are still increasing.
 - Estimations using global tropospheric measurements and atmospheric chemical models show that:
 - (a) The CFCs whose emissions are accurately known appear to have atmospheric lifetimes consistent with destruction in the stratosphere being their principal removal mechanism.
 - (b) CFC and chlorocarbon emissions inferred from atmospheric observations are consistent, approximately, with independent estimates of emissions based on industrial production and sales data. CFC-113 ($\text{CCl}_2\text{FCClF}_2$) is an exception: emissions based on atmospheric observations are significantly lower than those calculated by industry.

- (c) While CCl_4 in the atmosphere is declining at approximately 0.8% per year, the interhemispheric difference is effectively constant, indicating that there are still significant Northern Hemispheric (NH) emissions. Atmospheric measurements and estimates of developed countries' emissions indicate that developing countries have dominated world releases of CCl_4 after 1991. A recent investigation of stratospheric CCl_4 observations and some three-dimensional (3-D) model studies suggest that its lifetime is closer to 35 years, instead of the previously reported 42 years; if this shorter lifetime is correct, then larger emissions are indicated, presumably from developing countries.
- (d) Perfluorocarbons (PFCs) and sulfur hexafluoride (SF_6) continue to increase in the background atmosphere. They are not ozone depleters but are of potential concern because they are strong absorbers of infrared radiation on a per-molecule basis and, once released, they persist in the atmosphere for millennia.
- Simultaneous determinations of the stratospheric mixing ratio of a species and the age of the air can be used together with tropospheric measurements to estimate steady-state atmospheric lifetimes for species that lack tropospheric sinks. In general, the lifetimes obtained in this way are consistent with the model-derived lifetime ranges and lifetimes based on tropospheric measurements. However, the recommended reference lifetimes for CFC-11 (CCl_3F) and CCl_4 are approximately 45 and 35 years, respectively, which are shorter than the previously recommended estimates (50 and 42 years, respectively); some recent 3-D models also support these changes. Recommended reference lifetimes for major ozone-depleting source gases discussed in this chapter and also in Chapter 2 are summarized in Table 1-1.

Table 1-1. Summary of current (WMO, 1998) and previous (WMO, 1995) reference and observed steady-state lifetimes for several ozone-related source species. Lifetime is defined as the total amount of a compound in the atmosphere divided either by its total rate of removal or by its rate of destruction by tropospheric OH alone (values in parentheses). Additional information on calculated ranges for different models and lifetime-related uncertainties can be found in Tables 1-3, 1-4, 1-5, 1-6, and in Chapter 2 (Tables 2-2, 2-4, and 2-6).

Industrial Name	Chemical Formula	Lifetime, WMO (1998) ^a (years)	Lifetime, Observed Range (years)	Lifetime, WMO (1995) (years)
Nitrous oxide	N ₂ O	120	75 to 173 ^d	120
CFC-11	CCl ₃ F	45 ^f	29 to 76 ^e	50
CFC-12	CCl ₂ F ₂	100	77 to 185 ^e	102
CFC-113	CCl ₂ FCFClF ₂	85	54 to 143 ^d	85
Carbon tetrachloride	CCl ₄	35 ^f	21 to 43 ^d	42
H-1211	CBrClF ₂	11 ^f	10 to 31 ^d	20
H-1301	CBrF ₃	65	60 to 65 ^g	65
Methyl chloroform	CH ₃ CCl ₃	4.8 (5.7)	4.5 to 5.1 ^b	5.4
HCFC-22	CHClF ₂	11.8 (12.3)	7.0 to 14.4 ^c	13.3
HCFC-141b	CH ₃ CCl ₂ F	9.2 (10.4)	(h)	9.4
HCFC-142b	CH ₃ CClF ₂	18.5 (19.5)	(h)	19.5
HFC-134a	CH ₂ FCF ₃	13.6 (14.1)	(h)	14
HFC-23	CHF ₃	243 (255)	(h)	250
Methyl chloride	CH ₃ Cl	~1.3 (1.3)	(h)	1.5
Methyl bromide	CH ₃ Br	0.7 (1.8)	(h)	1.3
Methane	CH ₄	8.9 ⁱ (9.3)	(h)	10

^a The numbers in parentheses represent lifetimes for removal by tropospheric OH scaled to the total atmospheric lifetime of CH₃CCl₃ (4.8 years) derived by Prinn *et al.* (1995), and adopting CH₃CCl₃ lifetimes for ocean removal of 85 years and stratospheric removal of 45 years (Kaye *et al.*, 1994). Adopting a shorter stratospheric removal time of 37 years (Prinn *et al.*, 1995; see also Volk *et al.*, 1997) yields a lifetime for CH₃CCl₃ removal by tropospheric OH of 5.9 years which is within the uncertainty limits of the above (WMO, 1998) reference value.

^b Prinn *et al.*, 1995.

^c Miller *et al.*, 1998.

^d Volk *et al.*, 1997. Note that this analysis gives only stratospheric lifetimes. Additional loss of H-1211 in the troposphere (see Section 1.4.4) reduces its lifetime to 11 years. When considering recently updated emissions of H-1211 (see Figure 1-11) and observations, the Butler *et al.* (1998) lifetime evaluation approach leads to an H-1211 lifetime of 10 years.

^e For CFC-11, combined range of Volk *et al.* (1997) and updated values from Cunnold *et al.* (1997); for CFC-12, range covered by the central estimates of Volk *et al.* (1997) and updated central estimates from Cunnold *et al.* (1997).

^f WMO 1998 CFC-11, H-1211, and CCl₄ lifetimes are lower than WMO (1995) values to take account of recent estimates based on stratospheric observations and models. Note that some calculations in later chapters were carried out before these WMO (1998) values were finalized and therefore used WMO (1995) values instead.

^g Butler *et al.*, 1998.

^h Not available or not applicable.

ⁱ Lifetime as calculated by Prinn *et al.* (1995). The adjustment time for CH₄ recovery would be somewhat longer due to CH₄ feedback on CO and OH (WMO, 1995).

CHAPTER 2: SHORT-LIVED OZONE-RELATED COMPOUNDS

Fluorinated and Chlorinated Compounds

- The Montreal Protocol and its Amendments have caused dramatic changes in industrial halocarbon emissions. For example, industrial sales of methyl chloroform (CH_3CCl_3) have dropped by more than a factor of 3 from 1990 to 1995, resulting in decreases in its tropospheric concentration over this same period, approaching 40%. This decline in tropospheric CH_3CCl_3 (about 40 to 42 parts per trillion (ppt) atomic chlorine (Cl) yr^{-1} in 1996) is one of the principal causes for the recent downturn in total tropospheric Cl.
- Rapid growth in the tropospheric concentrations of several hydrochlorofluorocarbons (HCFCs) has occurred throughout the 1990s as expected from continuation of previous uses and from use as replacements for chlorofluorocarbons (CFCs). As a result, tropospheric Cl from HCFC-22, -141b, and -142b was increasing in mid-1996 by about 11 ppt yr^{-1} and accounted for an equivalent of approximately 5% of the Cl present in long-lived tropospheric gases. This increasing contribution to tropospheric Cl offsets some of the 1996 decline in tropospheric Cl associated with the decreasing tropospheric burden of CH_3CCl_3 . This can be contrasted with the total tropospheric Cl growth rate throughout the 1980s, which exceeded 100 ppt yr^{-1} .
- Significant growth has also been recorded for some hydrofluorocarbons (HFCs). HFC-134a has increased throughout the 1990s from non-detectable levels to slightly greater than 3 ppt. HFC-23 (a byproduct of HCFC-22 production) has tracked the tropospheric concentration of HCFC-22 since 1980 and is growing at about 0.6 ppt yr^{-1} from a mid-1995 abundance of approximately 11 ppt.
- Based on the most recent analysis of the CH_3CCl_3 observational record (including a refinement in calibration), the atmospheric lifetimes (with respect to reactive removal by hydroxyl radicals (OH)) of CH_3CCl_3 , HCFCs, and HFCs, have been reduced by about 15% since the 1994 Assessment (WMO, 1995; see Table 2-1). The 1995 Intergovernmental Panel on Climate Change Assessment (IPCC, 1996) mostly reflected these revisions, with a slightly smaller correction factor of about 10%.
- Using the recommended lifetimes for HCFCs and HFCs, emissions calculated by industry from sales and use data are in accordance with the current global abundances of HCFC-22 and HFC-134a. For HCFC-141b and -142b, the industry data underestimate the current global abundances by factors of approximately 1.3 and 2, respectively.
- New measurements of, and improved calibrations for, methyl chloride (CH_3Cl), the largest natural source of atmospheric Cl, suggest that its global average mixing ratio is about 550 ppt, a slight revision of the 600 ppt given in the 1994 Assessment (WMO, 1995). Despite new information on CH_3Cl sources, their sum accounts for only 40 to 80% of the current atmospheric burden of CH_3Cl . New information on the marine production of CH_3Cl suggests a much lower oceanic source strength than previously assumed (constituting about 7

to 13% of the total source flux required to balance the removal of CH_3Cl by OH). These data imply that biomass burning now appears to be the largest known source of atmospheric CH_3Cl , approximately three times greater than the ocean source.

- The total Cl determined from the average tropical tropopause or lower stratospheric mixing ratios of the anthropogenic chlorocarbons methylene chloride (CH_2Cl_2), chloroform (CHCl_3), and tetrachloroethene (C_2Cl_4), and from phosgene (COCl_2 , a product of chlorocarbon breakdown in the atmosphere), indicates that these short-lived compounds contribute about 100 ± 20 ppt of Cl to the stratosphere, or about 3% of the total organic Cl.

Methyl Bromide (CH_3Br)

- Recent measurements and intercomparison of calibration standards have confirmed that the average global mixing ratio of CH_3Br lies between 9 and 10 ppt, and that the interhemispheric ratio is 1.3 ± 0.1 (North/South), decreasing seasonally by as much as 0.2. Available data are not sufficient to determine the magnitude of CH_3Br trends since 1992.
- The amplitude of the seasonal behavior of CH_3Br shows wide geographical variability. The lack of an appreciable seasonal variation in the Southern Hemisphere (SH) suggests the existence of seasonality in other processes (sources or sinks) that offsets the signal for chemical removal by OH.
- Additional laboratory and shipboard measurements carried out since the 1994 Assessment (WMO, 1995) have changed our understanding of the ocean's role in the CH_3Br global budget. The ocean now appears to be a net sink, with an estimated net flux across the surface of about -21 Gg yr^{-1} , ranging from -3 to -32 Gg yr^{-1} . There is some evidence of seasonality in the saturation of CH_3Br at high latitudes, which suggests a close interplay between aquatic sources and sinks of CH_3Br and which further complicates narrowing the uncertainty in the global net flux across the ocean surface.
- New laboratory and field measurements and calculations utilizing global climatological data have increased the estimated total removal rates of CH_3Br . The magnitude of ocean uptake is -77 Gg yr^{-1} , with a range of -37 to -133 Gg yr^{-1} . Chemical removal in the ocean accounts for 70% of this estimate, with a newly identified biological ocean sink contributing the remaining 30%. Two different studies suggest a significant soil sink for CH_3Br . Although measured deposition velocities in similar soil types are consistent with each other, extrapolation to a global soil sink for CH_3Br yield estimates that differ widely due to utilization of different global soil type inventories. The best estimate for the soil sink for CH_3Br is -42 Gg yr^{-1} , with a range of -10 to -214 Gg yr^{-1} . Removal by atmospheric OH has been increased by 15% over the value in the 1994 Assessment (WMO, 1995) due to the impact of the recalibration of the CH_3CCl_3 data. The current estimate for OH removal is -86 Gg yr^{-1} , ranging from -65 to -107 Gg yr^{-1} . Thus the total removal rate of CH_3Br is -205 Gg yr^{-1} , with a range of -454 to -112 Gg yr^{-1} .

- No new important sources of CH₃Br have been identified. The total emission of CH₃Br from identified sources is 122 Gg yr⁻¹, with a range of 43 to 244 Gg yr⁻¹. The best-quantified source is fumigation, with a magnitude of 41 Gg yr⁻¹ and a range of 28 to 64 Gg yr⁻¹. Other anthropogenic sources include biomass burning (20 Gg yr⁻¹, ranging from 10 to 40 Gg yr⁻¹) and leaded gasoline use (5 Gg yr⁻¹, ranging from 0 to 10 Gg yr⁻¹). Estimates of ocean emissions of order 60 Gg yr⁻¹ can be directly deduced from the above estimates for ocean uptake and net ocean flux.
- The budget of atmospheric CH₃Br, calculated from our current understanding of sources and sinks, does not balance. Identified sinks (about 200 Gg yr⁻¹) outweigh identified sources (about 120 Gg yr⁻¹). The range in the imbalance is -315 to +36 Gg yr⁻¹, obtained by combining estimated ranges for each of the sources and sinks. Because these ranges do not represent a statistical uncertainty, we cannot ascribe a probability to obtaining a balanced budget. Still, uncertainties in sources and sinks cannot easily explain the discrepancy.
- The current best estimate of the lifetime of atmospheric CH₃Br, calculated from losses within the atmosphere, to the ocean, and to soils, is 0.7 (0.4 to 0.9) years, contrasted with 1.3 (0.8 to 1.7) years given in the 1994 Assessment (WMO, 1995). The range is estimated by calculating the separate impacts of uncertainties in each of the sinks. The change from the 1994 Assessment is due primarily to both an increase in the ocean sink and the identification of a soil uptake, with a smaller contribution from the increase in the atmospheric removal rate. The Ozone Depletion Potential (ODP) for CH₃Br, calculated using the above lifetime and a bromine (Br) efficiency factor of 58, is 0.4, with a range of 0.2 to 0.5. The ODP range is again calculated by considering the separate impacts of uncertainties in each of the parameters used for the ODP estimate. The bromine efficiency factor of 58 is greater than the value of 48 given in the 1994 Assessment due to improvements in our knowledge of stratospheric bromine chemistry.

Other Brominated Compounds

- Measurements of shorter-lived organic Br compounds (CH₂Br₂, CHBr₃, CH₂BrCl, CHBrCl₂, CHBr₂Cl, and C₂H₄Br₂) indicate that these chemicals contribute 5 to 10 ppt Br to the tropospheric organic Br burden. However, such measurements have not been part of long-term monitoring programs and the data are sporadic in time and location, with a bias toward coastal and oceanic regions. Variable concentrations of these compounds (ranging from 1.0 to 1.7 ppt) have been reported at the tropical tropopause, but the paucity of data and the high variability make it difficult to quantify their contribution to reactive Br in the lower stratosphere.

Methane (CH₄) and Carbon Monoxide (CO)

- The current best estimate for the total atmospheric lifetime of CH₄ is 8.9 ± 0.6 years. The lifetime decrease since the 1994 Assessment (WMO, 1995) reflects the impact of the CH₃CCl₃ recalibration.

- The burden of atmospheric CH₄ continues to increase, but the rate of growth is declining. A growth rate of about 3 to 4 ppb yr⁻¹ was reported for the 1996 to 1997 period, contrasting with an average increase rate of about 10 ppb yr⁻¹ in the late 1980s. Apart from the anomalously low growth period after the 1991 eruption of Mt. Pinatubo, the above growth rate is the lowest since the mid-1940s. These lower growth rates are in contrast with the commonly used scenarios of future CH₄ emissions.
- Ground-based networks for carbon monoxide (CO) monitoring continue to expand, with many laboratories beginning new CO-monitoring programs. A recent intercomparison of measurements showed that large differences still exist between groups, which may be related to the calibration scales used in the analyses.
- The long-term increase in CO observed in the Northern Hemisphere (NH) until the mid- to late 1980s reversed at that time, with a steady average decrease of 2% yr⁻¹ since 1990. This decrease continues today. No significant long-term trend in the SH has been deduced from measurements made over the past 20 years. However, periods of sharp decline in 1992 to 1993 and again in 1995 have yielded the lowest SH mixing ratios in the past two decades.

Table 2-1. Summary of current (WMO, 1998) and previous (WMO, 1995) reference and observed steady-state lifetimes for several ozone-related source species. Lifetime is defined as the total amount of a compound in the atmosphere divided by its total rate of removal (or by its rate of destruction by tropospheric OH alone; values in parentheses). Additional information on calculated ranges for different models and lifetime-related uncertainties can be found in Chapter 1 (Tables 1-3, 1-4, 1-5, 1-6) and in Tables 2-2, 2-4, and 2-6 of this chapter.

Industrial Name	Chemical Formula	Lifetime, WMO (1998) ^a (years)	Lifetime, Observed Range (years)	Lifetime, WMO (1995) (years)
Nitrous oxide	N ₂ O	120	75 to 173 ^d	120
CFC-11	CCl ₃ F	45 ^f	29 to 76 ^e	50
CFC-12	CCl ₂ F ₂	100	77 to 185 ^e	102
CFC-113	CCl ₂ FCClF ₂	85	54 to 143 ^d	85
Carbon tetrachloride	CCl ₄	35 ^f	21 to 43 ^d	42
H-1211	CBrClF ₂	11 ^f	10 to 31 ^d	20
H-1301	CBrF ₃	65	60 to 65 ^g	65
Methyl chloroform	CH ₃ CCl ₃	4.8 (5.7)	4.5 to 5.1 ^b	5.4
HCFC-22	CHClF ₂	11.8 (12.3)	7.0 to 14.4 ^c	13.3
HCFC-141b	CH ₃ CCl ₂ F	9.2 (10.4)	(h)	9.4
HCFC-142b	CH ₃ CClF ₂	18.5 (19.5)	(h)	19.5
HFC-134a	CH ₂ FCF ₃	13.6 (14.1)	(h)	14
HFC-23	CHF ₃	243 (255)	(h)	250
Methyl chloride	CH ₃ Cl	~1.3 (1.3)	(h)	1.5
Methyl bromide	CH ₃ Br	0.7 (1.8)	(h)	1.3
Methane	CH ₄	8.9 ⁱ (9.3)	(h)	10

^a The numbers in parentheses represent lifetimes for removal by tropospheric OH scaled to the total atmospheric lifetime of CH₃CCl₃ (4.8 years) derived by Prinn *et al.* (1995), and adopting CH₃CCl₃ lifetimes for ocean removal of 85 years and stratospheric removal of 45 years (Kaye *et al.*, 1994). Adopting a shorter stratospheric removal time of 37 years (Prinn *et al.*, 1995; see also Volk *et al.*, 1997) yields a lifetime for CH₃CCl₃ removal by tropospheric OH of 5.9 years, which is within the uncertainty limits of the above (WMO, 1998) reference value.

^b Prinn *et al.*, 1995.

^c Miller *et al.*, 1998.

^d Volk *et al.*, 1997. Note that this analysis gives only stratospheric lifetimes. Additional loss of H-1211 in the troposphere (see Section 1.4.4) reduces its lifetime to 11 years. When considering recently updated emissions of H-1211 (see Figure 1-11) and observations, the Butler *et al.* (1998) lifetime evaluation approach leads to an H-1211 lifetime of 10 years.

^e For CFC-11, combined range of Volk *et al.* (1997) and updated values from Cunnold *et al.* (1997); for CFC-12, range covered by the central estimates of Volk *et al.* (1997) and updated central estimates from Cunnold *et al.* (1997).

^f WMO (1998) CFC-11, H-1211, and CCl₄ lifetimes are lower than WMO (1995) values to take account of recent estimates based on stratospheric observations and models. Note that some calculations in later chapters of this 1998 Assessment were carried out before these WMO (1998) values were finalized and therefore used WMO (1995) values instead.

^g Butler *et al.*, 1998.

^h Not available or not applicable.

ⁱ Lifetime as calculated by Prinn *et al.* (1995). The adjustment time for CH₄ recovery would be somewhat longer due to CH₄ feedback on CO and OH (WMO, 1995).

CHAPTER 3: GLOBAL DISTRIBUTIONS AND CHANGES IN STRATOSPHERIC PARTICLES

Much progress has been made recently in our understanding of the two major classes of stratospheric particles: stratospheric sulfate aerosol (SSA), and polar stratospheric clouds (PSCs). Thermodynamic models have provided a clearer picture of particle behavior at low temperatures, while a richer and longer measurement suite has increased our knowledge of particle formation processes, the dispersal and decay of volcanic SSA, and particle climatology.

- There is no clear trend in background SSA from 1979 to 1997. SSA levels in late 1997 were below those observed before the 1991 Mt. Pinatubo eruption and are likely still decreasing. Hence, any anthropogenic contribution to the SSA layer must be smaller than previously estimated from observed changes from 1979 to 1989. Peak aerosol scattering ratios in 1997 were about 40% greater than those observed during 1979, but due to uncertainties and natural variability in the measurements, this difference must be viewed with caution at present.
- It is not clear that the 1979 minimum SSA period was truly free of volcanic influence. Recent model calculations of SSA production from known tropospheric sulfur sources significantly underestimate the 1979 observations. Other non-volcanic sources are thought to be insignificant.
- Post-volcanic SSA decay varies with time, space, and aerosol property. The e^{-1} decay time for column backscatter following the eruption of Mt. Pinatubo was about 1 year until 1994, and nearly twice as long (1.8 years) from 1994 to 1997. Derived surface areas decayed back to pre-Pinatubo levels in about 3.5 years at 25 km and about 5 years at 15 km. Surface area decayed 20-30% more slowly than backscatter or mass.
- PSC observations are still divided into two broad classes: Type 1 PSCs, containing nitric acid (HNO_3) as a major component, that form at temperatures above the water (H_2O) ice point; and Type 2 PSCs, containing predominantly H_2O ice particles. Most of the observations of Type 1 PSCs can be subclassified as Type 1b liquid particles or Type 1a solid particles. Other types of particles have been proposed to explain some specific observations.
- It is now generally accepted that Type 1b PSCs are supercooled ternary solution (STS) droplets that form from SSA without a nucleation barrier. Type 1a PSC particles are generally interpreted as solid nitric acid trihydrate (NAT), but understanding of the phase transition mechanisms leading to their formation is still poor. Better understanding of Type 1a PSCs is needed because solid particles play a significant role in denitrification.
 - Many of the Type 1b PSC observations occurred during ongoing fast synoptic cooling events, shortly after the air parcels experienced cold temperatures. Type 1a PSCs, in contrast, have been observed when synoptic temperatures were below the NAT existence temperature for several days. It now appears that theoretical models of Type 1a PSC formation may require knowledge of the air parcel thermal history.

- Mesoscale temperature fluctuations, especially over mountain ranges where such fluctuations can reach 20 K peak-to-peak, are important in PSC formation processes, particularly in the Arctic. The integral effect of such phenomena on polar ozone depletion is still unclear.
- Increases in source gases and cooling of the lower stratosphere from ozone depletion and increasing greenhouse gases favor increased formation and persistence of PSCs. However, an upward trend in PSC occurrence is not discernible in the present satellite data record due to the relatively short length of the record as well as the large variability in cloud sightings from year to year.

CHAPTER 4: OZONE VARIABILITY AND TRENDS

Non-Polar Ozone

TOTAL COLUMN OZONE

- The 1994 Assessment noted large negative trends in midlatitude total ozone in the 1980s, with an additional marked decrease in Northern Hemisphere midlatitude ozone following the large enhancement of stratospheric aerosol caused by the eruption of Mt. Pinatubo in 1991. By 1994, the transient effect on total ozone of the Mt. Pinatubo aerosols had largely disappeared. Since 1994, non-polar total ozone, while variable, has not shown an overall negative trend, and total ozone levels are now at a higher level than would be predicted by a linear extrapolation of the pre-Pinatubo trend. Extrapolation of the pre-Pinatubo trend of -2.9%/decade in Northern Hemisphere midlatitudes (25°-60°) would predict an ozone depletion relative to 1979 of -5.5% at the end of 1997, whereas instead the deviations have averaged about -4% in the last 2 or 3 years. Seasonally, the corresponding winter/spring (December-May) and summer/fall (June-November) changes averaged about -5.5% and -2.8%, respectively, whereas a linear extrapolation of the pre-Pinatubo trend would predict -7.6% and -3.4%, respectively. In the Southern Hemisphere (25°-60°), trend extrapolation would predict -7.2% depletion at the end of 1997, whereas the smoothed data indicate a 1997 value of about -4% (satellite) or -5% (ground).
- As shown in Table 4-1, trends in total ozone from January 1979 updated through the end of 1997 exhibit the now-familiar pattern of negative trends with the following features:
 1. Trends in both hemispheres in mid and high latitudes in all seasons are negative, large, and statistically significant.
 2. Trends in the equatorial regions (20°S to 20°N) are statistically nonsignificant.

Table 4-1. Total ozone trends in percent per decade and uncertainties (two standard errors) from Total Ozone Mapping Spectrometer (TOMS) data*.

Latitudes		Trend (%/decade)		
		Annual	Dec-May ¹	Jun-Nov ²
North	50°–65°	-3.7 ± 1.6	-4.4 ± 2.6	-2.8 ± 1.3
North	30°–50°	-2.8 ± 1.7	-3.8 ± 2.4	-1.7 ± 1.3
Equatorial	20°–20°	-0.5 ± 1.3	-0.3 ± 1.6	-0.7 ± 1.3
South	30°–50°	-1.9 ± 1.3	-2.4 ± 1.2	-1.4 ± 1.9
South	50°–65°	-4.4 ± 1.8	-3.4 ± 1.6	-5.2 ± 2.6

* Values in table are averages from Total Ozone Mapping Spectrometer (TOMS) trends in Table 4-5. Ground-based trends are shown in Table 4-4 for somewhat different latitude bands.

¹ North winter/spring and south summer/fall.

² North summer/fall and south winter/spring.

Ozone Trends

- In the middle and high latitudes, the overall ozone amount has declined during all months of the year, and the amplitude of the annual cycle for stations has decreased by about 15% mainly as a result of a decline in the maximum. In the Northern Hemisphere, the trends are much larger (more negative) in the winter and spring seasons (December-January-February, March-April-May) about -3 to -6%/decade, than in summer and fall (June-July-August, September-October-November), about -1 to -3%/decade.
- Regional trends in total ozone show some systematic differences among continental-scale regions at the same latitudes, e.g., Siberia, Europe, and North America. The longitudinal trend calculations using gridded data from TOMS show the strongest negative trends over Siberia in spring and large negative trends over Europe in winter and spring. North America shows relatively smaller trends in winter/spring.
- Total ozone levels at 60°N-60°S were at their lowest in 1993 in the aftermath of the Mt. Pinatubo eruption. Since that time, ground-based ozone values have remained fairly constant, whereas the Earth Probe (EP)-TOMS record, which began in 1996, shows global ozone to be about 2% higher. This discrepancy, which is not seen in the northern midlatitudes (the region where we have most confidence in the observational record) has not been resolved.
- New scientific understanding shows that quasi-decadal ozone oscillations have been induced by major volcanic eruptions in the past 20 years. The confounding influences of solar and volcanic effects on ozone time-series analyses could affect the interpretation of recent changes.

Vertical Ozone Distribution

- Based on the Stratospheric Aerosol and Gas Experiment (SAGE I/II) Version 5.96 data, there is no significant inter-hemispheric difference in upper stratospheric trends for data extended through 1996.
- Combined trends and uncertainties (including both statistical and systemic error) have been estimated from all available measurement systems. This was done only for the northern midlatitudes. The combined trends are negative at all altitudes between 10 and 50 km and are statistically significant at the 2-sigma level. The combined trend has two local maxima, $-7.4 \pm 4.6\%/decade$ at 15 km. The smallest trend deduced, $-2.0 \pm 1.8\%/decade$. Occurred at 30 km. This combined trend, representing the results from all the independent data sources, is an indicator of the robustness of the trend results.
- Statistically significant trends of -6 to 8%/decade have been found at 40-50 km altitude for the midlatitudes. There is good agreement between SAGE I/II and Umkehr. The Solar Backscatter Ultraviolet (SBUV/SBUV2) spectrometer combined record shows less-negative trends. There is a factor of 2 seasonal variation in the trends, with the maximum value in winter.
- Trends in the column amount of ozone above 20 km deduced from SAGE I/II are much less than the column trends deduced from TOMS. However, the TOMS-SAGE differences are consistent with the sonde trends below 20 km. There is also a consistent seasonal variation for the satellite and sonde data.
- There is good agreement between SAGE I/II trends and sonde trends over the altitude region from 15 to 27 km at northern latitudes for the time period 1980 to 1996. This is a significant improvement compared with previous comparisons due principally to the revision of the SAGE dataset. The agreement in the derived trends from SAGE II-only and the sondes is excellent for the period 1984-1996.
- Both sonde and SAGE data show that most of the column ozone loss at midlatitudes occurs between 10 and 25 km altitude, with peak loss between 15 and 20 km. The seasonal variation of the trend occurs primarily between 10 and 20 km, with largest trends in winter and spring.

Polar Ozone

ARCTIC OZONE

- In the Arctic vortex, extremely low ozone values were deduced in late-winter/spring (a loss of about 100 Dobson units (DU; m-atm cm) with extremes exceeding ~ 200 DU below the 1964-1976 averages) in 6 out of the last 9 years. They are comparable with the values recorded (episodically) in the areas adjacent to the vortex. The ozone deficiencies are observed mostly in the layer a few kilometers above the tropopause.

- In the spring seasons of 1993, 1995, 1996, and 1997, the difference in total ozone from the pre-1976 level was comparable with differences observed in the austral spring.

ANTARCTIC OZONE

- The large ozone losses continued at high latitudes in the Southern Hemisphere. The trends from 1979 in winter (June-July-August) are up to -6%/decade, and especially, in spring (September-October-November), up to -10%/decade, due to the influence of the Antarctic ozone hole. Trends in the summer months are smaller (-2 to -5%).
- Since the last Assessment, the monthly total ozone in September and October in Antarctica continued at a level of 40 to 55% below the pre-ozone-hole values, with up to a 70% decrease for periods of a week or so.
- At maximum expansion, the size of the ozone hole (defined as the area containing ozone values less than 220 DU) was nearly the same as during the early 1990s ($>20 \times 10^6$ km²).
- In the lower stratosphere, between 12 and 20 km, over the September-November period, the monthly-mean ozone content was, on the average, between 60 and 90% below the pre-ozone-hole values and at times nearly completely destroyed.

CHAPTER 5: TRENDS IN STRATOSPHERIC TEMPERATURES

Observations

- Datasets available for analyzing stratospheric temperature trends comprise measurements by radiosonde (1940s-present), satellite (1979-present), lidar (1979-present), and rocketsonde (periods varying with location, but most terminating by ~mid-1990s); meteorological analyses based on radiosonde and/or satellite data; and products based on assimilating observations using a general circulation model (GCM).
- The temporary global, annual-mean lower stratospheric (~50-100 hPa) warming (peak value ~1 K) associated with the aerosols from the Mt. Pinatubo volcanic eruption (see WMO, 1992, 1995), which lasted up to about 1993, has now given way to a relatively colder stratosphere.
- Radiosonde and satellite data indicate a cooling trend of the global, annual-mean lower stratosphere since ~1980. Over the period 1979-1994, the trend is ~0.6 K/decade. For the period prior to 1980, the radiosonde data exhibit a substantially weaker long-term cooling trend.
- Over the period 1979-1994 there is an annual-mean cooling of the Northern Hemisphere midlatitude lower stratosphere (~0.75 K/decade at 30-60°N). This trend is coherent amongst the various datasets with regard to the magnitude and statistical significance. Over the longer period 1966-1994, the available datasets indicate an annual-mean cooling at 30-60°N of ~0.3 K/decade.

- In the $\sim 15\text{-}45^\circ$ latitude belt of the Southern Hemisphere, the radiosonde record indicates an annual-mean cooling of the lower stratosphere of up to $\sim 0.5\text{-}1$ K/decade over the period 1979-1994. The satellite record also indicates a cooling of the lower stratosphere in this latitude belt; the cooling is statistically significant between about November and April.
- Substantial cooling ($\sim 3\text{-}4$ K/decade) is observed in the polar lower stratosphere during late winter/springtime in both hemispheres. An approximate decadal-scale cooling trend is evident in the Antarctic since about the early 1980s, and in the Arctic since about the early 1990s. However, the dynamical variability is large in these regions, particularly in the Arctic, and this introduces difficulties in establishing a high statistical significance of the trends.
- A cooling of the upper stratosphere (pressure < 3 hPa; altitude > 40 km) is apparent over the $60^\circ\text{N}\text{-}60^\circ\text{S}$ region from the annual-mean Stratospheric Sounding Unit (SSU) satellite data over the 1979-1994 period (up to ~ 3 K/decade near 50 km). There is a slight minimum in cooling in the middle stratosphere ($\sim 30\text{-}40$ km) between the maxima in the lower and upper stratosphere.
- Lidar and rocket data available from specific sites generally show a cooling over most of the middle and upper stratosphere ($\sim 30\text{-}50$ km) of 1 to 2 K/decade since ~ 1970 , with the magnitude increasing with altitude. The influence of the 11-year solar cycle is relatively large (>1 K) at these altitudes (>30 km).
- The vertical profile of the annual-mean stratospheric temperature change observed in the Northern Hemisphere midlatitude (45°N) over the 1979-1994 period is robust among the different datasets. The overall trend (Figure 5A) consists of a ~ 0.8 K/decade cooling of the $\sim 20\text{-}35$ km region, with the cooling trend increasing with height above (~ 2.5 K/decade at 50 km).

Model Results and Model-Observation Comparisons

- Model simulations based on the known changes in the stratospheric concentrations of various radiatively active species indicate that the depletion of lower stratospheric ozone is the dominant factor in the explanation of the observed global-mean lower stratospheric cooling trend ($\sim 0.5\text{-}0.6$ K/decade) for the period 1979-1990. The contribution to this trend from increases in well-mixed greenhouse gases is estimated to be less than one-fourth that due to ozone loss.
- Model simulations indicate that ozone depletion is an important causal factor in the latitude-month pattern of the decadal (1979-1990) lower stratospheric cooling. The simulated lower stratosphere in Northern and Southern Hemisphere midlatitudes, and in the Antarctic springtime, generally exhibits a statistically significant cooling trend over this period, consistent with observations.

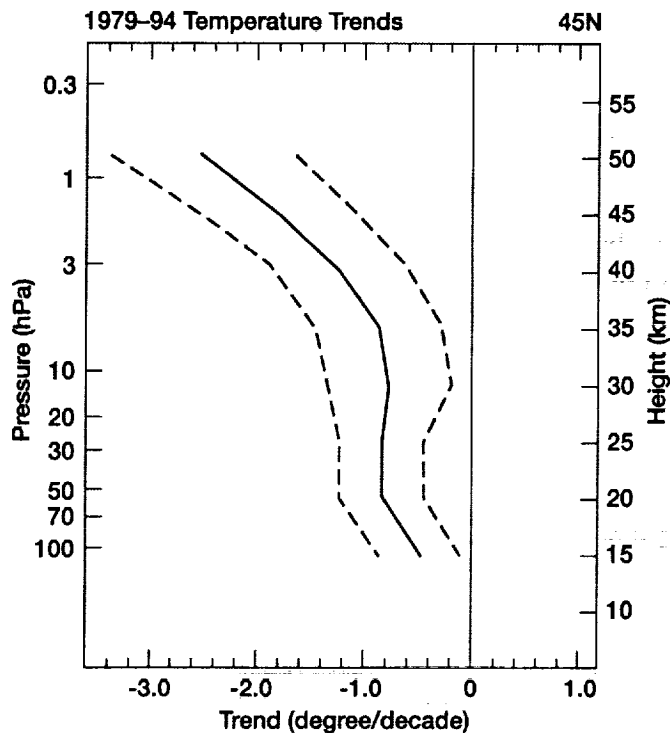


Figure 5A. Summary figure illustrating the overall mean vertical profile of temperature trend (K/decade) over the 1979-1994 period in the stratosphere at 45°N, as compiled using radiosonde, satellite, and analyzed datasets (Section 5.2.3.3). The vertical profile of the averaged trend estimate was computed as a weighted mean of the individual system trends shown in Figure 5-9, with the weighting being inversely proportional to the individual uncertainty. The solid line indicates the weighted trend estimate while the dashed lines denote the uncertainty at the 2-sigma level (note: Table 5-6 lists the numerical values of the trends and the uncertainty at the one-sigma level). (Figure assembled for this chapter in cooperation with the SPARC-Stratospheric Temperature Trends Assessment project.)

- The Fixed Dynamical Heating (FDH; equivalently, the pure radiative response) calculations yield a mid- to high-latitude annual-mean cooling that is approximately consistent with a GCM's radiative-dynamical response (Figure 5B); however, changes in circulation simulated by the GCM cause an additional cooling in the tropics, besides affecting the meridional pattern of the temperature decrease.
- FDH model results indicate that both well-mixed greenhouse gases and ozone changes are important contributors to the cooling in the middle and upper stratosphere; however, the computed upper stratospheric cooling is smaller than the observed decadal trend. Increased water vapor in the lower to upper stratosphere domain could also be an important contributor to the cooling; however, decadal-scale global stratospheric water vapor trends have not yet been determined.

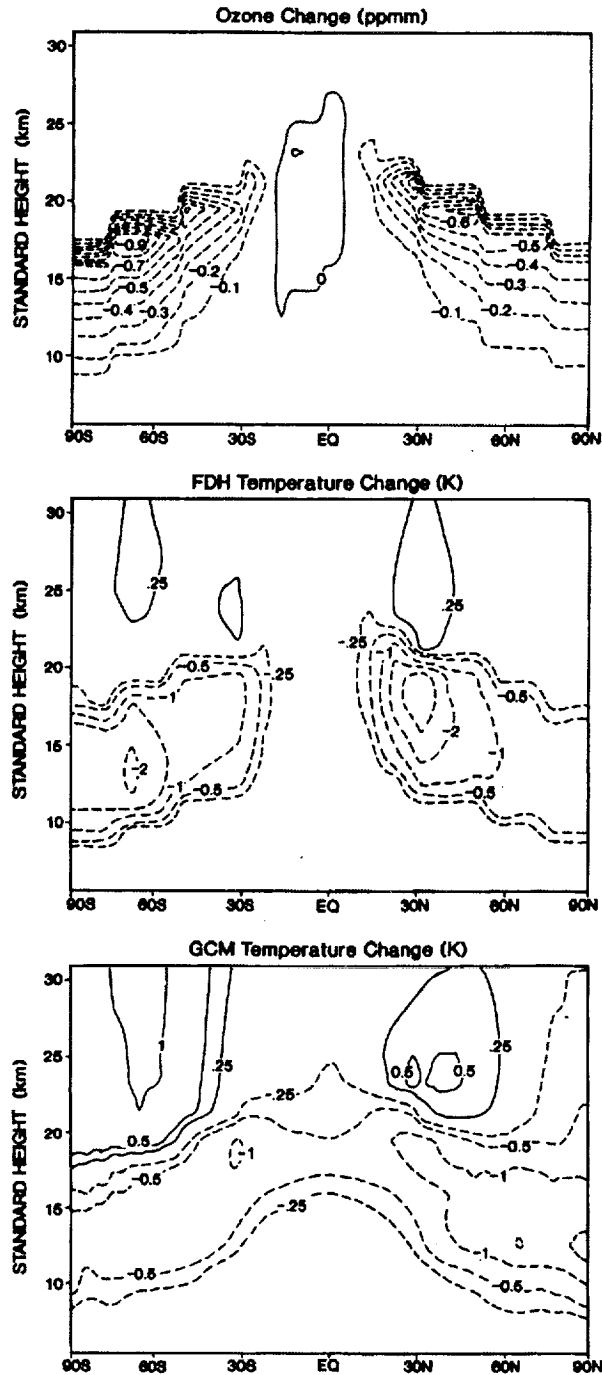


Figure 5B. Top panel: Idealized, annual-mean stratospheric ozone loss profile, based on Total Ozone Mapping Spectrometer (TOMS) and Stratospheric Aerosol and Gas Experiment (SAGE) satellite-observed ozone trends. Middle panel: Corresponding temperature change, as obtained using a Fixed Dynamical Heating (FDH) model, which illustrates the pure radiative response, and (bottom panel) a general circulation model (GCM), which illustrates the radiative-dynamical response (Section 5.3.3.1). (Adapted from Ramaswamy *et al.*, 1992, 1996).

- Model simulations of the response to the observed global lower stratospheric ozone loss in mid to high latitudes suggest a radiative-dynamical feedback leading to a warming of the middle and upper stratospheric regions, especially during springtime; however, while the modeled warming is large and can be statistically significant during the Antarctic spring, it is not statistically significant during the Arctic spring. Antarctic radiosonde observations indicate a statistically significant warming trend in spring at ~30 hPa (24 km) and extending possibly to even higher altitudes; this region lies above a domain of strong cooling that is approximately collocated with the altitude of the observed ozone depletion.
- There is little evidence to suggest that tropospheric climate changes (e.g., induced by greenhouse gas increases in the troposphere) and sea surface temperature variations have been dominant factors in the global-mean stratospheric temperature trend over the 1979-1994 period. The effect of potential shifts in atmospheric circulation patterns upon the decadal trends in global stratospheric temperatures remains to be determined.

CHAPTER 6: UPPER STRATOSPHERIC PROCESSES

Since the previous Assessment (WMO, 1995), an improved understanding of upper stratospheric processes has been gained through numerous atmospheric observations that have better defined long-term changes in ozone and better constrained our understanding of reactive hydrogen, nitrogen, and chlorine gases. The original hypothesis put forth in 1974 that a release of industrial chlorofluorocarbons (CFCs) to the atmosphere would lead to a significant reduction of upper stratospheric ozone, with the peak percentage decline occurring around 40 km, is now clearly confirmed.

- The global distributions calculated by current two-dimensional “assessment models” of the long-lived source gases (e.g., H₂O, methane (CH₄), nitrous oxide (N₂O), CFCs) of the radicals that catalyze ozone loss compare well with global observations. Consequently, the simplified representations of dynamics used by these models have proved to be useful for studies of the observed changes in upper stratospheric ozone (O₃) during the past several decades.
- Several independent recent studies show increases in upper stratospheric H₂O of about 55 to 150 parts per billion by volume (ppbv) per year from 1992 to 1996/1997, which cannot be explained by a concurrently observed downward trend in upper stratospheric CH₄ (about 15 ppbv/year). Should this rise in H₂O continue to occur, it could have important long-term radiative and photochemical consequences. However, changes in H₂O do not contribute a large fraction to the observed decline in upper stratospheric ozone over the last decades.
- Balloonborne observations of hydroxyl radicals (OH) and hydroperoxyl radicals (HO₂) near 40 km agree with calculated concentrations to within ±20%. Ground-based column observations of OH, which have a substantial contribution from the mesosphere, exhibit larger discrepancies with models. Satellite observations of OH near 50 km are considerably less than calculated using standard photochemical kinetics. These discrepancies are unlikely to have a substantial effect on calculated trends of upper stratospheric ozone.

- Comparisons of recent observations and model calculations show that the overall partitioning of reactive nitrogen and chlorine species is well understood. The previously noted discrepancy for the chlorine monoxide/hydrogen chloride ratio (ClO/HCl) has been resolved, provided allowance is made for production of HCl from a minor channel of the ClO + OH reaction, which is consistent with a recent laboratory study.
- Measurements of the total stratospheric chlorine loading demonstrate that long-lived organic chlorine compounds (mainly CFCs) released by anthropogenic activity are the dominant source of ClO, the chlorine compound that depletes O₃. The observed increases in upper stratospheric hydrogen chloride (HCl) and hydrogen fluoride (HF) are in excellent agreement with the rise of the chlorine and fluorine content of their organic source gases in the troposphere.
- An improved understanding of the relevant kinetic processes has resulted in close balance between the calculated production and loss of O₃ at 40 km (i.e., the long-standing difference between calculated and observed ozone abundance, the so-called “ozone deficit problem,” has been resolved at this altitude): Although there are remaining uncertainties regarding a possible ozone deficit at higher altitudes, the severity of this problem has been substantially reduced throughout the upper stratosphere.
- Several independent long-term datasets show a decline of the concentration of O₃ that peaks around 40 km altitude at a value of $7.4 \pm 1.0\%$ /decade. Photochemical model simulations likewise reveal a long-term decline of ozone throughout the upper stratosphere that is driven by the accumulation of anthropogenic chlorine. There is good quantitative agreement between the observed and simulated meridional and vertical structure of the long-term reductions in upper stratospheric ozone.

CHAPTER 7: LOWER STRATOSPHERIC PROCESSES

Chemical, microphysical, radiative-dynamical, and transport processes all play important roles in determining ozone abundance in the lower stratosphere. Since the last Assessment (WMO, 1995), there have been significant advances in our understanding of these processes and of the way in which they couple together to produce the observed distribution of ozone, and changes in this distribution.

Current Understanding of Lower Stratospheric Ozone Depletion

- The large ozone losses during spring over Antarctica continue unabated, with approximately the same magnitude and areal extent as in the early 1990s. The near-constant extent of seasonal column ozone losses from year to year reflects the near-complete destruction of ozone within the Antarctic lower stratosphere during springtime, and is consistent with our understanding of polar processes.
- Low abundances of late-winter/spring column ozone have been recorded both inside and outside the Arctic vortex in six of the last nine years. Observations show those years to be characterized by specific meteorological conditions: lower-than-normal late-winter/spring

Arctic temperatures, which lead to enhanced activated chlorine; and a more isolated vortex and weaker planetary-wave driving, which lead to less transport of ozone-rich air into the Arctic. Under these meteorological conditions, both chemistry and dynamics act to reduce the seasonal levels of column ozone.

- During these years of low late-winter/spring column ozone, high abundances of active chlorine have been observed inside the Arctic vortex, and chemical ozone losses inside the vortex have been unambiguously identified. These chemical losses are associated with activated chlorine augmented by bromine. The total seasonal chemical ozone losses within the vortex have been estimated to be approximately 100 milli-atm cm (Dobson units), although this magnitude is subject to considerable uncertainty.
- Low polar temperatures, an isolated vortex, and reduced wave driving are coupled processes that occur in concert in the stratosphere; but their intensity and duration are highly variable. With the present high chlorine loading and winter/spring temperatures close to the threshold for significant chlorine activation, late-winter/spring Arctic chemical ozone loss is particularly sensitive to meteorological conditions (temperature and vortex isolation). Thus, it is not possible to predict the year-to-year variations.
- The decadal trend in springtime Arctic depletion during the 1990s is reminiscent of the early years of the Antarctic ozone hole. However, while the decadal trend in the Antarctic during the late 1970s and 1980s was driven by the trend in chlorine loading, the decadal trend in the Arctic during the 1990s has been driven by a decadal change in late-winter/spring meteorological conditions in the presence of already high chlorine loading. Thus, a reduced chemical ozone loss in the coming years would not necessarily indicate chemical recovery. The Arctic will remain vulnerable to extreme seasonal loss as long as chlorine loading remains high.
- The major contribution to the midlatitude column ozone decline during the last two decades has come from decreases in the lower stratosphere. This region is influenced by local chemical ozone loss, enhanced by volcanic aerosol, and by transport from other regions. The vertical, latitudinal, and seasonal characteristics of the decadal depletion of midlatitude ozone are broadly consistent with the understanding that halogens are the primary cause. The expected low ozone amounts in the midlatitude lower stratosphere following the Mt. Pinatubo eruption, and the progressively smaller decreases in the following years as the volcanic aerosol loading decreased, further strengthened the connection between ozone destruction and anthropogenic chlorine. (In the absence of chlorine, an increase in sulfate loading is expected to increase ozone abundance.)
- The apparent leveling-off in midlatitude column ozone losses since the last Assessment is consistent with recovery from the large losses following the Mt. Pinatubo eruption as the volcanic aerosol loading slowly declined. Recent modeling studies have shown that it takes several years for the chemical effects of a volcanic eruption to disappear. Indeed, the trend in midlatitude ozone depletion during the 1980s (prior to Mt. Pinatubo) is now understood to have been exacerbated by volcanic influences during that decade.

Processes

- Chlorine activation in or on liquid particles in the lower stratosphere (both stratospheric sulfate aerosol (SSA) and supercooled ternary solutions (STS)) increases strongly with decreases in temperature. The rate coefficients are at least as large as those on solid polar stratospheric clouds (PSCs) close to nitric acid trihydrate (NAT) equilibrium temperatures. Thus, chlorine activation is to a first approximation controlled by temperature and water vapor pressure, and only secondarily by the phase of the condensed matter.
- Rapid polar ozone loss requires elevated chlorine monoxide (ClO) in the presence of sunlight. Maintenance of elevated ClO in late-winter/spring was previously thought to require denitrification. Since the last Assessment, new understanding has shown that cold liquid aerosol and/or repeated heterogeneous processing can also maintain elevated ClO in non-denitrified air.
- Some rate coefficients and photochemical parameters have been revised since the last Assessment. Although the impact of these findings has not yet been fully evaluated, our understanding of the lower stratosphere is not expected to change significantly. The lower measured rate coefficients for the reactions of iodine monoxide (IO) radicals mean that iodine may not contribute very significantly to the observed ozone depletion in the lower stratosphere.
- One of the most important new heterogeneous reactions identified since the last Assessment is the hydrolysis of bromine nitrate (BrONO_2), which serves to enhance odd hydrogen radicals (HO_x) and suppress nitrogen oxides (NO_x) and thereby plays a significant role in the midlatitude ozone chemistry.
- An individual stratospheric air parcel is made up of molecules that have spent differing amounts of time in the stratosphere. To calculate the composition of a given air parcel, one therefore needs to know the distribution of such times. The distribution varies as a function of height and latitude of the parcel. Different two-dimensional (2-D) and three-dimensional (3-D) model calculations of the distributions vary greatly and are generally inconsistent with measurements.
- The balance between radiation and dynamics controls upwelling and temperature in the tropics, and hence the amount of water vapor entering the stratosphere. This represents a potentially important mechanism by which stratospheric ozone depletion could be altered by changes in climate. The nature of this radiative-dynamical control is better understood since the last Assessment, although some important details remain unresolved.
- Constituent measurements show that the tropics are relatively isolated from midlatitudes, in some ways analogous to the wintertime polar vortex. The extent of isolation affects the budgets (and lifetimes) of chemical species. Simplified models that represent this dynamical feature (e.g., a leaky tropical pipe model) have been used to provide rough estimates of mixing time scales.

- Small-scale chemical tracer structure in the lower stratosphere, manifested as filaments or laminae, can arise from stirring by the large-scale flow. The importance of this process has been demonstrated since the last Assessment through transport calculations supported by in situ measurements. There have been significant advances in our understanding and quantification of this process, which affects mixing time scales in the lower stratosphere.
- Observations together with process-based modeling suggest that mesoscale PSC formation can activate chlorine in lee wave clouds. It is estimated that ozone can be destroyed downstream of such clouds for many days. Mesoscale chemical structure due to filamentation may also systematically impact rates of reactions (e.g., chlorine deactivation or ozone loss) on a larger spatial scale. However, the contribution of these two phenomena to midlatitude or polar ozone changes is yet to be quantified.

Quantification and Prediction of Ozone Changes

- Field measurements of the abundances of free radical catalysts involved in lower stratospheric ozone loss are consistent with model calculations and have enabled calculation of ozone loss rates in certain parts of the lower stratosphere. For example, it is now known that HO_x is the dominant catalytic ozone destroyer in the midlatitude stratosphere below ~20 km. However, observations in the lowest part of the extratropical stratosphere within a few km above the tropopause remain very limited.
- Two-dimensional models, despite their shortcomings, are useful for characterizing radiative/chemical effects in the present climate system. They are able to calculate variations in total ozone amounts that are broadly consistent with the observed midlatitude column ozone trend. In particular, the models reproduce the lower ozone amounts observed immediately following Mt. Pinatubo and the subsequent increases as the aerosol disappeared.
- The major hindrance for future prognosis of ozone levels in the Arctic is the limited ability of models to predict the dynamics (hence temperatures and transport), due to the inherent chaotic variability of the atmospheric circulation on interannual and decadal time scales.
- Dynamical forcing of the stratosphere by gravity-wave drag is now believed to be a more important effect than was previously realized. Most gravity-wave drag parameterizations remain crude. This represents a significant obstacle for general circulation modeling and prediction of stratospheric climate change.

CHAPTER 8: TROPOSPHERIC OZONE AND RELATED PROCESSES

A concerted effort continues in the deduction of trends in tropospheric ozone from the sparse in situ record. Trends are reported regionally or at stations where monitoring is conducted. Surface ozone increases, typically observed in Northern Hemisphere midlatitudes, have slowed considerably in the past decade. At the South Pole, there continues to be a decrease in surface ozone associated with the Antarctic lower stratospheric ozone depletion.

- Since the 1994 Assessment (WMO, 1995), a thorough evaluation of tropospheric ozone profiles can be summarized as follows:
 - Midlatitude: Three stations over Europe, which have had the greatest increases in free tropospheric ozone since 1970, show a major change in trends since 1980. Only Payerne shows an increase during the period 1980-1996; Uccle shows no change and Hohenpeissenberg a statistically marginal decrease. The two U.S. stations with regular ozonesonde launches (Wallops Island and Boulder) also show no significant change or a slight decrease since 1980. Of three Japanese stations, two show increases of 5-15%/decade, though not all significant; one station shows no trend. Canadian stations show a small decrease in free tropospheric ozone since 1980.
 - Tropics and Southern Hemisphere: There is only one tropical site with sufficient data for trends: Natal, Brazil, shows a 10-20%/decade increase only in the middle troposphere and possibly not significant; the record becomes too sparse for trends after 1992. There is no trend in free tropospheric ozone at Lauder, New Zealand, where the record began in 1986.
- Observations of ozone and other photochemically reactive species during field campaigns have been made with greater focus on understanding the interaction of chemistry and dynamics on local scales. Processes affecting reactive nitrogen species have been elucidated on several intensive campaigns. The free tropospheric nitric oxide (NO) and total reactive nitrogen climatology has been extended in aircraft campaigns in both Northern and Southern Hemispheres. Systematic sampling has extended the NO database along commercial aviation routes. Continental outflow downwind of industrial activity in Northern Hemisphere midlatitudes strongly enhances ozone budgets over large regions of the North Atlantic and North Pacific. Measurement campaigns in the tropics and subtropics show continental influences from long-range transport of biomass-burning emissions, although NO from lightning may also play a significant role in the tropical ozone budget.
 - Reliable instrumentation for hydroxyl radicals (OH), hydroperoxyl radicals (HO₂), and organic peroxy radicals (RO₂) has been a breakthrough development since the last Assessment. Intercomparisons on the ground, and model interpretation of ground-based and airborne OH and related measurements show that our theoretical understanding of OH is not complete. With the constraint of ancillary measurements, it can be shown that data-model discrepancies tend to be greatest under polluted conditions and that odd hydrogen (HO_x) sinks, rather than sources, are probably not accounted for. In the upper troposphere, under certain conditions, acetone and the recycling of peroxides following deep convective transport appear to be important HO_x sources. On a global scale, inferences about the total OH budget range from no trend in the past decade to a slightly positive trend.

- Model intercomparisons and uncertainty studies show that photolysis rates, representations of stratospheric-tropospheric exchange, and imprecise pathways in organic oxidation chains continue to limit the reliability of models used in interpretive ozone studies and predictions. Models continue to suggest intriguing possibilities for heterogeneous and multiphase reactions affecting ozone in a major way, but experimental confirmation is lacking for the most part.
- Large-scale ozone distributions calculated in global chemistry-transport models (CTMs) are in fair accord with the sparse measurements and historical ozone data. However, the agreement between models and measurements on regional and smaller scales is more difficult to achieve. The quality of simulations is probably most limited by the treatment of convection and other sub-grid dynamical processes as well as complex chemical pathways near ozone precursor source regions.

CHAPTER 9: ULTRAVIOLET RADIATION AT THE EARTH'S SURFACE

The advances and new findings that have occurred in the ultraviolet (UV) radiation field since the publication of the previous Assessment (WMO, 1995) include the following:

- The inverse relationship between decreasing ozone amount and increasing UV-B radiation has been reconfirmed and firmly established in both theory and measurements. The measured effects of ozone, albedo, altitude, clouds and aerosols, and geographic differences are much better understood.
- The number, distribution, and quality of UV-irradiance (energy per unit area per unit time) instruments have greatly improved throughout the world. However, there are still regions of sparse coverage.
- Well-calibrated UV-irradiance spectral time series are now available at some ground sites for periods of up to 9 years, where changes in UV-B irradiance have been detected (e.g., 1.5% per year at 300 nm, 0.8% per year at 305 nm) at midlatitudes (near 40°) that are consistent with expected changes from the decreasing amounts of ozone. However, the long-term stability needed for trend estimates has been demonstrated for only a few ground-based UV instruments. Either the records are not long enough or the instrument stability is insufficient to reliably determine decadal change at most midlatitude sites. Other factors limiting the detection of long-term trends are that clouds, albedo, aerosols, and short-term ozone changes produce local daily, monthly, and interannual changes that are larger than the long-term trend. It is important for long-term trend detection that both UV-A and UV-B be measured separately along with ancillary data (e.g., ozone and aerosols).
- The anomalous UV-trend estimates from the Robertson-Berger (RB) meter network located in the United States are now understood. Corrections have been applied to the data, which now show no significant trends for the latitude range of the instruments' locations. It was concluded that the data from the U.S. RB network alone are unsuitable for trend detection.

- Increases in UV-B irradiance in the Northern Hemisphere at high latitudes have been attributed to the low ozone amounts in the winter and spring of 1995, 1996, and 1997.
- New types of filter instruments have been developed, using narrower band pass at a few selected wavelengths and greater filter stability specifications than previous broadband instruments. These simpler instruments may yield results with accuracy comparable to that of grating spectroradiometers (5 to 10%) and should permit a wider geographical distribution of measuring sites for UV irradiance. This is especially important to address the lack of sufficient observing sites in some regions.
- New satellite estimates of global (latitude $\pm 65^\circ$) UV irradiance, which now include cloud, surface albedo, and aerosol effects, are available using radiative transfer models and measured radiances from Total Ozone Mapping Spectrometer (TOMS) instruments. The satellite-estimated UV irradiances have been compared with ground-based measurements at a single site, Toronto. The weekly-average results agree to within 5% for snow-free conditions. Further comparisons at other sites are necessary to validate the accuracy and applicability of the techniques over a wide range of observing conditions. This may be especially important when accounting for local aerosol extinctions.
- TOMS satellite data have been used to estimate long-term decadal changes in zonally averaged global and seasonal patterns in UV irradiance from 1979 to 1992. The results showed that the UV-B irradiances increased (see table below), while UV-A irradiances remained unchanged. At individual sites, changes in UV-A irradiances have occurred because of changes in local cloudiness and aerosol amounts.

Zonal Average UV-Erythemal Trends (Percent Increase per Decade) 1979 to 1992.

Latitude	January	April	July	October	Annual $\pm 2\sigma$
50° to 65°N	6	4	2	4	3.7 \pm 3
35° to 50°N	3	3	2	2	3 \pm 2.8
30°S to 30°N	0	0	0	0	0 \pm 2
35° to 50°S	4	2	2	6	3.6 \pm 2
50° to 65°S	4	5	8	14	9 \pm 6

- Zonally averaged UV-irradiance trend determinations from satellite data that include cloud effects yield numbers nearly identical to those from clear-sky estimates. However, the currently estimated UV trends are slightly lower than the clear-sky values in the 1994 Assessment because of the new TOMS ozone algorithm (see Chapter 4).

- Measurements at several ground sites have indicated differences between UV irradiances in the Northern and Southern Hemispheres that are larger than explained by the known differences in ozone amount and Sun-Earth separation. This may indicate that other factors such as aerosols could be involved. Satellite estimates show smaller irradiance differences between the hemispheres than do ground-based measurements.
- Several intercomparisons of UV-irradiance instruments of different types have been conducted in various countries. These have helped identify instrument capabilities and limitations. Currently, the best intercomparisons of different instruments at the same location are within $\pm 5\%$ absolute accuracy. However, this "best" accuracy estimate does not represent the general level of agreement between geographically distributed networks of similar and different instruments over extended periods of time. Significant improvements have been made to reduce errors in the cosine response, stray light rejection, and wavelength alignment.
- Expansion of the World Ozone and Ultraviolet Radiation Data Centre (WOUDC) in Canada and the European database, Scientific UV Data Management/UV Radiation in the Arctic; Past, Present, and Future (SUVDAMA/UVRAPPF), has significantly improved the availability and distribution of data to researchers studying the effects and behavior of UV-B radiation. Extensive sources of UV information have become available on the Internet.
- Significant improvements have been made in calibration of ground-based instruments. This has been achieved through instrument intercomparisons and the use of newly developed central calibration facilities, although additional calibration facilities would continue to meet needs. After validation, satellite estimations of UV irradiance may serve as a comparison standard between widely separated ground-based instruments in a manner similar to that used for the ground-based ozone network.
- Different classes of radiative transfer models have been intercompared and found to agree within 1% for irradiances. However, for some radiative transfer approximations (e.g., delta-Eddington) the gains in computational speed are offset by losses in accuracy. Two-stream models have accuracies on the order of 5% for moderate optical depths and can have errors exceeding 10% for large optical depths (small irradiances).
- Public interest related to UV exposure has been addressed by establishing a standardized UV index in many countries, based on estimates of ozone and, in some cases, cloud cover and surface albedo, to provide daily information about the intensity of UV radiation.

CHAPTER 10: CLIMATE EFFECTS OF OZONE AND HALOCARBON CHANGES

- **Increased penetration of UV radiation to the troposphere as a result of stratospheric ozone depletion leads to changes in key photochemical processes in the troposphere.** Model simulations have been used to estimate that a 1% decrease in global total ozone leads to a global increase of about 1.5% in the photolytic production of the first excited state of atomic oxygen, $O(^1D)$, from ozone. This results in a 0.7 to 1% increase in globally averaged tropospheric hydroxyl radical (OH). Since OH is the main oxidant for climatically important

gases, such as methane (CH₄), hydrochlorofluorocarbons (HCFCs), and hydrofluorocarbons (HFCs), this change would be expected to decrease their lifetimes. Stratospheric ozone depletion may have contributed 20 to 40% of the reduction in CH₄ growth rate, and 25 to 40% of the carbon monoxide (CO) surface concentration decrease during the two years following the Mt. Pinatubo volcanic eruption in 1991. The effect on those species whose lifetimes depend on OH has not yet been quantified.

- **The first systematic calculations of the effects of ozone changes on climate using a general circulation model (GCM) have been reported.** Previous assessments highlighted the climatic importance of ozone changes near the tropopause. When taking into account the impact of ozone changes on cloudiness, this GCM study suggests that changes in lower tropospheric ozone are of similar importance to changes near the tropopause. This study suggests that, because of the cloud interactions, the ozone change since the late 1970s may have resulted in a surface temperature change 20-30% smaller than that implied by radiative forcing. Given the known difficulties in modeling cloud processes in GCMs, the generality of conclusions drawn from a single model must be treated with caution.
- **The global-average radiative forcing due to changes in stratospheric ozone since the late 1970s is estimated to be $-0.2 \pm 0.15 \text{ Wm}^{-2}$.** The central value of this forcing estimate is about double the Intergovernmental Panel on Climate Change (IPCC, 1996) estimate, partly because the calculations now include the increased ozone losses during the 1990s. There remain uncertainties due to difficulties in defining the vertical profile of ozone change and in calculating the stratospheric temperature response to this change. The stratospheric ozone forcing may have offset about 30% of the forcing due to the increases in the well-mixed greenhouse gases since the late 1970s.
- **Recovery of stratospheric ozone would reduce the offset to the radiative forcing of the other greenhouse gases.** The ozone recovery will therefore lead to a more rapid increase in radiative forcing than would have occurred due to increases in other greenhouse gases alone.
- **The global-average radiative forcing due to increases in tropospheric ozone since preindustrial times is estimated to be $+0.35 \pm 0.15 \text{ Wm}^{-2}$.** This estimate is consistent with the IPCC (1996) estimate of $0.4 \pm 0.2 \text{ Wm}^{-2}$, but is based on a much wider range of model studies; significant uncertainties remain because of inter-model differences and the lack of data for evaluating the model results. Since the forcing due to the increases in “well-mixed” greenhouse gases since preindustrial times is about 2.5 Wm^{-2} , the tropospheric ozone changes may have enhanced this forcing by 10-20%.
- **Coupled ocean-atmosphere GCMs have been used to calculate the impact of stratospheric ozone loss on the thermal structure of the atmosphere.** The observed stratospheric ozone depletion appears to explain much of the observed temperature decrease in the lower stratosphere. The calculated altitude of the transition from tropospheric warming to stratospheric cooling is in better agreement with observations when ozone depletion is taken into account. The global average surface temperature is estimated to be about 0.1°C cooler over the past two decades as a result of the stratospheric ozone loss; this

can be compared with the calculated warming of about 0.3°C over the same period, due to well-mixed greenhouse gas increases.

- **The CFC-11 radiative forcing has been revised.** The currently recommended chlorofluorocarbon-11 (CFC-11) radiative forcing is 12% higher than the value used in IPCC (1990) and subsequent assessments. The change is primarily due to the use of an improved vertical profile of CFC-11. Because this gas was used as a reference in previous assessments to calculate the forcing for many other molecules, its change leads to revised radiative forcings recommendations for these gases.
- **Radiative forcings and Global Warming Potentials (GWPs) are presented for an expanded set of gases.** New categories of gases in the radiative forcing set include fluorinated organic molecules. For some of these gases, GWPs are not reliable, because laboratory data are not available for determination of the lifetimes. The direct GWPs have been calculated relative to carbon dioxide (CO₂) using an improved calculation of the CO₂ radiative forcing, the IPCC (1996) response function for a CO₂ pulse, and new values for the radiative forcing and lifetimes for a number of halocarbons. As a consequence of changes in the radiative forcing for CO₂ and CFC-11, the revised GWPs are typically 20% higher than listed in IPCC (1996). Indirect GWPs are also presented. The direct GWPs, for those species whose lifetimes are well characterized, are estimated to be accurate within ±35%, but the indirect GWPs are less certain.

CHAPTER 11: HALOCARBON SCENARIOS FOR THE FUTURE OZONE LAYER AND RELATED CONSEQUENCES

- **Different future scenarios for the release of ozone-depleting substances (ODSs) into the atmosphere will have different consequences for atmospheric halogen loading and therefore for stratospheric ozone and surface ultraviolet (UV) radiation.** Such scenarios indicate the sensitivity of the ozone layer to possible additional future control measures and illustrate the effects of compliance with the Montreal Protocol. The scenarios are not designed to yield exact predictions of future ozone amounts, which are affected also by other factors including possible interactions with climate change associated with the increasing atmospheric concentrations of greenhouse gases and aerosols. These factors are not considered here, both because of uncertainties in predictability and to enable a more direct and simple comparison of the relative impacts of different future ODS production/emission scenarios.
- **Large reductions in the production and atmospheric release of ODSs have been achieved by international regulations (Montreal Protocol and its Amendments and Adjustments).** Without such controls, and assuming a (perhaps conservative) 3% annual growth rate in production, ODSs would have led to an equivalent effective stratospheric chlorine (EESC) loading of about 17 parts per billion (ppb) in 2050. The control measures of the original Montreal Protocol (1987) reduce this to about 9 ppb; the London Amendments (1990) to about 4.6 ppb; and the Copenhagen Amendments (1992) to about 2.2 ppb (but with effective chlorine loading increasing again in the second half of the 21st century). The

Vienna Adjustments (1995) and the Montreal Amendments (1997) further reduce this to about 2.0 ppb (approximately the 1980 level) around the year 2050.

- **If there were to be an immediate stop to all emissions of human-made ODSs, including those currently in use, the future stratospheric halogen loading would not return to the 1980 level until about 2033.** On the other hand, with maximum production allowed by the current Protocol (Montreal Protocol and its Amendments and Adjustments as of 1997), the future stratospheric halogen loading is expected to decrease after about 1997 and to drop below the 1980 level in 2052.
- **Additional scenarios may affect the future ozone layer, although by amounts generally smaller than those already expected to be achieved by current regulations.** Relative to the current regulations (Montreal Protocol and its Amendments and Adjustments as of 1997), the equivalent effective chlorine loading above the 1980 level, integrated from now until the 1980 level is re-attained, could be decreased by
 - 9% by eliminating global Halon-1211 emissions in the year 2000, thus requiring the complete elimination of all new production and destruction of all Halon-1211 in existing equipment;
 - 7% by eliminating global Halon-1301 emissions in the year 2000, thus requiring the complete elimination of all new production and destruction of all Halon-1301 in existing equipment;
 - 5% by eliminating the global production of hydrochlorofluorocarbons (HCFCs) in the year 2004;
 - 2.5% by eliminating the global production of chlorofluorocarbons (CFCs) and carbon tetrachloride in the year 2004;
 - 1.6% by reducing the cap on HCFC production in developed countries from 2.8% to 2.0% and advancing the phase-out from the year 2030 to 2015, as well as more rapid intermediate reductions;
 - about 1% by eliminating the global production of methyl bromide in 2004.

The policy actions would advance the date at which the level of effective chlorine returns to the 1980 level by 1-3 years. It should be noted that if the currently allowed essential uses for metered dose inhalers (CFC-11, CFC-12, CFC-114) are extended from the year 2000 to 2004, the effective chlorine loading above the 1980 level would increase by 0.3%.

- **Illegal production of ozone-depleting substances may delay the recovery of the ozone layer.** For example, illegal production of, in total, 20-40 ktonnes per year of CFC-12 and CFC-113 for the next 10-20 years would increase the equivalent effective chlorine loading above the 1980 level, integrated from now until the year the 1980 level is re-attained, by 1%-

4% and delay the return to pre-1980 levels by about a year. Significant additional contributions may come from illegal production of halons.

- **Different scenarios of future effective chlorine loading lead to correspondingly different scenarios of future ozone amounts.** The exact ozone response is difficult to predict because of possible interactions with other global atmospheric changes. However, for the purpose of comparing the different scenarios, a simple scaling relationship between equivalent effective stratospheric chlorine loading and ozone depletion can be used if it is assumed that the ozone reductions observed during 1979-1991 were caused exclusively by the simultaneous increase in stratospheric effective chlorine. Within this approximation, the future evolution of ozone reductions follows closely the increases of effective chlorine above 1980 levels, with lowest ozone in about 1997, contemporaneous with maximum effective chlorine loading, and return to baseline (1980) values in 2052 (maximum production scenario) and 2033 (zero emissions scenario). At 45°N, the maximum reduction in the annually averaged ozone is expected to be about 15 Dobson units (DU), or about 4.3% lower than the 1980 value. At 45°S, the maximum reduction in the annually averaged ozone is expected to be about 20 DU, or about 6.2% lower than the 1980 value.
- **Decreases in the ozone column cause increases in surface UV radiation, if other factors (e.g., clouds, aerosols) remain unchanged.** For erythemally effective UV radiation (UV_{ery} , the integral of the product of the spectral irradiance and the spectral erythemal sensitivity), the temporal evolution of the scenario follows closely the increases of effective chlorine above 1980 levels, with highest UV irradiances in about 1997, contemporaneous with maximum effective chlorine loading, returning to baseline (1980) values in 2052 (maximum production scenario) and 2033 (zero emissions scenario). At 45°N, the maximum enhancement in the annually averaged UV_{ery} is expected to be about 4.7%, while at 45°S it is estimated to be about 8.1%.
- **Many other biological effects of UV exposure are recognized in addition to erythema and skin cancer induction.** These have a broad range of sensitivity to ozone changes, primarily because of different sensitivities of the biological effects to various wavelengths of radiation. In the few cases for which the biological spectral sensitivity functions (action spectra) are known, scaling factors are derived that allow estimation of the effective biological radiation for each of these effects, relative to the changes in erythemal radiation expected from future changes in effective stratospheric chlorine loading. The potential impacts of higher UV irradiances at the Earth's surface are discussed in detail by the UNEP Panel on the Environmental Effects of Ozone Depletion (UNEP, 1998b).
- **The compilation of Ozone Depletion Potentials (ODPs) has been updated and expanded.** The ODPs of halogen-containing molecules have been updated, relative to the previous Assessment, based on new estimates of atmospheric lifetimes.

CHAPTER 12: PREDICTING FUTURE OZONE CHANGES AND DETECTION OF RECOVERY

A range of models has been used to investigate future changes in ozone in response to changing atmospheric emissions of source gases and greenhouse gases. A significant advance is the use of three-dimensional (3-D) models in these studies. The detection of the beginning of recovery of ozone (where recovery is defined as the response of ozone to reductions in chemical ozone loss due to the halogens) is considered for the first time in this Assessment.

All other things being equal, stratospheric ozone levels should rise as the halogen loading falls in response to regulation. However, the future behavior of ozone will also be affected by the changing atmospheric abundances of methane (CH₄), nitrous oxide (N₂O), sulfate aerosol, and changing climate. Thus, for a given halogen loading in the future, the atmospheric ozone abundance will not be the same as found for that loading in the past. Because of these additional factors, observation of the beginning of ozone recovery is expected to be delayed beyond the time of maximum stratospheric halogen loading.

Model Predictions of Future Ozone

- Ten two-dimensional (2-D) models were used to investigate the response of ozone to past and future changes in halogen loading as well as CH₄, N₂O, and sulfate aerosol. The models provide a reasonable representation of the general structure of recent observed local and column ozone trends, giving credence to their ability to represent future ozone change.
 - In integrations to 2050, excluding the possibility of major volcanic eruptions in the future, the lowest global ozone is predicted to have occurred in the years immediately following the eruption of Mt. Pinatubo in 1991.
 - After 2000, ozone levels are predicted to recover slowly toward their pre-1980 values. The modeled recovery depends sensitively on the emission scenarios for the halogens, and for CH₄, N₂O, and sulfate aerosol density.
 - Increases in future CH₄ will shorten the recovery period. Increases in N₂O and sulfate aerosol surface area density will extend the recovery period. In one model that tested the effects of projected future CO₂ increases, the recovery period was shortened.
 - The methane scenario used here as a baseline had a lower growth rate than in previous Assessments and lengthened the modeled ozone recovery significantly. Understanding the methane trend is an important priority for understanding the future ozone recovery.
 - Model simulations show that future volcanic events at low inorganic chlorine (Cl_y) abundances will not significantly affect the rate of recovery.

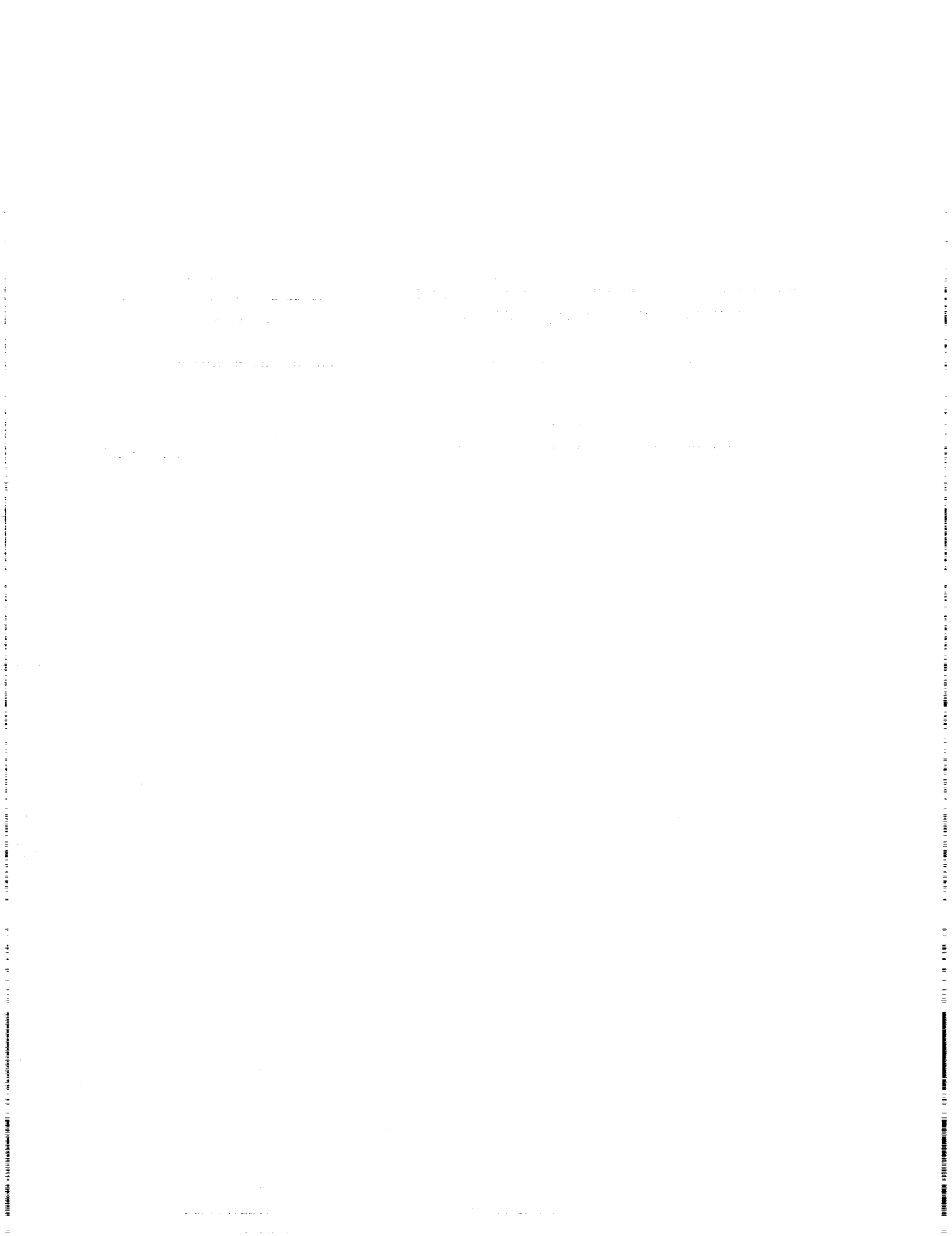
- Polar ozone loss in recent Northern Hemisphere winters has demonstrated a large dependence on meteorological conditions, and especially temperature. Those winters with the lowest polar lower stratospheric temperatures have shown largest ozone losses. Recovery of ozone is evidently strongly dependent on meteorological conditions.
- Advances in computing power have allowed the first simulations of future ozone using coupled 3-D models.
 - Three-dimensional models highlight that future Arctic ozone loss is very sensitive to changes in the strength, frequency, and timing of sudden warmings.
 - Three-dimensional models suggest that recovery of Arctic ozone is likely to be delayed past the maximum in stratospheric chlorine abundances and beyond that predicted by 2-D models. For example, coupled chemistry-climate models show greater ozone depletion in the Arctic in 2015 than 1995. The single model that has predicted trends out beyond 2015 shows a recovery of Arctic ozone beginning in the 2020s.
 - Model simulations indicate that observations of the onset of ozone recovery from halogen-induced depletion should be possible earlier in the Antarctic than in the Arctic.
 - At high latitudes throughout the stratosphere, there are considerable differences in the temperature response of general circulation models (GCMs) to increasing greenhouse gases that are associated with differences in modeled circulation changes.
 - Further validation of stratospheric GCMs is necessary for them to reach a consensus on predictions of chemistry-climate interactions in the stratosphere such as that now seen in predictions of surface parameters by climate models.

Detection of Recovery

- Observation of the beginning of ozone recovery, defined as the unambiguous detection of an increase toward pre-1980 ozone values, will be possible in the Antarctic before either the Arctic or midlatitudes. This is due to at least two factors: the smaller degree of variability in the Antarctic ozone loss phenomenon and the relatively smaller effect that future climate change will have on ozone loss in Antarctica.
- Antarctic ozone recovery indicators that have been identified include the geographical extent of the ozone hole region as measured by the 220-Dobson unit (DU) ozone contour, the total column ozone during October at South Pole and Halley stations, the amount of ozone depletion at the top of the ozone hole, in the 22-24 km region where the depletion chemistry is not saturated, and the rate of ozone decline during September in the 12-20 km region of maximum polar stratospheric cloud formation.
- Comparison of modeled ozone recovery with observations, and taking into account ozone variability, suggests that the beginning of recovery of the Antarctic ozone hole will likely not be detected before about 2020. The onset of the recovery of the bulk of the global ozone

layer may possibly not be unambiguously detected before 2030. Because of the large uncertainties in model predictions associated with changes in CH₄, N₂O, sulfate aerosol, and climate, these estimates are likewise uncertain; however, it is clear that the onset of ozone recovery will be delayed beyond the maximum in stratospheric halogens.

- A pre-recovery period, defined as a cessation of the worsening of global ozone depletion, may be observed during the next decade; however, a major volcanic eruption during this period would cause stratospheric chemical perturbations that would result in a further decline in ozone for several years. Over the longer term, future major volcanic eruptions occurring at decadal intervals would not be expected to alter eventual ozone layer recovery.
- Recovery of ozone from the effects of chlorine may be observed at an earlier time in the 40-km region, where the chemistry affecting ozone is relatively simple and volcanic effects are absent. However, climate change will likewise cause an increase in ozone in this region, possibly masking ozone recovery. In addition, because ozone in this region contributes only a few percent to the total column, observation of recovery at 40 km should not be interpreted as evidence for the recovery of the global ozone layer.



SECTION C

SUMMARY OF THE STRATOSPHERIC PROCESSES AND THEIR ROLE IN CLIMATE/INTERNATIONAL OZONE COMMISSION/GLOBAL ATMOSPHERIC WATCH (SPARC/IOC/GAW) ASSESSMENT OF TRENDS IN THE VERTICAL DISTRIBUTION OF OZONE

1. INTRODUCTION

One of the largest uncertainties in determining the effect of CFC's on stratospheric ozone has been the magnitude of the trends in the altitude region between 15 and 20 km. In the 1994 WMO-UNEP ozone assessment, SAGE was reported as giving trends up to $-0\pm 8\%$ per decade at northern mid-latitudes, while the ozonesonde stations gave a trend of $-\pm 3\%$ per decade. In 1996 the SPARC panel on Understanding Ozone Trends and the International Ozone Commission decided to collaborate, under the auspices of the World Climate Research Programme and the World Meteorological Organisation, on a study to carefully re-evaluate the ground-based and satellite data to resolve this discrepancy. The philosophy of the study was similar to that of the International Ozone Trends Panel of 1988 which addressed the total ozone measurements. The published literature was not simply reviewed, but a critical re-analysis and interpretation of the vertical profiles of ozone was performed. One of the principal aims of the report was to determine if there was sufficient confidence in the long-term measurement systems to use them for accurate determination of ozone trends in the stratosphere and troposphere. A major purpose of the study was to validate the quality of the data including quantification of the errors and to determine if there were any limitations in altitude or latitude.

The report is divided into three main chapters. Chapter 1 contains a description of how the various instruments work, and how ozone concentrations are calculated from the raw measurement. Particular attention is paid to the true vertical resolution of each instrument's measurement and to its long term calibration drift as well as to its precision and accuracy. Chapter 2 assesses how well the various measurements agree through a series of rigorous data comparisons. Traditional techniques based on zonal averages and on close matches in time and space are augmented by new techniques which classify the air mass according to its dynamic history. Chapter 3 discusses and uses the various methods available for calculating trends, as well as investigating how well the causes of the trends can be determined by statistical approaches.

2. FINDINGS

2.1 Validity of the Data Sets

Only four measurement techniques were identified that had produced records long enough to assess long term trends, SAGE (I and II), SBUV and SBUV2, Umkehr/Dobson and ozonesondes. The SAGE I and II satellite series extends from February 1979 to June 1996, with a three year interruption beginning November 1981. This series provides altitude coverage from the lower stratosphere to the stratopause. The SBUV-SBUV2 satellites (1978 to present) and the ground-based Umkehr/Dobson instruments (1957 to present) provide data sets for examining trends in the middle and upper stratosphere. Data from the ozonesonde network, started in the early 1960's, and extend to the present. This data set has the potential for providing trends in the lower stratosphere and troposphere. The report also assessed the ozone data quality from measurement systems which have operated over shorter time periods to validate the long term measurement systems above. The purpose of this approach was two-fold, (1) Was there any evidence that the SAGE algorithms produced errors in the measured ozone?, and (2) Was there any evidence for a long-term systematic error in the SAGE data which could affect the derived trends?

The measurement techniques of all the data sets were critically analysed from an instrumental and theoretical perspective. Changes in instrument performance and operation were considered as well as any errors or uncertainties produced in the algorithms used. Important issues include the correction in the SAGE data for the presence of aerosol (principally important below 20 km and in the aftermath of volcanic eruptions) and the pump correction for ozonesondes (important above 25 km). Tables of uncertainties have been composed which include not only the accuracy and precision of individual measurements, but also, for the first time for measurements of the vertical profile of ozone, estimates of the stability of the various systems over time. These were given as a function of altitude and latitude where appropriate and are being included in the estimates of the uncertainties in the trends given below. The drift uncertainties (2σ) are estimated to be less than 5% per decade for all measurements systems considered, with the exception of the Brewer-Mast ozonesonde in the troposphere (at 5 km).

The inter-comparisons were used to see if the drifts found between instruments with long term records were consistent with these estimates of stability. These inter-comparisons also included data covering shorter periods from the HALOE and MLS instruments on the UARS satellite and ground-based LIDAR and microwave instruments including those in the NDSC.

All SAGE II data used in the report were derived using the version 5.96 algorithm. The known error in the altitude registration of the SAGE I data was corrected according to Wang *et al.* (1996). It was found that the most important screening consideration was to eliminate SAGE II data contaminated by Mt. Pinatubo aerosol absorption. SAGE II ozone retrievals are affected by an inability to remove all the aerosol interference (although the current algorithm is better than previous versions). Based on comparisons with MLS, which is almost unaffected by high aerosol loading, it is recommended that between 1.5 and 2.5 years of data following the Pinatubo eruption be omitted from the SAGE II ozone data at pressures greater than 10 hPa. The detailed recommendations are given in the report as a function of pressure.

The upper altitude limit of SAGE II data for use in detecting trends was determined to be on the order of 50 km based on noise in SAGE II and inter-comparisons with HALOE. The lower altitude limit is less well determined, most likely because of low altitude atmospheric variability and aerosol effects on both the SAGE II measurements and the data used for comparisons. In most instances, the drifts and their associated uncertainties between SAGE II and correlative data start to increase below about 20 km, and they become much more variable thus limiting the lower altitude that can be validated. This is not to say that long-term trends derived from SAGE II are invalid in this range, only that for the measurements systems used in the inter-comparisons, a less definitive statement can be made about trend validity. The smallest long-term drifts that can be verified over the 20 km to 50 km altitude interval are in the range of $0.3\% \text{year}^{-1}$ when viewed as a function of latitude.

Between 20 and 40 km, the Dobson/Umkehr measurements constrain SAGE I/II drifts in a narrow latitude band in the northern mid-latitudes to $0.2 \pm 0.2\% \text{year}^{-1}$ and in the southern mid-latitudes to $0.3 \pm 0.3\% \text{year}^{-1}$ at the 95% confidence level. Globally averaged SAGE I/II trends over this altitude range are constrained by both ground-based and satellite measurements to be valid to a level on the order of $0.2\% \text{year}^{-1}$ at the 95% confidence level. It appears that the best agreement in trends occurs for SAGE II comparisons with other satellite data; although the Dobson/Umkehr comparisons provide equally good constraints in the northern and southern mid-latitudes.

The drifts for time series of coincident differences between SAGE II and other measurements for individual stations or latitudes are summarised in Figure 1. Values range from $\leq 0.3 \pm 0.15\% \text{year}^{-1}$ to $\sim 0.5 \pm 0.7\% \text{year}^{-1}$ (sondes, lidar, Umkehr, HALOE) for altitudes between 20 km and 35 km and $\leq 0.5 \pm 0.5\% \text{year}^{-1}$ to $\sim 1 \pm 1\% \text{year}^{-1}$ for altitudes between 35 km and 50 km. Only two systems (sondes and lidar) provide useful trend comparison data for the altitude range between 15 km and 20 km. Trends of matched pair (i.e. sonde minus SAGE II) differences at individual stations show significant variability, ranging up to $3\% \text{year}^{-1}$ at 15 km for Lauder; however, best agreement was obtained when the matched pair differences from the eight sonde stations used in the trend analyses (see section 2.2) were combined into a single time series to calculate the regression slope of the differences. No statistically significant differences were obtained for the combined time series, but the mean difference was about $0.25\% \pm 0.4\% \text{year}^{-1}$ in this lower stratosphere range above ~ 15 km altitude. This suggests that there is a fair degree of noise in the differences at individual stations due either to atmospheric variability, sampling, or instrumental effects; but it also suggests that SAGE II trends in the lower stratosphere are accurate to the $0.25\% \text{year}^{-1}$ level.

While no statistically significant drift was found between SAGE and the ozonesondes, differences in the absolute values of the measured ozone were found. The SAGE II absolute values agree with sondes in the altitude region between 20 km and 28 km to within a few %, but below 20 km SAGE II values start to increase relative to the sondes and reach values which are 15% to 20% larger at 15 km. The low altitude differences are latitudinally dependent which could indicate a problem with using the data for global trend calculations.

The globally averaged drifts of SAGE II versus SBUV, HALOE and MLS range from -0.06% to $-0.4\% \pm \sim 0.6\% \text{year}^{-1}$, i.e. SAGE II ozone has become more negative compared to the other instruments. These differences, although statistically insignificant, give a slight indication of a SAGE II drift with time (SAGE II trend is larger). SBUV2 differences with SAGE II are of opposite sign to SBUV, HALOE and MLS, but this is most likely due to algorithm effects brought on by a drifting orbit. Globally averaged analyses of the longest satellite time series - SBUV compared with the composite time series of SAGE I (1979-1981) and SAGE II (1984-89), designated SBUV(*) in Figure 1, shows agreement to $(-0.2\% \text{ to } 0.2\%) \pm 0.2\% \text{year}^{-1}$ in the altitude region between 20 km and 50 km.

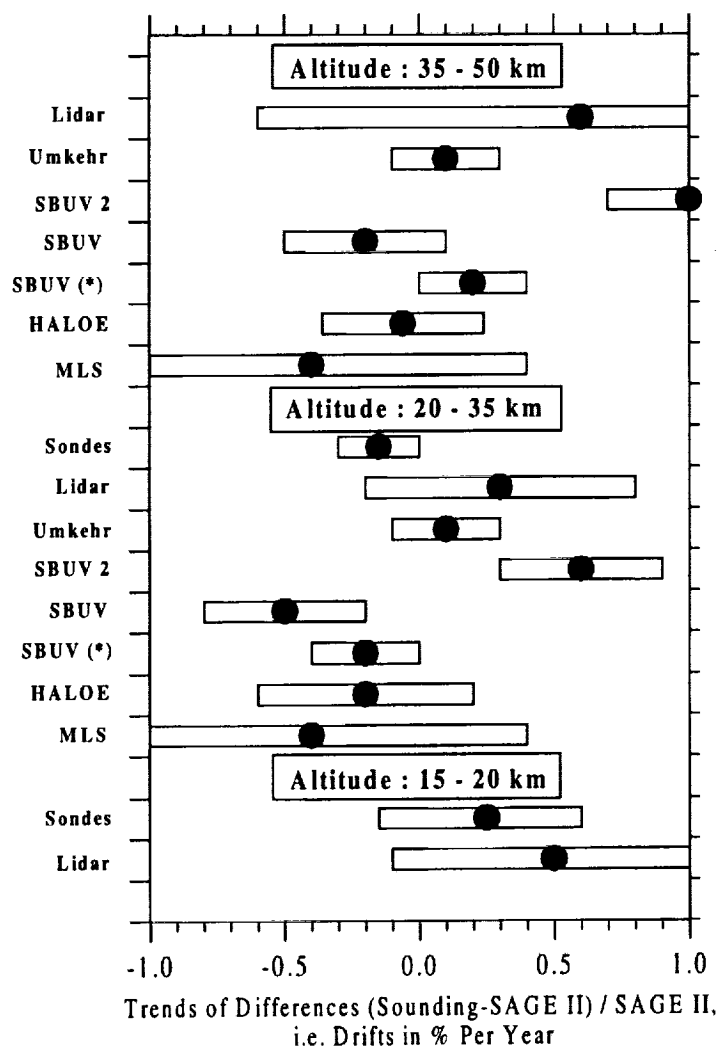


Figure 1. Trends of differences (i.e. drifts) between ozone measurements made by various ozone profiling instruments and SAGE II in % per year [(Sounding - SAGE II)/SAGE II]. Trends with ozonesondes are for the eight northern mid-latitude sounding stations used in Chapter 3 covering 36°N to 56°N. Umkehr differences are averages for eight Northern and Southern Hemisphere stations. Lidar differences are averages for the three stations with the longest records and number of coincidences exceeding 100 (Hohenpeissenberg, OHP and TMF). Trends of satellite differences (SBUV, SBUV2, HALOE and MLS) are presented as global means. The average differences are indicated by the dots and the bars represent the 95% confidence intervals of the drift estimations.

The results of a novel coordinate mapping (CM) study show general agreement with the conventional inter-comparisons, which rely on measurement space and time coincidence. Near 25 km, both the CM and conventional techniques show statistically significant regression slopes of differences in the 40-50°S (1-1.5%year⁻¹) and 60-70°S (~0.5%year⁻¹) regions. Differences between the two satellite measurements also appear in the CM analysis near 40-50°N in the same altitude range with the CM technique indicating a marginally significant positive drift of SAGE II relative to HALOE of $\sim 1 \pm 0.75\% \text{year}^{-1}$. At higher altitudes, CM results show insignificant drifts of less than 0.5%year⁻¹ in all regions except the polar summer latitudes. Differences in this region, which cannot be directly compared to conventional results, indicate statistically significant trends of differences, with SAGE ozone trends being larger relative to HALOE. A Lagrangian approach was tested which used air parcel trajectories to link measurements. This technique was only tested for a limited time period and so was unsuitable for use in assessing long-term stability, but it also shows great promise for applications in the future. Some evidence exists to suggest that SAGE I and SAGE II overlapping measurements are inconsistent (e.g., the comparisons with the ozonesonde measurements at Hohenpeissenberg, Payerne and Uccle), but the results are not statistically significant. It is recalled that SAGE I data have been corrected for a systematic reference height error of approximately 300 m (latitude dependent). The uncertainty in this correction for each latitude is approximately 100 m. Below 20 km altitude a simple upward shift of the SAGE I profiles (as assumed for this report) may be incorrect because of the large Rayleigh scattering contribution to the 0.6 nm extinction at these altitudes. A new inversion of the SAGE I data to correct the altitude registration problem would be preferable. Data can be used for trends with caution below 20 km, but more inter-comparisons are needed to draw firm conclusions.

Comparisons of ozonesondes in the stratosphere with other ozone profiling techniques show consistent results with agreement of about $\pm(3-5)\%$ at altitudes between the tropopause and 28 km. The precision of the different sonde types is better than $\pm 3\%$. Above 28 km the results are not consistent due to instrumental uncertainties (e.g. pump corrections and sensing solution changes) and caution must be used, at least for the non-ECC types of sondes, when applying the data for long-term trend determinations.

There is a dearth of sonde validation studies for the troposphere. Because of the small number of comparisons, only estimates about the reliability of the sonde data records below the tropopause can be made. In general, ECC-sondes provide much more consistent results than the other two types of sondes considered in the report. The precision of the ECC-sonde is better than $\pm (5-10)\%$ and shows a small positive bias of about 3%. Brewer Mast and KC79-sondes are less precise ($\pm(10-20)\%$), but there are no indications of any bias larger than $\pm 5\%$. Key issues of uncertainty are the background correction and the use of the total ozone normalisation factor.

The main reasons for observed differences between different sonde results from sounding stations using the same type of ozone sonde are believed to be due to differences in the preparation and correction procedures applied at the different launch sites. Although much progress has been made to improve the quality and homogeneity of the ozonesonde data since the last WMO Scientific Assessment of Stratospheric Ozone in 1994, there is still an urgent need

to investigate and intercompare the instrumental performance of the different sonde types as well as a need to revise and agree on procedures for preparation and data processing.

1.2 Trend Analyses

The statistical models used in the report were inter-compared using three test data sets. This comparison revealed only minor differences in trends obtained by the models. Somewhat greater differences were found in the uncertainties estimated for the trends and other variables included in the models. Results are most sensitive to the details of the models for time series with significant missing data. Quasi-decadal variations are a ubiquitous feature of ozone observations, in addition to QBO and faster time scale dynamical variability. Inclusion of these terms does not have a strong influence on the calculated trends for long time series. Much of the observed decadal change is approximately in phase with the solar cycle for the observational record, suggesting a solar mechanism. However, current model calculations of the solar effect show some inconsistencies with observations (in terms of magnitude and lower stratospheric response), and this limits confidence in our detailed understanding. It is also likely that a confusion exists between solar and volcanic signals for the recent record. Although these effects have relatively small impacts on the linear trend estimates, it does limit the ability to interpret decadal variability.

Figure 2 shows the mean trend vs. altitude at northern mid-latitudes obtained for combined measurement systems including estimated uncertainties from both the statistical and instrumental analyses. This averaging of trends from SAGE I/II, ozonesondes, Umkehr and SBUV is possible for the first time in a major assessment because there is now agreement between the systems in the regions where the measurements overlap. A few points are worth noting before discussing the trend findings further:

- (a) The trends below 20 km shown in figure 2 are found from the ozonesondes alone. There is now reasonable agreement in the trends at these altitudes between ozonesondes and SAGE I/II (which has occurred mainly as a result of the revised SAGE aerosol correction), but uncertainties in the SAGE I altitude registration below 20 km are considered too large for the SAGE I/II trends to be used in this context,
- (b) The ozone losses are statistically significant at all altitudes between 12 and 50 km,
- (c) There are two clear maxima in the trends, one around 40 km altitude, the other at about 15 km.

The upper stratosphere (altitudes between about 30 and 50 km) is a region where changes in ozone were originally predicted to occur. This is a region in which the chemistry should be dominated by gas-phase reactions. When the upper stratospheric data are fit to a standard statistical model, negative trends are found throughout the region with statistically significant peak values of -6 to -8% per decade at 40-45 km altitude. There is a factor of two seasonal variation, with a maximum negative trend in winter. There is no significant inter-hemispheric difference in upper stratospheric trends based on SAGE I/II version 5.96 data extended through 1996. There is good agreement between SAGE I/II and Umkehr. The SBUV-SBUV2 combined

record shows less negative trends. Less confidence is placed in the SBUV-SBUV2 result due to potential problems with the present version (6.1.2) of the NOAA-11 SBUV2 data.

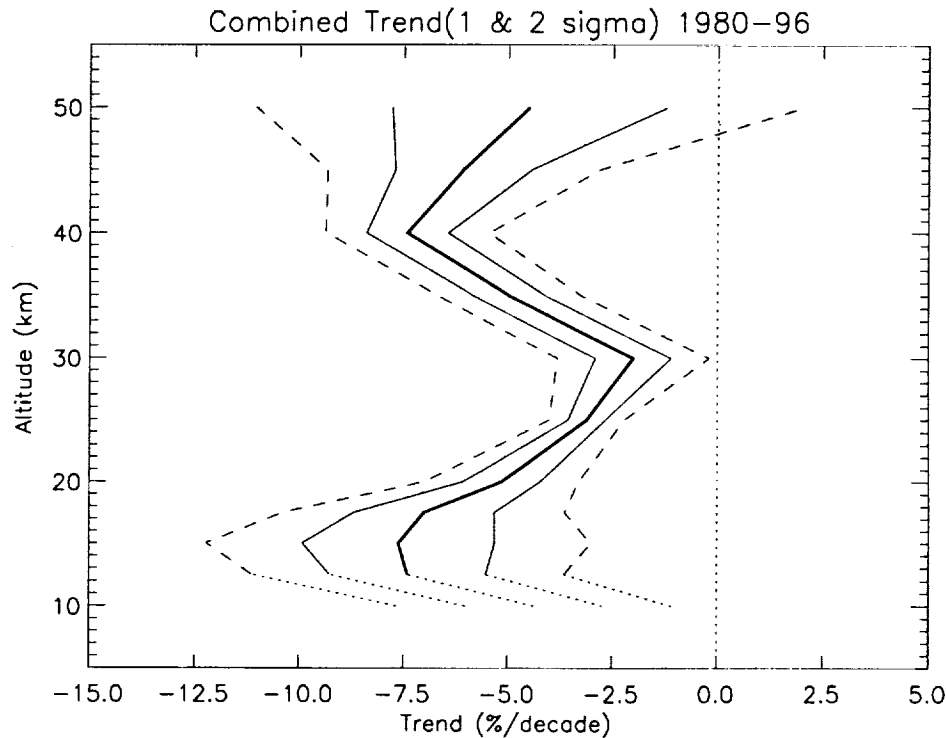


Figure 2. Estimate of the mean trend in the vertical distribution of ozone that has occurred over northern mid-latitudes from 1980-1996 (heavy solid line) calculated using the trends derived from SAGE I/II, ozonesondes, SBUV and Umkehr measurements. Combined uncertainties are shown as 1σ (light solid lines) and 2σ (dashed lines). The combined trends and uncertainties are extended down to 10 km as shown by the light dotted lines. The results below 15 km are a mixture of stratospheric and tropospheric trends and the exact numbers should be viewed with caution. Combined trends have not been extended lower into the troposphere because there are concerns regarding the representativeness of any mean trends derived from the small sample of sonde stations.

The lower stratosphere (altitudes below 30 km) is the region where much of the trend which has been deduced from column data is expected to occur. The primary trend instruments in this region are sondes (up to 27 km) and SAGE (20-30 km). For sondes, sampling of the data prior to trend analysis has as much or more effect on derived trends than do the details of the statistical model. The optimal selection criteria for the use of sonde data in trend analyses is a subject of debate. Trends from 8 individual stations in the northern mid-latitudes are negative throughout the lower stratosphere. They range from -3 to -11% per decade at 20 km and are statistically significant at all stations. The trends show little seasonal variability above 20 km. The seasonal variability in the trend in the ozone profile occurs mostly in the altitude range of 10-20 km. The exact time dependence of this seasonal variability is uncertain. European stations show a winter-spring maximum, while Canadian stations show a spring-summer maximum. Details of this seasonal maximum were somewhat different in the two analyses of the sonde data. There is a reasonable agreement between SAGE I/II trends and sonde trends over the altitude region from 15 to 27 km at northern mid-latitudes. The agreement between 15 and 20 km may be fortuitous.

SAGE II trends in the 15-20 km region in the tropics are much more negative than those in northern mid-latitudes but there are insufficient sonde records with which to compare these results (or those at southern mid-latitudes).

It is difficult to make generalisations concerning trends in tropospheric ozone. The only data from which to make conclusions is sonde data from a small number of stations. Trends calculated for Canadian stations are negative or near zero for the period from 1970 through 1996 and also for the period from 1980 through 1996. Trends calculated for 3 European stations are strongly positive for the period 1970 through 1996 but are essentially zero at two of these stations when data from 1980 through 1996 are considered. Trends calculated for the Japanese stations show a mixture of positive and insignificant for both time periods.

Trends in the column amount of ozone above 20 km deduced from SAGE I/II are much smaller than the column trends deduced from TOMS. The TOMS/SAGE differences are consistent with the sonde trends below 20 km. There is also a consistent seasonal variation between satellite and sonde data. Both indicate that the primary seasonal variation in mid-latitude ozone trends occurs at altitudes between 10 and 20 km with a clear maximum over northern mid-latitudes during the local winter-spring period and a much smaller seasonal cycle in the southern hemisphere.

REFERENCES

- Wang, H.J., D.M. Cunnold, and X. Bo, A critical analysis of SAGE ozone trends, *J. Geophys. Res.*, 101, 12,495-12,514, 1996.
- World Meteorological Organisation (WMO), Report of the International Ozone Trends Panel: 1988, Global Ozone and Monit. Network, WMO. Report No. 18, Geneva, 1990.
- WMO/UNEP, *Scientific assessment of ozone depletion: 1994*, Global Ozone and Monitoring Network, WMO. Report No. 37, Geneva, 1995.

SECTION D

POLICYMAKERS SUMMARY OF THE INTERGOVERNMENTAL PANEL ON CLIMATE CHANGE (IPCC) SPECIAL REPORT ON AVIATION AND THE GLOBAL ATMOSPHERE

This summary, approved in detail at a joint session of IPCC Working Groups I and III (San José, Costa Rica • 12-14 April 1999), represents the formally agreed statement of the IPCC concerning current understanding of aviation and the global atmosphere.

1. INTRODUCTION

This report assesses the effects of aircraft on climate and atmospheric ozone and is the first IPCC report for a specific industrial subsector. It was prepared by IPCC in collaboration with the Scientific Assessment Panel to the Montreal Protocol on Substances that Deplete the Ozone Layer, in response to a request by the International Civil Aviation Organization (ICAO)¹ because of the potential impact of aviation emissions. These are the predominant anthropogenic emissions deposited directly into the upper troposphere and lower stratosphere.

Aviation has experienced rapid expansion as the world economy has grown. Passenger traffic (expressed as revenue passenger-kilometers²) has grown since 1960 at nearly 9% per year, 2.4 times the average Gross Domestic Product (GDP) growth rate. Freight traffic, approximately 80% of which is carried by passenger airplanes, has also grown over the same time period. The rate of growth of passenger traffic has slowed to about 5% in 1997 as the industry is maturing. Total aviation emissions have increased, because increased demand for air transport has outpaced the reductions in specific emissions³ from the continuing improvements in technology and operational procedures. Passenger traffic, assuming unconstrained demand, is projected to grow at rates in excess of GDP for the period assessed in this report.

The effects of current aviation and of a range of unconstrained growth projections for aviation (which include passenger, freight, and military) are examined in this report, including the possible effects of a fleet of second generation, commercial supersonic aircraft. The report also describes current aircraft technology, operating procedures, and options for mitigating aviation's future impact on the global atmosphere. The report does not consider the local environmental effects of aircraft engine emissions or any of the indirect environmental effects of aviation operations such as energy usage by ground transportation at airports.

¹ ICAO is the UN specialized agency that has global responsibility for the establishment of standards, recommended practices, and guidance on various aspects of international civil aviation, including environmental protection.

² The revenue passenger-km is a measure of the traffic carried by commercial aviation: one revenue-paying passenger carried 1 km.

³ Specific emissions are emissions per unit of traffic carried, for instance, per revenue passenger-km.]

2. HOW DO AIRCRAFT AFFECT CLIMATE AND OZONE?

Aircraft emit gases and particles directly into the upper troposphere and lower stratosphere where they have an impact on atmospheric composition. These gases and particles alter the concentration of atmospheric greenhouse gases, including carbon dioxide (CO₂), ozone (O₃), and methane (CH₄); trigger formation of condensation trails (contrails); and may increase cirrus cloudiness—all of which contribute to climate change (see Box 1).

The principal emissions of aircraft include the greenhouse gases carbon dioxide and water vapor (H₂O). Other major emissions are nitric oxide (NO) and nitrogen dioxide (NO₂) (which together are termed NO_x), sulfur oxides (SO_x), and soot. The total amount of aviation fuel burned, as well as the total emissions of carbon dioxide, NO_x, and water vapor by aircraft, are well known relative to other parameters important to this assessment.

The climate impacts of the gases and particles emitted and formed as a result of aviation are more difficult to quantify than the emissions; however, they can be compared to each other and to climate effects from other sectors by using the concept of radiative forcing.⁴ Because carbon dioxide has a long atmospheric residence time (≈100 years) and so becomes well mixed throughout the atmosphere, the effects of its emissions from aircraft are indistinguishable from the same quantity of carbon dioxide emitted by any other source. The other gases (e.g., NO_x, SO_x, water vapor) and particles have shorter atmospheric residence times and remain concentrated near flight routes, mainly in the northern mid-latitudes. These emissions can lead to radiative forcing that is regionally located near the flight routes for some components (e.g., ozone and contrails) in contrast to emissions that are globally mixed (e.g., carbon dioxide and methane).

The global mean climate change is reasonably well represented by the global average radiative forcing, for example, when evaluating the contributions of aviation to the rise in globally averaged temperature or sea level. However, because some of aviation's key contributions to radiative forcing are located mainly in the northern mid-latitudes, the regional climate response may differ from that derived from a global mean radiative forcing. The impact of aircraft on regional climate could be important, but has not been assessed in this report.

Ozone is a greenhouse gas. It also shields the surface of the earth from harmful ultraviolet (UV) radiation, and is a common air pollutant. Aircraft-emitted NO_x participates in ozone chemistry. Subsonic aircraft fly in the upper troposphere and lower stratosphere (at altitudes of about 9 to 13 km), whereas supersonic aircraft cruise several kilometers higher (at about 17 to 20 km) in the stratosphere. Ozone in the upper troposphere and lower stratosphere is expected to increase in response to NO_x increases and methane is expected to decrease. At higher altitudes, increases in NO_x lead to decreases in the stratospheric ozone layer. Ozone precursor (NO_y) lifetimes in these regions increase with altitude, hence perturbations to ozone by aircraft depend on the altitude of NO_x injection and vary from regional in scale in the troposphere to global in scale in the stratosphere.

⁴ Radiative forcing is a measure of the importance of a potential climate change mechanism. It expresses the perturbation or change to the energy balance of the Earth-atmosphere system in watts per square meter (Wm⁻²). Positive values of radiative forcing imply a net warming, while negative values imply cooling.

Box 1. The Science of Climate Change

Some of the main conclusions of the Summary for Policymakers of Working Group I of the IPCC Second Assessment Report, published in 1995, which concerns the effects of all anthropogenic emissions on climate change, are the following:

- Increases in greenhouse gas concentrations since pre-industrial times (i.e., since about 1750) have led to a positive radiative forcing of climate, tending to warm the surface of the Earth and produce other changes of climate.
- The atmospheric concentrations of the greenhouse gases carbon dioxide, methane, and nitrous oxide (N₂O), among others, have grown significantly: by about 30, 145, and 15% respectively (values for 1992). These trends can be attributed largely to human activities, mostly fossil fuel use, land-use change, and agriculture.
- Many greenhouse gases remain in the atmosphere for a long time (for carbon dioxide and nitrous oxide, many decades to centuries). As a result of this, if carbon dioxide emissions were maintained at near current (1994) levels, they would lead to a nearly constant rate of increase in atmospheric concentrations for at least two centuries, reaching about 500 ppmv (approximately twice the pre-industrial concentration of 280 ppmv) by the end of the 21st century.
- Tropospheric aerosols resulting from combustion of fossil fuels, biomass burning, and other sources have led to a negative radiative forcing, which, while focused in particular regions and subcontinental areas, can have continental to hemispheric effects on climate patterns. In contrast to the long-lived greenhouse gases, anthropogenic aerosols are very short-lived in the atmosphere; hence, their radiative forcing adjusts rapidly to increases or decreases in emissions.
- Our ability from the observed climate record to quantify the human influence on global climate is currently limited because the expected signal is still emerging from the noise of natural variability, and because there are uncertainties in key factors. These include the magnitude and patterns of long-term natural variability and the time-evolving pattern of forcing by, and response to, changes in concentrations of greenhouse gases and aerosols, and land-surface changes. Nevertheless, the balance of evidence suggests that there is a discernible human influence on global climate.
- The IPCC has developed a range of scenarios, IS92a-f, for future greenhouse gas and aerosol precursor emissions based on assumptions concerning population and economic growth, land use, technological changes, energy availability, and fuel mix during the period 1990 to 2100. Through understanding of the global carbon cycle and of atmospheric chemistry, these emissions can be used to project atmospheric concentrations of greenhouse gases and aerosols and the perturbation of natural radiative forcing. Climate models can then be used to develop projections of future climate.
- Estimates of the rise in global average surface air temperature by 2100 relative to 1990 for the IS92 scenarios range from 1 to 3.5°C. In all cases the average rate of warming would probably be greater than any seen in the last 10,000 years. Regional temperature changes could differ substantially from the global mean and the actual annual to decadal changes would include considerable natural variability. A general warming is expected to lead to an increase in the occurrence of extremely hot days and a decrease in the occurrence of extremely cold days.
- Average sea level is expected to rise as a result of thermal expansion of the oceans and melting of glaciers and ice-sheets. Estimates of the sea level rise by 2100 relative to 1990 for the IS92 scenarios range from 15 to 95 cm.
- Warmer temperatures will lead to a more vigorous hydrological cycle; this translates into prospects for more severe droughts and/or floods in some places and less severe droughts and/or floods in other places. Several models indicate an increase in precipitation intensity, suggesting a possibility for more extreme rainfall events.

Water vapor, SO_x (which form sulfate particles) and soot⁵ play both direct and indirect roles in climate change and ozone chemistry.

⁵ Airborne sulfate particles and soot particles are both examples of aerosols. Aerosols are microscopic particles suspended in air.]

3. HOW ARE AVIATION EMISSIONS PROJECTED TO GROW IN THE FUTURE?

Global passenger air travel, as measured in revenue passenger-km, is projected to grow by about 5% per year between 1990 and 2015, whereas total aviation fuel use—including passenger, freight, and military⁶—is projected to increase by 3% per year, over the same period, the difference being due largely to improved aircraft efficiency. Projections beyond this time are more uncertain so a range of future unconstrained emission scenarios is examined in this report (see Table 1 and Figure 1). All of these scenarios assume that technological improvements leading to reduced emissions per revenue passenger-km will continue in the future and that optimal use of airspace availability (i.e., ideal air traffic management) is achieved by 2050. If these improvements do not materialize then fuel use and emissions will be higher. It is further assumed that the number of aircraft as well as the number of airports and associated infrastructure will continue to grow and not limit the growth in demand for air travel. If the infrastructure were not available, the growth of traffic reflected in these scenarios would not materialize.

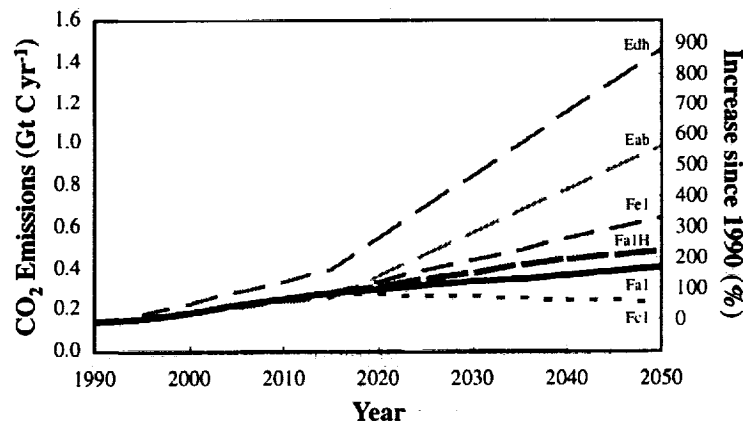


Figure 1. Total aviation carbon dioxide emissions resulting from six different scenarios for aircraft fuel use. Emissions are given in Gt C [or billion (10^9) tonnes of carbon] per year. To convert Gt C to Gt CO₂ multiply by 3.67. The scale on the righthand axis represents the percentage growth from 1990 to 2050. Aircraft emissions of carbon dioxide represent 2.4% of total fossil fuel emissions of carbon dioxide in 1992 or 2% of total anthropogenic carbon dioxide emissions. (Note: Fa2 has not been drawn because the difference from scenario Fa1 would not be discernible on the figure.)

IPCC [1992]⁷ developed a range of scenarios, IS92a-f, of future greenhouse gas and aerosol precursor emissions based on assumptions concerning population and economic growth, land use, technological changes, energy availability, and fuel mix during the period 1990 to 2100. Scenario IS92a is a mid-range emissions scenario. Scenarios of future emissions are not predictions of the future. They are inherently uncertain because they are based on different assumptions about the future, and the longer the time horizon the more uncertain these scenarios become. The aircraft emissions scenarios developed here used the economic growth and

⁶ The historical breakdown of aviation fuel burn for civil (passenger plus cargo) and military aviation was 64 and 36%, respectively, in 1976, and 82 and 18%, respectively, in 1992. These are projected to change to 93 and 7%, respectively, in 2015, and to 97 and 3%, respectively, in 2050.

⁷ IPCC, 1992: *Climate Change 1992: The Supplementary Report to the IPCC Scientific Assessment* [Houghton, J.T., B.A. Callander, and S.K. Varney (eds.)]. Cambridge University Press, Cambridge, UK, 200 pp.

population assumptions found in the IS92 scenario range (see Table 1 and Figure 1). In the following sections, scenario Fa1 is utilized to illustrate the possible effects of aircraft and is called the reference scenario. Its assumptions are linked to those of IS92a. The other aircraft emissions scenarios were built from a range of economic and population projections from IS92a-e. These scenarios represent a range of plausible growth for aviation and provide a basis

Table 1: Summary of future global aircraft scenarios used in this report.

Scenario Name	Avg. Traffic Growth per year (1990-2050) ¹	Avg. Annual Growth Rate of Fuel Burn (1990-2050) ²	Avg. Annual Economic Growth Rate	Avg. Annual Population Growth Rate	Ratio of Traffic 2050/1990	Ratio of Fuel Burn 2050/1990	Notes
Fa1	3.1%	1.7%	2.9% 1990-2025 2.3% 1990-2025	1.4% 1990-2025 0.7% 1990-2025	6.4	2.7	Reference scenario developed by ICAO Forecasting and Economic Support Group (FESG); mid-range economic growth from IPCC [1992]; technology for both improved fuel efficiency and NO _x reduction
Fa1H	3.1%	1.7%	2.9% 1990-2025 2.3% 1990-2100	1.4% 1990-2025 0.7% 1990-2100	6.4	2.7	Fa1 traffic and technology scenario with a fleet of supersonic aircraft replacing some of the subsonic fleet
Fa2	3.1%	1.7%	2.9% 1990-2025 2.3% 1990-2100	1.4% 1990-2025 0.7% 1990-2100	6.4	2.7	Fa1 traffic scenario; technology with greater emphasis on NO _x reduction, but slightly smaller fuel efficiency improvement
Fc1	3.1%	1.7%	2.9% 1990-2025 2.3% 1990-2100	1.4% 1990-2025 0.7% 1990-2100	6.4	2.7	FESG low-growth scenario technology as for Fa1 scenario
Fe1	3.1%	1.7%	2.9% 1990-2025 2.3% 1990-2100	1.4% 1990-2025 0.7% 1990-2100	6.4	2.7	FESG high-growth scenario technology as for Fa1 scenario
Eab	4.0%	3.2%			10.7	6.6	Traffic-growth scenario based on IS92a developed by Environmental Defense Fund (EDF); technology for very low NO _x assumed
Edh	4.7%	3.8%			15.5	9.4	High traffic-growth EDF scenario; Technology for very low NO _x assumed

¹ Traffic measured in terms of revenue passenger-km.

² All aviation (passenger, freight, and military).

for sensitivity analysis for climate modeling. However, the high growth scenario Edh is believed to be less plausible and the low growth scenario Fc1 is likely to be exceeded given the present state of the industry and planned developments.

4. WHAT ARE THE CURRENT AND FUTURE IMPACTS OF SUBSONIC AVIATION ON RADIATIVE FORCING AND UV RADIATION?

The summary of radiative effects resulting from aircraft engine emissions is given in Figures 2 and 3. As shown in Figure 2, the uncertainty associated with several of these effects is large.

4.1. Carbon Dioxide

Emissions of carbon dioxide by aircraft were 0.14 Gt C/year in 1992. This is about 2% of total anthropogenic carbon dioxide emissions in 1992 or about 13% of carbon dioxide emissions from all transportation sources. The range of scenarios considered here projects that aircraft emissions of carbon dioxide will continue to grow and by 2050 will be 0.23 to 1.45 Gt C/year. For the reference scenario (Fa1) this emission increases 3-fold by 2050 to 0.40 Gt C/year, or 3% of the projected total anthropogenic carbon dioxide emissions relative to the mid-range IPCC emission scenario (IS92a). For the range of scenarios, the range of increase in carbon dioxide emissions to 2050 would be 1.6 to 10 times the value in 1992.

Concentrations of and radiative forcing from carbon dioxide today are those resulting from emissions during the last 100 years or so. The carbon dioxide concentration attributable to aviation in the 1992 atmosphere is 1 ppmv, a little more than 1% of the total anthropogenic increase. This percentage is lower than the percentage for emissions (2%) because the emissions occurred only in the last 50 years. For the range of scenarios in Figure 1, the accumulation of atmospheric carbon dioxide due to aircraft over the next 50 years is projected to increase to 5 to 13 ppmv. For the reference scenario (Fa1) this is 4% of that from all human activities assuming the mid-range IPCC scenario (IS92a).

4.2. Ozone

The NO_x emissions from subsonic aircraft in 1992 are estimated to have increased ozone concentrations at cruise altitudes in northern mid-latitudes by up to 6%, compared to an atmosphere without aircraft emissions. This ozone increase is projected to rise to about 13% by 2050 in the reference scenario (Fa1). The impact on ozone concentrations in other regions of the world is substantially less. These increases will, on average, tend to warm the surface of the Earth.

Aircraft emissions of NO_x are more effective at producing ozone in the upper troposphere than an equivalent amount of emission at the surface. Also increases in ozone in the upper troposphere are more effective at increasing radiative forcing than increases at lower altitudes. Due to these increases the calculated total ozone column in northern mid-latitudes is projected to grow by approximately 0.4 and 1.2% in 1992 and 2050, respectively. However, aircraft sulfur and water emissions in the stratosphere tend to deplete ozone, partially offsetting the NO_x-induced ozone increases. The degree to which this occurs is, as yet, unquantified. Therefore, the impact of subsonic aircraft emissions on stratospheric ozone requires further evaluation. The largest increases in ozone concentration due to aircraft emissions are calculated to occur near the tropopause where natural variability is high. Such changes are not apparent from observations at this time.

4.3. Methane

In addition to increasing tropospheric ozone concentrations, aircraft NO_x emissions are expected to decrease the concentration of methane, which is also a greenhouse gas. These reductions in methane tend to cool the surface of the Earth. The methane concentration in 1992 is estimated here to be about 2% less than that in an atmosphere without aircraft. This aircraft-induced reduction of methane concentration is much smaller than the observed overall 2.5-fold increase since pre-industrial times. Uncertainties in the sources and sinks of methane preclude testing the impact of aviation on methane concentrations with atmospheric observations. In the reference scenario (Fa1) methane would be about 5% less than that calculated for a 2050 atmosphere without aircraft.

Changes in tropospheric ozone are mainly in the Northern Hemisphere, while those of methane are global in extent so that, even though the global average radiative forcings are of similar magnitude and opposite in sign, the latitudinal structure of the forcing is different so that the net regional radiative effects do not cancel.

4.4. Water Vapor

Most subsonic aircraft water vapor emissions are released in the troposphere where they are rapidly removed by precipitation within 1 to 2 weeks. A smaller fraction of water vapor emissions is released in the lower stratosphere where it can build up to larger concentrations. Because water vapor is a greenhouse gas, these increases tend to warm the Earth's surface, though for subsonic aircraft this effect is smaller than those of other aircraft emissions such as carbon dioxide and NO_x .

4.5. Contrails

In 1992, aircraft line-shaped contrails are estimated to cover about 0.1% of the Earth's surface on an annually averaged basis with larger regional values. Contrails tend to warm the Earth's surface, similar to thin high clouds. The contrail cover is projected to grow to 0.5% by 2050 in the reference scenario (Fa1), at a rate which is faster than the rate of growth in aviation fuel consumption. This faster growth in contrail cover is expected because air traffic will increase mainly in the upper troposphere where contrails form preferentially, and may also occur as a result of improvements in aircraft fuel efficiency. Contrails are triggered from the water vapor emitted by aircraft and their optical properties depend on the particles emitted or formed in the aircraft plume and on the ambient atmospheric conditions. The radiative effect of contrails depends on their optical properties and global cover, both of which are uncertain. Contrails have been observed as line-shaped clouds by satellites over heavy air traffic areas and covered on average about 0.5% of the area over Central Europe in 1996 and 1997.

4.6. Cirrus Clouds

Extensive cirrus clouds have been observed to develop after the formation of persistent contrails. Increases in cirrus cloud cover (beyond those identified as line-shaped contrails) are found to be positively correlated with aircraft emissions in a limited number of studies. About 30% of the

Earth is covered with cirrus cloud. *On average an increase in cirrus cloud cover tends to warm the surface of the Earth. An estimate for aircraft-induced cirrus cover for the late 1990s ranges from 0 to 0.2% of the surface of the Earth. For the Fa1 scenario, this may possibly increase by a factor of 4 (0 to 0.8%) by 2050; however, the mechanisms associated with increases in cirrus cover are not well understood and need further investigation.*

4.7. Sulfate and Soot Aerosols

The aerosol mass concentrations in 1992 resulting from aircraft are small relative to those caused by surface sources. Although aerosol accumulation will grow with aviation fuel use, aerosol mass concentrations from aircraft in 2050 are projected to remain small compared to surface sources. Increases in soot tend to warm while increases in sulfate tend to cool the Earth's surface. The direct radiative forcing of sulfate and soot aerosols from aircraft is small compared to those of other aircraft emissions. Because aerosols influence the formation of clouds, the accumulation of aerosols from aircraft may play a role in enhanced cloud formation and change the radiative properties of clouds.

4.8. What are the Overall Climate Effects of Subsonic Aircraft?

The climate impacts of different anthropogenic emissions can be compared using the concept of radiative forcing. The best estimate of the radiative forcing in 1992 by aircraft is 0.05 Wm^{-2} or about 3.5% of the total radiative forcing by all anthropogenic activities. For the reference scenario (Fa1), the radiative forcing by aircraft in 2050 is 0.19 Wm^{-2} or 5% of the radiative forcing in the mid-range IS92a scenario (3.8 times the value in 1992). According to the range of scenarios considered here, the forcing is projected to grow to 0.13 to 0.56 Wm^{-2} in 2050, which is a factor of 1.5 less to a factor of 3 greater than that for Fa1 and from 2.6 to 11 times the value in 1992. These estimates of forcing combine the effects from changes in concentrations of carbon dioxide, ozone, methane, water vapor, line-shaped contrails, and aerosols, but do not include possible changes in cirrus clouds.

Globally averaged values of the radiative forcing from different components in 1992 and in 2050 under the reference scenario (Fa1) are shown in Figure 2. Figure 2 indicates the best estimates of the forcing for each component and the two-thirds uncertainty range. The derivation of these uncertainty ranges involves expert scientific judgment and may also include objective statistical models. The uncertainty range in the radiative forcing stated here combines the uncertainty in calculating the atmospheric change to greenhouse gases and aerosols with that of calculating radiative forcing. For additional cirrus clouds, only a range for the best estimate is given; this is not included in the total radiative forcing.

The state of scientific understanding is evaluated for each component. This is not the same as the confidence level expressed in previous IPCC documents. This evaluation is separate from the uncertainty range and is a relative appraisal of the scientific understanding for each component. The evaluation is based on the amount of evidence available to support the best estimate and its uncertainty, the degree of consensus in the scientific literature, and the scope of the analysis. The total radiative forcing under each of the six scenarios for the growth of aviation is shown in Figure 3 for the period 1990 to 2050.

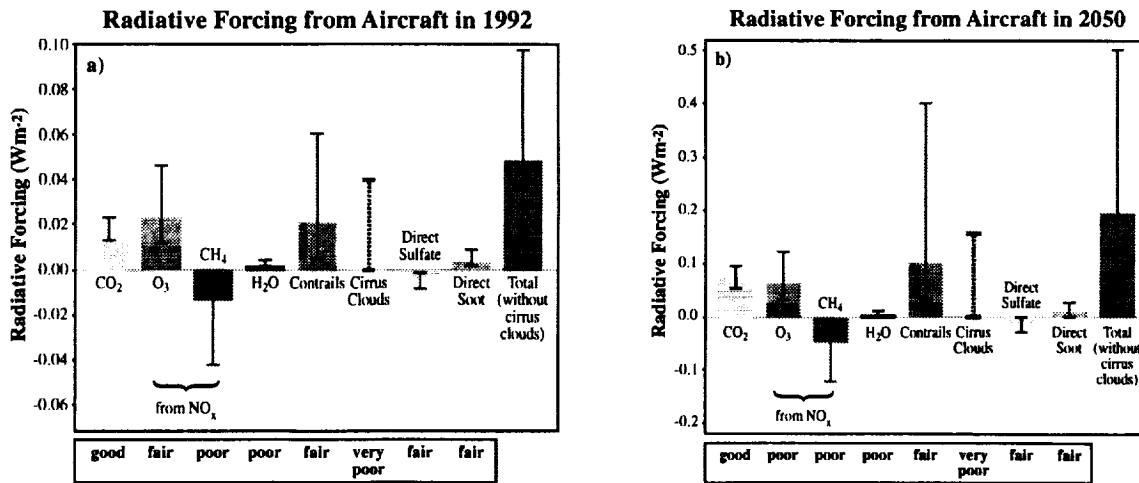


Figure 2. Estimates of the globally and annually averaged radiative forcing (Wm^{-2}) (see Footnote 4) from subsonic aircraft emissions in 1992 (2a) and in 2050 for scenario Fa1 (2b). The scale in Figure 2b is greater than the scale in 2a by about a factor of 4. The bars indicate the best estimate of forcing while the line associated with each bar is a two-thirds uncertainty range developed using the best knowledge and tools available at the present time. (The two-thirds uncertainty range means that there is a 67% probability that the true value falls within this range.) The available information on cirrus clouds is insufficient to determine either a best estimate or an uncertainty range; the dashed line indicates a range of possible best estimates. The estimate for total forcing does not include the effect of changes in cirrus cloudiness. The uncertainty estimate for the total radiative forcing (without additional cirrus) is calculated as the square root of the sums of the squares of the upper and lower ranges for the individual components. The evaluation below the graph (“good,” “fair,” “poor,” “very poor”) are a relative appraisal associated with each component and indicates the level of scientific understanding. It is based on the amount of evidence available to support the best estimate and its uncertainty, the degree of consensus in the scientific literature, and the scope of the analysis. This evaluation is separate from the evaluation of uncertainty range represented by the lines associated with each bar. This method of presentation is different and more meaningful than the confidence level presented in similar graphs from *Climate Change 1995: The Science of Climate Change*.

The total radiative forcing due to aviation (without forcing from additional cirrus) is likely to lie within the range from 0.01 to 0.1 Wm^{-2} in 1992, with the largest uncertainties coming from contrails and methane. Hence the total radiative forcing may be about 2 times larger or 5 times smaller than the best estimate. For any scenario at 2050, the uncertainty range of radiative forcing is slightly larger than for 1992, but the largest variations of projected radiative forcing come from the range of scenarios.

Over the period from 1992 to 2050, the overall radiative forcing by aircraft (excluding that from changes in cirrus clouds) for all scenarios in this report is a factor of 2 to 4 larger than the forcing by aircraft carbon dioxide alone. The overall radiative forcing for the sum of all human activities is estimated to be at most a factor of 1.5 larger than that of carbon dioxide alone.

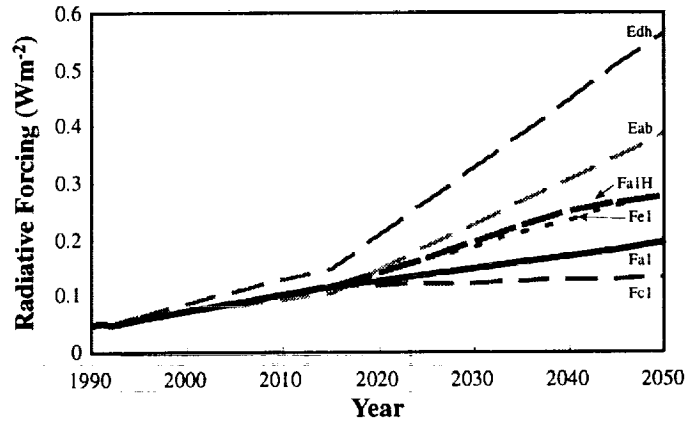


Figure 3. Estimates of the globally and annually averaged total radiative forcing (without cirrus clouds) associated with aviation emissions under each of six scenarios for the growth of aviation over the time period 1990 to 2050. (Fa2 has not been drawn because the difference from scenario Fa1 would not be discernible on the figure.)

The emissions of NO_x cause changes in methane and ozone, with influence on radiative forcing estimated to be of similar magnitude but of opposite sign. However, as noted above, the geographical distribution of the aircraft ozone forcing is far more regional than that of the aircraft methane forcing.

The effect of aircraft on climate is superimposed on that caused by other anthropogenic emissions of greenhouse gases and particles, and on the background natural variability. The radiative forcing from aviation is about 3.5% of the total radiative forcing in 1992. It has not been possible to separate the influence on global climate change of aviation (or any other sector with similar radiative forcing) from all other anthropogenic activities. Aircraft contribute to global change approximately in proportion to their contribution to radiative forcing.

4.9. What are the Overall Effects of Subsonic Aircraft on UV-B?

Ozone, most of which resides in the stratosphere, provides a shield against solar ultraviolet radiation. The erythemal dose rate, defined as UV irradiance weighted according to how effectively it causes sunburn, is estimated to be decreased by aircraft in 1992 by about 0.5% at 45°N in July. For comparison, the calculated increase in the erythemal dose rate due to observed ozone depletion is about 4% over the period 1970 to 1992 at 45°N in July.⁸ The net effect of subsonic aircraft appears to be an increase in column ozone and a decrease in UV radiation, which is mainly due to aircraft NO_x emissions. Much smaller changes in UV radiation are associated with aircraft contrails, aerosols, and induced cloudiness. In the Southern Hemisphere, the calculated effects of aircraft emission on the erythemal dose rate are about a factor of 4 lower than for the Northern Hemisphere.

⁸ This value is based on satellite observations and model calculations. See Scientific Assessment of Ozone Depletion: 1998, WMO Global Ozone Research and Monitoring Project – Report No. 44, 1999.

For the reference scenario (Fa1), the change in erythemal dose rate at 45°N in July in 2050 compared to a simulation with no aircraft is -1.3% (with a two-thirds uncertainty range⁹ from -0.7 to -2.6%). For comparison, the calculated change in the erythemal dose rate due to changes in the concentrations of trace species, other than those from aircraft, between 1970 to 2050 at 45°N is about -3%, a decrease that is the net result of two opposing effects: (1) the incomplete recovery of stratospheric ozone to 1970 levels because of the persistence of long-lived halogen-containing compounds, and (2) increases in projected surface emissions of shorter lived pollutants that produce ozone in the troposphere.

5. WHAT ARE THE CURRENT AND FUTURE IMPACTS OF SUPERSONIC AVIATION ON RADIATIVE FORCING AND UV RADIATION?

One possibility for the future is the development of a fleet of second generation supersonic, high speed civil transport (HSCT) aircraft, although there is considerable uncertainty whether any such fleet will be developed. These supersonic aircraft are projected to cruise at an altitude of about 19 km, about 8 km higher than subsonic aircraft, and to emit carbon dioxide, water vapor, NO_x, SO_x, and soot into the stratosphere. NO_x, water vapor, and SO_x from supersonic aircraft emissions all contribute to changes in stratospheric ozone. The radiative forcing of civil supersonic aircraft is estimated to be about a factor of 5 larger than that of the displaced subsonic aircraft in the Fa1H scenario. The calculated radiative forcing of supersonic aircraft depends on the treatment of water vapor and ozone in models. This effect is difficult to simulate in current models and so is highly uncertain.

Scenario Fa1H considers the addition of a fleet of civil supersonic aircraft that was assumed to begin operation in the year 2015 and grow to a maximum of 1,000 aircraft by the year 2040. For reference, the civil subsonic fleet at the end of the year 1997 contained approximately 12,000 aircraft. In this scenario, the aircraft are designed to cruise at Mach 2.4, and new technologies are assumed that maintain emissions of 5 g NO₂ per kg fuel (lower than today's civil supersonic aircraft which has emissions of about 22 g NO₂ per kg fuel). These supersonic aircraft are assumed to replace part of the subsonic fleet (11%, in terms of emissions in scenario Fa1). Supersonic aircraft consume more than twice the fuel per passenger-km compared to subsonic aircraft. By the year 2050, the combined fleet (scenario Fa1H) is projected to add a further 0.08 Wm⁻² (42%) to the 0.19 Wm⁻² radiative forcing from scenario Fa1 (see Figure 4). Most of this additional forcing is due to accumulation of stratospheric water vapor.

The effect of introducing a civil supersonic fleet to form the combined fleet (Fa1H) is also to reduce stratospheric ozone and increase erythemal dose rate. The maximum calculated effect is at 45°N where, in July, the ozone column change in 2050 from the combined subsonic and supersonic fleet relative to no aircraft is -0.4%. The effect on the ozone column of the supersonic component by itself is -1.3% while the subsonic component is +0.9%.

The combined fleet would change the erythemal dose rate at 45°N in July by +0.3% compared to the 2050 atmosphere without aircraft. The two-thirds uncertainty range for the combined fleet is -1.7% to +3.3%. This may be compared to the projected change of -1.3% for Fa1. Flying

⁹ The two-thirds uncertainty range means that there is a 67% probability that the true value falls within this range.

higher leads to larger ozone column decreases, while flying lower leads to smaller ozone column decreases and may even result in an ozone column increase for flight in the lowermost stratosphere. In addition, emissions from supersonic aircraft in the Northern Hemisphere stratosphere may be transported to the Southern Hemisphere where they cause ozone depletion.

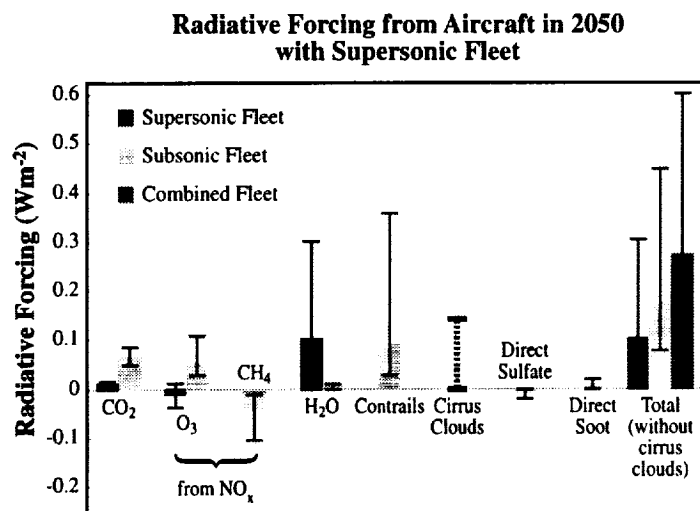


Figure 4. Estimates of the globally and annually averaged radiative forcing from a combined fleet of subsonic and supersonic aircraft (in Wm^{-2}) due to changes in greenhouse gases, aerosols, and contrails in 2050 under the scenarios Fa1H. In this scenario, the supersonic aircraft are assumed to replace part of the subsonic fleet (11%, in terms of emissions in scenario Fa1). The bars indicate the best estimate of forcing while the line associated with each is a two-thirds uncertainty range developed using the best knowledge and tools available at the present time. (The two-thirds uncertainty range means that there is a 67% probability that the true value falls within this range.) The available information on cirrus clouds is insufficient to determine either a best estimate or an uncertainty range; the dashed line indicates a range of possible best estimates. The estimate for total forcing does not include the effect of changes in cirrus cloudiness. The uncertainty estimate for the total radiative forcing (without additional cirrus) is calculated as the square root of the sums of the squares of the upper and lower ranges. The level of scientific understanding for the supersonic components are carbon dioxide, "good;" ozone, "poor;" and water vapor, "poor."

6. WHAT ARE THE OPTIONS TO REDUCE EMISSIONS AND IMPACTS?

There is a range of options to reduce the impact of aviation emissions, including changes in aircraft and engine technology, fuel, operational practices, and regulatory and economic measures. These could be implemented either singly or in combination by the public and/or private sector. Substantial aircraft and engine technology advances and the air traffic management improvements described in this report are already incorporated in the aircraft emissions scenarios used for climate change calculations. Other operational measures, which have the potential to reduce emissions, and alternative fuels were not assumed in the scenarios. Further technology advances have the potential to provide additional fuel and emissions reductions. In practice, some of the improvements are expected to take place for commercial reasons. The timing and scope of regulatory, economic, and other options may affect the introduction of improvements and may affect demand for air transport. Mitigation options for water vapor and cloudiness have not been fully addressed.

Safety of operation, operational and environmental performance, and costs are dominant considerations for the aviation industry when assessing any new aircraft purchase or potential engineering or operational changes. The typical life expectancy of an aircraft is 25 to 35 years. These factors have to be taken into account when assessing the rate at which technology advances and policy options related to technology can reduce aviation emissions.

6.1. Aircraft and Engine Technology Options

Technology advances have substantially reduced most emissions per passenger-km. However, there is potential for further improvements. Any technological change may involve a balance among a range of environmental impacts.

Subsonic aircraft being produced today are about 70% more fuel-efficient per passenger-km than 40 years ago. The majority of this gain has been achieved through engine improvements and the remainder from airframe design improvement. A 20% improvement in fuel efficiency is projected by 2015 and a 40 to 50% improvement by 2050 relative to aircraft produced today. The 2050 scenarios developed for this report already incorporate these fuel efficiency gains when estimating fuel use and emissions. Engine efficiency improvements reduce the specific fuel consumption and most types of emissions; however, contrails may increase and without advances in combustor technology NO_x emissions may also increase.

Future engine and airframe design involves a complex decision-making process and a balance of considerations among many factors (e.g., carbon dioxide emissions, NO_x emissions at ground level, NO_x emissions at altitude, water vapor emissions, contrail/cirrus production, and noise). These aspects have not been adequately characterized or quantified in this report.

Internationally, substantial research programs are in progress, with goals to reduce Landing and Take-off cycle (LTO) emissions of NO_x by up to 70% from today's regulatory standards, while also improving engine fuel consumption by 8 to 10%, over the most recently produced engines, by about 2010. Reduction of NO_x emissions would also be achieved at cruise altitude, though not necessarily by the same proportion as for Landing and Take-off. Assuming that the goals can be achieved, the transfer of this technology to significant numbers of newly produced aircraft will take longer—typically a decade. Research programs addressing NO_x emissions from supersonic aircraft are also in progress.

6.2. Fuel Options

There would not appear to be any practical alternatives to kerosene-based fuels for commercial jet aircraft for the next several decades. Reducing sulfur content of kerosene will reduce SO_x emissions and sulfate particle formation.

Jet aircraft require fuel with a high energy density, especially for long-haul flights. Other fuel options, such as hydrogen, may be viable in the long term, but would require new aircraft designs and new infrastructure for supply. Hydrogen fuel would eliminate emissions of carbon dioxide from aircraft, but would increase those of water vapor. The overall environmental

impacts and the environmental sustainability of the production and use of hydrogen or any other alternative fuels have not been determined.

The formation of sulfate particles from aircraft emissions, which depends on engine and plume characteristics, is reduced as fuel sulfur content decreases. While technology exists to remove virtually all sulfur from fuel, its removal results in a reduction in lubricity.

6.3. Operational Options

Improvements in air traffic management (ATM) and other operational procedures could reduce aviation fuel burn by between 8 and 18%. The large majority (6 to 12%) of these reductions comes from ATM improvements which it is anticipated will be fully implemented in the next 20 years. All engine emissions will be reduced as a consequence. In all aviation emission scenarios considered in this report the reductions from ATM improvements have already been taken into account. The rate of introduction of improved ATM will depend on the implementation of the essential institutional arrangements at an international level.

Air traffic management systems are used for the guidance, separation, coordination, and control of aircraft movements. Existing national and international air traffic management systems have limitations which result, for example, in holding (aircraft flying in a fixed pattern waiting for permission to land), inefficient routings, and sub-optimal flight profiles. These limitations result in excess fuel burn and consequently excess emissions.

For the current aircraft fleet and operations, addressing the above mentioned limitations in air traffic management systems could reduce fuel burned in the range of 6 to 12%. It is anticipated that the improvement needed for these fuel burn reductions will be fully implemented in the next 20 years, provided that the necessary institutional and regulatory arrangements have been put in place in time. The scenarios developed in this report assume the timely implementation of these ATM improvements, when estimating fuel use.

Other operational measures to reduce the amount of fuel burned per passenger-km include increasing load factors (carrying more passengers or freight on a given aircraft), eliminating non-essential weight, optimizing aircraft speed, limiting the use of auxiliary power (e.g., for heating, ventilation), and reducing taxiing. The potential improvements in these operational measures could reduce fuel burned, and emissions, in the range 2 to 6%.

Improved operational efficiency may result in attracting additional air traffic, although no studies providing evidence on the existence of this effect have been identified.

6.4. Regulatory, Economic, and Other Options

Although improvements in aircraft and engine technology and in the efficiency of the air traffic system will bring environmental benefits, these will not fully offset the effects of the increased emissions resulting from the projected growth in aviation. Policy options to reduce emissions further include more stringent aircraft engine emissions regulations, removal of subsidies and incentives that have negative environmental consequences, market-based options such as

environmental levies (charges and taxes) and emissions trading, voluntary agreements, research programs, and substitution of aviation by rail and coach. Most of these options would lead to increased airline costs and fares. Some of these approaches have not been fully investigated or tested in aviation and their outcomes are uncertain.

Engine emissions certification is a means for reducing specific emissions. The aviation authorities currently use this approach to regulate emissions for carbon monoxide, hydrocarbons, NO_x, and smoke. The International Civil Aviation Organization has begun work to assess the need for standards for aircraft emissions at cruise altitude to complement existing Landing and Take-off standards for NO_x and other emissions.

Market-based options, such as environmental levies (charges and taxes) and emissions trading, have the potential to encourage technological innovation and to improve efficiency, and may reduce demand for air travel. Many of these approaches have not been fully investigated or tested in aviation and their outcomes are uncertain.

Environmental levies (charges and taxes) could be a means for reducing growth of aircraft emissions by further stimulating the development and use of more efficient aircraft and by reducing growth in demand for aviation transportation. Studies show that to be environmentally effective, levies would need to be addressed in an international framework.

Another approach that could be considered for mitigating aviation emissions is emissions trading, a market-based approach which enables participants to cooperatively minimize the costs of reducing emissions. Emissions trading has not been tested in aviation though it has been used for sulfur dioxide (SO₂) in the United States of America and is possible for ozone-depleting substances in the Montreal Protocol. This approach is one of the provisions of the Kyoto Protocol where it applies to Annex B Parties.

Voluntary agreements are also currently being explored as a means of achieving reductions in emissions from the aviation sector. Such agreements have been used in other sectors to reduce greenhouse gas emissions or to enhance sinks.

Measures that can also be considered are removal of subsidies or incentives, which would have negative environmental consequences, and research programs.

Substitution by rail and coach could result in the reduction of carbon dioxide emissions per passenger-km. The scope for this reduction is limited to high density, short haul routes, which could have coach or rail links. Estimates show that up to 10% of the travelers in Europe could be transferred from aircraft to high-speed trains. Further analysis, including trade-offs between a wide range of environmental effects (e.g., noise exposure, local air quality, and global atmospheric effects) is needed to explore the potential of substitution.

7. ISSUES FOR THE FUTURE

This report has assessed the potential climate and ozone changes due to aircraft to the year 2050 under different scenarios. It recognizes that the effects of some types of aircraft emissions are well understood. It also reveals that the effects of others are not, because of the many scientific uncertainties. There has been a steady improvement in characterizing the potential impacts of human activities, including the effects of aviation on the global atmosphere. The report has also examined technological advances, infrastructure improvements, and regulatory or market-based measures to reduce aviation emissions. Further work is required to reduce scientific and other uncertainties, to understand better the options for reducing emissions, to better inform decisionmakers, and to improve the understanding of the social and economic issues associated with the demand for air transport.

There are a number of key areas of scientific uncertainty that limit our ability to project aviation impacts on climate and ozone:

- The influence of contrails and aerosols on cirrus clouds
- The role of NO_x in changing ozone and methane concentrations
- The ability of aerosols to alter chemical processes
- The transport of atmospheric gases and particles in the upper troposphere/lower stratosphere
- The climate response to regional forcings and stratospheric perturbations.

There are a number of key socio-economic and technological issues that need greater definition, including *inter alia* the following:

- Characterization of demand for commercial aviation services, including airport and airway infrastructure constraints and associated technological change
- Methods to assess external costs and the environmental benefits of regulatory and market-based options
- Assessment of the macroeconomic effects of emission reductions in the aviation industry that might result from mitigation measures
- Technological capabilities and operational practices to reduce emissions leading to the formation of contrails and increased cloudiness
- The understanding of the economic and environmental effects of meeting potential stabilization scenarios (for atmospheric concentrations of greenhouse gases), including measures to reduce emissions from aviation and also including such issues as the relative environmental impacts of different transportation modes.

SECTION E

ASSESSMENT OF THE EFFECTS OF HIGH-SPEED AIRCRAFT IN THE STRATOSPHERE: 1998 EXECUTIVE SUMMARY

INTRODUCTION

This report assesses the potential atmospheric impacts of a proposed hypothetical fleet of high speed civil transport (HSCT) aircraft. Civil supersonic transport aircraft were first developed in the 1970s, but, due to economic and environmental concerns, the number of commercial supersonic aircraft in regular service has been small (fewer than 20 aircraft). Recent developments in aviation technology and passenger demand, however, indicate that a substantially larger fleet of HSCTs may be environmentally and economically feasible in the next few decades. During the 1990s, the National Aeronautics and Space Administration (NASA) and the aerospace industry have embarked on a technology research and development program, the High-Speed Research Program, to facilitate technology development and help make widespread supersonic travel possible. The purpose of this report is to assess the effects of HSCTs on atmospheric composition and climate in order to provide a scientific basis for making technical, commercial, and environmental policy decisions regarding the HSCT fleet.

The work summarized here was carried out as part of NASA's Atmospheric Effects of Aviation Project (AEAP) (a component of the High-Speed Research Program) as well as other NASA, United States, and international research programs. Impacts of supersonic aircraft have been assessed previously in 1975 by the Climate Impact Assessment Program and by NASA in 1993 and 1995. Here we describe progress in understanding atmospheric processes and the current state of understanding of the atmospheric effects of HSCTs. The principal focus is on change in stratospheric ozone concentrations. The impact on climate change is also a concern. We delineate the principal uncertainties in atmospheric predictions and estimate the associated errors in predicted effects of HSCTs. The findings represent a broad consensus of the atmospheric research community, comprising the authors, contributors, and reviewers.

A. What are the emissions of greatest concern for the HSCT aircraft fleet?

The HSCT emissions of primary concern for stratospheric ozone and climate are **oxides of nitrogen (NO_x), water (H₂O), and aerosol particles and particle precursor gases.**

NO_x

Nitrogen oxides participate in a wide range of chemical processes that affect ozone. (a) The principal loss process for ozone in the middle and upper stratosphere involves NO_x radicals, and thus, exhaust that is transported to these regions will reduce ozone. The transport of NO_x from

HSCTs to altitudes above 22 km and accumulation at these altitudes is a critical question for the assessment. (b) In the lower stratosphere, NO_x radicals moderate ozone loss due to other radical species (hydrogen oxides (HO_x), chlorine oxides (ClO_x), bromine oxides (BrO_x)); thus addition of NO_x from HCST exhaust can either increase or decrease ozone in this region depending on the relative balance among the radicals. (c) In the polar winter stratosphere, nitrogen oxides participate in formation of polar stratospheric clouds (PSCs), which lead to large seasonal ozone loss in these regions, e.g., the Antarctic ozone "hole." The net effect of increasing NO_x depends on interactions between transport, heterogeneous chemistry, homogeneous chemistry, and the composition of the unperturbed atmosphere.

WATER

HSCT emissions could increase lower stratospheric water vapor by about 0.5 parts per million by volume (ppmv) (10 to 15% for a fleet of 500 aircraft) affecting climate, aerosol processes, and rates for chemical reactions. Warming of the lower atmosphere as a result of increased stratospheric water is predicted to be the main climatic effect of HSCTs, although the magnitude of this effect is not well determined at this time. The composition and growth of aerosol particles, including PSCs, is influenced because increased water vapor raises the condensation temperature. Increased water also increases the reactivity of aerosol toward gases, such as hydrogen chloride (HCl) and chlorine nitrate (ClONO_2), thus influencing the relative concentrations of radical species. Since water is the source of HO_x radicals, increased water leads directly to higher concentrations of HO_x . Model calculations suggest that the associated increase in HO_x is as important as changing NO_x for enhancing ozone loss.

AEROSOL PARTICLES

Repeated observations since 1994 consistently show that a large number of ultrafine (<20 nm diameter) aerosol particles exist in jet engine exhaust plumes, and that particle production increases as the sulfur content of fuel increases. Emission of small particles and sulfur dioxide (SO_2) can potentially increase aerosol surface area throughout the stratosphere which suppresses NO_x and enhances ozone loss by ClO_x and HO_x . Proposed mechanisms for small particle formation are still controversial, and the effects on particle abundance throughout the stratosphere are uncertain, but atmospheric ozone is definitely sensitive to changing aerosol conditions.

B. What factors determine the impact of HSCTs on stratospheric ozone?

The impacts of HSCTs depend on:

- The quantity of exhaust deposited (water, NO_x , particle mass and surface area) and its location in altitude and latitude;
- Atmospheric transport, especially the eventual accumulation of exhaust products in various parts of the stratosphere. The integration of changes in chemical rates for ozone loss and transport of ozone produces the perturbed ozone distribution;

- Microphysics (formation, growth, coagulation, and settling) of aerosol particles in the atmosphere;
- Chemical reactions of the exhaust products with aerosols, atmospheric radicals, and ozone; and
- The background state (meteorology and composition) of the future atmosphere onto which the HSCT perturbation is superimposed.

The linkage between transport, chemistry, aerosol microphysics, and the atmospheric background makes predicting ozone change due to HSCT emissions challenging.

C. What major progress has been accomplished since the previous HSCT assessment?

Great progress has been made in ozone assessment science since the previous HSCT assessment. Progress is led by new atmospheric observations and numerical model development. Observations paved the way for improved understanding and simulation of transport, chemistry, and emission processes. Models have been developed which are more soundly based in physical principles with fewer restrictive assumptions.

TRANSPORT DIAGNOSIS

Observations of chemical tracers, studies using analyzed meteorological fields and idealized models, and advances in theory have improved understanding and quantification of several key components of transport necessary to predicting the distribution of HSCT exhaust. *In situ* measurements of chemical tracers have been obtained within the previously data-sparse tropics. These observations permit quantitative diagnosis of key pathways for dispersal of HSCT exhaust into the upper stratosphere where chemical sensitivity to NO_x is high. Measurements of carbon dioxide (CO_2), sulfur hexafluoride (SF_6), and hydrogen fluoride (HF) over a range of latitude and altitude have enabled mean ages of air in the stratosphere to be determined. Age of air is a directly measured diagnostic related to stratospheric residence time and hence to the potential accumulation of HSCT exhaust in the stratosphere. The quantitative analysis of tropical transport and mean age provide stringent new tests of transport within numerical models. Comparison between observations and models is essential for assessing the uncertainty in the ozone perturbation and in developing more accurate models.

MODEL DEVELOPMENT

Three-dimensional (3-D) atmospheric models have been applied to the HSCT assessment for the first time. Three-dimensional models incorporate a more physically realistic representation of the atmosphere than two-dimensional (2-D) models. The modular design of the Global Modeling Initiative 3-D model has made it possible to test the different components of the model (e.g., the numerical transport algorithm and the source of the wind and temperature fields). Objective criteria for performance with respect to data have been applied. Thus, we discern differences among models in their response to the HSCT perturbation and begin to weigh their results. A major model-measurement comparison and model intercomparison (M&M II) has been conducted, and all

models in this assessment have been tested in comparison to a standard set of performance benchmarks. Also, the 2-D models have incorporated more complete process representations including those for aircraft aerosol exhaust, PSCs, heterogeneous reaction rates, and wave-driven mixing. These model developments give us more confidence in our physical representation of the stratospheric system.

CHEMISTRY

Improved confidence in chemistry has come about largely through observational data on chemicals not previously measured and more accurate data over a more comprehensive range of conditions, including the first in summer polar regions. Observations of key species and new laboratory measurements, placed in a diagnostic model framework, show good accuracy in partitioning components of reactive nitrogen, chlorine, and hydrogen in the models. This establishes confidence that we are not missing significant reactions or unknown species that would alter the calculated response of the chemical system to the HSCT perturbation.

EMISSIONS

The most important progress on emissions comes in confirming the importance of near-field production of small sulfate aerosol particles by HSCTs. New direct measurements for existing aircraft show formation of volatile ultra-fine aerosol particles in exhaust plumes from all aircraft sampled. In-flight measurements indicate that the number of particles is dependent on fuel sulfur content, while altitude chamber measurements show that sulfur emissions at the engine exit plane are primarily SO_2 . These observations support earlier inferences of a composition of sulfuric acid (H_2SO_4)/ H_2O for the volatile particles detected in the plume. Soot emissions from current aircraft engines are roughly two orders of magnitude lower in particle number density than volatile aerosols, and soot from HSCTs is expected to have a negligible effect on ozone and climate. Measurements of gaseous constituents, including HO_x and NO_x , emitted from current aircraft are consistent with expected emissions and plume models of gas-phase chemistry and dispersion. This reduces our uncertainty in applying current knowledge of emissions to the proposed future fleet.

D. What are the predicted impacts of the HSCT fleet on stratospheric ozone and climate?

Predictions of the impact of the future HSCT fleet have been calculated using a set of numerical models of chemistry and transport. Model calculations have been performed for a variety of scenarios to test a range of HSCT design parameters and atmospheric variations.

Based on a combination of model calculations and expert judgement, the estimated column ozone change in the Northern Hemisphere is -0.4% for a fleet of 500 HSCTs flying Mach 2.4 with an NO_x emission index (EI_{NO_x}) of 5 g/kg, EI_{SO_2} of 0.4 g/kg, and 10% of fuel sulfur converted to particles. Based on the same combination of model calculations and expert judgement for the uncertainty in component processes, the hemispheric ozone response will likely be in the range of -2.5 to +0.5%.

We also note that the maximum seasonal and latitudinal ozone changes will be greater than the hemispheric annual mean. Polar regions are a special concern. All models show their largest amount of column ozone loss at high latitudes and a minimum change in the tropics. The column ozone change is the sum of an ozone increase at lower stratospheric/upper tropospheric altitudes plus a decrease generally at and above the HSCT flight altitude. This balance between net production and loss is different for different models and depends strongly on latitude. The season of maximum change is not consistent among the models, with most predicting a springtime maximum ozone decrease but others a maximum in the summer or fall. These variations are connected to the models' sensitivity to chemical reactions in cold polar regions and PSC processes.

The climate forcing attributable to an HSCT fleet in the year 2050 is predicted to result in a warming which is small relative to that expected from other anthropogenic sources. The total radiative forcing from 1000 HSCTs is calculated to be $+0.1 \text{ W m}^{-2}$ in 2050. This HSCT number is a concern because the radiative forcing is disproportionately large for the amount of fuel used and equivalent to about 50% of the forcing from the entire projected subsonic fleet. Climate forcing is sensitive to HSCT emissions because the H_2O accumulation is localized in the lower stratosphere. The uncertainty in the HSCT climate forcing is estimated to be about a factor of 3 due to uncertainty in the exhaust accumulation and uncertainty in the temperature adjustment to a non-uniform perturbation of radiatively active gases in the stratosphere.

Several findings relevant to HSCT design issues come out of the atmospheric assessment. These are considered reliable notwithstanding uncertainties in model results, because they derive from basic understanding of stratospheric processes.

- The HSCT impact on ozone depends directly on total emissions, i.e., fleet size and fuel use.
- Water vapor, which is inherent to jet fuel combustion, accounts for a major part of the calculated stratospheric ozone impact. Increased water vapor in the stratosphere may also contribute to global climate warming.
- NO_x emissions are important. Although current atmospheric models do not show much relative sensitivity to very low ($\text{EI}_{\text{NO}_x} = 5$ to 10) emissions, higher NO_x emissions clearly increase the impact, especially for larger fleet sizes.
- Production of sulfate aerosol particles makes a significant contribution to the calculated ozone impact. This implies that low-sulfur fuel options and methods to control production of particle precursors should be explored.
- Flying the HSCT at lower altitudes reduces stratospheric impacts. The atmospheric residence time of the exhaust is decreased and the chemical sensitivity is reduced.
- Special issues are associated with exhaust build-up in polar regions, both winter and summer. Under current HSCT route scenarios, direct emissions into the polar vortex are minimal.

E. What are the major uncertainties in the prediction of HSCT impacts?

In several key areas, comparisons of model simulations and observational data challenge current model predictions.

TRANSPORT

Most exhaust will be emitted in the lower stratosphere in the Northern Hemisphere. Observations and models show that much of this exhaust will be carried downward into the troposphere and lost, but a fraction will be transported into the tropics, where it will be carried upward and mixed back into the mid-latitudes at higher altitudes. This material will increase stratospheric concentrations of total reactive nitrogen (NO_y), water vapor, and small particles globally. Predicting the magnitude of the fraction dispersed globally, and its residence time in the stratosphere, is a critical part of the assessment. There is a large difference among the models in the calculated accumulation of HSCT exhaust. Current models, both 2-D and 3-D, differ from diagnostic observations that test global stratospheric residence times. In particular, models predict a smaller mean age of stratospheric air, by about a factor of two, than inferred from observations. This tendency suggests that models may underestimate stratospheric residence times and the actual accumulation of exhaust that would occur in the atmosphere.

Transport uncertainties are also primarily responsible for models differing in their simulation of key trace species distributions, both from each other and from observations. To the extent that these model distributions do not match reality, the HSCT perturbation is superimposed on an incorrect background atmosphere. In particular, the model background NO_y controls the HSCT ozone response to a large extent, and no solution is known to simultaneously fix model comparisons to mean age and NO_y measurements.

AEROSOL EMISSIONS

The impact of HSCT emissions on stratospheric sulfate aerosol and the resultant effect on chemistry and ozone has emerged as one of the most important effects of aircraft in the stratosphere. Multi-phase reactions on sulfate particles strongly influence the balance among chemical ozone loss pathways in the lower stratosphere globally. More small volatile particles are formed in jet aircraft exhaust than previously expected, and the mechanism and control of this production are currently not well understood. Particle production has been shown to depend on fuel sulfur, but the particle emission yield for the HSCT is still very uncertain. Model calculations testing the atmospheric sensitivity to a range of particle emissions under differing atmospheric aerosol loadings, which are mainly controlled by volcanic eruptions, result in a range of impacts larger than that attributed to nitrogen oxides or water.

POLAR PROCESSES

Processes occurring at cold polar temperatures in winter are important to ozone because they initiate chlorine-catalyzed ozone destruction that is responsible for large seasonal ozone depletions (e.g., the "ozone hole"). Properly predicting the interaction of aircraft water, nitrogen oxides, and

particles with cold polar processes is an important component of the HSCT assessment. However, our basic understanding of how polar stratospheric clouds, sulfate aerosol, and gases interact to produce rapid polar ozone loss is not complete and simulation in global models is difficult. Test calculations show that inclusion of these processes does significantly alter the calculated impact of HSCT emissions by increasing polar ozone loss, but the amount of loss varies between models depending on their method of parameterization. In this assessment we have begun to quantify these previously unquantified effects, but the uncertainty is still significant.

CHEMISTRY

Recent measurements suggest inaccuracies in the chemical kinetic rates used in current model calculations of the partitioning of nitrogen oxides between NO_x radical and non-radical species. In general, models using current rates predict lower concentrations of radicals than observed, a tendency that would underestimate reductions in ozone. Known deficiencies in both transport and chemistry appear to lead to underestimation of ozone reduction due to HSCTs. Also, changes in the total ozone column due to HSCT exhaust result from a balance between ozone increases in the lower, aerosol-rich lower stratosphere and ozone losses in the NO_x -rich middle and upper stratosphere. Models differ in the magnitude of the vertical and latitudinal contributions to this critical balance.

THE FUTURE ATMOSPHERE

HSCTs would operate in a future stratosphere that will likely have different trace constituent mixing ratios and aerosol abundances. Climate change from increasing CO_2 will also change stratospheric temperatures and winds. Future changes in these and related quantities cannot be predicted with high accuracy. Since the effect of HSCT exhaust depends on the composition and meteorology of the background atmosphere, estimates of future changes in ozone are correspondingly uncertain. Changes in polar regions deserve special attention. In addition, the response to HSCT emissions has been tested in models with observations from current and past atmospheric conditions. The applicability to future conditions is less certain.

CLIMATE FORCING

The uncertainty in the HSCT climate forcing is estimated to be about a factor of 3. This is due to uncertainty in the exhaust accumulation and uncertainty in the temperature adjustment to a non-uniform perturbation of radiatively active gases in the stratosphere. This level of uncertainty, combined with the small magnitude of the calculated effect, makes it difficult to assess whether the HSCT climate impact is a serious concern or not.

F. Where do we stand now?

As a result of the progress on numerous aspects of the HSCT prediction problem, we are now able to predict the effects of stratospheric aviation with greater certitude than ever before. In this assessment a central value for the column ozone perturbation has been estimated based on model calculations, our understanding of the fundamental physics and chemistry of the atmosphere, and knowledge of the potential exhaust emissions. Uncertainties have been estimated for the key

processes in calculating HSCT ozone impacts and a range of uncertainty about the central value has been estimated. The sensitivity of the ozone change to a set of aircraft design and atmospheric variables has been assessed. Along with the assessment of ozone change, uncertainty, and sensitivity, we have identified the significant issues and reasons for concern about the accuracy and reliability of HSCT predictions. Taken together, these results should provide useful guidance for informed decisions on environmental policy and technology development for the HSCT aircraft. The status of several specific issues follows.

On stratospheric transport, the new measurement diagnostics and model comparisons allow us to begin to quantitatively evaluate model performance. Rapid model improvement will follow as specific shortcomings are addressed. Although the means to improvement are not all apparent, the new metrics will become part of standard procedure and models will respond. A limited number of 3-D model runs have been made for this assessment. A major emphasis will be diagnosing transport in 3-D models. These models are now on the verge of major advancement, almost certain to follow with further analysis and maturity. Until that time, though, stratospheric transport remains a major uncertainty for HSCT assessment.

Although the formation of particles in HSCT exhaust is not quantitatively predictable, the parametric studies used in this assessment limit the range of uncertainty in the chemical effect from this source. Continued process modeling and measurements should allow a mechanistic understanding of particle formation in current aircraft engine exhaust sufficient to better predict the formation of particles in HSCT plumes, thereby reducing the range used in this assessment. The processes controlling the background stratospheric aerosol distribution also need to be better quantified through systematic analysis of satellite and *in situ* observations.

Gas-phase photochemical mechanisms are generally understood and most are modeled within the combined uncertainties of the measurements and rate coefficients. Recent laboratory measurements are likely to resolve the NO_x/NO_y chemical issue identified for models used in this assessment. The possibility of missing chemical processes, which could invalidate our HSCT assessment, is significantly decreased, but continued observations are needed to minimize the risk.

We continue to be cautious about the potential effects of HSCTs in polar regions because of the demonstrated high sensitivity of ozone to changes there. This assessment does not find unexpectedly large changes near the poles, but we allow the possibility that we have not probed the full possible range of response. An upcoming measurement campaign should help to improve our ability to simulate ozone in polar regions and enhance HSCT assessment confidence. The natural evolution of climate research directed toward international climate assessments will further limit uncertainties in the state of the future atmosphere and the potential climate effects of HSCTs.

In summary, great progress has been made in understanding the potential effects of HSCTs in the atmosphere. However, we are not yet able to establish statistically rigorous error bounds on the effects of supersonic aircraft. We can carefully and critically develop a set of expert opinions on the likely ranges for future effects. To be more quantitative requires improvements in understanding and model capabilities not yet realized. We believe a strong foundation for future advances has been built: the enhanced capability to test models should pave the way for improved models in the future.

G. What can be done to reduce the uncertainties?

Research objectives consistent with the assessed sensitivities and the largest known uncertainties should include improved quantitative understanding of:

- *Transport and dynamics of the stratosphere.* Model differences from tracer observations (especially NO_y), underestimates of mean age, and the relation of residence time with HSCT exhaust accumulation make it a high priority to obtain improved knowledge of the rates for the residual mean circulation and improvements in data in the tropopause region.
- *Production of ultrafine aerosol particles by jet engines.* We need to understand the mechanism for particle production in current engines and the dependence on fuel sulfur well enough to predict HSCT particle production. Progress in understanding this phenomenon will follow from studying the process in the engine components, through the aircraft near field, and out to global scales.
- *Polar studies,* especially the mechanism for polar denitrification and the sensitivity of ozone loss in the Arctic to changes in H_2O , aerosols, and NO_y . These issues are the focus of the upcoming SAGE III Ozone Loss and Validation Experiment (SOLVE) mission.
- *Photochemistry,* laboratory studies, atmospheric observations, and analysis should continue with an emphasis on quantifying uncertainties and evaluating the potential for missing chemistry. Specific discrepancies in NO_x/NO_y partitioning must be resolved.
- *Continued development, evaluation, and refinement of models.* Fundamental processes represented in current models, with particular attention to transport, model resolution, and numerical artifacts require continued scrutiny. Methods for evaluating model performance, uncertainty quantification, and use of 3-D models should be continued.



SECTION F

MODELS AND MEASUREMENTS (M&M) INTERCOMPARISON II

EXECUTIVE SUMMARY

The Second Workshop on Stratospheric Models and Measurements (M&M II) is the continuation of the effort previously started in the first Workshop (M&M I, Prather and Remsberg [1993]) held in 1992. As originally stated, the aim of M&M is to provide a foundation for establishing the credibility of stratospheric models used in environmental assessments of the ozone response to chlorofluorocarbons, aircraft emissions, and other climate-chemistry interactions. To accomplish this, a set of measurements of the present day atmosphere was selected. The intent was that successful simulations of the set of measurements should become the prerequisite for the acceptance of these models as having a reliable prediction for future ozone behavior.

The choice of the measurements for M&M I was limited by data availability, and the emphasis on 2-D and 3-D assessment models. Other models such as climate models, air-trajectory models and assimilation models were not included in the consideration. In M&M II, the GSFC DAO assimilation model provided results for a number of transport experiments. In this report, we emphasize what was accomplished beyond M&M I.

A. New Data Used for M&M II

Almost all the data sets that were used for M&M I have been revised or replaced with better and more complete compilations. UARS satellite data sets are the primary ones being used for the middle and upper stratosphere. We chose to use the 1992 data as the basis for our comparison because it is the only full year for which there is CLAES data available. The CLAES data provide the very useful global coverage of N_2O , CH_4 , HNO_3 , and $ClONO_2$. In addition, data for O_3 , ClO , H_2O and CH_4 were available from MLS and HALOE. Many of the evaluations in M&M II relied on individuals to compile the UARS datasets for comparisons with the models. Future model comparisons will benefit from the climatological datasets constructed by the UARS Science Team, which were not available for M&M II but are now accessible (see <http://hyperion.gsfc.nasa.gov/Analysis/UARS/urap/home.html>).

The M&M II exercise has also benefited from additional data from various ER-2 aircraft campaigns (AASE II 91/92; SPADE 92/93; ASHOE/MAESA 94; STRAT 95/96; POLARIS 96/97) and balloon launches from the OMS program (Brazil, Alaska, Bill Brune, Geoff Toon). New data on SF_6 , CO_2 and H_2O provide diagnostics for transport rates, mean age of air, and propagation of seasonal cycles into the tropical lower stratosphere. Enhanced payload of the ER-2 provided in situ measured concentrations of OH and HO_2 . Data from the new $ClONO_2$ instrument also place additional constraints on partitioning of the chlorine species. Simultaneous measurements of NO_x and NO_y allow determination of the NO_x/NO_y ratio. New data on aerosol

surface areas and photolysis rates measurements provide additional constraints on our understanding of photochemical partitionings.

A climatology for ozone, consisting of monthly zonal mean column ozone and monthly ozone profiles as a function of latitude, was put together for M&M II. The column ozone climatology is based on ozone column data from 1988 to 1996 using TOMS on Nimbus-7, Meteor 3 and Earth Probe. The ozone profile is based on ozone sonde data between 0 and 28 km and SAGE II data between 20 and 60 km. In the region where the two datasets overlap (20-30 km), a weighted average is used with a heavier weighting for the sonde data at lower altitudes and a heavier weighting for the SAGE II data at higher altitudes.

B. Strategy for Model Testing

Ozone is the only species where there is long-term global coverage to derive a reliable climatology. However, using ozone by itself as a guide to choose the best transport and chemistry representations in a model is problematic since it is never clear whether a good ozone simulation in a particular model is achieved by having the correct combination of transport and chemistry or simply good fortune. A wrong transport rate in the model will give erroneous Cl_y and NO_y , which will produce an incorrect local ozone removal rate. The combination of the wrong transport with the wrong ozone removal rate could fortuitously result in a "correct" ozone simulation. This makes it impossible to use the agreement between observed and calculated ozone as the only criterion for having the correct transport.

Direct comparison of model simulated tracer distributions with observed distributions has limited value. In the case of observations from satellite platforms, one must take into account that the observations represent a specific year while the model results represent a climatological mean. Comparison of 3-D data with 2-D model results requires additional work since straight zonal averaging of the observation may overlook the effects from the wave motions that should be taken into account. This is particularly important for the winter hemisphere where planetary wave activities are stronger. In those cases, averaging by potential vorticity (PV) may help (see e.g. Randel *et al.*, 1998). Finally, observations from aircraft and balloon platforms may be affected by short term motions so that observations taken at a particular latitude and altitude may be sampling air that has been transported from another location. In those cases, use of alternative co-ordinates such as N_2O and PV would also help.

Comparison of radical species with model results are even more problematic. For example, discrepancies between model calculated and observed NO_2 concentration at a particular location could be due either to differences in NO_y concentrations, differences in partitioning (because of differences in local temperature, overhead ozone or air trajectory, treatments of heterogeneous reactions), or a combination of the two. In this report, the simulation is carried out for 1992, a period when the stratosphere was heavily perturbed by Pinatubo aerosols. Hence, the exercise provides a test bed for volcanic perturbations to stratospheric chemistry and the ways in which it is described in the models. However, the approaches to polar stratospheric cloud and volcanic heterogeneous chemistry were not 'standardized', and each modelling group made their own choices.

A number of theoretical developments enable us to develop a new strategy for model testing. Successful simulation of ozone depends on several processes. Therefore, it is difficult to identify the causes of the discrepancy between model results and observation. The current approach in M&M II identifies a number of independent tests for individual process simulated in the model (see Figure 1 and discussion below). Having the independent tests for the components provides a theoretical framework in which further adjustments could be made.

Testing components

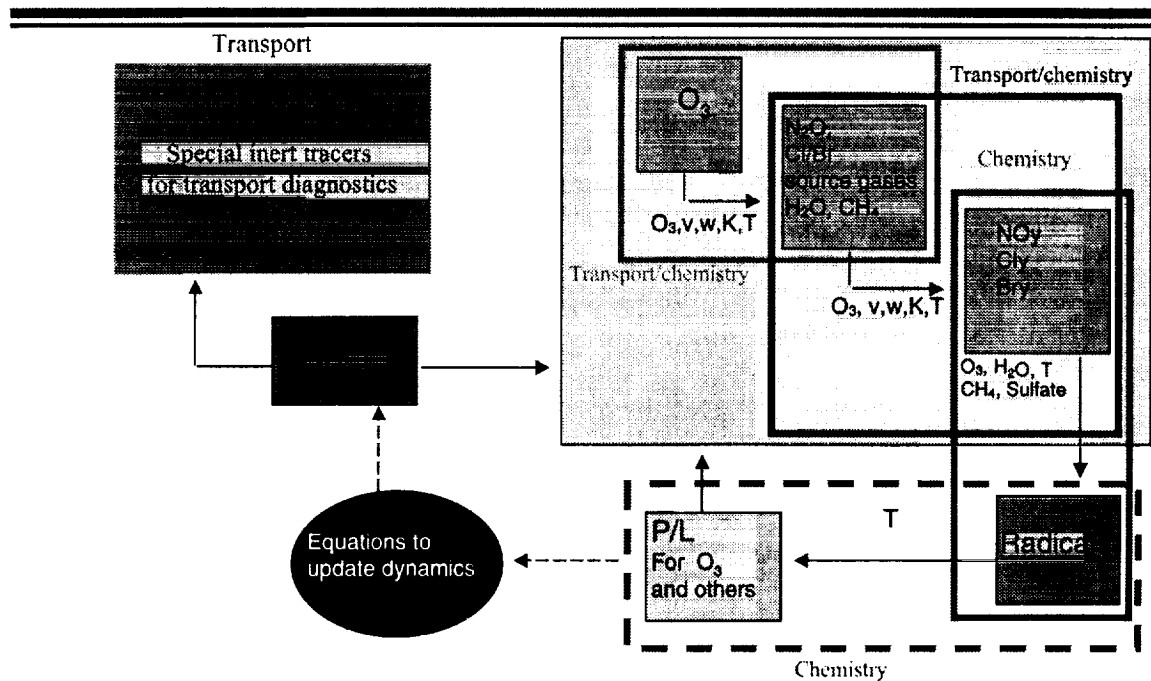


Figure 1. Testing different components of the model.

B.1 FOCUS ON TRANSPORT

Current thinking considers the lower stratosphere as being separated into the tropics, extra-tropics and the polar regions. The tropical lower stratosphere is dominated by upwelling from the tropopause. It is the region where source gases from the troposphere are transported into the stratosphere. In this region, the local concentration of ozone is maintained by a balance between net photochemical production and transport away from the region. Downward motions occur in the extra-tropics and the polar region. In both regions, local ozone concentration is determined by the balance between photochemical removal and transport into the region. In addition to the large scale motion as determined by advection, neighboring regions also communicate by irreversible transport associated with wave motions. In 2-D models, these are simulated by exchange of air between the two regions along isentropes whose rate is related to the horizontal eddy diffusion coefficient (K_{yy}). If the mixing ratio of a species is different in two neighboring

regions, this exchange of air will lead to a net transport of the species. Vertical motion (downward) and vertical mixing will carry material out of the extra-tropical lower stratosphere into the troposphere. Exchange along isentropes across the middle world is also thought to be important. This mixing connects the extra-tropical lower stratosphere and the tropical upper troposphere. Within this framework, the transport can be described by specifying the upwelling in the tropics, downward motions in the extra-tropics and polar regions, vertical mixing in each region, and the values of K_{yy} linking neighboring regions.

Progress has been made on understanding the individual components of transport in 2-D models. Heating rates calculated from observed ozone, temperature and aerosol [Eluszkiewicz *et al.*, 1996; Jackman *et al.*, 1996; Rosenlof, 1995] can be used to verify the heating rates associated with the residual circulation used in the models. In fact, several models (e.g. CSIRO, GSFC and LLNL) use heating rates calculated using observed fields to derive the residual circulation. Work by Minschwaner *et al.* [1996], Volk *et al.* [1996] and Schoeberl *et al.* [1997] provide a quantitative measure of the mixing rate between the tropics and mid-latitudes. Work by Hall *et al.* [1997] and Mote *et al.* [1998] provide measures of K_{zz} in the tropics in addition to upwelling velocity and mixing rate from mid-latitudes. With these works, a conceptual framework has been developed to identify the key transport processes in the lower stratosphere. Some of these parameters are related directly to observations (e.g., SF₆, CO₂) on the one hand, and can be derived as diagnostics from model output. Comparison of these model diagnostics with the values derived from observations provides a measure of how well the transport processes are simulated in each model.

The combinations of the data on long-lived tracers from satellite, aircraft and balloon platforms provide ample opportunity to study the correlation diagram for these species. As shown by Plumb and Ko [1992] and Plumb [1996], the slope of the correlation curve can be related to the ratio of the stratospheric lifetimes of the two species. The knowledge on the tropospheric growth rate of SF₆ allows one to translate relative lifetime to absolute lifetimes for comparison with model calculations [Volk *et al.*, 1997].

B.2 FOCUS ON CHEMISTRY

The local production and removal rates of long-lived species such as ozone, N₂O, and CH₄ depend on the local concentrations of the radicals and photolysis rates. Partitioning of the radicals in an air parcel is determined by the local concentration of ozone, H₂O, Cl_y, NO_y, Br_y and CH₄; and the solar illumination to which it is exposed. The solar illumination depends on the overhead column ozone and the exact trajectory of the motion. This is particularly important near the terminator as excursions in latitude would bring the parcel in and out of sunlight. Away from the terminator, the observed concentrations of the radicals at a particular latitude and longitude are found to correspond to the partitioning calculated for the air-parcel by assuming that the parcel is in photochemical equilibrium while executing exact zonal motion at the same latitude and altitude.

In situ observations of atmospheric trace species provided data for process studies of the partitioning of the radical species over a range of conditions with different sulfate loading and solar illumination. In a series of studies performed by Ross Salawitch [see e.g. Salawitch *et al.*,

1994], it was demonstrated that a photostationary box model constrained by observed values of sulfate surface area, temperature, NO_y , Cl_y , Br_y , H_2O , ozone, overhead column ozone and CH_4 can produce the observed partitioning of the radical species under a range of conditions. This method has been validated in the lower stratosphere using the data from the AASE II, ASHOE/MAESA, SPADE and POLARIS aircraft campaigns, and in the mid- to upper stratosphere using balloon data.

The above approach used to analyze the observations can be modified to examine photochemical partitioning in the models. Specifically, appropriate parameters are taken from the outputs of the assessment models to constrain the photostationary model. The radical concentrations calculated by the constrained photostationary model can be compared to the radical concentrations calculated by the assessment models. To the extent that the photostationary model can simulate the observed radicals using appropriate rate data, this provides verification of the photochemical solvers in the assessment models. The production and removal rates of the reservoir species calculated by the assessment models are also partially verified since they are determined by the radicals. The limitations of this approach are discussed in section 5.2.

C. Results of M&M II

The numerical experiments for M&M II were chosen so that the results from different models could be easily compared and that specific diagnostics which can be related to observations provide guidelines for the correct answers. The experiments can be separated into two groups. The first group involves simulations of chemical inert tracers and is used to provide diagnostics for transport. The second group uses the distributions (as functions of latitude, height and seasons) of chemical tracers simulated in the models (H_2O , Cl_y , NO_y , various source gases and ozone) for comparison with observations.

C.1 TRANSPORT EXERCISES

The transport exercises include the following:

- (1) simulation of a special tracer for diagnosing the age spectrum, and seasonal variation of the transport parameters (A-1 and A-2),
- (2) simulation of the distribution of an inert tracer using the boundary condition corresponding to the emission history of SF_6 (A-5),
- (3) simulation of the distribution of an inert tracer using the seasonally varying boundary condition corresponding to that of CO_2 (A-6),
- (4) simulation of the distributions of inert tracers released in the lower stratosphere, which represent HSCT emissions (A-3 and A-4).

The age spectrum [Hall and Plumb, 1994] encapsulates all the information required to reconstruct the stratospheric response to any tropospheric time series of a conserved tracer, and as such it summarizes transport in a chemistry-independent way. From this, the mean age can be

directly determined and compared with determinations from observations of SF₆ [e.g., Elkins *et al.*, 1996; Harnisch *et al.*, 1996] and from the observed trend in CO₂ [Boering *et al.*, 1995, 1996]. The response to a seasonally varying source can also be reconstructed. In principle, the full seasonal variation of the age spectrum, which cannot be fully determined from the single experiment A-1, is required to do this, and so experiment A-2 was designed to simulate seasonal tracers explicitly. However, it was found that the results of the seasonal tracer experiments could be reconstructed with little error from the age spectrum derived from experiment A-1.

The model calculations of mean age for the stratosphere were found to vary widely, by as much as a factor of 4. Moreover, compared to mean ages determined from observed SF₆ and CO₂ data, most models produced air that is too young throughout the stratosphere. Theoretical arguments indicate that stratospheric ages that are too young could result from a mean meridional circulation that is too strong, horizontal mixing between tropics and middle latitudes that is too weak, or vertical diffusion that is too strong [analyses of observed tracers indicates that vertical diffusion is negligible in the tropical atmosphere [Hall and Waugh 1997], but this may not be true of all the models]. Controlled comparisons between models differing in one or more of these circulation features are consistent with these arguments. A contribution from numerical errors (to which age calculations may be sensitive) cannot be ruled out, as no experiments were designed to compare transport schemes, but it is noteworthy that one pair of models, essentially identical except for their advection schemes, produced very similar magnitudes and distributions of stratospheric age.

The observation of propagation of the seasonal cycle of CO₂ [Boering *et al.*, 1996], and that of H₂O [Mote *et al.*, 1998] allows one to examine the upward propagation of a signal into the tropical lower stratosphere. Most models attenuated the signal too quickly; those that did not showed too rapid upward phase propagation. From the phase velocity and attenuation, and a third measurement such as mean age, one can deduce the tropical upwelling rate, the vertical eddy diffusion coefficient, and the rate extratropical air mixes into the tropics [Hall and Waugh, 1997; Mote *et al.*, 1998]. Compared to such deductions from observations, tropical upwelling in most models is too fast, consistent with the circulation being too strong from the age comparison. Vertical diffusion is also too large in many 2D models. Compared to the mixing rate time constant of about 15 months derived from several independent analyses of observations, most models are mixing the tropics and mid-latitudes too fast. This suggests that weak horizontal mixing is not the reason for the excessively young ages in most models.

Boering *et al.* [1996] suggested that the model-calculated mean age should be related to the residence time of materials deposited at the same rate (in mixing ratio unit) in the whole stratosphere. Indeed, it was found that model simulations of trace gases, not only of those with stratospheric sources, but also those with tropospheric sources, correlated extremely well with the age simulations. Model-to-model variation for tropospheric source gases is modest, but that for gases with stratospheric sources is substantial, being as large as a factor of 2 for Cl_y in the lower stratosphere and as much as a factor of 3 for the idealized HSCT emission simulation (experiments A-3 and A-4). Thus, model deficiencies in the simulation of age are indicative of serious transport errors that may impact the models' ability to simulate stratospheric composition, especially the stratospheric burden of HSCT emissions. This is an important step in the verification of model-computed changes in NO_y and H₂O due to aircraft emission, and

these results indicate that improvements in the simulation of stratospheric transport should be a high priority in future model development.

C.2 CHEMISTRY PARTITIONING

Testing chemistry partitioning in the models is performed as follows. First, the individual model was asked to simulate the 1992 atmosphere providing the calculated concentrations of the trace gases including the radical species. Appropriate parameters are taken from the outputs of the individual model to constrain the photostationary model of Salawitch. The radical concentrations calculated by the constrained photostationary model are used to verify the radical concentrations calculated by the assessment models.

The M&M I report identified a 30% difference in model calculated partitioning. Two separate photochemical benchmark exercises were carried out in 1994 to resolve this. As a result of these calculations, the participating models have identified the causes of these differences for their own models and modified them accordingly so that they produce the correct benchmark answers. As expected, the comparison with the constrained photostationary model confirms that the photochemical solvers used in most assessment models are in good agreement with the photostationary model.

In interpreting the chemistry test, one should be aware of the following two caveats. First, results of the photostationary model depend on the reaction rate constants used. With the current JPL-97 recommendation, some discrepancies between calculated results and observed results still exist. Most notable of these is the model ozone deficit at 40 km [Clancy *et al.* 1987 and references cited; Natarajan and Callis, 1991; Eluszkiewicz and Allen, 1993; Crutzen *et al.*, 1995; Dessler *et al.*, 1996; Osterman *et al.*, 1997; Summers *et al.*, 1997]. There are indications that models may underestimate the NO_x/NO_y ratio in the summer lower extra-tropical stratosphere [Sen *et al.*, 1998, Gao *et al.*, 1999, Danilin *et al.*, 1999]. Recent laboratory measurements [Brown *et al.* 1999 a,b] suggest that the rate recommendations for $\text{OH} + \text{NO}_2$ and $\text{OH} + \text{HNO}_3$ in JPL-97 may have to be revised. Second, the above procedure provides a valid test only for situations where heterogeneous chemistry is easily parameterized and where local photochemistry is rapid. It is well-known that behavior of the radicals depends on the air-parcel trajectory (temperature and solar illumination) in regions when the temperature is cold enough to trigger heterogeneous chemistry on surfaces. In addition, the long photochemical lifetimes of some reservoirs in the lowermost stratosphere (such as HNO_3 and HCl) imply that transport can influence chemical partitioning, and the local photostationary solution may not be appropriate. There remains a need to find ways to verify the PSC treatments in the models.

C.3 CHEMICAL TRACERS

In the following comparison, we emphasize specific aspects rather than direct comparison with observed concentrations:

- The model calculated atmospheric lifetimes of N_2O and several CFCs from the models are longer than those derived from observations by Volk *et al.* [1997] and Minschwaner *et al.* [1998]. Assuming that the photolysis rates are correct, the models would need a stronger

upwelling in the tropics and/or less mixing between the tropics and mid-latitudes to get longer lifetimes. Unfortunately, this conflicts with the requirement to get greater mean age of air at mid-latitudes.

- Because of zonal asymmetric motions, computation of the zonal mean of observed N_2O and CH_4 would underestimate the latitudinal gradient across the tropical barrier and polar vortex. The alternative way is to use PV to define an equivalent latitude. The gradient across the barrier defined this way is more pronounced. It is likely that unsuccessful simulations of the correct gradients across the region boundaries would imply incorrect exchange rates across the boundary.
- Analyses of the HNO_3 and N_2O measurements in the polar vortex suggest that correlative measurements of those two species provides an indication of removal of gas-phase HNO_3 by heterogeneous reactions and recovery of HNO_3 on the polar region.
- Model results show significant differences in NO_y and Cl_y (>50% at mid-latitudes, larger in the polar region) in the lower stratosphere. Differences in model calculated NO_y and Cl_y computed using specified source gases (N_2O for NO_y , CFCs for Cl_y) are even larger, indicating differences in transport as a major contributor.
- The UARS measurements provide information on seasonal behavior of NO , NO_2 , HNO_3 , HCl , $ClONO_2$, and ClO . The differences among model calculated concentrations for these species are large, reflecting the differences in NO_y and Cl_y , and different partitionings because of different local ozone. Given the large ranges covered by the model calculated values, the observed values generally lie within the model ranges most of the time. However, there is no one model that matches the observation in a consistent way.

C.4 OZONE COMPARISON

The comparison between model ozone and the ozone climatology shows the following:

- The model predicted columns are within $\pm 5\%$ of the climatology in the tropics, $\pm 15\%$ at mid-latitudes, and as much as 30% in polar region. The general tendency is to underestimate the tropical column and overestimate the column in the extra-tropics, consistent with too strong a circulation.
- Models that follow the JPL recommendation underestimate the ozone amount above 40 km (about 10% too little around 40km, up to 30% less at 60km). Calculations have shown that including a 6% yield of HCl from $OH + ClO$ will increase the model calculated ozone in this region.
- The calculated ozone is within 10% of the climatology between 25 km and 35 km in the tropics and mid-latitudes. The differences are as large as 30% at high latitudes in some models. Larger differences also occur in the lower stratosphere. The differences are largest in the extra tropics below 20 km where some models overestimate ozone by as much as 100% around 14 km.

- Concentrations of tropospheric ozone are more than a factor of 2 too low for many of the models.

Several other exercises were also included. While these results cannot be easily compared to observations, they provide some useful insights.

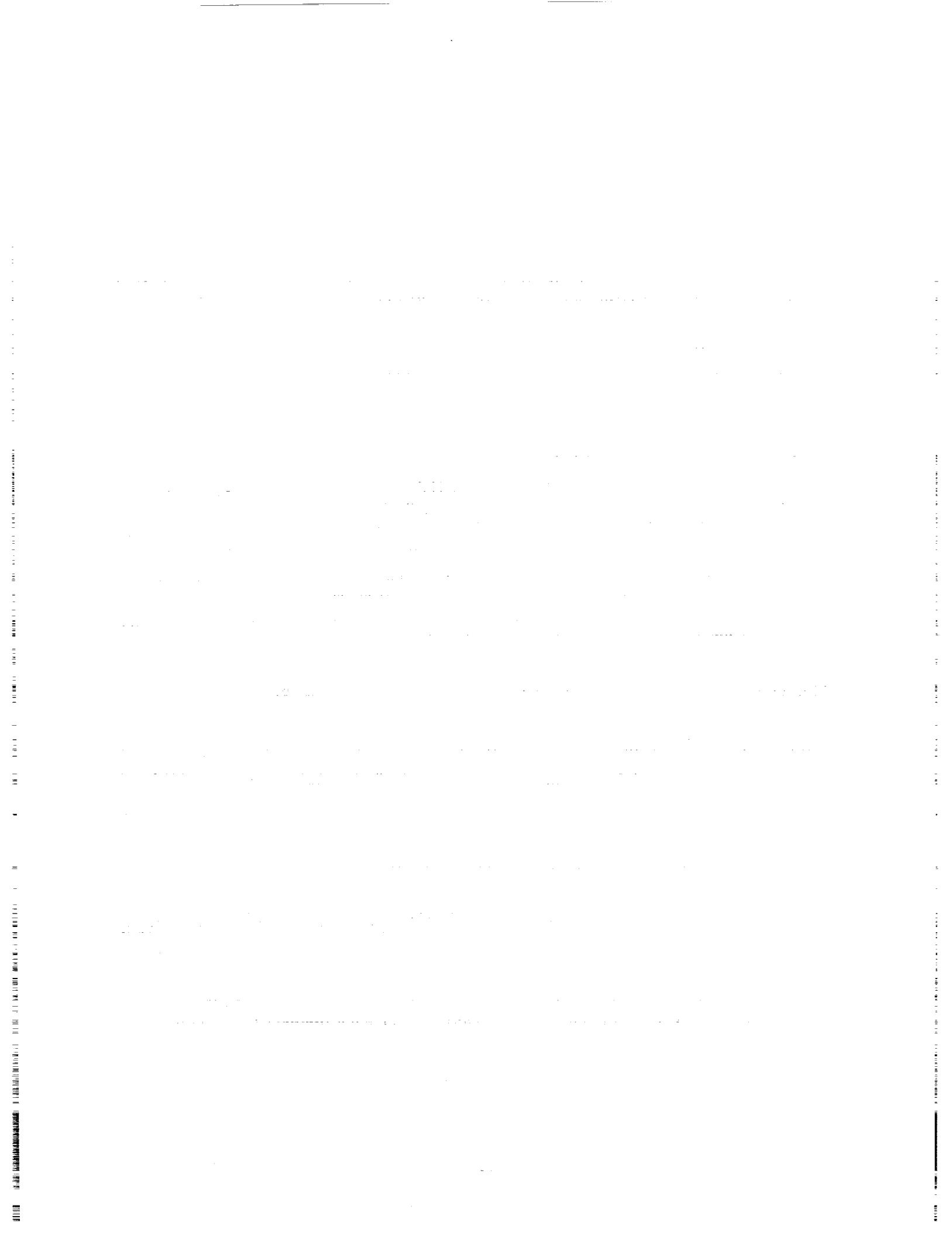
- The local ozone production and removal rates for the simulation of the 1992 atmosphere from different models were compared to each other. In spite of the large differences in NO_y , Cl_y , Br_y and H_2O concentrations, the calculated production and removal rates show many similarities. This suggests that there is internal buffering of the system.
- In another exercise, all the models used the same fixed ozone production and loss rates to compute ozone. This exercise highlighted how differences in transport affect the model computed ozone. Generally, the column ozone computed in this exercise for a model was fairly close to the column ozone calculated by the same model for the 1992 atmosphere even though the ozone production and loss rates used in two simulations were quite different.

REFERENCES

- Boering, K.A., E.J. Hirst, S.C. Wofsy, J.G. Anderson, B.C. Daube, Jr., A.E. Dessler, M. Lowenstein, M.P. McCormick, J.R. Podolske, E.M. Weinstock, and G.K. Yue, Measurements of stratospheric carbon dioxide and water vapor at northern mid-latitudes: Implications for troposphere-to-stratosphere transport, *Geophys. Res. Lett.*, 22, 2737-2740, 1995.
- Boering, K.A., S.C. Wofsy, B.C. Daube, H.R. Schneider, M. Lowenstein, and J.R. Podolske, Stratospheric transport rates and mean age distribution derived from observations of atmospheric CO_2 and N_2O , *Science*, 274, 1340-1343, 1996.
- Brown, S.S., R.K. Talukdar, and A.R. Ravishankara, Rate constants for the reaction $\text{OH} + \text{NO}_2 + \text{M} \rightarrow \text{HNO}_3 + \text{M}$ under atmospheric conditions, *Chem. Phys. Lett.*, 299, 277-284, 1999a.
- Brown, S.S., R.K. Talukdar, and A.R. Ravishankara, Reconsideration of the rate constant for the reaction of hydroxyl radicals with nitric acid, *J. Phys. Chem.*, in press, 1999b.
- Clancy, R.T., D.W. Rusch, R.J. Thomas, M. Allen, and R.S. Eckman, Model ozone photochemistry on the basis of Solar Mesospheric Explorers mesospheric observations, *J. Geophys. Res.*, 92, 3067-3080, 1987.
- Crutzen, P.J., J.-U. Grooz, C. Bruhl, R. Muller, J.M. Russell III, A reevaluation of the O_3 budget with HALOE UARS data: no evidence for the O_3 deficit, *Science*, 268, 705-708, 1995.
- Danilin, M.Y., J.M. Rodriguez, W. Hu, M.K.W. Ko, D.K. Weisenstein, J.B. Kumer, J.L. Mergenthaler, J.M. Russell III, M. Koike, G.K. Yue, N.B. Jones, and P.V. Johnston, Nitrogen species in the post-Pinatubo stratosphere: Model analysis utilizing UARS measurements, *J. Geophys. Res.*, 104, 8247-8262, 1999.

- Dessler, A.E., S.R. Kawa, D.B. Considine, J.W. Waters, L. Froidevaux, and J.B. Kumer, 393 UARS measurements of ClO and NO₂ at 40 km and 46 km and implications for the 394 model "ozone deficit", *Geophys. Res. Lett.*, 23, 339-342, 1996.
- Elkins, J. W., D.W. Fahey, J.M. Gilligan, G.S. Dutton, T.J. Baring, C.M. Volk, R.E. Dunn, R.C. Meyers, S.A. Montzka, P.R. Wamsley, A.H. Hayden, J.H. Butler, T. M. Thompson, T.H. Swanson, E.J. Dlugokencky, P.C. Novelli, D.F. Hurst, J.M. Lobert, S.J. Ciciora, R.J., McLaughlin, T.L. Thompson, R.H., Winkler, P.J. Fraser, L.P. Steele, and M.P. Lucarelli, Airborne gas chromatograph for in situ measurements of long-lived species in the upper troposphere and lower stratosphere, *Geophys. Res. Lett.*, 23, 347-350, 1996.
- Eluszkiewicz, J., and M. Allen, A global analysis of ozone deficit in the upper stratosphere and lower mesosphere, *J. Geophys. Res.*, 98, 1069-1082, 1993.
- Eluszkiewicz, J., D. Crisp, R. Zurek, L. Elson, E. Fishbein, L. Froidevaux, J. Waters, R. Grainger, A. Lambert, R. Harwood, and G. Peckham, Residual circulation in the stratosphere and lower mesosphere as diagnosed from Microwave Limb Sounder Data, *J. Atmos. Sci.*, 53, 217-240, 1996.
- Gao, R.S., D.W. Fahey, L.A. Del Negro, S. G. Donnelly, E.R. Keim, J.A. Neuman, E. Teverovski, P.O. Wennberg, T.F. Hanisco, E.J. Lanzendorf, M.H. Proffitt, J.J. Margitan, J.C. Wilson, J.W. Elkins, R.M. Stimpfle, R.C. Cohen, C.T. McElroy, T.P. Bui, R.J. Salawitch, S.S. Brown, A.R. Ravishankara, R.W. Portman, M.K.W. Ko, D.K. Weisensten, and P.A. Newman, A comparison of observations and model simulations of NO_x/NO_y in the lower stratosphere, *Geophys. Res. Lett.*, 26, 1153-1156, 1999.
- Geller, L.S., J.W. Elkins, J.M. Lobert, A.D. Clarke, D.F. Hurst, J.H. Butler, and R.C. Meyers, Tropospheric SF₆: Observed latitudinal distribution and trends, derived emissions, and interhemispheric exchange time, *Geophys. Res. Lett.*, 24, 675-678, 1997.
- Hall, T.M., and R.A. Plumb, Age as a diagnostic of stratospheric transport, *J. Geophys. Res.*, 99, 1059-1070, 1994.
- Hall, T.M., and D.W. Waugh, Tracer transport in the tropical stratosphere due to vertical diffusion and horizontal mixing, *Geophys. Res. Lett.*, 24, 1383-1386, 1997.
- Jackman, C. H., E. L. Fleming, S. Chandra, D. B. Considine, and J. E. Rosenfield, Past, present, and future modeled ozone trends with comparisons to observed trends, *J. Geophys. Res.*, 101, 28,753- 28,767, 1996.
- Minschwaner, K., A.E. Dessler, J.W. Elkins, C.M. Volk, D.W. Fahey, M. Lowenstein, J.R. Podolske, A.E. Roche, and K.R. Chen, Bulk properties of isotropic mixing into the tropics in the lower stratosphere, *J. Geophys. Res.*, 101, 9433-9439, 1996.
- Minschwaner, K., R.W. Carver, and B.P. Briegleb, Infrared radiative forcing and atmospheric lifetimes of trace species based on observations from UARS, *J. Geophys. Res.*, 103, 23243-23253, 1998.
- Mote, P.W., T.J. Dunkerton, M.E. McIntyre, E.A. Ray, P.H. Haynes, and J.M. Russell III, Vertical velocity, vertical diffusion, and dilution by mid-latitude air in the tropical lower stratosphere, *J. Geophys. Res.*, 103, 8651-8666, 1998.

- Natarajan, M., and L.B. Callis, Stratospheric Photochemical studies with Atmospheric Trace Molecule Spectroscopy (ATMOS) measurements, *J. Geophys. Res.*, *96*, 9361-9370, 1991.
- Osterman G.B., R.J. Salawitch, B. Sen, G.C. Toon, R.A. Stachnik, H.M. Pickett, J.J. Margitan, J.-F. Blavier, and D.B. Peterson, Balloon-borne measurements of stratospheric radicals and their precursors: Implications for the production and loss of ozone, *Geophys. Res. Lett.*, *24*, 1107-1110, 1997.
- Prather, M.J., and Remsberg, E.E., *The atmospheric effects of stratospheric aircraft: Report of the 1992 models and measurements workshop*, 3 volumes, NASA Reference Publication 1292, 1993.
- Randel, W.J., F. Wu, J.M. Russell, A. Roche, and J.W. Waters, Seasonal cycles and QBO variations in stratospheric CH₄ and H₂O observed in UARS HALOE data, *J. Atmos. Sci.*, *55*, 163-184, 1998.
- Rosenlof, K.H., Seasonal cycle of residual mean meridional circulation the stratosphere, *J. Geophys. Res.*, *100*, 5173-5191, 1995.
- Salawitch, R.J., S.C. Wofsy, P.O. Wennberg, R.C. Cohen, J.G. Anderson, D.W. Fahey, R.S. Gao, E.R. Keim, E. L. Woodbridge, R.M. Stimpfle, J.P. Koplw, D.W. Kohn, C.R. Webster, R.D. May, L. Pfister, E.W. Gottlieb, H.A. Michelsen, G.K. Yue, J.C. Wilson, C.A. Brock, H.H. Jonsson, J.E. Dye, D. Baumgardner, M.H. Proffitt, M. Loewenstein, J.R. Podolske, J.W. Elkins, G.S. Dutton, E.J. Hisntsa, A.E. Dessler, E.M. Wienstock, K.K. Kelly, K.A. Boering, B.C. Daube, K.R. Chan, S.W. Bowen, The distribution of hydrogen, nitrogen, and chlorine radicals in the lower stratosphere: Implications for changes in O₃ due to emission of NO_y from supersonic aircraft, *Geophys. Res. Lett.*, *21*, 2547-2550, 1994.
- Sen, B., G.C. Toon, G.B. Osterman, J-F Blavier, J.J. Margitan, R.J. Salawitch, and G.K. Yue, Measurements of reactive nitrogen in the stratosphere, *J. Geophys. Res.*, *103*, 3571-3585, 1998.
- Schoeberl, M.R., A.E. Roche, J.M. Russell III, D. Ortland, P.B. Hays, and J.W. Waters, An estimation of the dynamical isolation of the tropical lower stratosphere using UARS wind and trace gas observations of quasi-biennial oscillation, *Geophys. Res. Lett.*, *24*, 53-56, 1997.
- Summers, M.E., R.R. Conway, D.E. Siskind, M.H. Stevens, D. Offermann, M. Riese, P. Preusse, D.F. Strobel, J.M. Russell III, Implications of Satellite OH observations for middle atmospheric H₂O and Ozone, *Science*, *277*, 1967-1970, 1997.
- Volk, C. M., J.W. Elkins, D.W. Fahey, R.J. Salawitch, G.S. Dutton, J.M. Gilligan, M.H. Proffitt, M. Loewenstein, J.R. Podolske, K. Minschwaner, J.J. Margitan, and K.R. Chen, Quantifying transport between the tropical and mid-latitude lower stratosphere, *Science*, *272*, 1763-1768, 1996.
- Volk, C.M., J.W. Elkins, D.W. Fahey, G.S. Dutton, J.M. Gilligan, M. Loewenstein, J.R. Podolske, K.R. Chen, and M.R. Gunson, Evaluation of source gas lifetimes from stratospheric observations, *J. Geophys. Res.*, *102*, 25543-25564, 1997.



SECTION G

PHOTOCHEMISTRY OF OZONE LOSS IN THE ARCTIC REGION IN SUMMER (POLARIS) END OF MISSION STATEMENT

This summary is a compilation of research and activities performed by the investigators of the Photochemistry of Ozone Loss in the Arctic Region in Summer (POLARIS) aircraft campaign. The campaign was based at the NASA Ames Research Center, Moffett Field, California; Fort Wainwright U. S. Army Base, Fairbanks, Alaska; and Barbers Point Naval Air Station, Hawaii between March and September 1997. The mission was co-sponsored by NASA's Office of Mission to Planet Earth and Office of Aeronautics.

INTRODUCTION

The POLARIS aircraft campaign was designed to understand the seasonal behavior of polar stratospheric ozone as it changes from very high concentrations in spring down to very low concentrations in autumn. This behavior has been attributed to an increased role of NO_x catalytic cycles for ozone destruction during periods of prolonged solar illumination such as occur at high latitudes during summer. The detail with which current photochemical models can describe this large natural change in ozone serves as an indication of how well the role of increased stratospheric NO_x from anthropogenic sources can be quantified.

The campaign primarily utilized the NASA ER-2 and balloon platforms based in Fairbanks, Alaska to make measurements of select species within the reactive nitrogen (NO_y), halogen (Cl_y), and hydrogen (HO_x) families; aerosols; and other long-lived species in the lower and middle stratosphere. The POLARIS campaign included a total of 30 ER-2 flights and 3 balloon flights in 3 deployment periods in 1997: 17 April to 15 May, 24 June to 13 July, and 3 to 27 September. The flight dates for each are included in the Appendix. These measurements along with computer models of the atmosphere as well as meteorological and satellite data are being used to evaluate spring-summer-fall ozone changes due to chemistry and transport at high latitudes.

The POLARIS web page (<http://cloud1.arc.nasa.gov/polaris/index.html>) provides additional details on the mission, including overview, goals, logistics, schedule, platform payloads, and science and support team members. The POLARIS flight logs and science and support team lists are included in the Appendix.

DEPLOYMENT DESCRIPTIONS

Phase I

This ER-2 flight series covered a latitude range from 13°N to 90°N at cruise altitudes near 20 km in the lower stratosphere. On most flights, vertical coverage extended from ~15 to 21 km at selected latitudes. Several vertical profiles were obtained between cruise altitude and the surface at the two deployment sites, NASA Ames Research Center (37°N) and Fairbanks (65°N).

This flight series achieved a number of science goals including: 1) penetration into the northern polar vortex on 26 April 1997 (the polar vortex had unusually low ozone and persisted for an exceptionally long period during the spring of 1997; see *Geophysical Research Letters*, 24, at http://www.agu.org/pubs/toc/gl/gl_24_22.html for a series of articles describing these low ozone values); 2) completion of both sunrise (30 April 1997) and sunset (9 May 1997) flights at high latitudes in the stratosphere, with the data indicating unusual asymmetries in trace-gas behavior in low-angle illumination; 3) penetration into stratospheric air masses that had experienced continuous sunlight for periods ranging from 1 to 12 days (2, 6, and 13 May 1997) and that revealed important observational-model (photochemical steady-state and trajectory) discrepancies with respect to NO_x concentrations; and 4) a launch of the Advanced Earth Observing System (ADEOS) Validation Campaign balloon payload.

Phase II

With the ER-2 based solely in Fairbanks during Phase II, the latitude survey range extended only from 47.7°N to 90°N in the lower stratosphere. Vertical coverage to 21 km in the Fairbanks region was quite good because of stacked flights on 30 June 1997 and 10 July 1997, with vertical profiles over the 15- to 20-km altitude range near 47.7°N and 90°N.

This flight series achieved a number of science goals including: 1) sampling of midsummer polar air that had undergone continuous solar exposure for an extended period; 2) Observations from the Middle Stratosphere (OMS) balloon flights using the *in situ* and MkIV solar absorption interferometer payloads to altitudes in excess of 30 km (performed coincidentally with the ER-2); and 3) sampling of winter polar vortex fragments in midsummer.

Phase III

Phase III ER-2 flights included latitudes extending from 90°N to 3°S in the lower stratosphere. Both sunrise and sunset flights in late summer were conducted over the Fairbanks region, similar to those flown in Phase I. In addition, a midday solar zenith angle flight was flown on 19 September 1997, providing a nearly full scan of solar zenith angles from sunrise to sunset.

As the final component of this phase, the ER-2 transited to Barbers Point, Hawaii on 21 September 1997, performed a flight to slightly south of the equator on 23 September 1997, and returned to Ames on 25 September 1997. Vertical profiles from the ground to 21 km occurred at Fairbanks, Hawaii and NASA Ames Research Center, with profiles over the 15- to 20-km altitude range near 3°S and 90°N.

POLARIS SCIENCE SUMMARY

Ozone Evolution during the Summer of 1997

The total ozone values during 1997 generally followed the typical summer evolution. Figure 1 displays longitudinally (zonally) averaged total ozone between November 1996 and October 1997 as observed by the Earth Probe Total Ozone Mapping Spectrometer (TOMS) satellite instrument. Superimposed on the plots are the POLARIS ER-2 flight tracks over the course of the deployment (dark vertical lines). The TOMS satellite data display the very strong mid-latitude maximum of ozone during the northern spring. Note also the anomalous polar low of ozone in late March and April 1997 (see *GRL* articles referred to earlier). POLARIS flights nearly sampled the entire equator-to-pole ozone gradient at an altitude of about 20 km during the first deployment. The TOMS data show the April polar low quickly recovered to normal high values in May. As the season evolved, total ozone gradually decreased in the mid- to high latitudes, with the largest decreases in the polar region. This differential decrease led to the development of the normal summer polar low and mid-latitude belt of high ozone. The second POLARIS deployment sampled the period of greatest total ozone decline during late June, and covered the region of the mid-latitude belt of high ozone. The final POLARIS deployment in September sampled the polar region during the period of minimum ozone values in the Northern Hemisphere annual cycle.

In situ sampling of ozone occurred over the entire POLARIS period via the ER-2, ozone sondes, and the OMS flights. Remote sensing measurements of ozone were conducted from both ground and balloon observations. Figure 2 displays ozonesonde profile data taken over the course of the summer period at Fairbanks, Alaska (triangles at bottom indicate sonde launch dates) with ER-2 flights superimposed as white vertical lines, and the tropopause indicated by the thick white horizontal line. The contours of ozone partial pressure decrease over the course of the summer period. For example, 16-nbar contours are apparent during April, but only values of ~12 nbar are present during September. Ozone levels above ~28 km show small changes over the entire period, while the tropopause shows rather minor variations. These ozone partial pressure decreases are reflected in the decrease of total ozone concentrations during summer as observed by TOMS in Figure 1, and illustrate how the ozone changes are confined to the lower stratosphere.

1997 Northern Summer Meteorology

The meteorological situation was generally consistent with climatology. The spring (April and early May) was anomalous because of the persistence of the winter polar vortex. Figure 3 displays zonally averaged winds for the Northern Hemisphere as determined from the Goddard Space Flight Center (GSFC) Goddard Earth Observing System-Stratospheric Transport of Atmospheric Tracers (GEOS-STRAT) analyses over the course of the POLARIS period. The temperature contours are shown with long dashed lines and the tropopause is shown as a thick horizontal line. POLARIS ER-2 flight tracks during the respective months are indicated by the white lines.

Westerly stratospheric winds (solid line contours) during April 1997 were much stronger than expected, since the polar vortex usually breaks down in late March or early April. The first POLARIS flight to the north pole on 26 April 1997 was able to reach just inside the northern polar

vortex. The zonal monthly mean gives a somewhat distorted picture, since the vortex was offset into the Eastern Hemisphere over northern Siberia, and the winds considerably weakened over the course of the month. By mid-May, the vortex had deteriorated, with winds slowed to their normal easterly circulation (dotted line contours). By June, the stratosphere was generally dominated by easterlies, although atmospheric waves of considerable amplitude extended into the stratosphere over the course of the deployment. By the final phase of the deployment in September, polar winds were beginning to make the transition to the winter westerly circulation. The descending westerly phase of the quasi-biennial oscillation (QBO) dominated the tropical circulation during the entire POLARIS period. These descending westerlies are seen at the equator above 30 hPa in April, and centered at about 50 hPa in September.

Twice-daily balloon observations at Fairbanks show the descent of the easterly winds during the early-May period. Figure 4 displays zonal winds from these sondes over the course of the POLARIS period over Fairbanks (contours are 10 m s^{-1} with westerly winds as solid line contours, and easterly winds as dashed line contours). The disappearance of the strong westerly winds is just apparent at the end of April, with the corresponding appearance of the normal summer easterlies. The westerlies reappear over Fairbanks in August, just prior to the third POLARIS deployment.

In addition to the general wind behavior, note that the variability of the winds decreases quite dramatically with altitude. At altitudes near the tropopause, the day-to-day variation of the zonal wind is quite large. At higher altitudes this variation is markedly less. Because of the easterly winds in the stratosphere, synoptic-scale waves cannot penetrate into the middle stratosphere, and wind variability falls off with increasing altitude. This lessening of wind variability results in reduced mixing by these synoptic systems. Based on this type of wind variability, mixing ought to be strongest near the tropopause, and significantly decrease at altitudes above $\sim 400 \text{ K}$.

Air will remain on an isentropic surface in the absence of any diabatic heating processes. Typical diabatic heating rates are quite small during the summer period, hence the cross isentropic mass flux should be small. The diabatic heating rates have been calculated for the entire summer period over the polar region (see Figure 5). At the start of the first POLARIS deployment, diabatic heating rates (contours with thin solid lines denote positive values while those with thin dotted lines denote negative values) were positive because of the colder polar temperatures resulting from the persistent vortex. This situation quickly changed, and there were generally small diabatic cooling rates in the polar region. Typical values of diabatic cooling were approximately -0.5 K/day or about 15 K per month isentropic change. Since ozone has a vertical gradient of $\sim 0.02 \text{ ppmv/K}$ in the lower stratosphere, this diabatic cooling rate leads to an ozone increase of $\sim 0.3 \text{ ppmv}$ over a 1-month time scale, representing an $\sim 15\%$ increase of ozone on the 480-K isentropic surface solely from downward diabatic advection.

Observations Highlights

- Stratospheric Nitrogen Chemistry

NO , NO_2 , and total odd nitrogen were measured during all three of the POLARIS deployments. The measurements of the ratio NO_x/NO_y ($\text{NO}_x = \text{NO} + \text{NO}_2$) were consistently higher than

modeled (photochemical steady-state, trajectory, and three-dimensional (3-D)) values throughout the POLARIS campaign. Flights in May and September that revisited the same air mass several times over the course of five hours provide important information on the possible explanations for this discrepancy. Specifically, we made observations that provide information on the rates of N_2O_5 formation after sunset, N_2O_5 photolysis at sunrise, and on the rate of change of NO_x during the afternoon. Simultaneous observations of OH in the afternoon provide further restrictions on the possible mechanisms for the unexpectedly high NO_x . Models that reproduce the observations may be more sensitive (exhibit greater ozone loss) to added nitrogen oxide such as might occur via the emissions from aircraft than the current generation of models. However, buffering by HO_x and halogens modify the NO_x impact on ozone, and complicate the issue of whether additional NO_x from aircraft will increase ozone loss.

The NO_x/NO_y ratio changed dramatically over the three phases of the mission. NO_x/NO_y ratios varied from 0.07 to 0.28 and maximized around summer solstice when periods of photolysis were nearly continuous at high latitudes over the course of the day. These observations are consistent with a reduction in heterogeneous N_2O_5 hydrolysis due to the suppression of N_2O_5 formation. In addition, the concentration of BrONO_2 is reduced around summer solstice due to higher photolysis loss, which further reduces formation of HNO_3 .

The NO_2 measurements from the laser-induced fluorescence instrument compared well with the photolysis-chemiluminescence measurements. In addition, these observations compared well with simple, constrained models based on measurements of NO, ozone, and the solar radiation field. Small differences in calibration between the two measurement approaches will be evaluated in the laboratory over the next few months.

While the NO_x/NO_y ratio is poorly represented by most models, the observed NO_2/NO ratio is accurately predicted using a photochemical steady-state model. Photolysis of NO_2 (i.e., $J(\text{NO}_2)$) is derived from standard photolysis models using satellite data, ER-2 constituent observations, and Ultraviolet-Visible (UV-Vis) observations from the Composition and Photodissociative Flux Measurement (CPFM) instrument. These rates show some discrepancies, but generally agree to within 5%. Calculations of $J(\text{NO}_2)$ at high solar zenith angles (SZA) ($89^\circ < \text{SZA} < 91^\circ$) have been evaluated using *in situ* measurements of NO_x and ozone. It was found that the height of clouds beneath the ER-2 can affect the calculated value of $J(\text{NO}_2)$ at high SZAs by as much as 20%. With cloud height values derived from satellite observations, the calculated $J(\text{NO}_2)$ values agree well with those derived from NO_x and ozone measurements.

- Ozone Loss Rates

Preliminary calculations using *in situ* measurements of NO_x , HO_x , and ClO show that NO_x dominates the destruction of ozone in the summer Arctic stratosphere, with significant contributions from the HO_x cycles. Calculations of mid-latitude spring ozone loss rates during the Stratospheric Photochemistry, Aerosol, and Dynamics Expedition (SPADE) campaign showed that HO_x catalysis was the dominant ozone loss process. Near the summer solstice, the ozone destruction rate due to NO_x reached 13% per month, compared to 5% per month by HO_x and halogen cycles combined. The net ozone change reached -16% per month during that period.

Estimates of ozone loss (without production) have been computed using the GSFC 3-D chemical transport model (CTM) which is driven by winds derived from the Data Assimilation Office (DAO) GEOS data assimilation system (DAS). Figure 6 displays these ozone loss rates (percent per month) as a function of latitude and time on the 525-K isentropic surface over the course of the POLARIS campaign (white vertical lines show latitudinal range of POLARIS flights). Shown are total loss rates from all species (top), NO_x (middle panel), and HO_x (lower panel). Ozone losses in the model are principally driven by HO_x and NO_x chemistry. The NO_x catalytic loss exceeds that of the HO_x cycles at polar latitudes. These loss processes are largest in the polar region during periods of continuous sunlight in midsummer during the second POLARIS deployment, and fall to smaller values in the third deployment.

The net photochemical change of ozone using a photochemical steady-state model was -10 to -15% per month near 20 km, peaking during Phase I and at high latitudes during Phase II. The altitude range of net photochemical loss of ozone extended to ~24 km for the first MkIV flight during May, and extended to ~30 km for the second flight during July. The net photochemical loss rate of ozone is sensitive to the production rate of ozone, which increases as overhead ozone column falls and as the noontime solar zenith angle experienced by an air mass falls. Indeed, changes in the net photochemical change of ozone between various phases of POLARIS, and as a function of latitude during a specific phase, are driven as much by a variation in ozone production as by changes in NO_x . Both the ozone loss rates based on radical measurements, and the model based ozone loss rates generally were consistent with the observed ozone decreases over the course of the summer.

- Stratospheric Chlorine Budget

The payload of the ER-2 includes a number of measurements of chlorine-containing species, including ClO; HCl; ClONO₂, CFC-11, CFC-12, CFC-113, CCl₄, and CH₃CCl; plus a number of other halocarbons. These observations represent a large fraction of both the organic and inorganic chlorine reservoirs in the lower stratosphere. The ClONO₂ instrument provided its first measurements during the POLARIS deployments. ER-2 measurements of ClO, HCl, and ClONO₂ are very consistent with measurements of organic chlorine compounds. In addition, the measured ratio of ClO/ClONO₂ is in excellent agreement with the modeled photochemical steady-state value. The sum of the inorganic chlorine species, ClO, ClONO₂, and HCl, is in excellent agreement with the value inferred from organic chlorine measurements from the Airborne Chromatograph for Atmospheric Trace Species (ACATS) and Whole Air Sampler (WAS) instruments. These measurements place exacting constraints on our understanding of the chemical mechanisms involved in chlorine partitioning, and suggest that our current understanding of stratospheric chlorine chemistry is very good.

In addition to the ER-2 observations, MkIV and Far-Infrared Spectrometer (FIRS) balloon-borne observations during Phases I and II also showed excellent agreement with our understanding of chlorine partitioning. The new *in situ* ER-2 measurements of ClONO₂ obtained during POLARIS add great confidence to our understanding of processes that regulate reactive chlorine at 20 km, and are entirely consistent with these balloon-borne remote measurements of ClONO₂ obtained by MkIV and FIRS.

- Sunrise and Sunset Flights and HO_x Chemistry

Early summer sunrise/sunset flights were conducted during the first POLARIS deployment, while late summer sunrise/sunset flights were flown in the third deployment. These observations will be of value in addressing the diurnal chemistry of radicals in the lower stratosphere. In particular, the flights confirm the important role of the heterogeneous reaction of BrONO₂ + H₂O in explaining the behavior of HO_x, since concentrations of OH and HO₂ are significantly higher at high solar zenith angle than expected. The observations of HO_x radicals during the third deployment are very consistent with observations made during Phase I, suggesting that our current understanding of diurnal HO_x chemistry in the lower stratosphere is quite good.

- Polar Vortex Samples

Unusually low ozone values were observed in March 1997 inside the polar vortex by the Earth Probe TOMS, ADEOS TOMS, and Upper Atmosphere Research Satellite (UARS) Halogen Occultation Experiment (HALOE) satellite instruments. Because of these unusual observations, the first POLARIS flight from Fairbanks on 26 April 1997 was directed at making measurements inside the stratospheric polar vortex. The ER-2 flight went on a direct path from Fairbanks to the north pole. Meteorological forecasts showed that the edge of the polar vortex was near the pole, with the bulk of the vortex offset into the Eastern Hemisphere. The vortex edge was observed near the pole, based upon various trace gas observations (e.g., methane, N₂O, SF₆, NO_y, and CO₂). Nitrous oxide (N₂O) dropped to ca. 80 parts per billion by volume (ppbv), while other chemical and particle tracers showed comparable behavior. Measurements made inside the vortex on this flight did indeed show low values of ozone with respect to long-lived tracers such as nitrous oxide. The most convincing evidence for a polar ozone deficit was observed in the polar dive on this flight, between 400 and 470 K. Measurements of ozone deep within the vortex were inaccessible because the stationary position of the vortex was beyond the permitted ER-2 operational flight region.

- Midsummer Vortex Fragments

Long-lived trace-gas measurements during the second POLARIS deployment showed anomalously low values in a relatively narrow layer near 20 km. A particular filament sampled by the ER-2 showed N₂O values down to 50 ppbv. The OMS payload also made measurements in this anomalous layer and in a higher layer at ~30 hPa. These layers are too vertically narrow to be observed by satellite instruments (such as Stratospheric Aerosol and Gas Experiment (SAGE) or HALOE). Three-dimensional transport model predictions of such layers have been previously described in the literature, but have heretofore been unobserved. The layers appear to be remnants of the polar vortex following the late spring breakup. These observations indicate that vortex fragments can survive at least two months following vortex breakup. Previous analysis using an advection-diffusion model together with SPADE ER-2 data and trajectory calculations, suggested that during spring, vortex filaments are mixed into the background field within 25 to 30 days [Vaugh *et al.*, 1997]. Preliminary results indicate that during summer the time scale for the large-scale flow to reduce the scale of these filaments down to mixing scales is twice as large as during winter/spring.

- Ozone Transport Effects

Ozone changes on a potential temperature surface are not solely a result of photochemistry. As was observed in the second POLARIS deployment, transport significantly altered the CO_2 - N_2O relationship for values of N_2O less than 200 ppbv. The CO_2 data suggest that features of the ozone- N_2O correlation plots are due primarily to end-point mixing between vortex remnants and mid-latitude air.

Long-lived tracer-tracer relationships are relatively independent of potential temperature. Hence, CO_2 data suggest that a significant region of middle stratospheric air at high latitudes was not significantly affected by transport during the summer, although the influence of transport on ozone is difficult to define accurately because gradients between mid- and high latitudes are weak. However, the persistence of winter vortex remnants well into the summer (see previous item) provides direct support for the idea that high-latitude air is isolated from lower latitudes.

Tracer correlations from the WAS in the lower stratosphere suggest that the Arctic stratosphere was dynamically isolated during the spring-through-autumn period of POLARIS. One example of this behavior was the relatively slow increase inferred for hydrochlorofluorocarbons (HCFCs) (e.g., HCFC-141b) in the 20-km region compared to temporal increases in the troposphere and the stratospheric increases found during the STRAT missions at lower latitudes.

Survey flights to the tropics in early summer and late summer show the development of a very strong latitude gradient in long-lived trace gases such as N_2O , CO_2 , SF_6 , H_2O , and CH_4 . This gradient development indicates that these long-lived trace gases were continuously injected into the tropical stratosphere, but had not intruded into the high latitudes.

- Stratospheric Transport

The mean age of air provides extremely important information for our understanding of the stratosphere, and an important test of transport in two-dimensional (2-D) and 3-D models. The mean age also provides a measure of the time that high-speed civil transport (HSCT) exhaust will spend in the stratosphere. The mean age of air observed over Fairbanks on 20 June was 6.8 years. This air is older than calculated by models, indicating that at high summertime latitudes, HSCT exhaust will likely accumulate in greater amounts than models currently predict.

Tracer-tracer correlations obtained from aircraft and balloons show clear differences among tropical, mid-latitude, and polar vortex air. These differences are pronounced in correlation diagrams for species such as CH_4 , N_2O , and CFC-11. These correlation diagrams show evidence of mixing between the tropics and mid-latitudes, and between the polar vortex and mid-latitudes.

- Gravity Wave Mixing

The POLARIS wind measurements on all three deployments were dominated in the vertical profiles by inertia-gravity waves with peak-to-peak amplitudes of about 10 m/s. The correlations of these wind fluctuations with tracer profiles were generally quite low, consistent with the generally accepted idea that these waves are NOT responsible for the major filamentation of trace constituents

in the stratosphere. Horizontal excursions associated with inertial period fluctuations of these amplitudes are at most ~100 km, creating relatively small perturbations of trace-gas profiles. A number of observed small “dents” in the tracer profiles were associated with these wind fluctuations.

Weak turbulence (as indicated by high-frequency vertical wind fluctuations) was correlated with strong vertical shears associated with the inertia-gravity waves. This observation, and the small dents in the tracer profiles related to the waves, suggests that the role of inertia-gravity waves in the summer Arctic stratosphere is to generate some of the mixing that breaks down the strong tracer filaments.

An interesting case arose on 10 July 1997, where a fortuitous and unplanned change in the flight path caused the aircraft to fly back and forth through a breaking mountain wave. Notably, the turbulence in this case was five times greater than in the strongest inertia-gravity wave case. Also, the amplitude of the mountain wave decreased to very small values at the highest flight leg, indicating that the mountain wave energy is absorbed by the decreasing very weak winds in the summer Arctic stratosphere.

- Organic Fluorine Growth Rate

Analysis of air from tropospheric samples collected in the Northern Hemisphere by L. Heidt and W. Pollock of the National Center for Atmospheric Research (NCAR) allowed a reasonable definition of the growth rate of selected organic fluorine gases since 1977. Preliminary examination of the measurements from POLARIS, still underway as of this writing, indicate concentration distributions in the stratosphere that are consistent with measured tropospheric growth rates. As a result, HFC-143a (CH_3CF_3) appears to have tropospheric growth rates and mixing ratios of sufficient magnitude that this compound could be used as another independent tracer of stratospheric age, in addition to SF_6 and CO_2 .

- Particle Observations

The Focused Cavity Aerosol Spectrometer-Condensation Nucleus Counter (FCAS-CNC) data contain many interesting features, including aircraft plumes and large increases in nuclei-mode particle concentrations near 20 km in mid-latitudes not associated with any obvious plumes or tracer fluctuations. These regions of unexpectedly high particle concentration are unprecedented in our measurement record and will be investigated further.

Preliminary analysis of samples indicates that the sulfate aerosol concentration is in agreement with estimates for this region of the atmosphere. Soot, as collected on wire impactor samples, is found at concentrations one to two orders of magnitude less than sulfate aerosol. The soot results will be used to evaluate the potential role of soot surface reactions in the partitioning of reactive nitrogen and ozone loss rates.

FIGURE CAPTIONS

Figure 1. Values of total column ozone from the Total Ozone Mapping Spectrometer (TOMS) instrument on the Earth Probe satellite shown as a function of latitude during 1997. Contour lines are labeled in Dobson Units (DU, m-atm cm) and separated by 25 DU. No observations are available for the white open areas at high latitudes. The dark vertical lines represent the range of latitude on individual ER-2 flight tracks during POLARIS.

Figure 2. Values of ozone in nbar as a function of altitude and pressure during the April to September period of 1997. Contours are separated by 2 nbars. Observations are from ozone sondes launched from Fairbanks, Alaska, (65°N) on dates marked by triangles at the bottom of the figure. The thin white vertical lines represent the altitude range of ER-2 flights during POLARIS. The thick white horizontal line represents the tropopause.

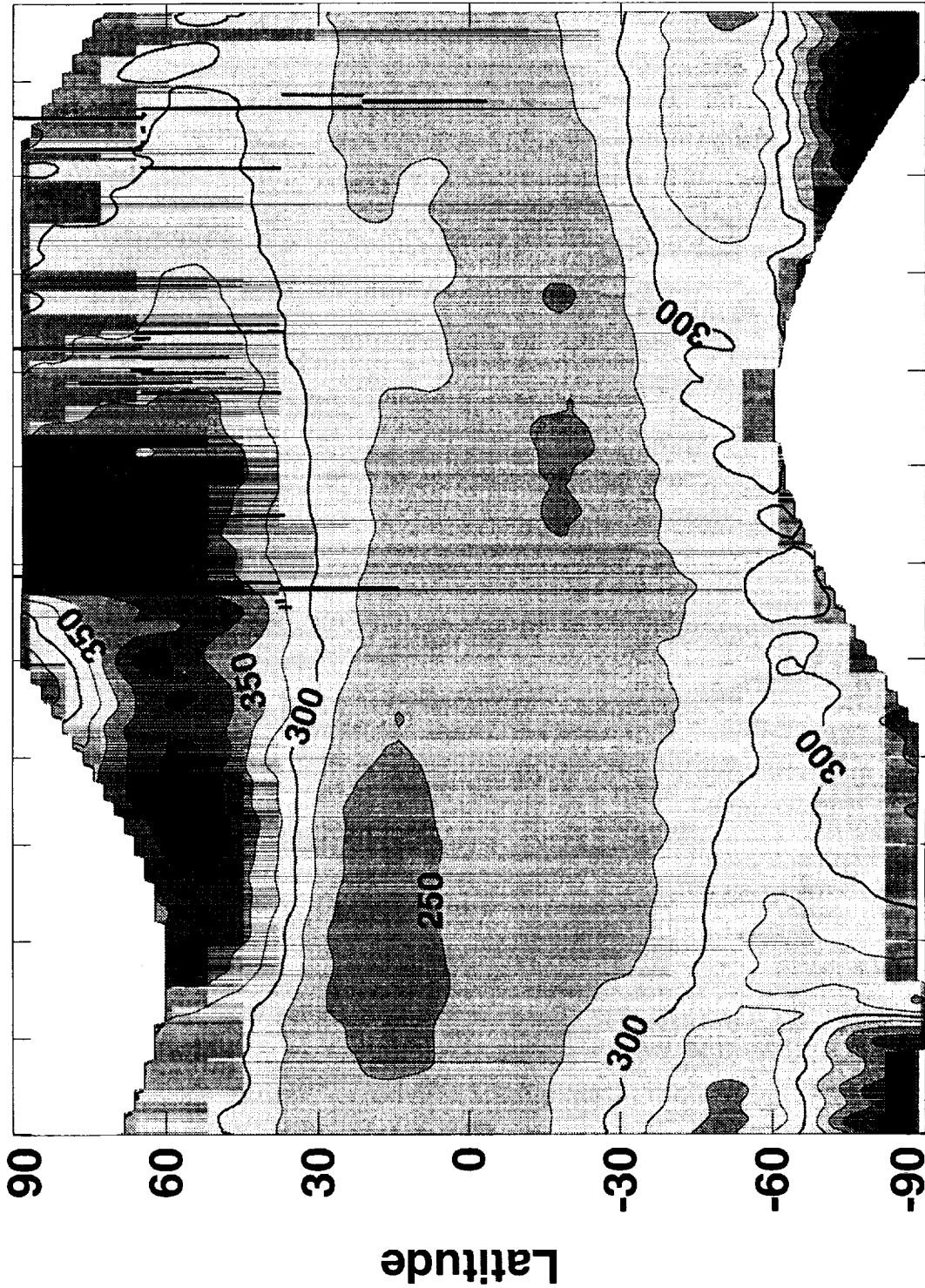
Figure 3. Vertical distribution of winds and temperatures as function of latitude and month during POLARIS. Zonally averaged winds for the Northern Hemisphere are determined from the Goddard Space Flight Center (GSFC) Goddard Earth Observing System-Stratospheric Transport of Atmospheric Tracers (GEOS-STRAT) analyses over the course of the POLARIS period. Contours show wind in units of m s^{-1} with intervals of 5 m s^{-1} (thin solid lines (westerly) and dotted lines (easterly)). The temperatures are superimposed as dashed lines, while the tropopause is superimposed as the thick solid line. POLARIS ER-2 flights during the respective months are indicated by the white lines.

Figure 4. Vertical distribution of zonal winds over Fairbanks, Alaska (65°N) as a function of time during POLARIS as observed with twice-daily balloon soundings. Contours are in intervals of 10 m s^{-1} with westerly winds as solid lines and easterly winds as dashed lines. The tropopause is shown as the thick white line and POLARIS ER-2 flights are indicated by the white vertical lines. The thin dot-dash lines are potential temperature contours in K.

Figure 5. Vertical distribution of diabatic heating rates as a function of northern latitudes for each month of POLARIS. Contours with thin solid lines denote positive values and those with thin dotted lines denote negative values. The thick solid line denotes zero heating rate. Contours intervals are 0.5 K day^{-1} . The tropopause is shown as the unlabelled thick solid line and POLARIS ER-2 flights are indicated by the white lines. The long dashed lines indicate potential temperature in K with contour intervals of 100K.

Figure 6. Estimates of ozone loss (without production) using the GSFC 3-D chemical transport model (CTM) as driven by winds derived from the Data Assimilation Office (DAO) GEOS data assimilation system (DAS). Ozone loss rates in percent per month are shown as a function of latitude and time on the 500-K isentropic surface over the course of the POLARIS campaign where the white vertical lines show the latitudinal range of POLARIS flights. Loss rates are shown for all species (top), NO_x (middle panel), and HO_x (lower panel).

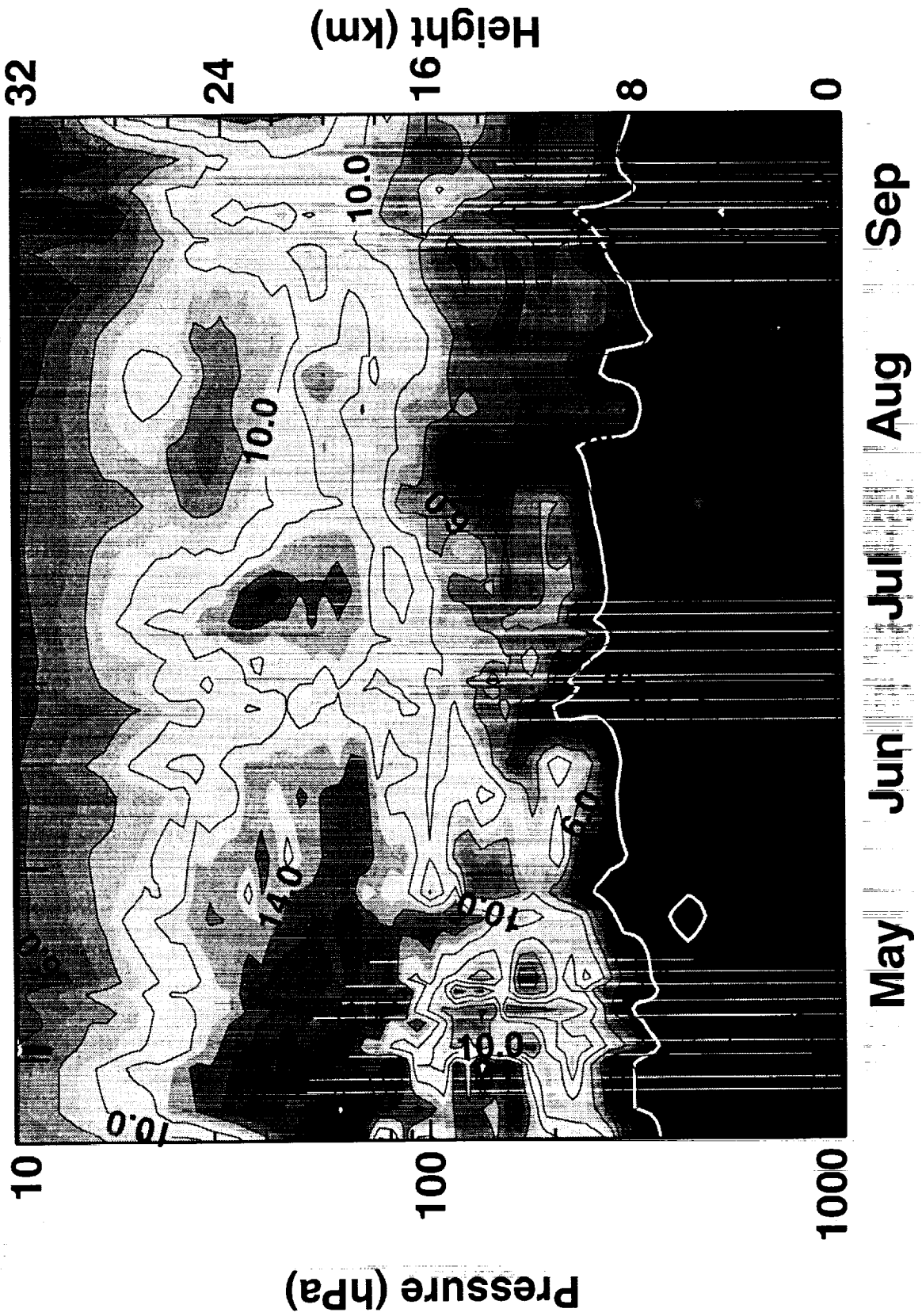
TOMS 1996-97

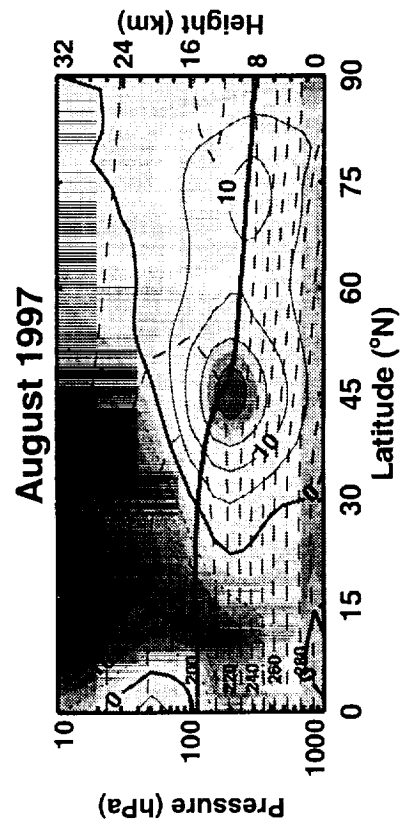
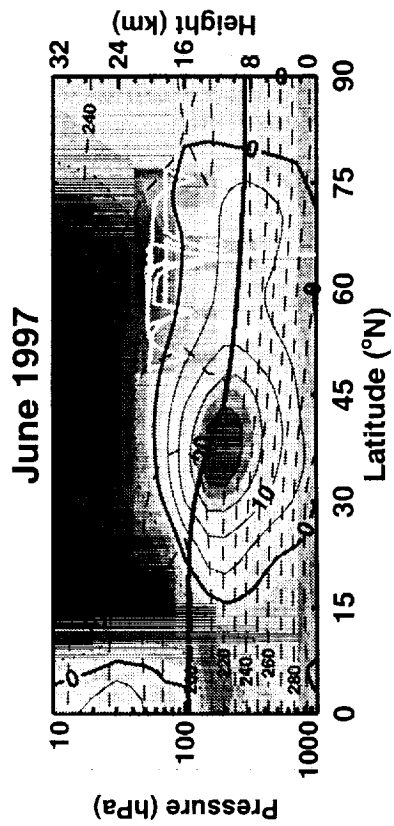
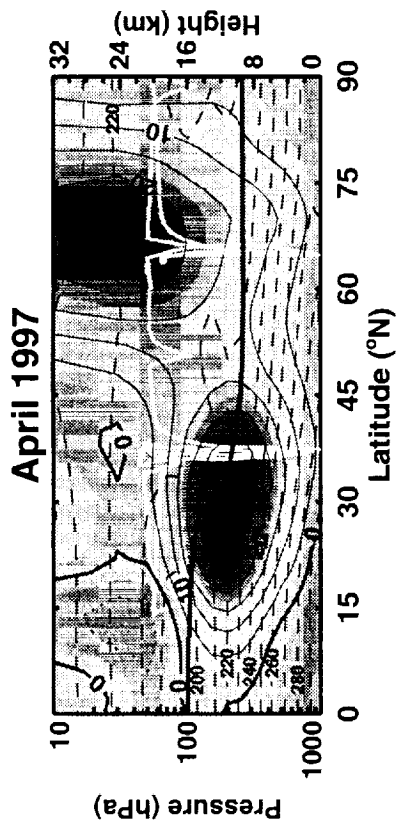
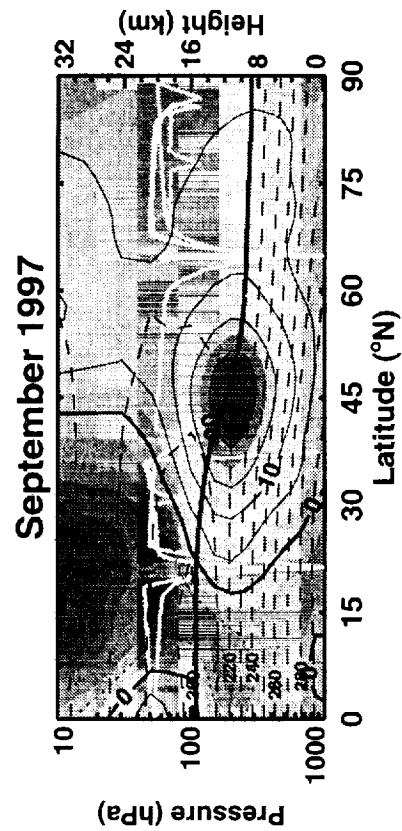
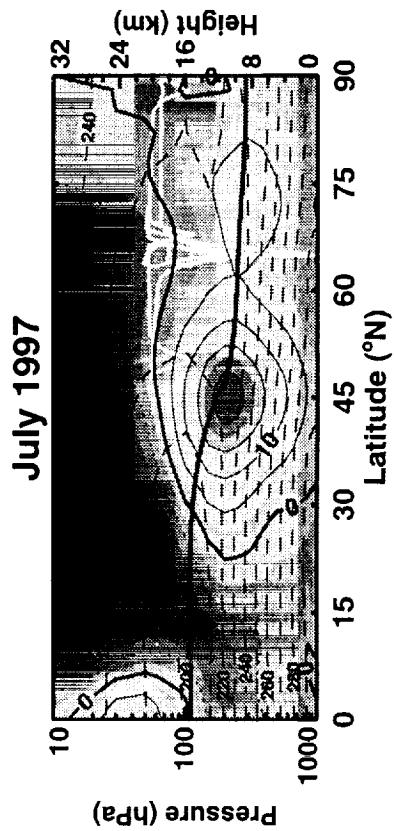
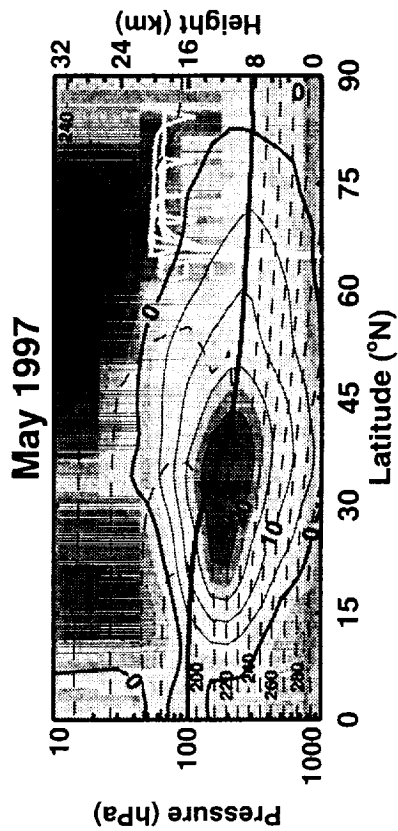


NSA Nov Dec Jan Feb Mar Apr May Jun Jul Aug Sep Oct

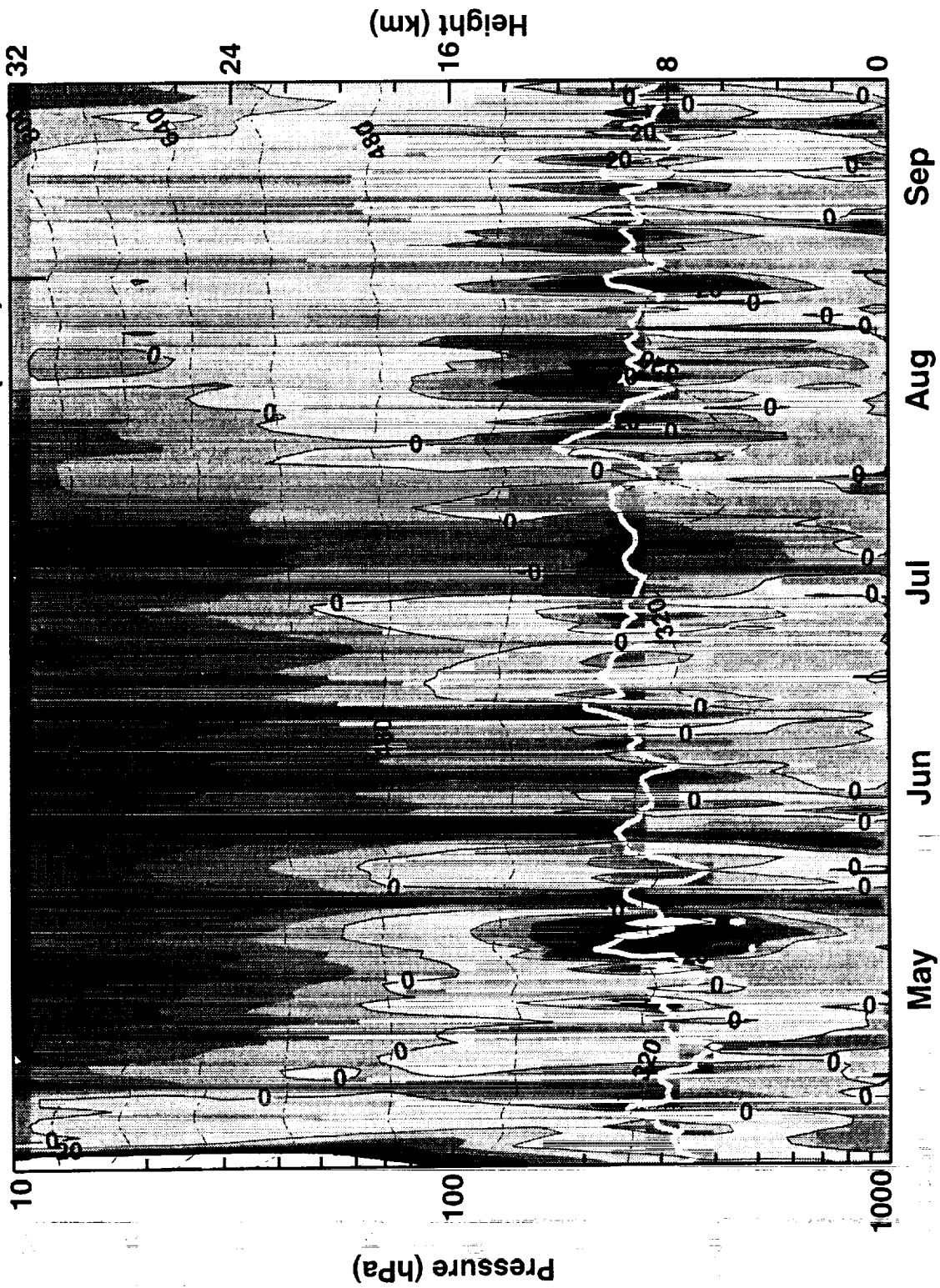
10/27/97 12:08

1997 UA Fairbanks ozone (nbar)

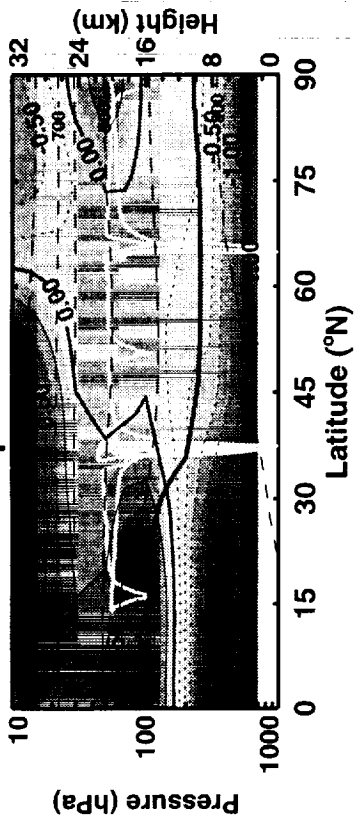




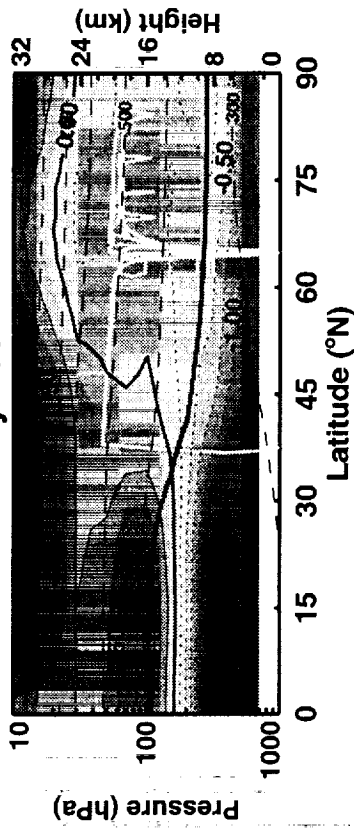
1997 RAOB Fairbanks u-wind (m/s)



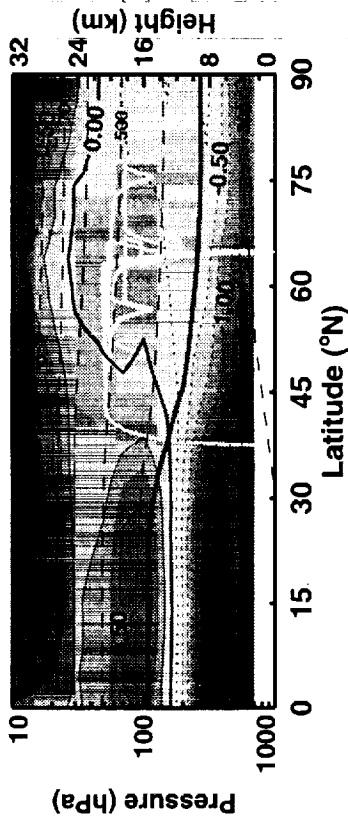
April 1997



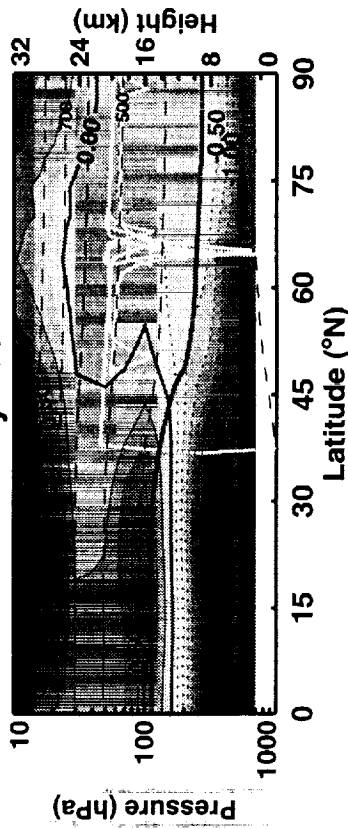
May 1997



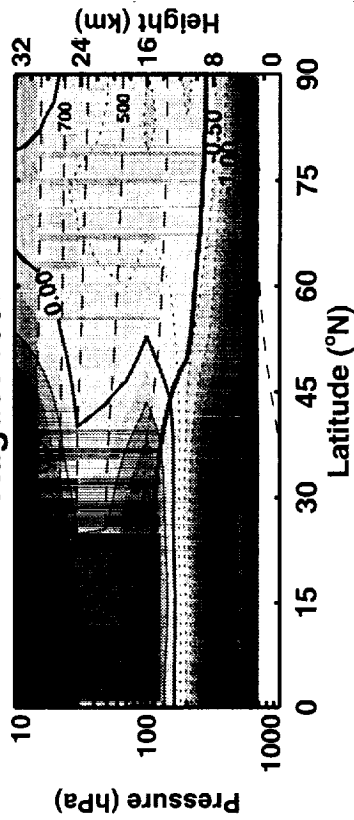
June 1997



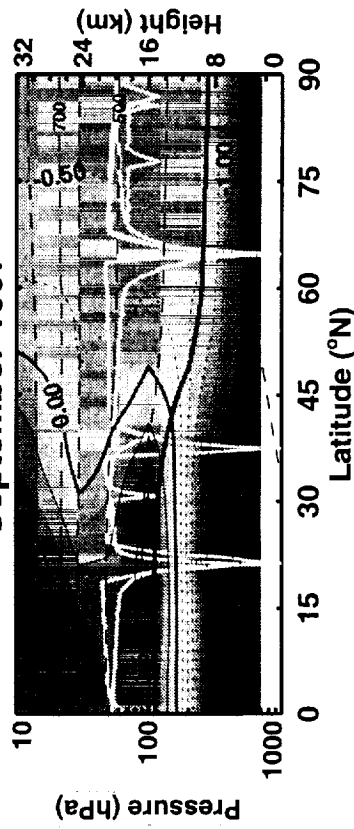
July 1997



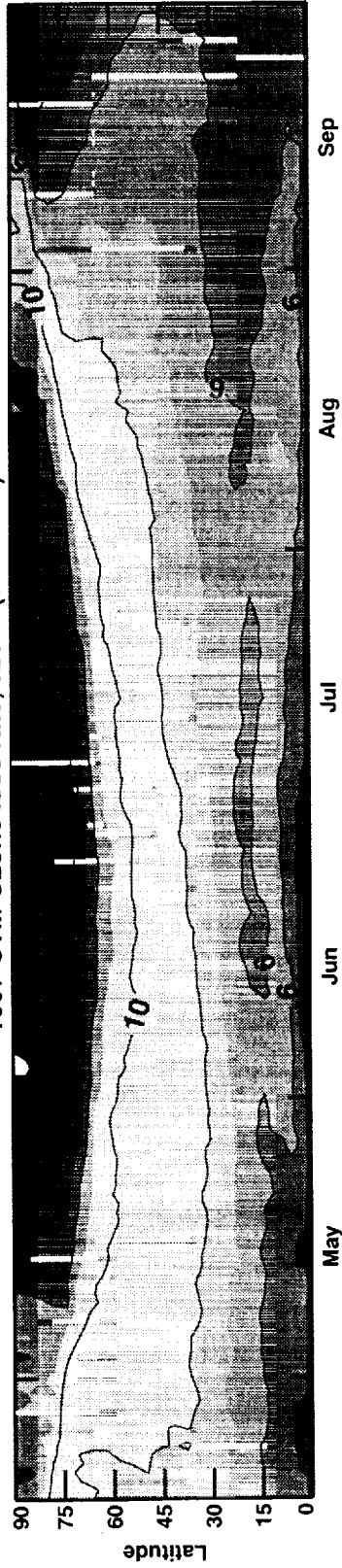
August 1997



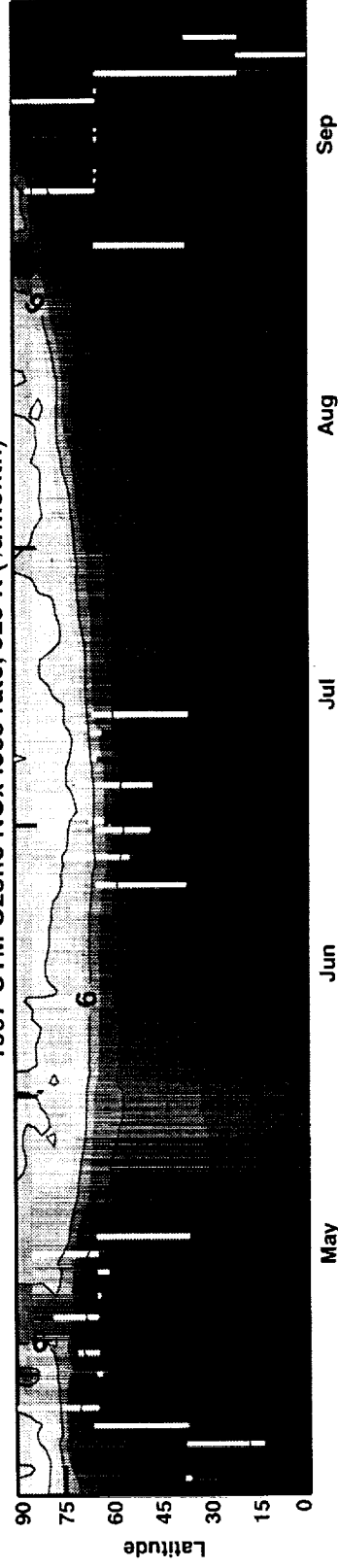
September 1997



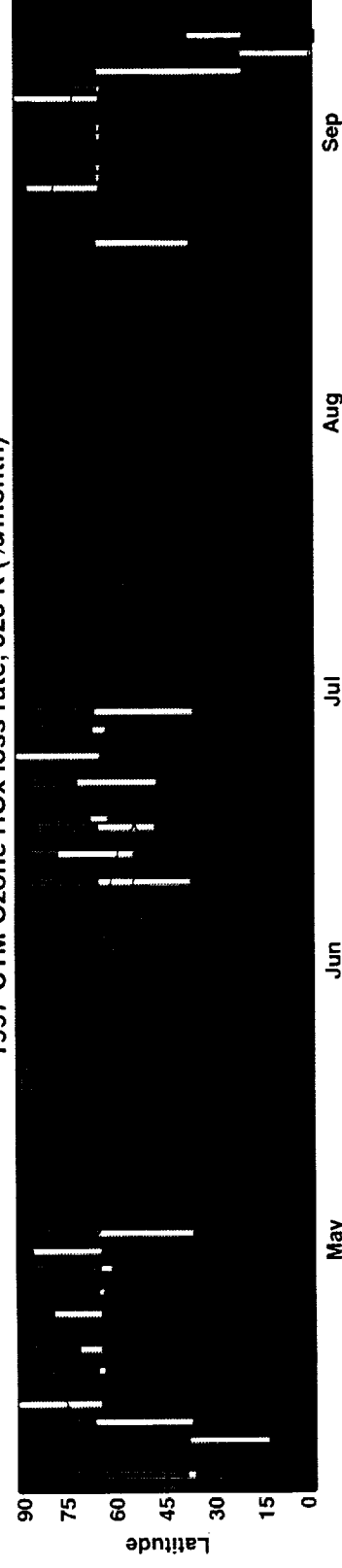
1997 CTM Ozone loss rate, 525 K (%/month)



1997 CTM Ozone NOx loss rate, 525 K (%/month)



1997 CTM Ozone HOx loss rate, 525 K (%/month)



APPENDIX

POLARIS ER-2 Flight Log

Requested Flight Hours: 190.00
 Augment (5/97): 40.00
 Total: 230.00

<u>DATE</u> <u>(YYMMDD)</u>	<u>Sortie</u>	<u>POLARIS ft.</u>	<u>Flt. time</u>	<u>Pilot</u>	<u>Comments</u>
<i>Test Flights</i>					
970106			2.00		CIONO ₂ test flight
970108			6.00		CIONO ₂ test flight
970112			6.00		CIONO ₂ test flight
970114			6.00		CIONO ₂ test flight
Subtotal:	20.00 hours				
<i>Phase I</i>					
970416	97-081	97-01	2.00	Collette	2-hr check flight
970418	97-082	97-02	5.00	Nystrom	5-hr check flight
970422	97-083	97-03	7.75	Porter	8-hr south survey from Ames
970424	97-085	97-04	6.00	Collette	Transit Ames to Ft. W.
970426	97-086	97-05	8.00	Nystrom	8-hr to NP/into vortex
970430	97-087	97-06	6.50	Collette	SZA flight (2:10-08:45)
970502	97-088	97-07	7.58	Nystrom	Photolysis - Canada
970506	97-089	97-08	6.83	Collette	Photolysis - 2 dips, Canada
970509	97-090	97-09	6.17	Collette	Sunset flight
970511	97-091	97-10	4.92	Nystrom	Stack flight
970513	97-092	97-11	6.67	Collette	Photolysis
970515	97-093	97-12	5.33	Collette	Return transit Ft. W. to Ames
Subtotal:	72.75 hours				
Cumulative:	92.75 hours				

Phase II

970623	97-115	97-13	5.25	Broda	Transit Ames to Ft. W.
970626	97-116	97-14	7.75	Porter	Photolysis - 77°N-54°N, 2 dips
970629	97-117	97-15	6.75	Broda	Photolysis - South to 53°N, 2 dips
970630	97-118	97-16	4.58	Porter	OMS intercomparison
970704	97-119	97-17	8.25	Porter	Photolysis - north/south
970708	97-120	97-18	8.00	Broda	Photolysis to NP, Broda 2000 hours
970710	97-121	97-19	5.50	Broda	Stairstep
970712	97-122	97-20	5.50	Porter	Return transit Ft. W. to Ames

Subtotal: 51.58 hours

Cumulative: 144.33 hours

Phase III

970902			5.50	Barrilleaux	Transit Ames to Ft. W.
970905			0.00		Canceled - control panel problem
970906			0.00		Canceled - autopilot problem
970907			0.00		Canceled - autopilot problem
970908	97-152	97-22	7.75	Nystrom	Photolysis flight
970909			0.00		Abort sunset - autopilot
970910	97-153	97-23	0.50	Barrilleaux	Abort after takeoff - autopilot
970911	97-154	97-24	4.25	Nystrom	Sunset flight
970912			0.00		Abort sunrise - fog
970913			0.00		Open House
970914	97-155	97-25	6.40	Barrilleaux	Sunrise (HO _x fail)
970915	97-156	97-26	6.70	Nystrom	Sunrise (HO _x fail)
970917			0.00		Abort photolysis - MMS fail
970918	97-157	97-27	8.00	Barrilleaux	Photolysis - North Pole
970919	97-158	97-28	7.30	Porter	East-west constant altitude
970921	97-159	97-29	7.33	Nystrom	Transit Ft. W. to Barbers Pt.
970923	97-160	97-30	8.00	Broda	South survey (2nd dive aborted)
970925	97-161	97-31	6.00	Nystrom	Return transit Barbers Pt. to Ames

Subtotal: 62.23 hours

Cumulative: 206.56 hours

POLARIS Balloon Flight Log

970430	ADEOS payload
970508	ADEOS - MkIV payload
970630	OMS <i>in situ</i> payload
970704	MkIV payload
970708	OMS <i>in situ</i>

POLARIS Principal Investigators

POLARIS ER-2 Aircraft Instruments

J. Anderson and E. Hintsa	Harvard University	Water Vapor (H ₂ O)
J. Anderson, R. Stimpfle, and R. Cohen	Harvard University Harvard University University of California, Berkeley	Chlorine Nitrate (ClONO ₂)
J. Anderson and P. Wennberg	Harvard University	High-Altitude OH Experiment (HO _x)
E. Atlas	National Center for Atmospheric Research	Whole Air Sampler (WAS)
D. Baumgardner and B. Gandrud	National Center for Atmospheric Research	Multiangle Aerosol Spectrometer Probe (MASP)
K. Boering and S. Wofsy	Harvard University	High-Sensitivity Fast-Response CO ₂ Analyzer
P. Bui	NASA Ames Research Center	ER-2 Meteorological Measurement System (MMS)
J. Elkins	NOAA Climate Monitoring and Diagnostics Laboratory	Airborne Chromatograph for Atmospheric Trace Species (ACATS)
R.-S. Gao	NOAA Aeronomy Lab	Reactive Nitrogen (NO/NO _y)
B. Gary	Jet Propulsion Laboratory	Microwave Temperature Profiler (MTP)
M. Loewenstein	NASA Ames Research Center	Airborne Tunable Laser Absorption Spectrometer (ATLAS)

T. McElroy	Atmospheric Environment Service/ Canada	Composition and Photodissociative Flux Measurement (CPFM)
R. May	Jet Propulsion Laboratory	Water Vapor (H ₂ O)
M. Proffitt and J. Margitan	NOAA Aeronomy Lab Jet Propulsion Laboratory	Dual-Beam UV-Absorption Ozone Photometer (O ₃)
R. Stachnik	Jet Propulsion Laboratory	Submillimeterwave Limb Sounder
A. Strawa	NASA Ames Research Center	Ames Particle Measurement System (APS)
C. Webster	Jet Propulsion Laboratory	Aircraft Laser Infrared Absorption Spectrometer (ALIAS)
J. Wilson	University of Denver	Focused Cavity Aerosol Spectrometer (FCAS) and Condensation Nuclei Counter (CNC)

Observations from the Middle Stratosphere (OMS) Balloon Instruments

K. Boering and S. Wofsy	Harvard University	Carbon Dioxide (CO ₂)
J. Elkins	NOAA Climate Monitoring and Diagnostics Laboratory	Lightweight Airborne Chromatograph Experiment (LACE)
M. Loewenstein	NASA Ames Research Center	Argus
J. Margitan	Jet Propulsion Laboratory	Dual-Beam UV-Absorption Ozone Photometer (O ₃)
S. Oltmans	NOAA Climate Monitoring and Diagnostics Laboratory	Water Vapor (H ₂ O)
C. Webster	Jet Propulsion Laboratory	Aircraft Laser Infrared Absorption Spectrometer II (ALIAS II)

Theoretical Modeling Projects, Ancillary Measurements, and Mission Support

M. Hitchman	University of Wisconsin
R. Kawa	NASA Goddard Space Flight Center
M. Ko	Atmospheric and Environmental Research, Inc.
L. Lait	NASA Goddard Space Flight Center
S. Lloyd	Johns Hopkins University
L. Pfister	NASA Ames Research Center
R. Pierce	NASA Langley Research Center
R. Salawitch	Jet Propulsion Laboratory
S. Solomon	NOAA Aeronomy Laboratory
S. Strahan	NASA Goddard Space Flight Center
A. Tuck	NOAA Aeronomy Laboratory
D. Waugh	Monash University (Australia)
S. Wofsy	Harvard University

Operations Management

J. Barrilleaux	NASA Ames Research Center
A. Cartledge	NASA Ames Research Center

ER-2 Pilots

J. Barrilleaux	NASA Ames Research Center
K. Broda	Lockheed
W. Collette	Lockheed
J. Nystrom	Lockheed
D. Porter	Lockheed

Project Office

D. Fahey	NOAA Aeronomy Laboratory	Project Scientist
P. Newman	NASA Goddard Space Flight Center	Project Scientist
S. Hipskind	NASA Ames Research Center	Project Manager
M. Craig	NASA Ames Research Center	Deputy Project Manager
K. Wolfe	Computer Sciences Corporation	Project Coordinator
Q. Allison	SIMCO	Logistics Coordinator
S. Gaines	Sterling Software	Data Exchange and Archive/Network Manager

Program Management

M. Kurylo	NASA Headquarters and National Institute of Standards and Technology	Program Scientist/UARP Manager
R. Lawrence	NASA Goddard Space Flight Center	AEA Project Manager
R. Kawa	NASA Goddard Space Flight Center	AEA Project Scientist
J. Kaye	NASA Headquarters	ACMAP Manager
J. Huning and G. Shelton	NASA Headquarters	Airborne Science Office Program Managers
E. Condon	NASA Ames Research Center	Atmospheric Observations Mgr.
P. DeCola	Johns Hopkins University and NASA Headquarters	Assistant UARP Manager

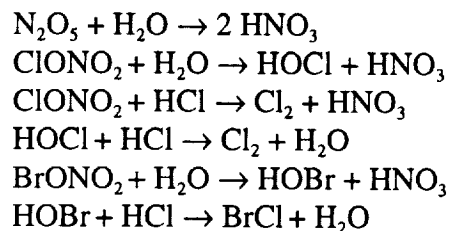
SECTION H

CHEMICAL KINETICS AND PHOTOCHEMICAL DATA FOR USE IN STRATOSPHERIC MODELING: SUPPLEMENT TO EVALUATION NUMBER 12 OF THE NASA PANEL FOR DATA EVALUATION

SCOPE OF THE EVALUATION

In the past, the NASA Panel on Data Evaluation reviewed the entire set of reactions presented in the previous compilations, updating the recommendations and increasing the scope of the review in response to changes in the published literature. For the current release, the Panel has focused on a selected subset of the kinetic and photochemical parameters presented in the JPL 97-4 evaluation [1]. The most important criterion which guided the scope of the present evaluation was an analysis of the sensitivities and uncertainties of reactions with respect to ozone depletion. Guidance in this selection was obtained from several recent sensitivity analysis studies including those of Dubey *et al.* [2], Thompson and Stewart [3] and Chen *et al.* [4]. The reaction lists from these studies were used to identify those processes which play a particularly important role in ozone depletion calculations. Reactions were selected for inclusion (somewhat subjectively) if there were significant uncertainties in the laboratory data or if significant time had elapsed since the last evaluation. Another selection criterion was importance in the interpretation of atmospheric field measurements. For example, the OH + NO₂ reaction has a significant effect on the ratio of NO_x and NO_y which is measured with high precision by aircraft instruments. On this basis, this reaction and several others were included in the present update.

Because of the significant impact of heterogeneous reactions in the polar and mid-latitude lower stratosphere and rapid progress in laboratory investigations of these processes, several heterogeneous reactions were included in the present evaluation. We currently lack guidance from multi-dimensional model sensitivity analyses as to which heterogeneous processes contribute the largest degrees of uncertainty to current models of stratospheric chemistry. However, available box model calculations indicate that uncertainties in heterogeneous reactions can lead to significant uncertainties in calculated ozone levels. Six reactions were identified as key heterogeneous processes most often included in current stratospheric photochemical models. These reactions are:



While each of these six reactions occurs to a greater or lesser extent on the full range of stratospheric aerosol surfaces, we have restricted this review to the three most frequently studied and/or believed to be the most likely present in the stratosphere: water ice, nitric acid trihydrate, and liquid sulfuric acid/water mixtures (typically ~40 to 80 wt.% H_2SO_4). This selection of aerosol surface compositions covers those found in most current stratospheric models.

Table 1. Rate Constants for Second Order Reactions

Reaction	A-Factor ^a	E/R±ΔE/R	k(298 K) ^a	f(298) ^b	Notes ^c
<u>O(¹D) Reactions</u>					
O(¹ D) + H ₂ O → OH + OH	2.2x10 ⁻¹⁰	0±100	2.2x10 ⁻¹⁰	1.2	A2 A6
O(¹ D) + N ₂ O → N ₂ + O ₂	4.9x10 ⁻¹¹	0±100	4.9x10 ⁻¹¹	1.3	A2 A7
→ NO + NO	6.7x10 ⁻¹¹	0±100	6.7x10 ⁻¹¹	1.3	A2 A7
<u>HO_x Reactions</u>					
O + HO ₂ → OH + O ₂	3.0x10 ⁻¹¹	-(200±50)	5.9x10 ⁻¹¹	1.1	B 2
OH + O ₃ → HO ₂ + O ₂	1.5x10 ⁻¹²	880±100	7.8x10 ⁻¹⁴	1.2	B 6
OH + HO ₂ → H ₂ O + O ₂	4.8x10 ⁻¹¹	-(250±100)	1.1x10 ⁻¹⁰	1.3	B10
HO ₂ + O ₃ → OH + 2O ₂	2.0x10 ⁻¹⁴	680 +200 -100	2.0x10 ⁻¹⁵	1.3	B12
<u>NO_x Reactions</u>					
O + NO ₂ → NO + O ₂	5.6x10 ⁻¹²	-(180±50)	1.0x10 ⁻¹¹	1.1	C 1
OH + HNO ₃ → H ₂ O + NO ₃	(See Note)			1.2	C 9
NO + O ₃ → NO ₂ + O ₂	3.0x10 ⁻¹²	1500±200	1.9x10 ⁻¹⁴	1.1	C20
<u>ClO_x Reactions</u>					
O + ClO → Cl + O ₂	3.0x10 ⁻¹¹	-(70±70)	3.8x10 ⁻¹¹	1.15	F 1
OH + ClO → Cl + HO ₂	7.4x10 ⁻¹²	-(270±100)	1.8x10 ⁻¹¹	1.4	F10
→ HCl + O ₂	3.2x10 ⁻¹³	-(320±150)	9.5x10 ⁻¹³	3	F10
OH + HCl → H ₂ O + Cl	2.6x10 ⁻¹²	350±100	8.0x10 ⁻¹³	1.1	F12
Cl + O ₃ → ClO + O ₂	2.3x10 ⁻¹¹	200±100	1.2x10 ⁻¹¹	1.15	F49
Cl + CH ₄ → HCl + CH ₃	9.6x10 ⁻¹²	1360±75	1.0x10 ⁻¹³	1.05	F55

TABLE 1. (Continued)

Reaction	A-Factor ^a	E/R±ΔE/R	k(298 K) ^a	f(298) ^b	Notes ^c
BrO_x Reactions					
BrO + ClO → Br + OClO	9.5 × 10 ⁻¹³	(-550±150)	6.0 × 10 ⁻¹²	1.25	G36
→ Br + ClOO	2.3 × 10 ⁻¹²	(-260±150)	5.5 × 10 ⁻¹²	1.25	G36
→ BrCl + O ₂	4.1 × 10 ⁻¹³	(-290±150)	1.1 × 10 ⁻¹²	1.25	G36

a Units are cm³/molecule-s.

b f(298) is the uncertainty factor at 298 K. To calculate the uncertainty at other temperatures, use the expression:

$$f(T) = f(298) \exp \left[\frac{\Delta E}{R} \left(\frac{1}{T} - \frac{1}{298} \right) \right]$$

Note that the exponent is absolute value.

c Notes refer to detailed information which is provided in the full NASA Data Panel report issued as a Jet Propulsion Laboratory Laboratory publication. Shaded areas indicate changes or additions since JPL 97-4.

Table 2. Rate Constants for Association Reactions

Reaction	Low Pressure Limit ^a		High Pressure Limit ^b		Notes ^c
	$k_o(T) = k_o^{300} (T/300)^{-n}$	n	$k_{\infty}(T) = k_{\infty}^{300} (T/300)^{-m}$	m	
O + O ₂ → O ₃	(6.0±0.5) (-34)	2.4±0.2	-	-	
O + NO → NO ₂	(9.0±2.0) (-32)	1.5±0.3	(3.0±1.0) (-11)	0±1.0	C1
OH + NO ₂ → HNO ₃	(2.4±0.1) (-30)	3.1±0.2	(1.7±0.2) (-11)	2.1±0.3	C4
NO ₂ + NO ₃ → N ₂ O ₅	(2.0±0.2) (-30)	4.4±0.4	(1.4±0.1) (-12)	0.7±0.4	C6
ClO + NO ₂ → ClONO ₂	(1.8±0.3) (-31)	3.4±0.2	(1.5±0.4) (-11)	1.9±0.5	F8
ClO + ClO → Cl ₂ O ₂	(2.2±0.2) (-32)	3.1±0.2	(3.4±0.5) (-12)	1.0±1.0	F10
BrO + NO ₂ → BrONO ₂	(5.2±0.4) (-31)	3.2±0.8	(6.9±0.4) (-12)	2.9±0.1	G2

$$k_f([M], T) = \left(\frac{k_o(T)[M]}{1 + \left(\frac{k_o(T)[M]}{k_{\infty}(T)} \right)} \right)^{0.6} \left\{ 1 + \left[\log_{10} \left(\frac{k_o(T)[M]}{k_{\infty}(T)} \right) \right]^{-2} \right\}^{-1}$$

The values quoted are suitable for air as the third body, M.

a Units are cm⁶/molecule²-sec.

b Units are cm³/molecule-sec.

c Notes refer to detailed information which is provided in the full NASA Data Panel report issued as a Jet Propulsion Laboratory Laboratory publication. Shaded areas indicate changes or additions since JPL 97-4.

Table 3. Equilibrium Constants

Reaction	A/cm ³ molecule ⁻¹	B±ΔB/°K	K _{eq} (298 K)	f(298 K) ^a	Note ^b
NO ₂ + NO ₃ → N ₂ O ₅	3.0x10 ⁻²⁷	10991±200	3.1x10 ⁻¹¹	1.2	4
ClO + ClO → Cl ₂ O ₂	1.27x10 ⁻²⁷	8744±500	7.0x10 ⁻¹⁵	1.3	11

$$K/\text{cm}^3 \text{ molecule}^{-1} = A \exp(B/T) [200 < T/K < 300]$$

^a f(298) is the uncertainty factor at 298 K. To calculate the uncertainty at other temperatures, use the expression:

$$f(T) = f(298) \exp \left[\frac{\Delta E}{R} \left(\frac{1}{T} - \frac{1}{298} \right) \right]$$

^b Notes refer to detailed information which is provided in the full NASA Data Panel report issued as a Jet Propulsion Laboratory Laboratory publication. Shaded areas indicate changes or additions since JPL 97-4.

Table 4. Gas/Surface Reaction Probabilities (γ)

Gaseous Species	Surface Type	Surface Composition	T(K)	γ	Uncertainty Factor	Notes ^a
$N_2O_5 + H_2O \rightarrow 2HNO_3$						
N_2O_5	Water Ice	$H_2O(s)$	188-195	0.02	2	14
	Liquid Water	$H_2O(l)$	260-295	See Note*	See	15
	Nitric Acid Ice	$HNO_3 \cdot 3H_2O(s)$	200	4×10^{-4}	Note	16
	Sulfuric Acid	$H_2SO_4 \cdot nH_2O(l)$	195-300	See Note*	3	17
					See Note	
$HOCl + HCl(s) \rightarrow Cl_2 + H_2O$						
$HOCl$	Water Ice	$H_2O(s) \cdot HCl(s)$	195-200	0.2	2	40
	Nitric Acid Ice	$HNO_3 \cdot 3H_2O(s) \cdot HCl(s)$	195-200	0.1	2	40
	Sulfuric Acid	$H_2SO_4 \cdot nH_2O(l)$	198-209	See Note*	See Note	41
$ClONO_2 + H_2O(s) \rightarrow HOCl + HNO_3$						
$ClONO_2$	Water Ice	$H_2O(s)$	180-200	0.3	3	43
	Nitric Acid Ice	$HNO_3 \cdot 3H_2O(2)$	185-202	0.004	3	44
	Sulfuric Acid	$H_2SO_4 \cdot nH_2O(l)$	200-265	See Note*	See Note	45
$ClONO_2 + HCl(s) \rightarrow Cl_2 + HNO_3$						
$ClONO_2$	Water Ice	$H_2O(s)$	180-200	0.3	3	47
	Nitric Acid Ice	$HNO_3 \cdot 3H_2O \cdot HCl$	185-210	0.2	2	48
	Sulfuric Acid	$H_2SO_4 \cdot nH_2O(l) \cdot HCl(l)$	195-235	See Note*	See Note	49
$HOBr + HCl(s) \rightarrow BrCl + H_2O$						
$HOBr$	Water Ice	$H_2O(s) \cdot HBr(s)$	228	0.3	3	57
	Sulfuric Acid	$H_2SO_4 \cdot nH_2O$ (60-69 wt% H_2SO_4)	198-218	See Note		57
$BrONO_2 + H_2O \rightarrow HOBr + HNO_3$						
$BrONO_2$	Water Ice	$H_2O(s)$	190-200	0.3	2	59
	Sulfuric Acid	$H_2SO_4 \cdot nH_2O$	210-300	See Note	See Note	60
					Note	

* γ is temperature dependent

a Notes refer to detailed information which is provided in the full NASA Data Panel report issued as a Jet Propulsion Laboratory Laboratory publication. Shaded areas indicate changes or additions since JPL 97-4.

REFERENCES

1. DeMore, W. B., S. P. Sander, D. M. Golden, R. F. Hampson, M. J. Kurylo, C. J. Howard, A. R. Ravishankara, C. E. Kolb and M. J. Molina "Chemical Kinetics and Photochemical Data for Use in Stratospheric Modeling," Jet Propulsion Laboratory, 1997.
2. Dubey, M. K., G. P. Smith, W. S. Hartley, D. E. Kinnison and P. S. Connell, 1997, *Geophys. Res. Lett.*, *24*, 2737-2740.
3. Thompson, A. M. and R. W. Stewart, 1991, *J. Geophys. Res.*, *96*, 13,089-13,108.
4. Chen, L., H. Rabitz, D. B. Considine, C. H. Jackman and J. A. Shorter, 1997, *J. Geophys. Res.*, *102*, 16,201-16,214.

SECTION I

AUTHORS, CONTRIBUTORS, AND REVIEWERS

SECTION A: Introduction

AUTHORS

Philip L. DeCola	NASA Headquarters	US
Jack A. Kaye	NASA Headquarters	US
Michael J. Kurylo	National Institute of Standards and Technology/NASA Headquarters	US

COORDINATING EDITORS

Rose M. Kendall	Computer Sciences Corporation	US
Kathy A. Wolfe	Computer Sciences Corporation	US

SECTION B: Scientific Assessment Of Ozone Depletion: 1998

ASSESSMENT CO-CHAIRS

Daniel L. Albritton	National Oceanic and Atmospheric Administration	US
Piet J. Aucamp	Ptersa Environmental Consultants	South Africa
G�rard M�gie	Service d'A�ronomie du CNRS	France
Robert T. Watson	The World Bank	US

AUTHORS AND CONTRIBUTORS

FREQUENTLY ASKED QUESTIONS ABOUT OZONE

Coordinator

Gerard Megie	Service d'Aeronomie du CNRS	France
--------------	-----------------------------	--------

PART 1. HALOCARBON, OZONE AND TEMPERATURE CHANGES

Chapter 1: Long-Lived Ozone-Related Compounds

Chapter Lead Authors

Ronald G. Prinn	Massachusetts Institute of Technology	US
R. Zander	Universit� de Li�ge	Belgium

Coauthors

Derek M. Cunnold	Georgia Institute of Technology	US
James W. Elkins	NOAA Climate Monitoring and Diagnostics Laboratory	US
Andreas Engel	Universität Frankfurt	Germany
Paul J. Fraser	CSIRO Division of Atmospheric Research	Australia
Michael R. Gunson	California Institute of Technology/Jet Propulsion Laboratory	US
Malcolm K.W. Ko	Atmospheric and Environmental Research, Inc.	US
Emmanuel Mahieu	Université de Liège	Belgium
Pauline M. Midgley	M & D Consulting	Germany
James M. Russell III	Hampton University	US
C. Michael Volk	Universität Frankfurt	Germany
Ray F. Weiss	University of California at San Diego	US

Contributors

Donald R. Blake	University of California at Irvine	US
James H. Butler	NOAA Climate Monitoring and Diagnostics Laboratory	US
David W. Fahey	NOAA Aeronomy Laboratory	US
Jochen Harnisch	Max-Planck-Institut für Aeronomie	Germany
Dana E. Hartley	Georgia Institute of Technology	US
Dale F. Hurst	NOAA Climate Monitoring and Diagnostics Laboratory/CIRES	US
Nicholas B. Jones	National Institute of Water & Atmospheric Research Ltd. (NIWA)	New Zealand
Manfred Maiss	Max-Planck-Institut für Chemie	Germany
Archie McCulloch	ICI Chemicals & Polymers Ltd.	UK
Stephen A. Montzka	NOAA Climate Monitoring and Diagnostics Laboratory	US
David E. Oram	University of East Anglia	UK
Stuart A. Penkett	University of East Anglia	UK
Curtis P. Rinsland	NASA Langley Research Center	US
Ross J. Salawitch	California Institute of Technology/Jet Propulsion Laboratory	US
Sue M. Schauffler	National Center for Atmospheric Research	US
Ulrich Schmidt	Universität Frankfurt	Germany
Peter G. Simmonds	University of Bristol	UK
Thayne M. Thompson	NOAA Climate Monitoring and Diagnostics Laboratory	US
Geoffrey C. Toon	California Institute of Technology/Jet Propulsion Laboratory	US

Chapter 2: Short-Lived Ozone-Related Compounds

Chapter Lead Authors

Michael J. Kurylo	National Institute of Standards and Technology; NASA Headquarters	US
José M. Rodríguez	Atmospheric and Environmental Research, Inc.	US

Coauthors

Meinrat O. Andreae	Max-Planck-Institut für Chemie	Germany
Elliot L. Atlas	National Center for Atmospheric Research	US
Donald R. Blake	University of California at Irvine	US
James H. Butler	NOAA Climate Monitoring and Diagnostics Laboratory	US
Shyam Lal	Physical Research Laboratory	India
David J. Lary	Centre for Atmospheric Science, University of Cambridge	UK
Pauline M. Midgley	M & D Consulting	Germany
Stephen A. Montzka	NOAA Climate Monitoring and Diagnostics Laboratory	US
Paul C. Novelli	NOAA Climate Monitoring and Diagnostics Laboratory	US
Claire E. Reeves	University of East Anglia	UK
Peter G. Simmonds	University of Bristol	UK
L. Paul Steele	CSIRO Division of Atmospheric Research	Australia
William T. Sturges	University of East Anglia	UK
Ray F. Weiss	University of California at San Diego	US
Youko Yokouchi	National Institute for Environmental Studies	Japan

Contributors

Derek M. Cunnold	Georgia Institute of Technology	US
Ed Dlugokencky	NOAA Climate Monitoring and Diagnostics Laboratory	US
James W. Elkins	NOAA Climate Monitoring and Diagnostics Laboratory	US
David E. Etheridge	CSIRO Division of Atmospheric Research	Australia
Paul J. Fraser	CSIRO Division of Atmospheric Research	Australia
Dana E. Hartley	Georgia Institute of Technology	US
Malcolm K.W. Ko	Atmospheric and Environmental Research, Inc.	US
Sasha Madronich	National Center for Atmospheric Research	US
Emmanuel Mahieu	Université de Liège	Belgium
Andrew Matthews	National Institute of Water & Atmospheric Research Ltd. (NIWA)	New Zealand
Archie McCulloch	ICI Chemicals & Polymers Ltd.	UK
David E. Oram	University of East Anglia	UK
John J. Orlando	National Center for Atmospheric Research	US
Stuart A. Penkett	University of East Anglia	UK
Sue M. Schauffler	National Center for Atmospheric Research	US
Shari A. Yvon-Lewis	NOAA Atlantic Oceanographic and Meteorological Laboratory	US

Chapter 3: Global Distributions and Changes in Stratospheric Particles

Chapter Lead Authors

Sophie Godin	Service d'Aéronomie du CNRS	France
Lamont R. Poole	NASA Langley Research Center	US

Coauthors

Slimane Bekki	Service d'Aéronomie du CNRS	France
Terry Deshler	University of Wyoming	US
Niels Larsen	Danmarks Meteorologiske Institut	Denmark
Thomas Peter	Max-Planck-Institut für Chemie	Germany

Contributors

Alberto Adriani	Consiglio Nazionale della Ricerca Istituto di Fisica dell'Atmosfera	Italy
John Barnes	NOAA Climate Monitoring and Diagnostics Laboratory	US
Richard Bevilacqua	Naval Research Laboratory	US
Christine David	Service d'Aéronomie du CNRS	France
Guido Di Donfrancesco	Consiglio Nazionale della Ricerca Istituto di Fisica dell'Atmosfera	Italy
Michael Fromm	Computational Physics, Inc.	US
Mark Hervig	University of Wyoming	US
Horst Jäger	Fraunhofer-Institut für Atmosphärische Umweltforschung	Germany
Beiping Luo	Zhenjiang Rietschle Machinery Company, Ltd.	China
Roland Neuber	Alfred Wegener Institute	Germany
Mary Osborn	Science Applications International Corporation	US
Wolfgang Renger	Deutsche Forschungsanstalt für Luft- und Raumfahrt	Germany
Larry Thomason	NASA Langley Research Center	US
Osamu Uchino	Japan Meteorological Agency	Japan
Martin Wirth	Deutsche Forschungsanstalt für Luft- und Raumfahrt	Germany

Chapter 4: Ozone Variability and Trends

Chapter Lead Authors

Rumen D. Bojkov	World Meteorological Organization	Switzerland
Robert Hudson	University of Maryland	US

Coauthors

Lane Bishop	AlliedSignal Inc.	US
Vitali Fioletov	Atmospheric Environment Service	Canada
James M. Russell III	Hampton University	US
Richard Stolarski	NASA Goddard Space Flight Center	US
Osamu Uchino	Japan Meteorological Agency	Japan
Christos Zerefos	Aristotle University of Thessaloniki	Greece

Contributors

Roger Atkinson	Bureau of Meteorology	Australia
Dimitrios S. Balis	Aristotle University of Thessaloniki	Greece
P.K. Bhartia	NASA Goddard Space Flight Center	US

H. Claude	Meteorological Observatory Hohenpeißenberg	Germany
Lawrence E. Flynn	Software Corporation of America	US
Robert Guicherit	Netherlands Organization for Applied Scientific Research (TNO)	The Netherlands
Fumio Hasebe	Ibaraki University	Japan
G.J. Labow	Raytheon STX Inc.	US
Jennifer A. Logan	Harvard University	US
Richard D. McPeters	NASA Goddard Space Flight Center	US
Alvin J. Miller	NOAA NWS Climate Prediction Center	US
Rolf Müller	Forschungszentrum Jülich	Germany
Ruben Piacentini	Planetario y Observatorio de Rosario	Argentina
William J. Randel	National Center for Atmospheric Research	US
Herman Smit	Forschungszentrum Jülich	Germany
B.H. Subbaraya	Physical Research Laboratory	India
Kleareti Tourpali	Aristotle University of Thessaloniki	Greece
Peter von der Gathen	Alfred Wegener Institute	Germany
Ahmed Zand	Tehran University	Iran
Members of the SPARC/IOC Profile Trends Panel		

Chapter 5: Trends in Stratospheric Temperatures

Chapter Lead Authors

Marie-Lise Chanin	Service d'Aéronomie du CNRS	France
V. Ramaswamy	NOAA Geophysical Fluid Dynamics Laboratory	US

Coauthors

Dian J. Gaffen	NOAA Air Resources Laboratory	US
William J. Randel	National Center for Atmospheric Research	US
Richard B. Rood	NASA Goddard Space Flight Center	US
Masato Shiotani	Hokkaido University	Japan

Contributors

James K. Angell	NOAA Air Resources Laboratory	US
J. Barnett	Oxford University	UK
Piers M. de F. Forster	University of Reading	UK
Melvyn E. Gelman	NOAA NWS Climate Prediction Center	US
James Hansen	NASA Goddard Institute for Space Studies	US
Philippe Keckhut	Service d'Aéronomie du CNRS	France
Yuri Koshelkov	Central Aerological Observatory	Russia
Karin Labitzke	Freie Universität Berlin	Germany
J.-J. Roger Lin	Research and Data Systems Corporation	US
E.V. Lysenko	Central Aerological Observatory	Russia
John Nash	U.K. Meteorological Office	UK

Alan O'Neill	University of Reading	UK
M. Daniel Schwarzkopf	NOAA Geophysical Fluid Dynamics Laboratory	US
Keith P. Shine	University of Reading	UK
Richard Swinbank	NASA Goddard Space Flight Center	US
Osamu Uchino	Japan Meteorological Agency	Japan

PART 2. ADVANCES IN UNDERSTANDING THE PROCESSES INVOLVED

Chapter 6: Upper Stratospheric Processes

Chapter Lead Authors

Rolf Müller	Forschungszentrum Jülich	Germany
Ross J. Salawitch	California Institute of Technology/Jet Propulsion Laboratory	US

Coauthors

Paul J. Crutzen	Max-Planck-Institut für Chemie	Germany
William A. Lahoz	University of Reading	UK
Gloria L. Manney	California Institute of Technology/Jet Propulsion Laboratory	US
Ralf Toumi	Imperial College	UK

Contributors

David B. Considine	University of Maryland; NASA Goddard Space Flight Center	US
Simon J. Evans	Imperial College	UK
Jens-Uwe Groöß	Forschungszentrum Jülich	Germany
Charles H. Jackman	NASA Goddard Space Flight Center	US
Kenneth W. Jucks	Harvard-Smithsonian Center for Astrophysics	US
Douglas E. Kinnison	Lawrence Livermore National Laboratory	US
Alvin J. Miller	NOAA NWS Climate Prediction Center	US
Gary A. Morris	Valparaiso University	US
Gerald E. Nedoluha	Naval Research Laboratory	US
Cynthia D. Nevison	National Center for Atmospheric Research	US
William J. Randel	National Center for Atmospheric Research	US
A.R. Ravishankara	NOAA Aeronomy Laboratory	US
James M. Russell III	Hampton University	US
Karen H. Sage	NASA Langley Research Center	US
Michelle L. Santee	California Institute of Technology/Jet Propulsion Laboratory	US
David E. Siskind	Naval Research Laboratory	US
Michael E. Summers	Naval Research Laboratory	US
Jörg Trentmann	Max-Planck-Institut für Chemie	Germany
Ray H.J. Wang	Georgia Institute of Technology	US
Jerry Ziemke	Software Corporation of America	US

Chapter 7: Lower Stratospheric Processes

Chapter Lead Authors

A.R. Ravishankara	NOAA Aeronomy Laboratory	US
Theodore G. Shepherd	University of Toronto	Canada

Coauthors

Martyn Chipperfield	Centre for Atmospheric Science, University of Cambridge	UK
Peter Haynes	Centre for Atmospheric Science, University of Cambridge	UK
Randy Kawa	NASA Goddard Space Flight Center	US
Thomas Peter	Max-Planck-Institut für Chemie	Germany
Alan Plumb	Massachusetts Institute of Technology	US
Bob Portmann	NOAA Aeronomy Laboratory	US
William J. Randel	National Center for Atmospheric Research	US
Darryn Waugh	Johns Hopkins University	US
Doug Worsnop	Aerodyne Research, Inc.	US

Contributors

Stephan Borrmann	Universität Mainz	Germany
Byron Boville	National Center for Atmospheric Research	US
Ken Carslaw	Max-Planck-Institut für Chemie	Germany
Rod Jones	Centre for Atmospheric Science, University of Cambridge	UK
Mike Mozurkewich	York University	Canada
Rolf Müller	Forschungszentrum Jülich	Germany
Donal O'Sullivan	NorthWest Research Associates, Inc.	US
Gilles Poulet	Laboratoire de Combustion et Systèmes Réactifs du CNRS	France
Michel Rossi	Ecole Polytechnique Fédérale de Lausanne	Switzerland
Stan Sander	California Institute of Technology/Jet Propulsion Laboratory	US

Chapter 8: Tropospheric Ozone and Related Processes

Chapter Lead Authors

Jos Lelieveld	Institute for Marine and Atmospheric Research Utrecht (IMAU)	The Netherlands
Anne M. Thompson	NASA Goddard Space Flight Center	US

Coauthors

Roseanne D. Diab	University of Natal	South Africa
Oystein Hov	Norsk Institutt for Luftforskning (NILU)	Norway
Dieter Kley	Forschungszentrum Jülich	Germany
Jennifer A. Logan	Harvard University	US

Ole J. Nielsen	Risø National Laboratory	Denmark
William R. Stockwell	Fraunhofer-Institut für Atmosphärische Umweltforschung	Germany
Xiuji Zhou	Chinese Academy of Meteorological Sciences	China

Contributors

Robert Guicherit	Netherlands Organization for Applied Scientific Research (TNO)	The Netherlands
Daniel J. Jacob	Harvard University	US
Michael Kuhn	Fraunhofer-Institut für Atmosphärische Umweltforschung	Germany
Jana B. Milford	University of Colorado	US
Howard W. Sidebottom	University College Dublin	Ireland
Johannes Stähelin	Eidgenössische Technische Hochschule Hönggerberg	Switzerland

PART 3. IMPACTS OF OZONE CHANGES

Chapter 9: Ultraviolet Radiation At The Earth's Surface

Chapter Lead Authors

Jay R. Herman	NASA Goddard Space Flight Center	US
Richard L. McKenzie	National Institute of Water & Atmospheric Research Ltd. (NIWA)	New Zealand

Coauthors

Susana Diaz	Centro Austral de Investigaciones Cientificas (CADIC)	Argentina
James B. Kerr	Atmospheric Environment Service	Canada
Sasha Madronich	National Center for Atmospheric Research	US
Gunther Seckmeyer	Fraunhofer-Institut für Atmosphärische Umweltforschung	Germany

Contributors

Germar Bernhard	Fraunhofer-Institut für Atmosphärische Umweltforschung	Germany
Mario Blumthaler	Universität Innsbruck	Austria
Barry A. Bodhaine	NOAA Climate Monitoring and Diagnostics Laboratory	US
C. Rocky Booth	Biospherical Instruments, Inc.	US
Edward Celarier	Software Corporation of America	US
Piers M. de F. Forster	University of Reading	UK
Nickolay Krotkov	Raytheon STX Inc.	US
Jacqueline Lenoble	Université des Sciences et Technologies de Lille 1	France
Kirsti Leszczynski	Radiation and Nuclear Safety Authority (STUK)	Finland
Craig S. Long	NOAA NWS Climate Prediction Center	US
Bernhard Mayer	Fraunhofer-Institut für Atmosphärische Umweltforschung	Germany
Forrest Mims	Sun Photometer Atmospheric Network	US
Patrick Neale	Smithsonian Environmental Research Center	US

Ruben Piacentini	Planetario y Observatorio de Rosario	Argentina
Ken G. Ryan	Industrial Research Limited	New Zealand
Harry Slaper	National Institute of Public Health and the Environment (RIVM)	The Netherlands
James R. Slusser	Colorado State University	US
Russell Wooldridge	IDEA Corporation	US
Christos Zerefos	Aristotle University of Thessaloniki	Greece

Chapter 10: Climate Effects of Ozone and Halocarbon Changes

Chapter Lead Authors

Claire Granier	Service d'Aéronomie du CNRS; NOAA Aeronomy Laboratory	France/US
Keith P. Shine	University of Reading	UK

Coauthors

John S. Daniel	NOAA Aeronomy Laboratory	US
James Hansen	NASA Goddard Institute for Space Studies	US
Shyam Lal	Physical Research Laboratory	India
Frode Stordal	Norsk Institutt for Luftforskning (NILU)	Norway

Contributors

Slimane Bekki	Service d'Aéronomie du CNRS	France
Lane Bishop	AlliedSignal Inc.	US
Jan Fuglestad	Universitetet I Oslo Centre for International Climate and Environmental Research	Norway
Jan-Eiof Jonson	Universitetet I Oslo	Norway
Sasha Madronich	National Center for Atmospheric Research	US
Gunnar Myhre	Universitetet I Oslo	Norway

PART 4. PREDICTIONS OF FUTURE CHANGES

Chapter 11: Halocarbon Scenarios for the Future Ozone Layer and Related Consequences

Chapter Lead Authors

Sasha Madronich	National Center for Atmospheric Research	US
Guus J.M. Velders	National Institute of Public Health and the Environment (RIVM)	The Netherlands

Coauthors

John S. Daniel	NOAA Aeronomy Laboratory	US
Murari Lal	Indian Institute of Technology	India
Archie McCulloch	ICI Chemicals & Polymers Ltd.	UK
Harry Slaper	National Institute of Public Health and the Environment (RIVM)	The Netherlands

Contributors

Mack McFarland	DuPont Fluoroproducts	US
Pauline M. Midgley	M & D Consulting	Germany
Nelson A. Sabogal	United Nations Environment Programme	Kenya
Susan Solomon	NOAA Aeronomy Laboratory	US
Donald J. Wuebbles	University of Illinois	US

Chapter 12: Predicting Future Ozone Changes and Detection of Recovery

Chapter Lead Authors

David J. Hofmann	NOAA Climate Monitoring and Diagnostics Laboratory	US
John A. Pyle	Centre for Atmospheric Science, University of Cambridge	UK

Coauthors

John Austin	U.K. Meteorological Office	UK
Neal Butchart	U.K. Meteorological Office	UK
Charles H. Jackman	NASA Goddard Space Flight Center	US
Douglas E. Kinnison	Lawrence Livermore National Laboratory	US
Franck Lefèvre	Météo-France, Centre National de Recherches Météorologiques	France
Giovanni Pitari	Università degli Studi dell'Aquila	Italy
Drew Shindell	NASA Goddard Institute for Space Studies	US
Ralf Toumi	University of Cambridge	UK
Peter von der Gathen	Alfred Wegener Institute	Germany

Contributors

Slimane Bekki	Service d'Aéronomie du CNRS; University of Cambridge	France/UK
Christoph Brühl	Max-Planck-Institut für Chemie	Germany
Peter S. Connell	Lawrence Livermore National Laboratory	US
Martin Dameris	Deutsche Forschungsanstalt für Luft- and Raumfahrt	Germany
Eric L. Fleming	Space Applications Corporation	US
Stacey M. Hollandsworth	Space Applications Corporation	US
Samuel J. Oltmans	NOAA Climate Monitoring and Diagnostics Laboratory	US
Lakshman Randeniya	CSIRO Telecommunications and Industrial Physics	Australia
Markus Rex	Alfred Wegener Institute	Germany

Bjoerg Rognerud	Universitetet I Oslo	Norway
Sergei P. Smyshlyaev	Russian State Hydrometeorological Institute	Russia
Hubert Teysse�re	M�t�eo-France, Centre National de Recherches M�t�eorologiques	France
Guus J.M. Velders	National Institute of Public Health and the Environment (RIVM)	The Netherlands
Debra K. Weisenstein	Atmospheric and Environmental Research, Inc.	US
Jerry Ziemke	Software Corporation of America	US

CHAPTER EDITORIAL CONTRIBUTORS

Chapter 1: Long-Lived Ozone-Related Compounds

Nada Derek	CSIRO Division of Atmospheric Research	Australia
L. Kubrick	Massachusetts Institute of Technology	US
Kathy A. Wolfe	Computer Sciences Corporation	US
Diane Zander	Universit� de Li�ge	Belgium

Chapter 2: Short-Lived Ozone-Related Compounds

Kathy A. Wolfe	Computer Sciences Corporation	US
----------------	-------------------------------	----

Chapter 5: Trends in Stratospheric Temperatures

Gail Haller	NOAA Geophysical Fluid Dynamics Laboratory	US
Cathy Raphael	NOAA Geophysical Fluid Dynamics Laboratory	US
Jeff Varanyak	NOAA Geophysical Fluid Dynamics Laboratory	US

Chapter 6: Upper Stratospheric Processes

Stephan B�ttcher	Tel Aviv University	Israel
------------------	---------------------	--------

Chapter 7: Lower Stratospheric Processes

LeAnn Droppleman	NOAA Aeronomy Laboratory	US
------------------	--------------------------	----

Chapter 8: Tropospheric Ozone

Matthew G. Seybold	Steven Myers and Associates Corporation/ NASA Goddard Space Flight Center	US
--------------------	--	----

Chapter 11: Scenarios for the Future Ozone Layer and Related Consequences

Chris Fischer	National Center for Atmospheric Research	US
---------------	--	----

Chapter 12: Predicting Future Ozone Changes and Detection of Recovery

Ann Thorne	NOAA Climate Monitoring and Diagnostics Laboratory	US
------------	--	----

REVIEWERS

Daniel L. Albritton	National Oceanic and Atmospheric Administration	US
Georgios T. Amanatidis	European Commission	Belgium
James K. Angell	NOAA Air Resources Laboratory	US
Pieter J. Aucamp	Ptersa Environmental Consultants	South Africa
Linnea Avallone	University of Colorado	US
Darrel Baumgardner	National Center for Atmospheric Research	US
Lane Bishop	AlliedSignal Inc.	US
Mario Blumthaler	Universität Innsbruck	Austria
Greg Bodeker	National Institute of Water & Atmospheric Research Ltd. (NIWA)	New Zealand
Barry A. Bodhaine	NOAA Climate Monitoring and Diagnostics Laboratory	US
Rumen D. Bojkov	World Meteorological Organization	Switzerland
Guy Brasseur	National Center for Atmospheric Research	US
Christoph Brühl	Max-Planck-Institut für Chemie	Germany
William H. Brune	Pennsylvania State University	US
Neal Butchart	U.K. Meteorological Office	UK
Pablo O. Canziani	Universidad de Buenos Aires	Argentina
Daniel Cariolle	Météo-France, Centre National de Recherches Météorologiques	France
Marie-Lise Chanin	Service d'Aéronomie du CNRS	France
Cathy Clerbaux	Service d'Aéronomie du CNRS	France
Michael Coffey	National Center for Atmospheric Research	US
R.A. Cox	Centre for Atmospheric Science, University of Cambridge	UK
Paul J. Crutzen	Max-Planck-Institut für Chemie	Germany
John S. Daniel	NOAA Aeronomy Laboratory	US
Richard Derwent	U.K. Meteorological Office	UK
Susana Diaz	Centro Austral de Investigaciones Cientificas (CADIC)	Argentina
Ed Dlugokencky	NOAA Climate Monitoring and Diagnostics Laboratory	US
Thomas Duafala	Tri-Cal Research Division	US
Dieter H. Ehhalt	Institut für Chemie und Dynamik der Geosphäre	Germany
James W. Elkins	NOAA Climate Monitoring and Diagnostics Laboratory	US
Christine A. Ennis	NOAA Aeronomy Laboratory/CIRES	US
David W. Fahey	NOAA Aeronomy Laboratory	US
Jack Fishman	NASA Langley Research Center	US
Piers M. de F. Forster	University of Reading	UK
J. Paul F. Fortuin	Koninklijk Nederlands Meteorologisch Instituut (KNMI)	The Netherlands
Paul J. Fraser	CSIRO Division of Atmospheric Research	Australia
Lucien Froidevaux	California Institute of Technology/Jet Propulsion Laboratory	US
Marvin A. Geller	State University of New York at Stony Brook	US
Sophie Godin	Service d'Aéronomie du CNRS	France
Allen Goldstein	College of Natural Resources	UK
George S. Golitsyn	Russian Academy of Sciences	Russia
Claire Granier	Service d'Aéronomie du CNRS; NOAA Aeronomy Laboratory	France/US
William B. Grant	NASA Langley Research Center	US

Robert Guicherit	Netherlands Organization for Applied Scientific Research (TNO)	The Netherlands
Neil R.P. Harris	European Ozone Research Coordinating Unit	UK
Alain Hauchecorne	Service d'Aéronomie du CNRS	France
Didier Hauglustaine	National Center for Atmospheric Research	US
Jay R. Herman	NASA Goddard Space Flight Center	US
David J. Hofmann	NOAA Climate Monitoring and Diagnostics Laboratory	US
James R. Holton	University of Washington	US
Robert Hudson	University of Maryland	US
Drusilla Hufford	U.S. Environmental Protection Agency	US
Abdel Moneim Ibrahim	Egyptian Meteorological Authority	Egypt
Mohammad I. Ilyas	Universiti Sains Malaysia	Malaysia
Ivar S.A. Isaksen	Universitetet I Oslo	Norway
Tomoyuki Ito	Japan Meteorological Agency	Japan
Evgeny A. Jadin	Central Aerological Observatory	Russia
Rod Jones	Centre for Atmospheric Science, University of Cambridge	UK
Torben S. Jørgensen	Danmarks Meteorologiske Institut	Denmark
David Karoly	Monash University	Australia
Jack A. Kaye	NASA Headquarters	US
Hennie Kelder	Koninklijk Nederlands Meteorologisch Instituut (KNMI)	The Netherlands
James B. Kerr	Atmospheric Environment Service	Canada
Jhoon Kim	Korea Aerospace Research Institute	Republic of Korea
Volker Kirchhoff	Instituto Nacional de Pesquisas Espaciais (INPE)	Brazil
Malcolm K.W. Ko	Atmospheric and Environmental Research, Inc.	US
Kunihiko Kodera	Meteorological Research Institute	Japan
Yutaka Kondo	Nagoya University	Japan
Janusz Krzyscin	Polish Academy of Sciences	Poland
Michael J. Kurylo	National Institute of Standards and Technology; NASA Headquarters	US
Murari Lal	Indian Institute of Technology	India
Yuan-Pern Lee	National Tsing Hua University	Taiwan
Jos Lelieveld	Institute for Marine and Atmospheric Research Utrecht (IMAU)	The Netherlands
Joel M. Levy	NOAA Office of Global Programs	US
Jennifer A. Logan	Harvard University	US
Craig S. Long	NOAA NWS Climate Prediction Center	US
Sasha Madronich	National Center for Atmospheric Research	US
Jerry D. Mahlman	NOAA Geophysical Fluid Dynamics Laboratory	US
Andrew Matthews	National Institute of Water & Atmospheric Research Ltd. (NIWA)	New Zealand
M. Patrick McCormick	Hampton University	US
Archie McCulloch	ICI Chemicals & Polymers Ltd.	UK
Mack McFarland	DuPont Fluoroproducts	US
Danny McKenna	Forschungszentrum Jülich	Germany
Richard L. McKenzie	National Institute of Water & Atmospheric Research Ltd. (NIWA)	New Zealand
Gérard Mégie	Service d'Aéronomie du CNRS	France

Pauline M. Midgley	M & D Consulting	Germany
Alvin J. Miller	NOAA NWS Climate Prediction Center	US
Philippe Mirabel	Université Louis Pasteur	France
Masa Miyauchi	Japan Meteorological Agency	Japan
Mario J. Molina	Massachusetts Institute of Technology	US
Rolf Müller	Forschungszentrum Jülich	Germany
Hideaki Nakane	National Institute for Environmental Studies	Japan
Paul A. Newman	NASA Goddard Space Flight Center	US
Samuel J. Oltmans	NOAA Climate Monitoring and Diagnostics Laboratory	US
Michael Oppenheimer	Environmental Defense Fund	US
Stuart A. Penkett	University of East Anglia	UK
Joyce Penner	University of Michigan	US
Thomas Peter	Max-Planck-Institut für Chemie	Germany
Michel Pirre	Service d'Aéronomie du CNRS	France
Jean-Pierre Pommereau	Service d'Aéronomie du CNRS	France
Lamont R. Poole	NASA Langley Research Center	US
Michael Prather	University of California at Irvine	US
M. Margarita Préndez	Universidad de Chile	Chile
Ronald G. Prinn	Massachusetts Institute of Technology	US
John A. Pyle	Centre for Atmospheric Science, University of Cambridge	UK
V. Ramaswamy	NOAA Geophysical Fluid Dynamics Laboratory	US
William J. Randel	National Center for Atmospheric Research	US
A.R. Ravishankara	NOAA Aeronomy Laboratory	US
George C. Reid	NOAA Aeronomy Laboratory	US
Henning Rodhe	Stockholms Universitet	Sweden
José M. Rodríguez	Atmospheric and Environmental Research, Inc.	US
James M. Rosen	University of Wyoming	US
James M. Russell III	Hampton Univesity	US
Keith R. Ryan	CSIRO Telecommunications and Industrial Physics	Australia
Nelson A. Sabogal	United Nations Environment Programme	Kenya
Ross J. Salawitch	California Institute of Technology/Jet Propulsion Laboratory	US
Eugenio Sanhueza	Instituto Venezolano de Investigaciones Cientificas (IVIC)	Venezuela
Ulrich Schmidt	Universität Frankfurt	Germany
Ulrich Schumann	Deutsche Forschungsanstalt für Luft- und Raumfahrt	Germany
Theodore G. Shepherd	University of Toronto	Canada
Keith P. Shine	University of Reading	UK
Susan Solomon	NOAA Aeronomy Laboratory	US
Johannes Stähelin	Eidgenössische Technische Hochschule Hönggerberg	Switzerland
Leopoldo Stefanutti	Istituto di Ricrea sulle Onde Elettromagnetiche del Consiglio Nazionale della Richerche	Italy
William R. Stockwell	Fraunhofer-Institut für Atmosphärische Umweltforschung	Germany
B.H. Subbaraya	Physical Research Laboratory	India
Petteri Taalas	Finnish Meteorological Institute	Finland
Xiao-Yan Tang	Peking University	China
Anne M. Thompson	NASA Goddard Space Flight Center	US
Brian Toon	University of Colorado	US

Michael Trainer	NOAA Aeronomy Laboratory	US
Osamu Uchino	Japan Meteorological Agency	Japan
Jan C. van der Leun	University Hospital	The Netherlands
Karel Vanicek	Czech Hydrometeorological Institute	Czech Republic
Guus J.M. Velders	National Institute of Public Health and the Environment (RIVM)	The Netherlands
Guido Visconti	Università degli Studi dell'Aquila	Italy
Andreas Volz-Thomas	Forschungszentrum Jülich	Germany
Wei-Chyung Wang	State University of New York at Albany	US
Joe Waters	California Institute of Technology/Jet Propulsion Laboratory	US
Robert T. Watson	The World Bank	US
Ray F. Weiss	University of California at San Diego	US
Paul O. Wennberg	California Institute of Technology	US
James C. Wilson	University of Denver	US
Donald J. Wuebbles	University of Illinois	US
Vladimir Yushkov	Central Aerological Observatory	Russia
Ahmed Zand	Tehran Unversity	Iran
R. Zander	Université de Liège	Belgium
Christos Zerefos	Aristotle University of Thessaloniki	Greece

OZONE PEER-REVIEW MEETING

Les Diablerets, Switzerland

June 1-5, 1998

Daniel L. Albritton	National Oceanic and Atmospheric Administration	US
Georgios T. Amanatidis	European Commission	Belgium
Pieter J. Aucamp	Ptersa Environmental Consultants	South Africa
Lane Bishop	AlliedSignal Inc.	US
Rumen D. Bojkov	World Meteorological Organization	Switzerland
Marie-Lise Chanin	Service d'Aéronomie du CNRS	France
R.A. Cox	Centre for Atmospheric Science, University of Cambridge	UK
Paul J. Crutzen	Max-Planck-Institut für Chemie	Germany
John S. Daniel	NOAA Aeronomy Laboratory	US
Susana Diaz	Centro Austral de Investigaciones Cientificas (CADIC)	Argentina
Thomas Duafala	Tri-Cal Research Division	US
Dieter H. Ehhalt	Institut für Chemie und Dynamik der Geosphäre	Germany
James W. Elkins	NOAA Climate Monitoring and Diagnostics Laboratory	US
Christine A. Ennis	NOAA Aeronomy Laboratory/CIRES	US
David W. Fahey	NOAA Aeronomy Laboratory	US
Paul J. Fraser	CSIRO Division of Atmospheric Research	Australia
Lucien Froidevaux	California Institute of Technology/Jet Propulsion Laboratory	US
Marvin A. Geller	State University of New York at Stony Brook	US
Sophie Godin	Service d'Aéronomie du CNRS	France
Claire Granier	Service d'Aéronomie du CNRS; NOAA Aeronomy Laboratory	France/US
Neil R.P. Harris	European Ozone Research Coordinating Unit	UK
Jay R. Herman	NASA Goddard Space Flight Center	US

David J. Hofmann	NOAA Climate Monitoring and Diagnostics Laboratory	US
James R. Holton	University of Washington	US
Robert Hudson	University of Maryland	US
Abdel Moneim Ibrahim	Egyptian Meteorological Authority	Egypt
Mohammad I. Ilyas	Universiti Sains Malaysia	Malaysia
Ivar S.A. Isaksen	Universitetet I Oslo	Norway
Rod Jones	Centre for Atmospheric Science, University of Cambridge	UK
James B. Kerr	Atmospheric Environment Service	Canada
Michael J. Kurylo	National Institute of Standards and Technology; NASA Headquarters	US
Murari Lal	Indian Institute of Technology	India
Jos Lelieveld	Institute for Marine and Atmospheric Research Utrecht (IMAU)	The Netherlands
Jennifer A. Logan	Harvard University	US
Sasha Madronich	National Center for Atmospheric Research	US
M. Patrick McCormick	Hampton University	US
Mack McFarland	DuPont Fluoroproducts	US
Danny McKenna	Forschungszentrum Jülich	Germany
Richard L. McKenzie	National Institute of Water & Atmospheric Research Ltd. (NIWA)	New Zealand
Gérard Mégie	Service d'Aéronomie du CNRS	France
Rolf Müller	Forschungszentrum Jülich	Germany
Hideaki Nakane	National Institute for Environmental Studies	Japan
Paul A. Newman	NASA Goddard Space Flight Center	US
Samuel J. Oltmans	NOAA Climate Monitoring and Diagnostics Laboratory	US
Stuart A. Penkett	University of East Anglia	UK
Thomas Peter	Max-Planck-Institut für Chemie	Germany
Lamont R. Poole	NASA Langley Research Center	US
M. Margarita Préndez	Universidad de Chile	Chile
John A. Pyle	Centre for Atmospheric Science, University of Cambridge	UK
V. Ramaswamy	NOAA Geophysical Fluid Dynamics Laboratory	US
William J. Randel	National Center for Atmospheric Research	US
A.R. Ravishankara	NOAA Aeronomy Laboratory	US
José M. Rodríguez	Atmospheric and Environmental Research, Inc.	US
James M. Russell III	Hampton University	US
Nelson A. Sabogal	United Nations Environment Programme	Kenya
Ross J. Salawitch	California Institute of Technology/Jet Propulsion Laboratory	US
Eugenio Sanhueza	Instituto Venezolano de Investigaciones Cientificas (IVIC)	Venezuela
Theodore G. Shepherd	University of Toronto	Canada
Keith P. Shine	University of Reading	UK
Susan Solomon	NOAA Aeronomy Laboratory	US
William R. Stockwell	Fraunhofer-Institut für Atmosphärische Umweltforschung	Germany
B.H. Subbaraya	Physical Research Laboratory	India
Petteri Taalas	Finnish Meteorological Institute	Finland
Osamu Uchino	Japan Meteorological Agency	Japan
Jan C. van der Leun	University Hospital	The Netherlands
Karel Vanicek	Czech Hydrometeorological Institute	Czech Republic

Guus J.M. Velders	National Institute of Public Health and the Environment (RIVM)	The Netherlands
Robert T. Watson	The World Bank	US
Ray F. Weiss	University of California at San Diego	US
Donald J. Wuebbles	University of Illinois	US
Ahmed Zand	Tehran University	Iran
R. Zander	Université de Liège	Belgium
Christos Zerefos	Aristotle University of Thessaloniki	Greece

Sponsoring Organizations Liaisons

Rumen D. Bojkov	World Meteorological Organization	Switzerland
K.M. Sarma	United Nations Environment Programme	Kenya
Daniel L. Albritton	National Oceanic and Atmospheric Administration	US
Michael J. Kurylo	National Institute of Standards and Technology; NASA Headquarters	US
Georgios T. Amanatidis	European Commission	Belgium

Coordinating Editor

Christine A. Ennis	NOAA Aeronomy Laboratory/CIRES	US
--------------------	--------------------------------	----

Editorial Staff

Debra Dailey-Fisher	NOAA Aeronomy Laboratory	US
Christine C. Sweet	NOAA Environmental Research Laboratories	US
Jeanne S. Waters	NOAA Aeronomy Laboratory	US

Publication Design and Layout

VISUAL SCIENCE INC.

Dave Gallant
Elizabeth J. Graves
Scott Lininger
Julianne Snider

Conference Coordination and Documentation

Rumen D. Bojkov	World Meteorological Organization	Switzerland
Marie-Christine Charrière	World Meteorological Organization	Switzerland
Christine A. Ennis	NOAA Aeronomy Laboratory/CIRES	US
Jeanne S. Waters	NOAA Aeronomy Laboratory	US

Conference Support

Catherine A. Burgdorf	NOAA Aeronomy Laboratory/CIRES	US
Marie-Christine Charrière	World Meteorological Organization	Switzerland
Rose M. Kendall	Computer Sciences Corporation	US
Jeanne S. Waters	NOAA Aeronomy Laboratory	US
Kathy A. Wolfe	Computer Sciences Corporation	US

Computing and Networking Support

Catherine A. Burgdorf	NOAA Aeronomy Laboratory/CIRES	US
Walter J. Harrop	NOAA Aeronomy Laboratory	US
Ken Jamieson	NOAA Aeronomy Laboratory/CIRES	US
Sarah Thompson	NOAA Aeronomy Laboratory/CIRES	US

SECTION C: Summary of the Stratospheric Processes and Their Role in Climate/International Ozone Commission/Global Atmospheric Watch (SPARC/IOC/GAW) Assessment of Trends in the Vertical Distribution of Ozone

CO-CHAIRS

Neil Harris	European Ozone Research Coordinating Unit	UK
Robert Hudson	University of Maryland	US

CHAPTER 1

Lead Authors

David Hofmann	NOAA Climate Monitoring and Diagnostics Laboratory	US
Clive Rodgers	University of Oxford	UK

Authors

Dirk DeMuer	Royal Meteorological Institute (KMI)	Belgium
Lucien Froidevaux	NASA Jet Propulsion Laboratory	US
Sophie Godin	Service d'Aeronomie, CNRS	France
Larry Gordley	GATS, Inc., VA	US
Ernest Hilsenrath	NASA Goddard Space Flight Center	US
Rich McPeters	NASA Goddard Space Flight Center	US
Mike Newchurch	University of Alabama	US
Dave Rusch	University of Colorado	US
Sam Oltmans	NOAA Climate Monitoring and Diagnostics Laboratory	US
Joe Zawodny	NASA Langley Research Center	US

CHAPTER 2

Lead Authors

James M. Russell III	Hampton University	US
Herman G. J. Smit	Forschungszentrum Jülich	Germany

Co-Authors

Robert J. Atkinson	Meteorology CRC, Bureau of Meteorology	Australia
Brian J. Connor	National Institute of Water and Atmospheric Research	New Zealand
Derek M. Cunnold	Georgia Institute of Technology	US
Lawrence E. Flynn	NOAA National Environmental Satellite, Data and Information Services	US
Sophie Godin	Service d'Aeronomie, CNRS	France
Stacey Hollandsworth	Space Applications Corporation	US
James B. Kerr	Atmospheric Environment Service	Canada
A. J. Miller	NOAA National Centers for Environmental Prediction	US
Gary A. Morris	University of Maryland, Baltimore	US
Rich McPeters	NASA Goddard Space Flight Center	US
Mike Newchurch	University of Alabama	US
Dave Rusch	University of Colorado	US
Larry W. Thomason	NASA Langley Research Center	US
Ray H. J. Wang	Georgia Institute of Technology	US

Contributors

Gerard Ancellet	Service d'Aeronomie, CNRS	France
Matthias Beekmann	Service d'Aeronomie, CNRS	France
Greg Bodeker	National Institute of Water and Atmospheric Research	New Zealand
Rumen Bojkov	World Meteorological Organization	Switzerland
Ellen J. Brinksmas	Vrije Universiteit, Amsterdam	Netherlands
Hans Claude	Deutscher Wetterdienst	Germany
Hugo De Backer	Institute Royal Meteorologique de Belgique	Belgium
Pierre Heanet	Schweizerische Meteorologische Anstalt	Switzerland
Bryan Johnson	NOAA Climate Monitoring and Diagnostics Laboratory	US
N. Kämpfer	Universität Bern	Switzerland
Gordon J. Labow	NASA Goddard Space Flight Center	US
Ulf Köhle	Deutscher Wetterdienst	Germany
I. Stuart McDermid	NASA Jet Propulsion Laboratory/Caltech	US
Thomas McGee	NASA Goddard Space Flight Center	US
Hideaki Nakane	National Institute for Environmental Studies	Japan
Samuel Oltmans	NOAA Climate Monitoring and Diagnostics Laboratory	US
Francis J. Schmidlin	NASA Goddard Space Flight Center	US
Johannes Staehelin	Eidgenössische Technische Hochschule, Zurich	Switzerland
Wolfgang Steinbrecht	Deutscher Wetterdienst	Germany
Daan P. J. Swart	Rijksinstituut voor Volksgezondheid en Milieu	Netherlands
David Tarasick	Atmospheric Environment Service	Canada
Osamu Uchino	Japan Meteorological Agency	Japan
Pierre Viatte	Schweizerische Meteorologische Anstalt	Switzerland
Joseph M. Zawodny	NASA Langley Research Center	US

CHAPTER 3

Lead Authors

Richard Stolarski	NASA Goddard Space Flight Center	US
William Randel	National Center for Atmospheric Research	US

Co-Authors

Lane Bishop	Allied Signal, Inc.	US
Derek Cunnold	Georgia Institute of Technology	US
Dirk DeMuer	Royal Meteorological Institute (KMI)	Belgium
Sophie Godin	Service d'Aeronomie, CNRS	France
Stacey Hollandsworth	Space Applications Corporation	US
Lon Hood	University of Arizona	US
Jennifer Logan	Harvard University	US
Jim Miller	NOAA National Centers for Environmental Prediction	US
Mike Newchurch	University of Alabama	US
Sam Oltmans	NOAA Climate and Diagnostics Laboratory	US
Osamu Uchino	Meteorological Research Institute	Japan
Ray H. J. Wang	Georgia Institute of Technology	US

REVIEWERS

Roger Atkinson	Atmosphere Watch Section	Australia
John Burrows	University of Bremen	Germany
Arthur Downey	Atmosphere Watch Section	Australia
Herb Fischer	Forschungszentrum Karlsruhe	Germany
John Gille	National Center for Atmospheric Research	US
Rod Jones	University of Cambridge	UK
Brian Kerridge	Rutherford Appleton Laboratory	UK
Richard McKenzie	National Institute of Water and Atmospheric Research	New Zealand
Howard Roscoe	British Antarctic Survey	UK
Yasuhiro Sasano	National Institute for Environmental Studies	Japan
Susan Solomon	NOAA	US
Geraint Vaughan	University of Wales	UK

SECTION D: Policymakers Summary of the Intergovernmental Panel on Climate Change (IPCC) Special Report on Aviation and the Global Atmosphere

AUTHORS AND CONTRIBUTORS

Chapter 1: Introduction

Lead Authors

J. H. Ellis	Federal Express Corporation	US
N. R. P. Harris	European Ozone Research Coordination Unit	UK
D. H. Lister	DERA	UK
J. E. Penner	University of Michigan	US

Review Editor

B. S. Nyenzi	Directorate of Meteorology	Tanzania
--------------	----------------------------	----------

Chapter 2: Impacts of Aircraft Emissions on Atmospheric Ozone

Coordinating Lead Authors

R. G. Derwent	Meteorological Office	UK
R. R. Friedl	Jet Propulsion Laboratory	US

Lead Authors

I. L. Karol	Main Geophysical Observatory	Russia
H. Kelder	KNMI	The Netherlands
V. W. J. H. Kirchoff	Instituto Nacional de Pesquisas Espaciais	Brazil
T. Ogawa	National Space Development Agency of Japan	Japan
M. J. Rossi	Ecole Polytechnique Federale de Lausanne	Switzerland
P. Wennberg	California Institute of Technology	US

Contributors

T. K. Berntsen	University of Oslo	Norway
C. H. Brühl	Max-Planck Institut für Chemie	Germany
D. Brunner	KNMI	The Netherlands
P. Crutzen	Max-Planck Institut für Chemie	Germany
M. Y. Danilin	Atmospheric and Environmental Research, Inc.	US
F. J. Dentener	Institute for Marine and Atmospheric Research	The Netherlands
L. Emmons	Space Physics Research Laboratory	US
F. Flatoy	Geophysics Institute	Norway
J. S. Fuglestedt	University of Oslo	Norway

T. Gerz	DLR Institut für Physik der Atmosphäre	Germany
V. Grewe	DLR Institut für Physik der Atmosphäre	Germany
D. Hauglustaine	CNRS Service Aeronomie	France
G. Hayman	AEA Technology	UK
O. Hov	Ministry of Environment	Norway
D. Jacob	Harvard University	US
C. E. Johnson	Meteorological Office	UK
M. Kanakidou	Centre des Faibles Radioactivités	France
B. Kärcher	DLR Institut für Physik der Atmosphäre	Germany
D. E. Kinnison	Lawrence Livermore National Laboratory	US
A. A. Kiselev	Main Geophysical Observatory	Russia
I. Köhler	DLR Institut für Physik der Atmosphäre	Germany
J. Lelieveld	Institute of Marine and Atmospheric Research	The Netherlands
J. Logan	Harvard University	US
J. F. Müller	Belgian Institute for Space Aeronomy	Belgium
J. E. Penner	University of Michigan	US
H. Petry	University of Köln	Germany
G. Pitari	Università Degli Studi dell' Aquila	Italy
R. Ramarosan	ONERA	France
F. Rohrer	Forschungszentrum Jülich	Germany
E. V. Rozanov	University of Illinois	US
K. Ryan	CSIRO	Australia
R. J. Salawitch	Jet Propulsion Laboratory	US
R. Sausen	DLR Institut für Physik der Atmosphäre	Germany
U. Schumann	DLR Institut für Physik der Atmosphäre	Germany
R. F. Slemr	Fraunhofer-Gesellschaft, Institut für Atmosphärische, Umweltforschung	Germany
D. Stevenson	Meteorological Office	UK
F. Stordal	Norwegian Institute for Air Research	Norway
A. Strand	Geophysics Institute	Norway
A. Thompson	NASA Goddard Space Flight Center	US
G. Velders	RIVM	The Netherlands
P. F. J. van Velthoven	KNMI	The Netherlands
P. Valks	RIVM	The Netherlands
Y. Wang	Georgia Institute of Technology	US
X. W. M. F. Wauben	KNMI	The Netherlands
D. K. Weisenstein	Atmospheric and Environmental Research, Inc.	US

Review Editor

A. Wahner	Forschungszentrum Jülich	Germany
-----------	--------------------------	---------

Chapter 3: Aviation-Produced Aerosols and Cloudiness

Coordinating Lead Authors

D. W. Fahey	NOAA Aeronomy Laboratory	US
U. Schumann	DLR Institut für Physik der Atmosphäre	Germany

Lead Authors

S. Ackerman	University of Wisconsin	US
P. Artaxo	University of Sao Paulo, Instituto de Fisica	Brazil
O. Boucher	Université de Lille	France
M. Y. Danilin	Atmospheric and Environmental Research, Inc.	US
B. Kärcher	DLR Institut für Physik der Atmosphäre	Germany
P. Minnis	NASA Langley Research Center	US
T. Nakajima	Center for Climate System Research, University of Tokyo	Japan
O. B. Toon	University of Colorado	US

Contributors

J. K. Ayers	Analytical Services and Materials, Inc.	US
T. K. Berntsen	Center for International Climate and Environmental Research	Norway
P. S. Connell	Lawrence Livermore National Laboratory	US
F. J. Dentener	Ulrecht University, Institute for Marine and Atmospheric Research	The Netherlands
D. R. Doelling	NASA Langley Research Center	US
A. Döpelheuer	DLR Institut für Physik der Antriebstechnik	Germany
E. L. Fleming	NASA Goddard Space Flight Center	US
K. Gierens	DLR Institut für Physik der Atmosphäre	Germany
C. H. Jackman	NASA Goddard Space Flight Center	US
H. Jäger	Fraunhofer-Gesellschaft, Institut für Atmosphärische, Umweltforschung	Germany
E. J. Jensen	NASA Ames Research Center	US
G. S. Kent	NASA Langley Research Center	US
I. Köhler	DLR Institut für Physik der Atmosphäre	Germany
R. Meerkötter	DLR Institut für Physik der Atmosphäre	Germany
J. E. Penner	University of Michigan	US
G. Pitari	Università Degli Studi dell' Aquila	Italy
M. J. Prather	University of California at Irvine	US
J. Ström	University of Stockholm	Sweden
Y. Tsushima	Center for Climate System Research, University of Tokyo	Japan
C. J. Weaver	NASA Goddard Space Flight Center	US
D. K. Weisenstein	Atmospheric and Environmental Research, Inc.	US

Review Editor

K.-N. Liou UCLA, Department of Atmospheric Sciences US

Chapter 4: Modeling the Chemical Composition of the Future Atmosphere

Coordinating Lead Authors

I. Isaksen University of Oslo Norway
C. H. Jackman NASA Goddard Space Flight Center US

Lead Authors

S. L. Baughcum The Boeing Company US
F. J. Dentener Institute for Marine and Atmospheric Research The Netherlands
W. L. Grose NASA Langley Research Center US
P. Kasibhatla Duke University US
D. E. Kinnison Lawrence Livermore National Laboratory US
M. K. W. Ko Atmospheric and Environmental Research, Inc. US
J. C. McConnell York University Canada
G. Pitari Università Degli Studi dell' Aquila Italy
D. Wuebbles University of Illinois US

Contributors

T. K. Berntsen University of Oslo Norway
M. Y. Danilin Atmospheric and Environmental Research, Inc. US
R. S. Eckman NASA Langley Research Center US
E. L. Fleming NASA Goddard Space Flight Center US
M. Gauss University of Oslo Norway
V. Grewe DLR Institut für Physik der Atmosphäre Germany
R. Harwood University of Edinburgh UK
D. Jacob Harvard University US
H. Kelder KNMI The Netherlands
J.-F. Muller Belgian Institute for Space Aeronomy Belgium
M. J. Prather University of California at Irvine US
H. Rogers University of Cambridge UK
R. Sausen DLR Institut für Physik der Atmosphäre Germany
D. Stevenson Meteorological Office UK
P. F. J. van Velthoven KNMI The Netherlands
M. van Weele KNMI The Netherlands
P. Vohralik CSIRO Australia
Y. Wang Georgia Institute of Technology US
D. K. Weisenstein Atmospheric and Environmental Research, Inc. US

Review Editor

J. Austin Meteorological Office UK

Chapter 5: Solar Ultraviolet Irradiance at the Ground

Coordinating Lead Authors

J. E. Frederick University of Chicago US
K. R. Ryan CSIRO Australia

Lead Authors

A. F. Bais Aristotle University of Thessaloniki Greece
J. B. Kerr Atmospheric Environment Service Canada
B. Wu Institute of Atmospheric Physics (Deceased) China

Contributors

R. Meerkötter DLR Institut für Physik der Atmosphäre Germany
I. C. Plumb CSIRO Australia

Review Editor

C. Zerefos Aristotle University of Thessaloniki Greece

Chapter 6: Potential Climate Change from Aviation

Coordinating Lead Authors

M. J. Prather University of California at Irvine US
R. Sausen DLR Institut für Physik der Atmosphäre Germany

Lead Authors

A. S. Grossman Lawrence Livermore National Laboratory US
J. M. Haywood Meteorological Office UK
D. Rind NASA Goddard Institute of Space Studies US
B. H. Subbaraya ISRO HQ India

Contributors

P. M. Forster University of Reading UK
A. K. Jain University of Illinois US
M. Ponater DLR Institut für Physik der Atmosphäre Germany
U. Schumann DLR Institut für Physik der Atmosphäre Germany

W.-C. Wang	State University of New York at Albany	US
T. M. L. Wigley	NCAR	US
D. J. Wuebbles	University of Illinois	US

Review Editor

D. Yihui	China Meteorological Administration	China
----------	-------------------------------------	-------

Chapter 7: Aircraft Technology and Its Relation to Emissions

Coordinating Lead Authors

J. S. Lewis	Rolls Royce Plc.	UK
R. Niedzwiecki	NASA Lewis Research Center	US

Lead Authors

D. W. Bahr	G. E. Aircraft Engines (Retired)	US
S. Bullock	Rolls Royce Plc.	UK
N. Cumpsty	Cambridge University	UK
W. Dodds	General Electric Company	US
D. DuBois	The Boeing Company	US
A. Epstein	Massachusetts Institute of Technology	US
W. W. Ferguson	Pratt & Whitney Aircraft	US
A. Fiorentino	Pratt & Whitney Aircraft	US
A. A. Gorbatko	CIAM	Russia
D. E. Hagen	University of Missouri-Rolla	US
P. J. Hart	Allison Engine Company	US
S. Hayashi	National Aerospace Laboratory	Japan
J. B. Jamieson	Consultant	UK
J. Keerebrock	Massachusetts Institute of Technology	US
M. Lecht	DLR Institut für Physik der Antriebstechnik	Germany
B. Lowrie	Rolls Royce Plc.	UK
R. C. Miake-Lye	Aerodyne Research Inc.	US
A. K. Mortlock	The Boeing Company	US
C. Moses	Sowthwest Research Institute	US
K. Renger	Airbus Industrie	France
S. Sampath	Pratt & Whitney Canada Inc.	Canada
J. Sanborn	Allied Signal Engines	US
B. Simon	Motoren-und-Turbinen-Union	Germany
A. Sorokin	CLAMECOLEN	Russia
W. Taylor	Exxon Research and Energy Co.	US
I. Waitz	MIT Gas Turbine Laboratory	US
C. C. Wey	Army Vehicle Propulsion Directorate	US
P. Whitefield	University of Missouri-Rolla	US
C. W. Wilson	Combustion and Emissions Group Propulsion	UK

S. Wu	Beijing University of Aeronautics and Astronautics	China
-------	--	-------

Contributors

S. L. Baughcum	The Boeing Company	US
A. Döpelheuer	DLR Institut für Physik der Antriebstechnik	Germany
H. J. Hackstein	AI/EE-T Engineering Directorate	Germany
H. Mongia	General Electric Company	US
R. R. Nichols	The Boeing Company	US
C. Osonitsch	Gulfstream	US
R. Paladino	University of Missouri-Rolla	US
M. K. Razdan	Allison Engine Company	US
M. Roquemore	WL/POSF	US
P. A. Schulte	DLR Institut für Physik der Atmosphäre	Germany
D. J. Sutkus	The Boeing Company	US

Review Editor

M. Wright	Consultant	UK
-----------	------------	----

Chapter 8: Air Transport Operations and Relation to Emissions

Coordinating Lead Author

G. Bekebrede	NLR	The Netherlands
--------------	-----	-----------------

Lead Authors

D. Dimitriu	Romanian Air Transport	Romania
L. Dobbie	IATA	
V. Galotti	ICAO	
A. Liewen	Eurocontrol Agency	Belgium
S. Nakao	Japan Airlines	Japan
D. Raper	Manchester Metropolitan University	UK
H. Somerville	British Airways	UK
R. L. Wayson	University of Central Florida	US
S. Webb	The Weinberg Group, Inc.	US

Contributors

A. Gil	Airports Council International	Switzerland
D. R. Marchi	Airports Council International	US
B. Miaillier	Eurocontrol Airspace and Navigation	Belgium
B. O. Nas	SAS	Sweden
J. Templeman	The Boeing Company	US

E. Fleuti	Zurich Airport Authority	Switzerland
M. Mann	DETR	UK
H. Somerville	British Airways	UK

Review Editor

C. V. Oster, Jr.	Indiana University	US
------------------	--------------------	----

EXPERT REVIEWERS

Albania

E. Demiraj Bruci	Hydrometeorological Institute
------------------	-------------------------------

Australia

E. Curran	Bureau of Meterology
K. Ryan	CSIRO
J. Zillman	Bureau of Meterology

Austria

M. Blumthaler	Innsbruck University
T. Glöckel	Federal Environment Agency
K. Radunsky	Federal Environment Agency

Belgium

G. T. Amanatidis	EC/DGX11-DT
D. Brockhagen	The Greens in the European Parliament
A. Lieuwen	Eurocontrol Agency
K. Smeekens	VITO
J.-P. van Ypersele	Université Catholique De Louvain
M. Vanderstraeten	OSTC

Brazil

V. W. J. H. Kirchhoff	Instituto Nacional de Pesquisas Espaciais
-----------------------	---

Canada

J. Masterton	Atmospheric Environment Service
T. McElroy	Atmospheric Environment Service

Chile

L. Gallardo Klenner
M. Fiebig-Wittmack

CONAMA
Universidad de La Serena

China

D. Yihui
Z. Jingmeng
B. Wu
S. Wu

China Meteorological Administration
China Meteorological Administration (Deceased)
Institute of Atmospheric Physics (Deceased)
Beijing University of Aeronautics and Astronautics

Czech Republic

J. Pretel

Hydrometeorological Institute

Denmark

T. S. Jorgensen
B. Kuemmel
N. Larsen
H. Lyse Nielsen

Danish Meteorological Institute
KVL
Danish Meteorological Institute
Danish Environment Protection Agency

European Commission

G. Angeletti
R. Dunker
M. Raquet

Finland

R. Korhonen
M. Kulmala
I. Savolainen

VTT-Energy
University of Helsinki
VTT-Energy

France

J.-J. Becker
O. Boucher
D. Cariolle
M. Desaulty
M. Gillet
M. Kanakidou
L. Michaelis
P. Vesseron
R. von Wrede

Mission Interministérielle de l'Effet de Serre
Laboratoire d'Optique Atmosphérique
Meteo-France
SNECMA
Mission Interministérielle de l'Effet de Serre
Centre des Faibles Radioactivités
OECD/International Energy Agency
Mission Interministérielle de l'Effet de Serre
Airbus Industrie

Germany

C. H. Brühl	Max-Planck Institut für Chemie	Germany
P. Crutzen	Max-Planck Institut für Chemie	Germany
M. Ernst	Federal Ministry for the Environment	
P. Fabian	LBI	
N. Gorisson	Federal Environmental Agency	
B. Kärcher	DLR Institut für Physik der Atmosphäre	Germany
D. Kley	Institut für Chemie der KFA Jülich GmbH	Germany
H. G. Klug	Daimler-Benz Aerospace Airbus GmbH	
P. Koepke	Meteorologisches Institut München	
A. Petzold	DLR Institut für Physik der Atmosphäre	Germany
R. Sausen	DLR Institut für Physik der Atmosphäre	Germany
H. Schlager	DLR Institut für Physik der Atmosphäre	Germany
U. Schumann	DLR Institut für Physik der Atmosphäre	Germany
G. Seckmeyer	Fraunhofer-Institut für Atmosphäre	
B. Simon	Motoren-und-Turbinen-Union	Germany
W. Stockwell	Fraunhofer-Institut für Atmosphäre	
J. Szodruch	Deutsche Aerospace Airbus GmbH	
M. Treber	Germanwatch	
F. Walle	Leiter Umweltfragen	
H. Weyer	DLR Institut für Physik der Antriebstechnik	Germany

IATA

B. Bourke
J. de la Camera
L. Dobbie
A. Hardeman
R. Walder
G. Zaccagnini

ICAO

A. Costaguta
J. Crayston
G. Finnsson

Israel

Y. Rudisch Weizmann Institute of Science

Italy

V. Satancesaria
G. Visconti

IROE-CNR
Università Degli Studi dell' Aquila

Japan

Y. Kondo

Nagoya University

Kenya

C. K. Gatebe
P. M. Mbuthi
J. K. Njihia

University of Nairobi
Ministry of Energy
Kenya Meteorological Department

New Zealand

V. Gray
M. R. Manning
R. McKenzie

Coal Research Association of New Zealand
NIWA
National Institute of Water and Atmospheric Research Ltd

Norway

K. Alfsen
M. Asen
T. K. Berntsen
O. Christophersen
J. S. Fuglestedt
A. Gaustad
O. Hov
I. Isaksen
S. Lindahl
M. V. Pettersen
K. Rypdal

CICERO
Ministry of Environment
University of Oslo
Ministry of Environment
University of Oslo
Norwegian Civil Aviation Administration
Ministry of Environment
University of Oslo
Norwegian Ministry of Transport
State Pollution Control Authority
Central Bureau of Statistics

Russia

A. A. Gorbatko
I. L. Karol
A. Sorokin

CIAM
Main Geophysical Observatory
CLAM, ECOLEN

Sierra Leone

O. Davidson

Sierra Leone University

Slovenia

A. Kranjc Hydrometeorological Institute

Spain

B. Artinano CIEMAT
J. M. Ciseneros National Meteorological Institute
E. Fernandez INTA
M. Gil INTA
J. C. Rodriguez Murillo Centro de Ciencias Medioambientales
I. Sastre DGAC

Sweden

N. E. Nertun Scandanavian Airlines
K. J. Noone University of Stockholm
K. Pleijel Swedish Environmental Research Institute
J. Ström University of Stockholm
L. Westermark Swedish Commission on Climate Change

Switzerland

W. Bula Federal Office for Civil Aviation
B. C. Cohen UNECE Committee on Energy
C. Frohlich World Radiation Center
J. Romero Federal Office of Environment, Forest, and Landscape
J. Staehelin ETH Atmospheric Physics Laboratory
S. Wenger Federal Office for Civil Aviation

The Netherlands

H. Kelder KNMI
J. W. Nieuwenhuis Ministry of Housing
M. Osterman Royal Netherlands Meteorological Institute
H. J. Pulles Netherlands Civil Aviation Authority
G. Velders Air Research Lab, RIVM

Uganda

B. Apuuli Department of Meteorology

UNEP

N. Sabogal

UNFCCC

N. Höhne
D. Tirpak

United Kingdom

I. Colbeck	University of Essex
P. M. Forster	University of Reading
B. Gardiner	British Antarctic Survey
J. Houghton	IPCC WGI Co-Chairman
C. Hulme	British Airways
C. Hume	British Aerospace
L. R. Jenkinson	Department of Aeronautical and Automotive Engineering and Transport Studies
C. Johnson	DETR
P. R. Jonas	UMIST
D. Lary	University of Cambridge
D. S. Lee	DERA
D. H. Lister	DERA
A. McCulloch	AFEAS/ICI C&P
N. J. Mills	DERA
K. Morris	British Airways
P. Newton	DTI
K. Pearson	DETR
A. Pyle	University of Cambridge
M. Rossell	DETR
K. Shine	University of Reading
J. Tilston	DERA

United States of America

H. Aylesworth, Jr.	Aerospace Industries Association
S. L. Baughcum	The Boeing Company
J. Begin	Northwest Airlines Inc.
F. J. Berardino	Gellman Research Associates Inc.
K. Boering	University of California
T. Carmichael	Coalition for Clean Air
L. Chang	Environmental Protection Agency
U. Covert	Massachusetts Institute of Technology
R. Cuthbertson	The Boeing Company
P. J. De Mott	Colorado State University
S. Dollyhigh	NASA Langley Research Center
D. DuBois	The Boeing Company
J. H. Ellis	Federal Express Corporation
D. Ercegovic	NASA Langley Research Center

A. Fiorentino	Pratt & Whitney Aircraft
N. Fitzroy	GE (Retired)
S. Gander	Center for Clean Air Policy
M. Geller	New York State University
A. Gettelman	US Climate Action Network
T. E. Graedel	IGBP/IGAC, AT&T Bell Laboratories
K. Green	Consultant
W. L. Grose	NASA Langley Research Center
M. Guynn	NASA Langley Research Center
P. Hamill	San Jose State University
S. Henderson	The Boeing Company
J. Holton	University of Washington
C. H. Jackman	NASA Goddard Space Flight Center
D. Jacob	Harvard University
R. Kassel	Natural Resources Defense Council
G. Kent	NASA Langley Research Center
H. Kheshgi	EXXON
E. Levina	Center for Clean Air Policy
J. Levy	NOAA
J. Logan	Harvard University
S. P. Lukachko	Massachusetts Institute of Technology
B. Manning	Environmental Protection Agency
R. Marshall	Pratt & Whitney Aircraft
J. Montgomery	American Airlines
A. Mortlock	The Boeing Company
C. Newberg	Environmental Protection Agency
R. Nichols	The Boeing Company
R. Niedzwiecki	NASA Lewis Research Center
R. C. Oliver	Institute for Defence Analyses
M. Oppenheimer	Environmental Defense Fund
J. Pershing	US Department of State
A. Petsonk	Environmental Defense Fund
B. Pierce	NASA Langley Research Center
L. R. Poole	NASA Langley Research Center
R. Pueschel	NASA Ames Research Center
V. Ramaswamy	Geophysical Fluid Dynamics Laboratory
A. R. Ravishankara	NOAA Aeronomy Laboratory
D. Rind	NASA Goddard Institute of Space Studies
R. Rubenstein	Environmental Protection Agency
C. Russo	NASA Lewis Research Center
A. Schafer	Massachusetts Institute of Technology
K. Shah	NASA Goddard Institute of Space Studies
S. F. Singer	Science and Environmental Policy Project
R. Stolarski	NASA Goddard Space Flight Center
W. Strack	Modern Technologies Corp
L. Thomason	NASA Langley Research Center

A. Thompson	NASA Goddard Space Flight Center
K. E. Trenberth	National Center for Atmospheric Research
A. Vedantham	Richard Stockton College of New Jersey
D. Victor	Council for Foreign Relations
W.-C. Wang	State University of New York at Albany
S. G. Warren	University of Washington
S. Webb	The Weinberg Group Inc.
H. L. Wesoky	Federal Aviation Administration

SECTION E: Assessment of the Atmospheric Effects of High-Speed Aircraft in the Stratosphere: 1998

ASSESSMENT CHAIR

S. Randolph Kawa	NASA Goddard Space Flight Center	US
------------------	----------------------------------	----

LEAD AUTHORS

James G. Anderson	Harvard University	US
Steven L. Baughcum	Boeing Company	US
Charles A. Brock	University of Denver	US
William H. Brune	Pennsylvania State University	US
Ronald C. Cohen	University of California, Berkeley	US
Douglas E. Kinnison	National Center for Atmospheric Research (formerly affiliated with Lawrence Livermore National Laboratory)	US
Paul A. Newman	NASA Goddard Space Flight Center	US
Jose M. Rodriguez	University of Miami	US
Richard S. Stolarski	NASA Goddard Space Flight Center	US
Darryn Waugh	Johns Hopkins University	US
Steven C. Wofsy	Harvard University	US

COORDINATING EDITORS

Rose M. Kendall	Computer Sciences Corporation	US
Kathy A. Wolfe	Computer Sciences Corporation	US

CONTRIBUTORS AND REVIEWERS

Donald E. Anderson	The Johns Hopkins University Applied Physics Laboratory/NASA Goddard Space Flight Center	US
Kristie A. Boering	University of California, Berkeley	US
Lisa Chang	US Environmental Protection Agency	US
Martyn Chipperfield	University of Leeds	UK
Med Colket	United Technologies Research Center/Pratt & Whitney	US
David Considine	University of Maryland	US
Robert Cuthbertson	Boeing Commercial Airplane Group	US

Willard J. Dodds	General Electric Aircraft Engines	US
Anne R. Douglass	NASA Goddard Space Flight Center	US
James W. Elkins	NOAA Climate Monitoring and Diagnostics Laboratory	US
David W. Fahey	NOAA Aeronomy Laboratory	US
Randall R. Friedl	Jet Propulsion Laboratory	US
Marvin A. Geller	State University of New York, Stony Brook	US
William L. Grose	NASA Langley Research Center	US
Tom F. Hanisco	Harvard University	US
James R. Holton	University of Washington	US
Charles H. Jackman	NASA Goddard Space Flight Center	US
Harold S. Johnston	University of California, Berkeley	US
Bernd Kärcher	DLR Institute for Atmospheric Physics	Germany
Jack A. Kaye	NASA Headquarters	US
Malcolm K. W. Ko	Atmospheric and Environmental Research, Inc.	US
Charles E. Kolb	Aerodyne Research, Inc.	US
Michael J. Kurylo	National Institute of Standards and Technology/NASA Headquarters	US
Richard J. Lawrence	NASA Goddard Space Flight Center	US
Richard C. Miake-Lye	Aerodyne Research, Inc.	US
Mario J. Molina	Massachusetts Institute of Technology	US
Alan K. Mortlock	Boeing Company	US
Joyce E. Penner	University of Michigan	US
Michael J. Prather	University of California, Irvine	US
David H. Rind	NASA Goddard Institute for Space Studies	US
Helen Rogers	University of Cambridge	UK
Richard B. Rood	NASA Goddard Space Flight Center	US
Douglas Rotman	Lawrence Livermore National Laboratory	US
Keith R. Ryan	Commonwealth Scientific and Industrial Research Organization (CSIRO)	Australia
Ulrich Schumann	DLR Institute for Atmospheric Physics	Germany
Sergei Smyshlyaev	State University of New York, Stony Brook	US
Saadat A. Syed	Pratt & Whitney	US
Darin W. Toohey	University of Colorado, Boulder	US
Peter Vohralik	Commonwealth Scientific and Industrial Research Organization (CSIRO)	Australia
Debra Weisenstein	Atmospheric and Environmental Research, Inc.	US
Howard L. Wesoky	Federal Aviation Administration	US
Allen H. Whitehead	NASA Langley Research Center	US

SECTION F: Models and Measurements (M&M) Intercomparison II Summary

N. Andronova	University of Illinois, Urbana-Champaign	US
Steven L. Baughcum	Boeing Company	US
Praful P. Bhatt	Science Applications International Corporation	US
Kristie A. Boering	University of California, Berkeley	US

Guy P. Brasseur	Max-Planck-Institut für Meteorologie	US
Donald E. Brown	Science Applications International Corporation	US
Christoph Brühl	Max-Planck-Institut für Chemie	Germany
Martyn P. Chipperfield	University of Leeds	UK
Peter S. Connell	Lawrence Livermore National Laboratory	US
David B. Considine	University of Maryland, College Park	US
Anne R. Douglass	NASA Goddard Space Flight Center	US
Victor L. Dvortsov	State University of New York, Stony Brook	US
Richard S. Eckman	NASA Langley Research Center	US
James W. Elkins	NOAA Climate Monitoring and Diagnostics Laboratory	US
Eric L. Fleming	Steven Myers and Associates, Corp.	US
Randall R. Friedl	Jet Propulsion Laboratory	US
Rolando R. Garcia	National Center for Atmospheric Research	US
Volker Grewe	DLR Institute for Atmospheric Physics	Germany
William L. Grose	NASA Langley Research Center	US
Timothy M. Hall	NASA Goddard Institute for Space Studies	US
Bryan J. Hannegan	University of California, Irvine	US
Matthew H. Hitchman	University of Wisconsin, Madison	US
Theresa Y. Huang	National Center for Atmospheric Research	US
Charles H. Jackman	NASA Goddard Space Flight Center	US
Dylan B. A. Jones	Harvard University	US
Igor L. Karol	A. I. Voeikov Main Geophysical Observatory	Russia
S. R. Kawa	NASA Goddard Space Flight Center	US
Jack A. Kaye	NASA Headquarters	US
Rose M. Kendall	Computer Sciences Corporation	US
Rashid Khosravi	National Center for Atmospheric Research	US
Douglas E. Kinnison	National Center for Atmospheric Research	US
Malcolm K. W. Ko	Atmospheric and Environmental Research, Inc.	US
Larissa Kogan	Harvard University	US
Gordon Labow	NASA Goddard Space Flight Center	
Jean Lerner	NASA Goddard Institute for Space Studies	US
Jennifer A. Logan	Harvard University	US
Richard D. McPeters	NASA Goddard Space Flight Center	US
Philip W. Mote	Northwest Research Associates, Inc.	US
S. Nossal	University of Wisconsin	US
Samuel J. Oltmans	NOAA Climate Monitoring and Diagnostics Laboratory	US
Jae H. Park	NASA Langley Research Center	US
Giovanni Pitari	Universita' degli Studi L'Aquila	Italy
R. Alan Plumb	Massachusetts Institute of Technology	US
Michael J. Prather	University of California, Irvine	US
Patrick N. Purcell	Science Applications International Corporation	US
William J. Randel	National Center for Atmospheric Research	US
Lakshman Randeniya	Commonwealth Scientific and Industrial Research Organization (CSIRO)	Australia
Philip J. Rasch	National Center for Atmospheric Research	US
Ellis E. Remsberg	NASA Langley Research Center	US

David H. Rind	NASA Goddard Institute for Space Studies	US
Curtis P. Rinsland	NASA Langley Research Center	US
Jose M. Rodriguez	University of Miami	US
Helen L. Rogers	University of Cambridge	UK
Richard B. Rood	NASA Goddard Space Flight Center	US
Joan E. Rosenfield	General Sciences Corporation	US
Douglas Rotman	Lawrence Livermore National Laboratory	US
Eugene V. Rozanov	University of Illinois, Urbana-Champaign	US
Keith R. Ryan	Commonwealth Scientific and Industrial Research Organization (CSIRO)	Australia
Karen H. Sage	Science Applications International Corporation	US
Ross J. Salawitch	Jet Propulsion Laboratory	US
M. E. Schlesinger	University of Illinois, Urbana-Champaign	US
Hans R. Schneider	Harvard University	US
Courtney Scott	Atmospheric and Environmental Research, Inc.	US
Sergey P. Smyshlyaev	State University of New York, Stony Brook	US
Randy Soderholm	Computer Sciences Corporation	US
Susan Solomon	NOAA Aeronomy Laboratory	US
Benedikt Steil	Max-Planck-Institut fur Chemie	Germany
XueXi Tie	National Center for Atmospheric Research	US
Peter F. Vohralik	Commonwealth Scientific and Industrial Research Organization (CSIRO)	Australia
Darryn W. Waugh	The Johns Hopkins University	US
Clark J. Weaver	Applied Research Corporation	US
Chu-feng Wei	University of Illinois, Urbana-Champaign	US
Debra K. Weisenstein	Atmospheric and Environmental Research, Inc.	US
Kathy A. Wolfe	Computer Sciences Corporation	US
Donald J. Wuebbles	University of Illinois	US
F. Yang	University of Illinois, Urbana-Champaign	US
Valery A. Yudin	State University of New York, Stony Brook	US
Xin Zhu	University of California, Irvine	US
Vladimir A. Zubov	A. I. Voeikov Main Geophysical Observatory	Russia

SECTION G: POLARIS End-of-Mission Statement

David W. Fahey	NOAA Aeronomy Laboratory	US
Paul A. Newman	NASA Goddard Space Flight Center	US

Co-Project Scientists on behalf of the POLARIS Science Team
(see Section G for detailed list)

SECTION H: Chemical Kinetics and Photochemical Data for Use in Stratospheric Modeling: Supplement to Evaluation Number 12 of the NASA Panel for Data Evaluation

AUTHORS

William B. DeMore	Jet Propulsion Laboratory	US
Randall R. Friedl	Jet Propulsion Laboratory	US
David M. Golden	SRI International	US
Robert F. Hampson	National Institute of Standards and Technology	US
Robert E. Huie	National Institute of Standards and Technology	US
Charles E. Kolb	Aerodyne Research, Inc.	US
Michael J. Kurylo	National Institute of Standards and Technology	US
Mario J. Molina	Massachusetts Institute of Technology	US
Geert Moortgat	Max-Planck-Institut für Chemie	Germany
A. R. Ravishankara	NOAA Aeronomy Laboratory	US
Stanley P. Sander	Jet Propulsion Laboratory	US

